Engineering innate immunology in cardiovascular disease models and regenerative medicine

Trinity College Dublin
Coláiste na Tríonóide, Baile Átha Cliath
The University of Dublin

A thesis submitted to the University of Dublin in partial fulfilment of the requirements for the degree of

Doctor in Philosophy

Sinead O'Rourke B.A. (Hons)

January 2023

Supervisor: Prof. Michael Monaghan

Co-supervisor: Prof. Aisling Dunne

Declaration

I declare that this thesis has not been submitted as an exercise for a degree at this or any other university and it is entirely my own work.

I agree to deposit this thesis in the University's open access institutional repository or allow the Library to do so on my behalf, subject to Irish Copyright Legislation and Trinity College Library conditions of use and acknowledgement.

I consent to the examiner retaining a copy of the thesis beyond the examining period, should they so wish (EU GDPR May 2018).

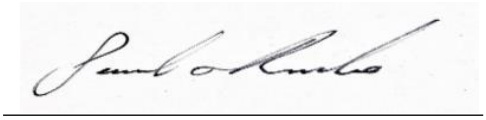

Sinead O'Rourke

Acknowledgements

I would like to first extend my sincere thanks and gratitude to my supervisor and mentor Prof. Michael Monaghan, firstly for providing me with the opportunity to undertake this PhD and secondly for your continued support throughout the project. Thank you for always pushing me to do my best, and continuously seeing the value in the work I have done. Your enthusiasm for all data, (even the negative data) is something I hope to carry with me in my future work.

I also would like to thank my co-supervisor, and mentor Prof. Aisling Dunne. I can still remember very clearly the day I nervously stepped into your office as an undergraduate, to ask about the possibility of pursuing a PhD. I am forever grateful for your belief in me then, and right up to now, that I had what it takes to reach this point. Thank you for your time, patience, and continuous support and encouragement through all the unexpected turns of the last 4 years.

Thank you to my thesis committee, Prof. Fred Sheedy and Prof. Dave Hoey, for your ongoing input and advice through the progression of this work.

I would like to thank all current and previous members of the Monaghan and Dunne lab, who have helped me throughout the course of my project. Thank you to Matteo, for your invaluable help with all my PEDOT and bioreactor experiments and beyond, as well as your patience for my never-ending questions and practice drills for the bioreactor set up. Thank you to Nuno, not only for every FLIM experiment you willingly carried out for me, but for all the laughs and chats we have shared since starting together in the lab. Thank you to Meena, who I shared the thrill (but mostly pain) of iPSC culture with. I am truly grateful for your support and friendship, especially in the final months of experiments. I would also like to thank Giuseppe for all he contributed to make the Monaghan lab a friendly work environment. Thank you also to Dinorath, who very much took me under her wing when I first started, doing everything she could to help me start up experiments.

Thank you, Hannah, who over the last 4+ years I have forged a firm friendship with (whether she likes it or not). In all sincerity, thank you for being an extra pair of hands when I planned too much in one day, a sympathetic ear when I needed to vent, advisor on all things flow-related, and an incredible friend during this PhD. Thank you to my fellow immuno-engineer Lianne, for your help with all things lab-related (too many to list!), and your reliability for a coffee-run, as well as a good hug when needed. Thank you to Eva, for all your help and training at the beginning of my project, and all the laughs we've shared since then. Thank you to Gearóid, you have been a brilliant addition to the Dunne lab, and I wish you the best of luck with your own PhD.

Thank you to all members of 3.12, past and present, who have made the lab such an enjoyable place to work. Thank you, Vivienne, as it is safe to say without you the lab

would crumble! Thank you to Michelle for great chats and advice, Tracey for your kind words of encouragement over the years, and Eoin for all your help with Seahorse, Endnote, and phlebotomy! Thank you, Andy and Simon for help with monocytes, and Alanna and Richard for good chats and laughs over the years. Thank you Cliodhna for your friendship and dedicated commitment to the Late Night Crew and thank you Seán for the numerous delivery runs and help around the lab. Thank you, Juber, Lowela, and Aziz, who have been great additions to the 3.12 group over the last two years. Thank you to Mei for your kindness, generosity and help in the lab. Thank you, Claudia, for always being there to share a good laugh, trouble shoot a western blot, or empathise with me on any PhD woes, more often than not with biscuits at hand. Thank you also to Barry and Aoife for your help with all things flow-related!

A special thank you to Emilio, for the countless times you have cheered me on, made me laugh, and gone out of your way to help me in the lab. You are a terrific scientist and a wonderful friend, and I am so grateful to have shared this time with you.

Thank you to all the staff and students in TBSI who have helped me throughout this project. Thank you to Jer Hayes, Gavin Davis, and Sarah mcComish for all your iPSC help. Thank you to Gavin McManus for your help and expertise with confocal. Thank you to Coilín Boland for all your help with cholesterol crystal synthesis. Thank you to Stephane for your ever willing support with experiments. Thank you to the prep room staff, Audrey, Martha, Roisín, Brian, Trudy, and Edith who have all supported me at some point, whether it was emergency supply of lab reagents or kind words of encouragement. It has been a pleasure to get to know you all. A special shout out also beyond TBSI to Shannon Cox from the Curtis Clock lab, RCSI, who was always willing to share reagents and western blot wisdom with me.

I would also like to acknowledge all past and present members of TCBE who I have met along the years. They are truly a team of brilliant minds, and it has been a privilege to be a member of such a fantastic department. I greatly look forward to continuing my research journey with you all.

I would like to acknowledge my friends, Derv, Stef, Shannon, Niamh, Chrissy, and Izzy, who are not only a brilliant support group, but a group of amazing scientists in their own right. Thank you to the Coldrick family, Julie, Ken, Jack, Amy and Luke for your enthusiasm and interest in my work, and always cheering me on throughout the years.

To Kenny, for being by my side every step of the way, I cannot put into words how much you mean to me. Thank you for being there to pick me up when I'm low and celebrating every win with me. I know I will do the same for you to get you over the PhD finish line. Here's to our future as doctors.

To my sister Aisling, who knows me better than any other, thank you for always being there. Our evening debriefs always meant I was ending even the toughest of days with a good laugh.

Lastly, I would like to dedicate this thesis to my parents, Brian and Anne. I think it would truly take me a whole additional thesis to express my gratitude for everything you have done for me. You have been my number one supporters and I owe all my success to your constant support and guidance through the years. Thank you, Dad, for every time you sat at the kitchen table with me to brainstorm an idea, every lift home after a long day, and keeping me level-headed and focused on the end point, especially in the final few months. Thank you, Mom, for everything, but especially for always encouraging me to speak up, ask questions, and have confidence in myself. I love you both so dearly.

It makes no damn sense! Compels me though…

— Knives Out 2019

Summary

Heart failure is the leading cause of death worldwide with atherosclerosis and myocardial infarction remaining prominent causes. It is now widely accepted that the inflammatory response holds a key role in advancing both cardiovascular disease and heart failure, and as a result, anti-inflammatory therapies have garnered significant interest in the last decade to combat disease. In particular, targeting the inflammatory action of macrophages, an innate immune cell population known for their adverse pathological role in both cardiovascular disease and heart failure, shows great promise. However, advances in immunomodulatory therapies, including those which target macrophages, remain limited in humans. This is in part due to substantial gaps in our knowledge regarding the interactions of the immune response in the heart at a cellular level and further complicated by the fact that current disease models either fail to incorporate a multicellular environment, or are carried out in animal models, which can largely lack translational capacity. The aim of this thesis, therefore, was to assess the role of macrophages in the cardiac environment at a simpler cellular level, with the intention of elucidating the functional role of macrophages in the heart, gaining insight to the mechanisms which advance CVD, and ultimately identifying potential therapeutic strategies for future treatments of heart failure. To achieve this, I explored several different factors which can influence macrophage function in the cardiac environment, including cell-cell interactions with cardiomyocytes, endogenous athero-associated DAMPs, and the physical stimulus: electrical stimulation.

First, I assessed the interactions between primary human macrophages and induced pluripotent stem cell-derived cardiomyocytes, in order to understand how cardiomyocyte cross-talk influences macrophage function. It was observed in this study that cardiomyocytes potentially have an immunomodulatory effect on blood-derived macrophages, limiting the production of pro-inflammatory cytokine IL-6 and chemokine IL-8. However, detailed characterisation of this response was limited by the adverse effects of B-27™ supplement, a media component necessary for the culture of induced pluripotent stem cell-derived cardiomyocytes.

The second study of this thesis investigated the impact of cholesterol crystals on primary human macrophages. It was demonstrated in this chapter that cholesterol crystals

promote polarisation of macrophages towards a pro-inflammatory M1 phenotype, with increased expression of M1 associated genes and IL-8 production. This pro-inflammatory response was accompanied by increased rates of glycolysis in macrophages. Inhibition of glycolysis either directly through inhibition of the glycolytic enzymes Hexokinase II (HK2), or PFKFB3, or else indirectly through inhibition of PKM2 (found to be a critical mediator of macrophage metabolic reprogramming) abrogated the pro-inflammatory phenotype induced by cholesterol crystals. As a result of this study, significant insight was gained regarding the inner mechanisms which drive macrophage-mediated inflammation in atherosclerosis, while furthermore highlighting immunometabolism as a novel therapeutic target to combat this disease.

The third study of this thesis investigated the impact of electrical stimulation on macrophage phenotype and function. It was observed in this work that electrical stimulation promotes polarisation of primary human macrophages towards an anti-inflammatory M2 phenotype, with increased expression of M2 associated genes and pro-regenerative growth factors. Additionally, electrical stimulation restricted classical activation of macrophages with either LPS or cholesterol crystals. This work has allowed us to shed some light on how homeostasis of macrophages is potentially maintained in the heart while additionally, presenting a novel therapeutic strategy to harness anti-inflammatory, pro-regenerative responses across multiple injury and defence microenvironments.

Based on the above findings, the fourth and final study of this thesis assessed the response of macrophages to the electroconductive material PEDOT: PSS, for future applications of electrically stimulated macrophages. PEDOT: PSS was found to be well tolerated by primary human macrophages, not only identifying the material as a compatible platform for macrophage culture *in vitro*, but also providing insight to future success of the material *in vivo* as PEDOT: PSS failed to elicit a foreign body response in macrophages.

Collectively, the work in this thesis has provided novel insight to the function of human macrophages in the cardiac environment, providing insight to the chemical and physical factors which shape the supportive role of macrophages, while additionally

demonstrating the cellular mechanisms responsible for adverse function of this cell population in cardiovascular disease.

List of Publications, conference proceedings, awards

First Author Publications

O'Rourke S., Neto N., Devilly E., Shanley L., Fitzgerald H., Monaghan M.G., Dunne A., Cholesterol crystals drive metabolic reprogramming and M1 polarisation in primary human macrophages. *Atherosclerosis* 2022.

O'Rourke S., Dunne A., Monaghan M.G. The Role of Macrophages in the Infarcted Myocardium: Orchestrators of ECM Remodelling. *Frontiers in Cardiovascular Medicine* 2019.

Co-Author publications

Shanley L., Fitzgerald H., **O'Rourke S.,** Dunne A. Endogenous drivers of altered immune cell metabolism. *Experimental Biology and Medicine* 2022.

Fitzgerald H., **O'Rourke S.,** Desmond E., Neto N., Monaghan M.G., Tosetto M., Doherty J., Ryan E., Doherty G., Nolan D., Fletcher J., Dunne A. The Trypanosoma brucei-derived ketoacids, Indole Pyruvate and Hydroxyphenylpyruvate, induce HO-1 expression and suppress inflammatory responses in human dendritic cells. *Antioxidants* 2022.

Neto N., **O'Rourke S**., Zhang M., Fitzgerald H., Dunne A., Monaghan M.G. Non-Invasive classification of macrophage polarisation by 2P-FLIM and machine learning. *eLife Sciences* 2022.

Shanley L., Mahon O., **O'Rourke S.,** Neto N., Monaghan M.G., Kelly D. J., Dunne A. Hydroxyapatite particle size differentially alters macrophage metabolism. *Acta Biomaterialia* 2023.

Conference proceedings

*presenting author

O'Rourke S*., Solazzo M., Dunne A., Monaghan M.G. External delivery of electrical stimulation promotes M2 macrophage polarisation: Implications in regenerative tissue engineering. Trinity Centre for Biomedical Engineering Annual Research Day. Dublin, Ireland. 6th of December 2022. Oral presentation.

O'Rourke S.*, Neto N., Devilly E., Shanley L., Fitzgerald H.K., Dunne A., Monaghan M.G. Targeting metabolism in cardiovascular disease: investigating metabolic reprogramming of macrophages in atherosclerosis as a novel therapeutic strategy. Irish Society of Immunology Meeting 2022. Kildare, Ireland. 1st-2nd September 2021. Poster presentation

O'Rourke S.*, Neto N., Devilly E., Shanley L., Fitzgerald H.K., Dunne A., Monaghan M.G. Targeting metabolism in cardiovascular disease: investigating metabolic reprogramming of macrophages in atherosclerosis as a novel therapeutic strategy. British Society of Immunology Congress Meeting 2021. Edinburgh, Scotland. 28th of November – 1st of December 2021. Poster presentation

O'Rourke S.*, Neto N., Devilly E., Shanley L., Fitzgerald H.K., Dunne A., Monaghan M.G. Targeting metabolism in cardiovascular disease: investigating metabolic reprogramming of macrophages in atherosclerosis as a novel therapeutic strategy. British Society for Cardiovascular Research Autumn meeting 2021. Oral presentation.

O'Rourke S.*, Neto N., Devilly E., Shanley L., Fitzgerald H.K., Dunne A., Monaghan M.G. Immunometabolism in atherosclerosis: Investigating cholesterol crystals as potent drivers of metabolic reprogramming and M1 macrophage polarisation. Keystone eSymposia; Innate Immunity: Mechanisms and modulation. Virtual conference 12-15th April. Poster presentation.

O'Rourke S.*, Neto N., Dunne A., Monaghan M.G. Immune modulation in atherosclerosis: Investigating cholesterol crystals as potent drivers of metabolic reprogramming and M1 macrophage polarisation. Drexel Immune Modulation and Engineering Symposium. 11-13th November 2020. Oral Presentation.

O'Rourke S.*, Solazzo, M., Dunne, A. Monaghan, M. G. The Assessment of Macrophage Response to Electroconductive Biomaterials. Irish Society for Immunology Meeting 2019. Dublin, Ireland. 19th - 20th September 2019. Poster Presentation.

O'Rourke S.*, Dunne A., Monaghan, M.G. The Influence of Electroconductive Materials on Macrophage Phenotype. 25th Bioengineering in Ireland 2019. Limerick, Ireland. 18th-19th January 2019. Oral Presentation.

Awards

1st Place, "Thesis in 3", Trinity Centre for Biomedical Engineering Winter Symposium, 2020

2nd Place "5x5" Oral presentation, Trinity Immunometabolism Forum, 2021

1st Place Oral presentation, British Society for Cardiovascular Research Autumn meeting 2021

2nd Place "BHI People's choice" oral abstract prize, British Society for Cardiovascular Research Autumn meeting 2021

Abbreviations

2-DG	2-Deoxyglucose
ACAT	Acyl-Coenzyme A:cholesterol Acyltransferases
ATP	Adenosine triphosphate
CCL2/MCP-1	Monocyte chemoattractant protein-1
CCR2	Chemokine receptor type 2
CD	Cluster differentiation
CHC	Cholesterol crystals
CM	Cardiomyocyte
CNT	Carbon nanotube
CRP	C-Reactive protein
CTnT	Cardiac troponin T
CVD	Cardiovascular disease
CX3CR1	CX3C motif chemokine receptor 1/Fractalkine receptor
DAMP	Damage associated molecular pattern
DQ-ova	DQ-ovalbumin
ECAR	Extracellular acidification rate
ECL	Electrochemiluminescence
ECM	Extracellular matrix
EF	Electric field
ER	Endoplasmic reticulum
ES	Electrical stimulation
ESC	Embryonic stem cell
FAO	Fatty acid oxygen pathway
FAS	Fatty acid synthesis pathway
FBS	Foetal bovine serum
FLIM	Fluorescence lifetime imagine microscopy
FMO	Fluorescence minus one
G6P	Glucose-6-phosphate
GOPS	3-glycidyloxypropyl)trimethoxysilane
HEK	Human embryonic kidney
HIF1α	Hypoxia inducible factor 1 alpha
HK2	Hexokinase II
ICAM	Intracellular adhesion molecule
ICP	Intrinsic conjugated polymers
IFNγ	Interferon gamma
IGF-1	Insulin growth factor 1
IL	Interleukin
iNOS	Inducible nitric oxide synthase
iPSC	Induced pluripotent stem cell
IS	Infarction size
LDL/OX-LDL	Low-density lipids/ Oxidised low-density lipids
LPS	Lipopolysaccharide
M-CSF	Macrophage colony stimulation factor
MFF	Mitochondrial fission factor

MI	Myocardial infarction
MLC2a	Myosin light chain atrial
MMP	Matrix metalloproteinase
MSC	Mesenchymal stem/stromal cell
mTOR	Mammalian target of rapamycin
NF-Kb	Nuclear factor kappa-light-chain-enhancer of activated B cells
NO	Nitrogen oxide
NP	Nanoparticles
OCR	Oxygen consumption rate
PAMP	Pathogen associated molecular pattern
PBMC	Peripheral blood mononuclear cells
PDGF	Platelet derived growth factor
PEDOT: PSS	Poly(3,4-ethylenedioxythiophene) polystyrene sulfonate
PEGDE	Poly(ethylene glycol)diglycidyl ether
PKM2	Pyruvate kinase isoform 2
PPP	Pentose phosphate pathway
PRR	Pathogen recognition receptor
ROS	Reactive oxygen species
SCN	Voltage-gated sodium channel
SD	Standard deviation
SEM	Standard error of the mean
TCA	Tricarboxylic acid
TGF-β	Tissue growth factor beta
TLR	Toll-like Receptor
TNF	Tumour necrosis factor
VCAM	Vascular cell adhesion molecule
VEGF	Vascular endothelial growth factor

Table of Contents

Table of Figures

Table of Tables

Chapter 1 : Introduction

1.1 Cardiovascular disease and heart failure

Heart failure is defined as a debilitating cardiovascular condition whereby the heart is not capable of pumping enough blood to meet the energy demands of the body. Despite advances in modern medicine, heart failure remains a challenge to the health care system both at a national and international level. In Ireland, the overall prevalence rate of heart failure is approximately 2% (approximately 90,000 people diagnosed every year) [1]. This equates to one in five people suffering from heart failure over their lifetime with the rate of incidence increasing with the ageing population. Heart failure is a common consequence of cardiovascular diseases (CVD), and usually occurs following incidence of injury to the heart, such as myocardial infarction (MI) (also known as a heart attack). MI refers to mass cardiomyocyte death as a result of an occlusion of oxygen (known as ischemia). Due to the limited regenerative capacity of the heart, this mass cell death significantly impairs cardiac function [2]. Damage to the myocardium also triggers an inflammatory response which often becomes dysregulated, leading to tissue fibrosis and the generation of non-contracting scar tissue which further limits cardiac function [3]. Atherosclerosis is the most common cause of MI, as build-up of plaque in the inner lining of arteries leads to a blocked supply of oxygen to the heart. Our understanding of both atherosclerosis and MI has evolved over the years, with inflammation, primarily driven by macrophages, now accepted as playing a key pathological role [3, 4].

1.2 Macrophages

Macrophages are key innate immune cells arising from early developmental stages to reside in the tissue or else from circulating monocytes in the blood. Circulating monocytes are recruited to sites of injury or pathogen invasion by specific signals, including cytokines and chemokines released by local cells. Once recruited, monocytes differentiate into macrophages. A defining feature of macrophages is their plasticity, which allows them to produce a tailored response to local microenvironment stimuli. Classical activation of macrophages occurs in response to pathogen-associated molecular patterns (PAMPs) such as lipopolysaccharide (LPS) or endogenous damage associated molecular patterns (DAMPs) [5]. This results in a pro-inflammatory phenotype, often denoted in the literature as an M1 phenotype [6]. Alternative

activation of macrophages is known to arise from stimulation with anti-inflammatory cytokines such as interleukin 4 (IL-4) or IL-10, resulting in an anti-inflammatory phenotype, often referred to as M2. While this M1/M2 classification provides useful framework to understand macrophage function, this represents merely two ends of a broad spectrum of macrophage phenotype and function. Indeed, numerous subsets of macrophage phenotype can exist, sharing properties of both the typical M1 and M2 classification. Additionally, macrophages exhibit great plasticity, capable of shifting from a pro-inflammatory role to an anti-inflammatory and pro-reparative phenotype, depending on their surrounding environment [6, 7]. Therefore, macrophage form and function is often context dependent.

1.3 The role of macrophages in CVD and heart failure

Inflammation, driven largely by innate immune cells, is a key feature of plaque formation and rupture in atherosclerosis. Neutrophils, natural killer cells, dendritic cells, and macrophages have all been shown to reside within the plaque and drive the inflammatory response [8]. Macrophages in particular, play a central role in the development and destabilisation of atherosclerotic plaques [8, 9]. Macrophages in atherosclerotic lesions actively participate in ingestion of lipoproteins, resulting in the formation of foam cells. The accumulation of foam cells leads to increased lipid storage and plaque growth. Meanwhile non-foamy macrophages exhibit a classical pro-inflammatory phenotype in atherosclerotic lesions, secreting pro-inflammatory cytokines and reactive oxygen species (ROS) which directly affect smooth muscle cells, thus leading to thinning of the fibrous cap surrounding plaques and eventual plaque rupture [10].

In MI, macrophages are key regulators of tissue repair following loss of cardiomyocytes (CMs) [11]. In the early stages of MI, monocytes infiltrate the heart where they differentiate to M1 macrophages in response to necrotic cells. This pro-inflammatory population clears cell debris through phagocytosis and induces breakdown of the extracellular matrix (ECM). Phagocytosis of cell debris promotes a phenotypic switch in macrophages towards the anti-inflammatory M2 phenotype. M2 macrophages secrete high levels of anti-inflammatory, pro-reparative factors such as IL-10 and growth factor transforming growth factor beta (TGFβ), thus resolving the inflammatory response as

well as activating local cells such as fibroblasts to promote ECM repair and tissue regeneration. Both M1 and M2 phenotypes are necessary for effective cardiac repair following MI, however sustained activation of macrophages leads to continuous secretion of growth factors, pro-inflammatory cytokines, and matrix metalloproteinases (MMPs) responsible for ECM breakdown. Continued breakdown of ECM as well as overproduction of ECM components by myofibroblasts (activated fibroblasts) leads to adverse remodelling of ECM and results in fibrotic scar tissue, therefore limiting cardiac function.

1.4 Current limitations in immunomodulating therapies for heart failure

Given the observed role of inflammation in the pathogenesis of CVD and heart failure, more current studies have begun to focus on modulating the immune response as a potential therapeutic strategy. Several clinical trials have been carried out which target mediators of inflammation, including pro-inflammatory cytokines tumour necrosis factor (TNF) and IL-1β [12-15]. Use of IL-1β inhibitor Canakinumab in the CANTOS trial, resulted in a 25% risk reduction of CVD in patients [3]. Targeting IL-1β also reduced the risk of new MI events in patients with previous history of infarction [3]. However, use of general immunosuppressants such as corticosteroids in patients post MI has yielded conflicting results. While some trials have reported potential benefits, generally these treatments have failed to provide a significant cardio-protective effect [16]. It is possible that non-specific suppression of inflammation is insufficient to alleviate the adverse effects associated with infarction, with more targeted approaches required.

Specifically targeting macrophages has shown great promise in improving prognostic outcome for animal models of MI. For example, selective targeting of the chemokine receptor CCR2 effectively prevents monocyte/macrophage infiltration to the heart following MI, and as a result, significantly reduces infarct size in murine models, in addition to reducing levels of pro-inflammatory cytokines and ventricular remodelling [17, 18]. Such results not only affirm the significant role of macrophages in heart failure following MI, but also highlight the potential of these cells as an effective therapeutic target. However, to allow for further development of such therapies, greater understanding of the role of macrophages in the heart is required. Indeed, there are still considerable gaps in our knowledge regarding macrophage interactions in the cardiac

environment, and how precisely these interactions are regulated. Much of what we have learned to date regarding the role of macrophages and the inflammatory response in heart failure arises from animal models. While these studies have proven constructive in delineating the impact of the inflammatory response post MI, the caveat, as always with animal models, is the disparity between animal studies and human clinical trials. Furthermore, much of these studies fail to examine the pathological interactions which drive heart failure at a simpler cellular level.

1.5 Research objective and specific aims

The appreciation for the role of macrophages in CVD and heart failure marks these cells as a prime therapeutic target in combatting the disease. However, advances in immunomodulatory therapies, specifically those which target macrophages remain limited in humans. This in part is due to the substantial gaps of knowledge of the precise role of macrophages in the cardiac environment. Additionally, much of what we have learned regarding the role of macrophages in CVD arise from animal models, which can lack translational capacity to humans, thus limiting the development and success of novel therapies in clinical trials. To address this limitation, the overall objective of this thesis is to examine the role of macrophages in the cardiac environment for therapeutic applications. There are numerous factors which can influence macrophage function in this environment, such as endogenous DAMPs, cell-cell interactions, and physical cues from the environment itself. Therefore, several objectives have been identified to achieve the overall aim of this thesis.

Objective 1: Investigate the cellular interactions between primary human macrophages and induced pluripotent stem cell derived cardiomyocytes (iPSC-CMs).

Objective 2: Study the impact of athero-associated DAMPs: cholesterol crystals on macrophage phenotype and function

Objective 3: Determine the impact of electrical stimulation on primary human macrophages

Objective 4: Characterise macrophage response to the electroconductive biomaterial PEDOT: PSS, for future applications of electrically stimulated macrophages.

Chapter 2 : Literature review

The majority of the work in this chapter has been peer reviewed and published in O'Rourke SA, Dunne A, Monaghan MG. The Role of Macrophages in the Infarcted Myocardium: Orchestrators of ECM Remodeling. Front Cardiovasc Med. 2019 Jul 31;6:101. doi: 10.3389/fcvm.2019.00101. PMID: 31417911; PMCID: PMC6685361.

2.1 Heart failure and its global impact

Heart failure is a global pandemic, accounting for 31% of deaths worldwide [19]. Health expenditures associated with heart failure are substantial and expected to increase dramatically with an ageing population [20]. MI is the most common form of acute cardiac injury attributing to heart failure, and while there have been significant advances in therapies, mortality and morbidity remain high. Our understanding of MI has evolved in recent years with inflammation driven by macrophages now recognised as playing a key pathological role in the progression of tissue remodelling and fibrosis which, in turn, limits cardiac function. A greater appreciation of the role of the inflammatory response and specifically, the interaction of macrophages within the cardiac environment, is required in order to provide greater insight into tissue remodelling and disease progression within the myocardium, as well as revealing therapeutic targets for the treatment of heart failure.

2.2 Multicellularity of the heart

The myocardium is a multicellular complex tissue comprised of a range of distinct cell-types. Cardiomyocytes (CMs) constitute approximately one third of resident myocardial cells by number [21], with the remaining two thirds referred to as non-excitable cells (non-CMs) such as fibroblasts, smooth muscle cells, endothelial cells, autonomic motor neurons, and immune cells such as mast cells and macrophages [22]. While CMs possess inherent conduction capabilities which mediate the characteristic contractile forces of the heart, non-CMs are responsible for matrix deposition, vascularization and autonomic regulation [23]. CMs and non-CMs communicate via biochemical signalling through cytokine and growth factor secretion [23, 24]. Such signals arise, for example, during development and regulation and include the release of vascular endothelial growth factor (VEGF) which activates endothelial cells to initiate angiogenesis [25], or in response to trauma or injury, where signalling is mediated by pro-inflammatory cytokines such as TNF [26, 27]. Numerous networks also exist between non-CMs such as fibroblasts and macrophages, working in tangent to maintain the structural integrity of the heart. Fibroblasts are traditionally defined as cells of mesenchymal origin, arising from bone marrow derived cells known as fibrocytes [28, 29]. Cardiac fibroblasts produce the necessary components for the construction of the extracellular matrix

(ECM) in order to maintain the integrity of the myocardium [28]. As a result, fibroblasts have been highlighted as key mediators of both normal cardiac function and the remodelling response to injury [24, 28, 30]. In addition to producing components of the ECM, fibroblasts are also observed to secrete regulatory proteins and matrix metalloproteinases (MMPs) as well as their corresponding inhibitors (SCN of metalloproteinases), thus maintaining a well-controlled balance for ECM homeostasis [31].

2.3 Macrophages – key drivers of the innate immune response

Macrophages (and their precursors, monocytes) are key mediators of the innate immune response involved in the recognition, phagocytosis, and elimination of pathogens. They exist as both circulating and tissue resident cells within the body and have the ability to change their function and phenotype based on environmental cues [32]. While they exist as a heterogenous population they can be broadly classified as M1 or M2 macrophages [7]. M1 macrophages are traditionally associated with a pro-inflammatory response, and are referred to as classically activated macrophages, induced by interferon gamma (IFNγ), lipopolysaccharide (LPS), and TNF. When stimulated, M1 macrophages secrete high levels of pro-inflammatory cytokines IL-12, IL-23, IL-1 and IL-6 [5]. M2 macrophages, or "alternatively activated" macrophages exhibit an anti-inflammatory, pro-regenerative phenotype largely due to their ability to secrete high levels of anti-inflammatory cytokines including IL-10 and growth factors such as VEGF, as well as MMPs [5]. In murine models, M1 and M2 macrophages are distinguished from one another through the expression of the inflammatory monocyte marker Ly6C. $Ly6C^{high}$ monocytes are preferentially recruited to sites of inflammation and exhibit an M1 pro-inflammatory phenotype while $Ly6C^{low}$ monocytes represent the non-classical population and differentiate into M2 macrophages to promote tissue healing and angiogenesis [33].

While the M1/M2 paradigm proves useful as a preliminary introduction to these innate immune cells, the full story is not as black and white. The macrophage phenotype exhibits more plasticity than historically assumed, and M1/M2 classification merely represents two extremes of a continuum of activated states. For example, macrophages treated with the pathogen associated molecule, LPS, exhibit a reduced phagocytic

capacity compared to macrophages treated with the endogenous cytokine, IFNγ. While both produce pro-inflammatory mediators, LPS-polarized macrophages are now referred to as M1b macrophages, while IFNγ-polarized macrophages are referred to as M1a macrophages [5, 34]. Distinct M2 macrophage subsets also exist. For example, M2a macrophages are induced by IL-4 and IL-13 and have a pre-dominantly anti-inflammatory phenotype, secreting high levels of IL-10 and IL-1 receptor antagonist as a means of dampening the inflammatory response. M2b macrophages, on the other hand, exhibit both pro and anti-inflammatory responses, producing IL1β, TNF and IL-6 as well as IL-10 in response to LPS stimulation. M2c macrophages are induced by IL-10 and secrete high levels of TGF-β. They assume a regenerative, pro-healing phenotype and play a major role in promoting tissue repair and silencing the inflammatory response. These cells also play a significant role in matrix deposition [7]. More recently, M2d and M2f phenotypes have also been characterised [35, 36]. M2d macrophages are activated by Toll-like receptor (TLR) agonists and adenosine A2a receptor agonists. In response, these cells secrete high levels of VEGF and IL-10, and in turn downregulate TNF and IL-12 production [36]. M2f cells are induced by efferocytosis which involves the removal of apoptotic cells by macrophages. This process is similar to phagocytosis, however, it involves distinct receptors and signalling pathways and results in the secretion of high levels of TGF-β, prostaglandin E2 (PGE2) and platelet activating factor (PAF), all of which are known to inhibit LPS-induced proinflammatory cytokine production [37].

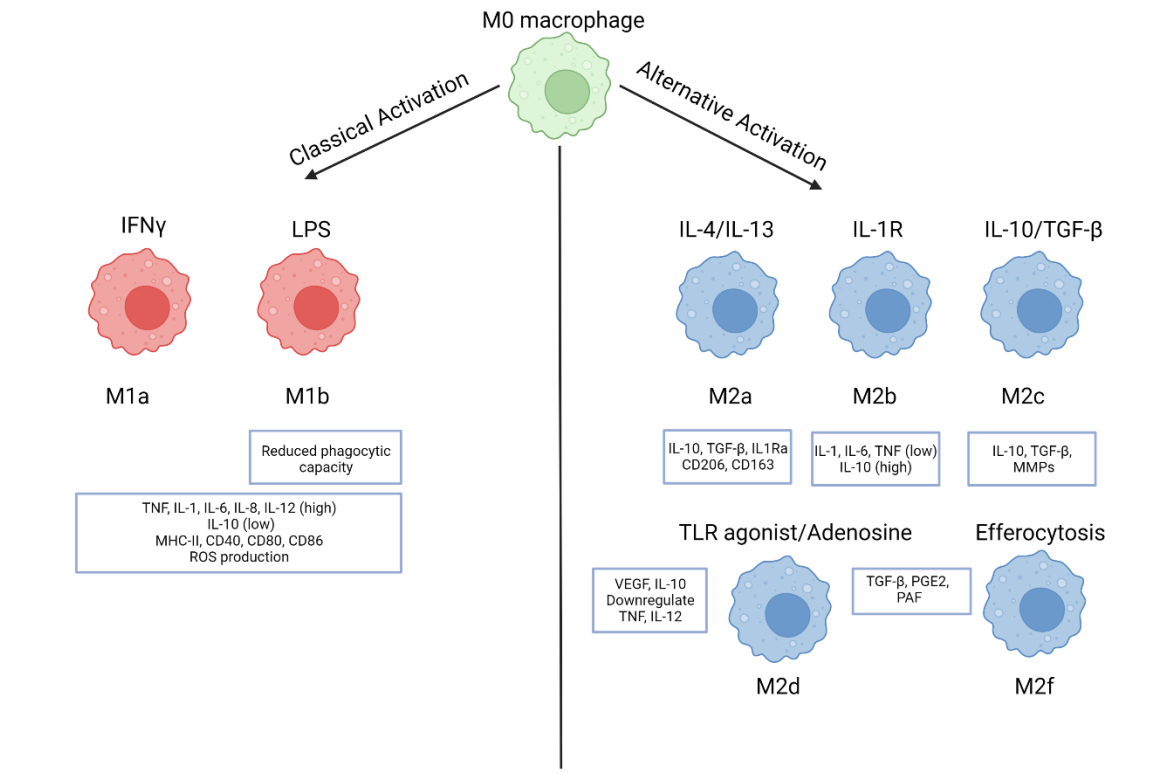

Figure 2-1 - Summary of various subsets of macrophage phenotype

2.4 Macrophage metabolism

In addition to the substantial advances made in the characterisation of macrophage phenotype, recent studies have also revealed that macrophages undergo metabolic reprogramming, whereby distinct metabolic pathways are upregulated or altered in the cell to support the energy demands of specific cell functions [38, 39].

In a resting state, macrophages typically utilise the tricarboxylic acid (TCA) cycle via cellular respiration to generate adenosine triphosphate (ATP) molecules. These act as the main source of energy for the cell. Cellular respiration is a multi-step catabolic process beginning with the breakdown of glucose. Glucose is taken into the cell via glucose transporters (GLUT1 – GLUT4), where it is passed through the various stages of glycolysis, all of which takes place in the cytosol of the cell. Glucose is first converted to glucose 6-phosphate (G6P) by HK2 which is the first rate-limiting step of the pathway. G6P is then shuttled through various reactions until the end-product, pyruvate, is formed, along with two ATP molecules. While the process of glycolysis is relatively fast, the yield of ATP is low. Energy production can however be increased when pyruvate is oxidised to form acetyl-CoA, which then enters the TCA cycle, inside the mitochondria.

This leads to the formation of CO_2 and the conversion of NAD^+ to NADH, which facilitates electron transport through a proton gradient. This, in turn, activates ATP synthase and fuels the generation of 32 ATP molecules. The process of acetyl-CoA formation and oxidative phosphorylation only occurs in the presence of oxygen and is termed aerobic respiration. Under anaerobic conditions, pyruvate is formed at the end stage of glycolysis and is simply converted to lactate, which is subsequently transported out of the cell.

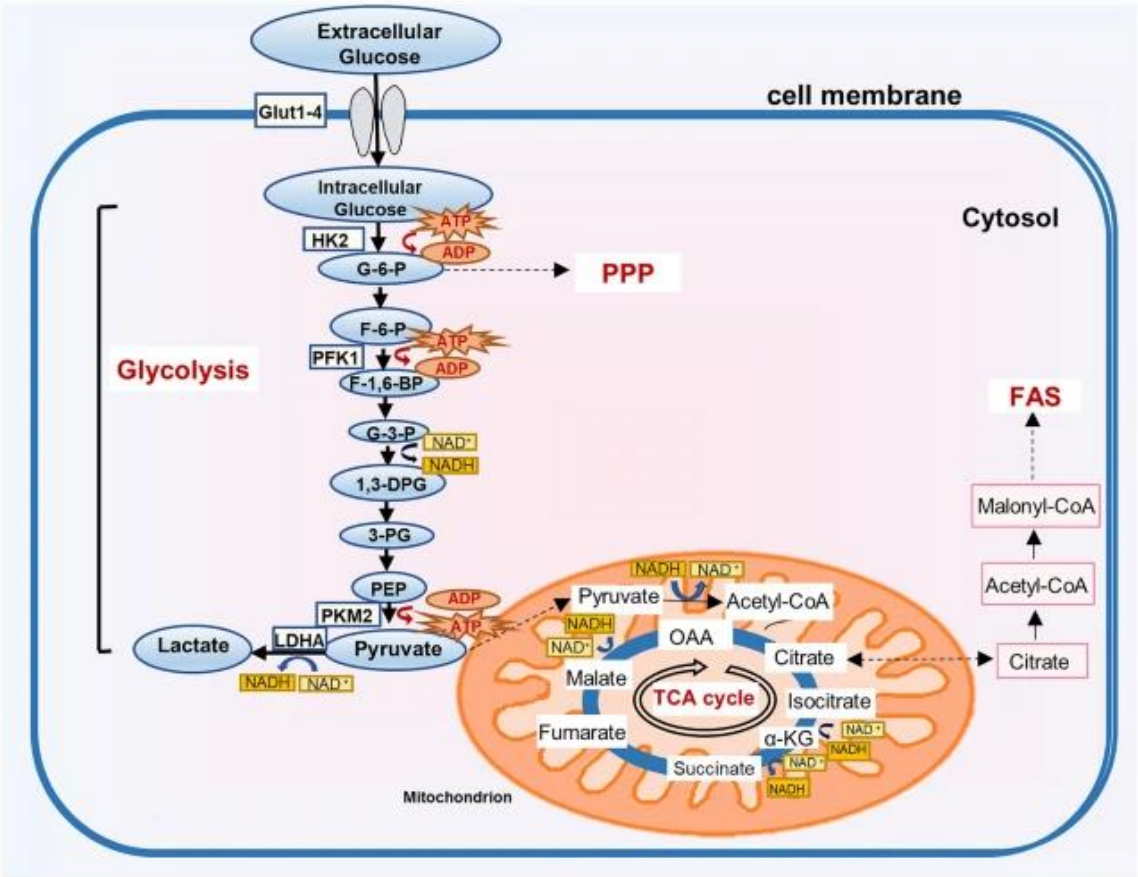

Figure 2-2 - Simplified schematic of glucose metabolism and cellular respiration - Adapted from Hu C., et al 2022.

Glycolysis occurs in the cytoplasm, converting glucose into pyruvate. Under anaerobic conditions, pyruvate is converted to lactate which is shuttled out of the cell. Under aerobic conditions, pyruvate is converted to acetyl CoA, which then enters the TCA cycle. Intermediates in glucose metabolism can flow to other metabolic pathways, such as PPP and FAS.

The process of oxidative phosphorylation is time consuming compared to glycolysis, however the pay-off in ATP production makes it a reliable source of steady-state energy for resting macrophages. Upon activation, however, macrophages undergo significant metabolic reprogramming to meet the energy demands of a rapid immune response. Classically activated, M1 macrophages, undergo a metabolic switch to favour glycolysis as their prime energy source, with LPS and IFNγ both known to drive elevated levels of glycolysis over oxidative phosphorylation [40]. This rapid increase in glycolysis occurs regardless of the presence of oxygen, a phenomenon first observed in cancer cells in 1956, and entitled the "Warburg" effect [41].

In murine macrophages, enhanced glycolysis coincides with an increase in the pentose phosphate pathway (PPP) which generates fundamental co-factors such as NADPH, as well as nucleotides and amino acids that allow for the generation of nitric oxide (NO) following upregulation of inducible nitric oxide synthase (iNOS). iNOS mediated NO production causes backflow of electrons within the mitochondria, therefore impairing oxidative phosphorylation and driving production of reactive oxygen species (ROS) [42]. In human macrophages, iNOS expression is limited, and LPS stimulation causes an upregulation of both glycolysis and oxidative phosphorylation initially, however, over time, the cells steer towards glycolysis as the predominant source of ATP, thus mirroring the response observed in murine cells [43, 44]. Increased rates of glycolysis also results in the rapid production of important intermediates of fatty acid metabolism, such as citrate, which feeds into the fatty acid synthesis (FAS) pathway [45], further fuelling rapid inflammatory responses [46, 47].

The up-regulation of glycolysis is controlled in part by the transcription factor, hypoxia inducible factor alpha (HIF1α), which is responsible for the transcription of various pro-glycolytic factors as well as pro-inflammatory cytokines such as IL-1β [48]. Under resting conditions, HIF1α is continuously turned over in the cytosol however, in the presence of inflammatory stimuli such as LPS, HIF1α is stabilised in macrophages by the metabolite succinate, which is generated in excess from the TCA cycle [49]. The expression of HIF1α itself is promoted by an isoform of pyruvate kinase known as pyruvate kinase M2 (PKM2) [50]. While PKM1 is responsible for the conversion of phosphoenolpyruvic acid to pyruvate at the end stage of glycolysis, PKM2 typically exists as a non-enzymatically

active tetramer in the cytosol of the cell under homeostatic conditions. In LPS-activated macrophages, PKM2 forms a dimer which is capable of translocating to the nucleus of the cell, and subsequently promotes expression of HIF1α. As a result, PKM2 contributes to the increased glycolytic profile observed in M1 macrophages [50].

Warburg metabolism leads to an accumulation of lactate as a by-product, which in turn can act as a feedback mechanism to further regulate macrophage phenotype and function. Removal of lactate build-up by oxidation to pyruvate, fuels the TCA cycle and contributes to redox balance of NAD+ and NADH in the electron transport chain [51, 52]. Accumulated lactate can also be shuttled back into the cell via surface membrane transporters known as MCTs. Once inside the cell, lactate has been shown to promote epigenetic changes, through modifications to histone proteins, whereby lactyl groups are added to lysine residues on the protein [53]. This histone lysine lactylation has been shown to promote expression of M2-promoter genes in M1 activated macrophages, suggesting a role for lactate in M1-M2 transitions to resolve inflammation and promote tissue repair [51, 53].

In contrast to M1 macrophages, IL-4-activated M2 macrophages favour oxidative phosphorylation as their primary source of energy [54]. ATP derived from oxidative phosphorylation is more well sustained compared to ATP sources in M1 macrophages and allows for increased expression of pro-regenerative genes associated with tissue repair [55]. M2 macrophages also exhibit elevated levels of arginase 1 (Arg-1), which in turn, increases production of citrulline in the cell, and largely contributes to tissue repair and resolution of inflammation. Oxidative phosphorylation in M2 macrophages is fuelled by fatty oxidation (FAO) whereby fatty acids are broken down to acetyl-CoA units, for use in the TCA cycle [56, 57]. As a result, alternatively activated macrophages are often characterised by both their commitment to the TCA cycle, and upregulation of FAO processes.

The mammalian target of rapamycin (mTOR) is thought to be a critical regulator of M2 metabolic reprogramming, specifically mTOR complex 2 (mTORC2). mTOR is a member of the PI3K-related kinase protein family, functioning through two complexes, mTOR complex 1 (mTORC1) and mTOR complex 2 (mTORC2). Each complex holds specific functions in cell signalling and metabolism [58]. mTORC1 is known to promote increased

glycolysis in classically activated macrophages, in addition to regulating FAS [59]. mTORC2 in contrast, is essential for M2 metabolic reprogramming, as demonstrated through selective inhibition of the mTOR complex 2 subunit protein Rictor [60, 61]. Deletion of Rictor diminishes glucose uptake, oxidative phosphorylation and FAO in IL-4 treated macrophages, thus inhibiting alternative activation of the cell [61]. Meanwhile, deletion of the Rictor protein fails to impact M1 polarisation, highlighting the specific role of mTORC2 in M2 metabolism.

The stark differences in metabolism between pro- and anti-inflammatory macrophages allows for metabolic profiling of these cells within a heterogenous population and suggests an underlying role for immunometabolism in inflammatory disease. However, much like the nomenclature of the M1/M2 paradigm, macrophage metabolism is not as simple as a clear switch between glycolysis and oxidative phosphorylation, as exemplified by the early upregulation of both pathways in LPS-activated human macrophages. Further study is clearly required to better elucidate the metabolic pathways responsible for specific macrophage form and function.

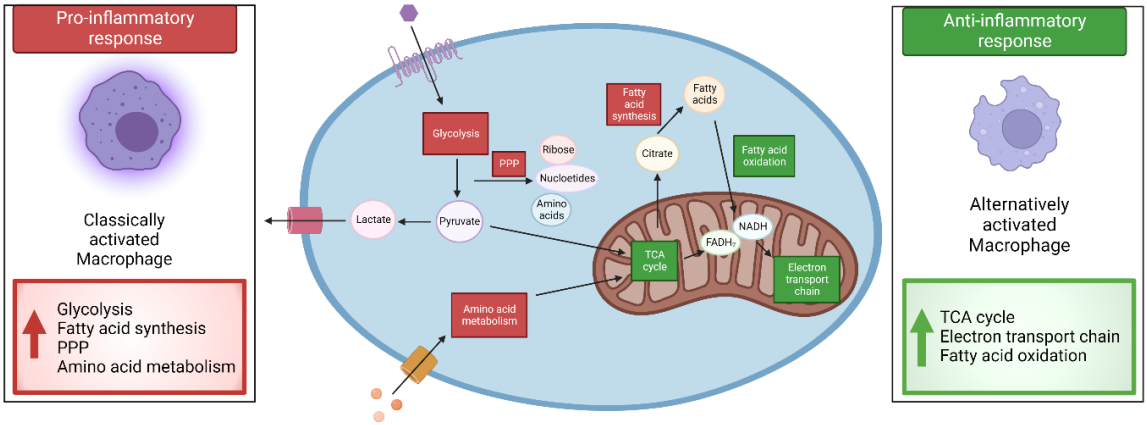

Figure 2-3 – Schematic summary highlighting the contrasting activating states of macrophages and the corresponding metabolic profiles. Adapted from Shanley L., et al 2022

2.5 Tissue resident macrophages of the heart

Tissue resident macrophages exist at various sites throughout the body and can include microglia in the brain and Kuppfer cells in the liver [62]. The heart, being no exception;

contains its own resident macrophages which possess a specific role in the regulation of cardiac function [63]. The distinction between tissue residing cardiac macrophages and circulating monocyte-derived macrophages has become a considerable area of focus in recent years [64]. While long established tissue resident cells appear to facilitate coronary development and tissue homeostasis, it appears that monocyte-derived infiltrating cells have a predominant role in tissue injury and destruction. This highlights that macrophages, whether circulating or permanently residing, originate from diverse lineages, and as a result have different functions.

2.5.1 $CCR2^+$ and $CCR2^-$ resident macrophages

Gene mapping of cardiac resident macrophages reveals two distinct lineages arising at the embryonic stage and postnatal stage [65]. Developmental studies of early cell migration in murine models affirms this, with the earliest cardiac resident macrophages derived from an erythromyeloid progenitor in the yolk sac [66]. These progenitor macrophages migrate out of the yolk-sac either directly to the developing myocardium or else to the foetal liver, where they progress to haemopoietic stem cells and eventually cardiac tissue-resident macrophages [66]. Postnatally, monocyte-derived macrophages can also migrate to the myocardium to become tissue resident macrophages [67]. These embryonic and postnatal resident cells can be distinguished from one another based on expression of the chemokine receptor, CCR2 [65]. This receptor and its corresponding ligand, chemokine ligand 2 (CCL2), also known as monocyte chemoattractant protein 1 (MCP-1), play an important role in monocyte/macrophage migration. Studies have demonstrated that $CCR2^+$ cardiac resident macrophages are derived from monocytes while $CCR2^-$ macrophages originate from the embryonic developmental stage [65, 68]. Furthermore, $CCR2^-$ macrophages undergo local proliferation in order to replenish their population whereas $CCR2^+$ macrophages are repopulated by monocyte-derived macrophages extravasating into the myocardium [65]. Both $CCR2^+$ and $CCR2^-$ cell populations orchestrate diverse responses following traumatic events such as MI. $CCR2^+$ cells facilitate monocyte recruitment into the heart following MI via CCR2-MCP1 mediated trafficking and secrete high levels of pro-inflammatory mediators including IL-1β, TNF and IL-6 [68]. Not surprisingly,

depletion of this cell population has resulted in reduced infarct size in a murine model of MI [68].

Conversely, $CCR2^-$ macrophages appear to play an immune-modulatory, pro-regenerative role, expressing high levels of growth factors including Insulin-like growth factor 1 (IGF1) and Platelet-derived growth factor C (PDGF-C) [68]. Depletion of this $CCR2^-$ population has enhanced monocyte/macrophage infiltration to the heart and further implicates these cells as potential immune-modulators during MI [68, 69]. In addition to immune modulatory functions, recent studies have also demonstrated that $CCR2^-$ macrophages express high levels of the voltage-gated sodium channel, SCN4, and sodium channel modulator, FGF13, suggesting that macrophages can modulate the electrical activity of cardiomyocytes [65, 70]. Fracktalkine receptor ($CX3CR1^+$) expressing resident macrophages have also been reported to facilitate conductivity, further implicating their role in regular functioning of the heart and broadening the role of macrophages beyond local inflammation and immune modulation [70]. It is not yet clear if both $CCR2^+$ and $CCR2^-$ macrophages contribute to the electrical homeostasis of the heart and, given that both subsets express the CX3CR1 receptor [71], delineation of the direct impact of these individual cell-types on cellular conductivity is a promising avenue of exploration.

2.6 The role of inflammation in heart failure

2.6.1 Atherosclerosis

Atherosclerosis is the leading cause of MI and stroke [72]. Initially believed to be the result of passive lipid accumulation in the arterial wall, research of the last two decades has redefined the condition as a chronic inflammatory disease, with macrophages well established as key mediators [8, 9, 73]. The key initiating step of atherosclerosis is the accumulation of apolipoprotein-B containing liposomes, largely originating from the liver, and oxidised to form low-density lipoproteins (LDLs). Accumulation of these lipoproteins beneath the endothelial layer of blood vessels activates endothelial cells to secrete chemokines such as MCP-1 and IL-8, which in turn leads to the recruitment of monocytes that subsequently differentiate into macrophages. Activated macrophages attempt to remove the modified/oxidised lipoproteins, however, a lack of negative feedback in this system causes dysregulation of lipid metabolism in macrophages, and as

a result, the cells become transformed into lipid-laden foam cells. These foam cells form a fatty streak within the artery, and attribute to the formation of atheromatous plaques (also known as atheromas) at the site, marking the early stage of atherosclerosis.

As the disease progresses, internalized lipoproteins are digested in the lysosome, which converts lipids to free cholesterol that can either be released completely from the cell or transported to the endoplasmic reticulum (ER). However, the enrichment of the ER membrane with free cholesterol causes a defect in the Acyl-Coenzyme A: cholesterol Acyltransferases 1 (ACAT1) system, which normally acts to convert free cholesterol to an inert cholesteryl ester. This dysregulation of cholesterol efflux and lipid metabolism causes prolonged stress on the ER, causing foam cells to undergo apoptosis. Not only is free cholesterol toxic to the cell, but its further accumulation within the cell enhances inflammation via TLR signalling and the activation of nuclear factor-κB (NF-κB). As a result, macrophages show increased expression of pro-inflammatory genes, and secrete cytokines such as TNF and IL-1β into the surrounding environment, thus exacerbating the local inflammatory response.

Apoptotic cells cannot be effectively cleared from the plaque as the successful removal of dying cells requires intact lipid metabolism and this eventually leads to secondary necrosis. As plaque formation progresses, a lipid rich necrotic core forms, with smooth muscle cells forming a fibrous cap around the core. Thinning of the fibrous cap in advanced plaques leaves the site vulnerable to rupture, thus leading to arterial occlusion and myocardial infarction.

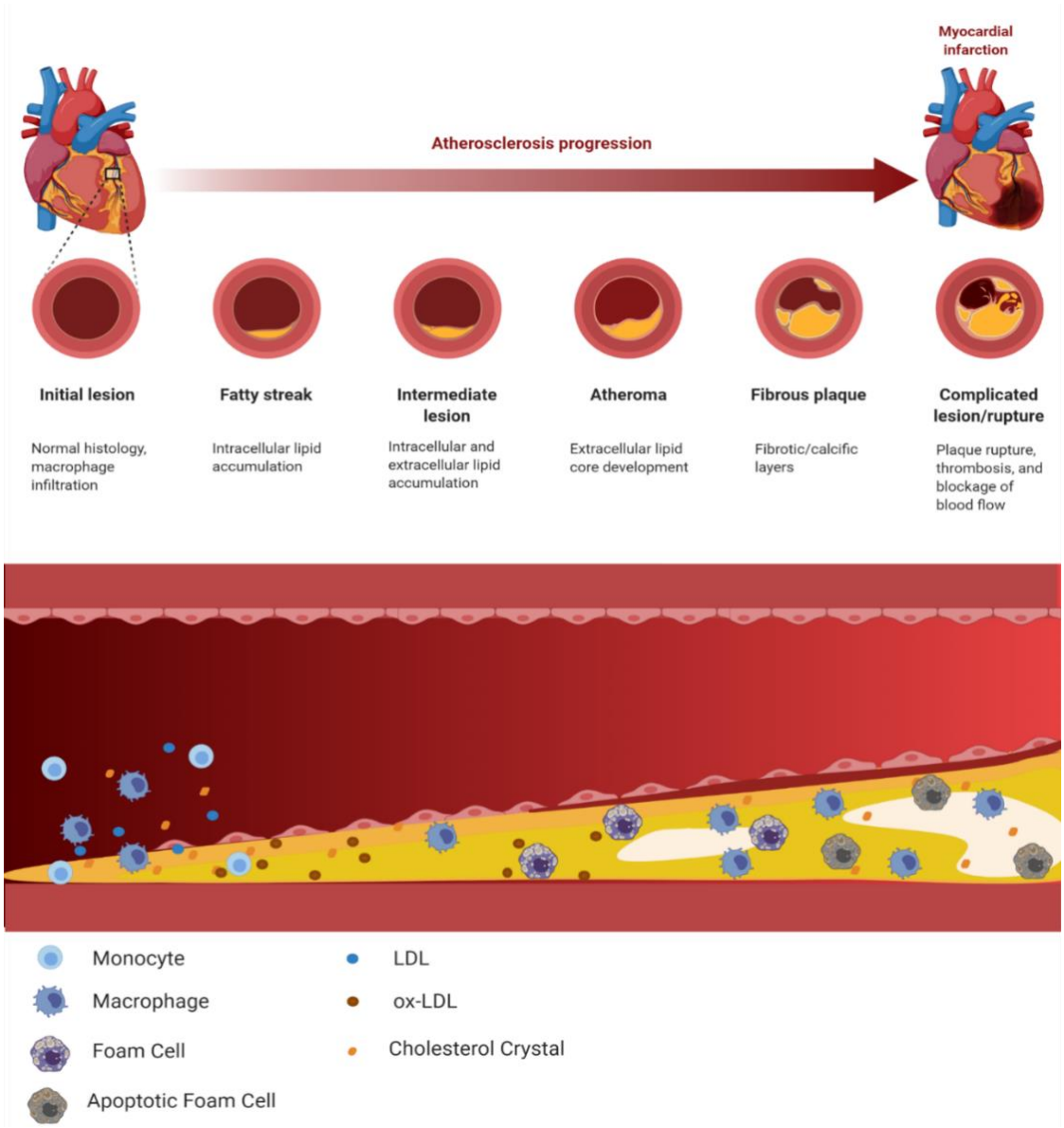

Figure 2-4 - Schematic summary of atherosclerotic plaque formation and progression.

ApoB-lipids accumulate beneath the subendothelial layer of the artery and are oxidised to Ox-LDL. Endothelial cells recruit monocytes to the site, which differentiate to macrophages and attempt to clear the accumulated lipids. Dysregulated lipid metabolism causes macrophages to transform into foam cells. Continuous secretion of pro-inflammatory cytokines and chemokines leads to further recruitment of monocytes and macrophages to the site. A fibrous cap comprised of smooth muscle cells forms over the plaque. Defective removal of apoptotic cells and lipids leads to continuous activation of macrophages and secondary necrosis. A rich necrotic core begins to form. Meanwhile, thinning of the fibrous cap due to matrix degradation and apoptotic smooth muscle cells decreases stability of the plaque. The plaque ruptures, leading to platelet activation and aggregation, and thus thrombosis and vessel occlusion.

Inflammation, driven largely by innate immune cells, is a key feature of plaque formation and rupture in atherosclerosis. Neutrophils, natural killer cells, dendritic cells and macrophages have all been shown to reside within the plaque and drive the inflammatory response [8]. Macrophages appear to be particularly detrimental to the process, releasing numerous factors which advance plaque formation [9]. Interestingly, transcriptome analysis of distinct plaque macrophage subsets in mice revealed that non-foamy, rather than lipid-loaded foamy macrophages are pro-inflammatory and are likely the cells that drive lesion inflammation [74]. Macrophage inflammasome signalling has proven essential for necrotic core formation in advanced atherosclerosis [75]. Both Ox-LDL and cholesterol crystals, found within atherosclerotic plaques, have been shown to activate the NLRP3 inflammasome and induce secretion of IL-1β in macrophages [75-77]. This is supported by *in vivo* studies whereby selective deletion of NLRP3 in LDL deficient mice, resulted in decreased lesions and plaques stabilisation [75]. Additionally, TNF and nitric oxide secreted by pro-inflammatory macrophages within the lesion can trigger apoptosis in smooth muscle cells, contributing to thinning of the fibrous cap surrounding the plaque [78]. This is further enhanced through macrophage derived MMPs, in particular MMP2 and MMP9, which break down the matrix surrounding the cap, thus weakening its structure and destabilising the plaque as a whole. Sustained activation of macrophages therefore is regarded as a primary cause of disease progression in atherosclerosis and makes macrophages worthy candidates for targeted therapy.

2.6.2 Myocardial infarction and ischemia

MI refers to mass cardiomyocyte death as a result of ischemia, which is often worsened by a subsequent reperfusion of oxygen supply, and the ensuing inflammatory response [79]. This association between inflammation and adverse cardiac events is well acknowledged. Multiple studies have demonstrated that elevated pro-inflammatory cytokine production in the heart correlates with worsening outcome [14, 80-82]. Furthermore, inhibition of pro-inflammatory cytokines such as TNF, which is heavily implicated in cardiac disease, results in improved cardiac function in rat models of heart failure [26, 27]. Two classifications of infarction are often presented, both which occur as a result of ischemia. Acute MI is caused by an atherosclerotic plaque rupture causing coronary artery occlusion and cardiac tissue damage due to ischemia. Chronic MI refers

to continued loss of cardiomyocytes from gradual and prolonged ischemia, often greater than 8 weeks. The vast amount of cell death following MI poses a detriment, as the heart itself possesses a limited regenerative capacity [2]. Left untreated, cardiac tissue undergoes extensive remodelling to compensate for cell loss and to maintain structural integrity. The inflammatory response facilitates the removal of necrotic cells in addition to tissue remodelling [11]. However, extensive remodelling imposes stress on the heart, instigating maladaptive mechanisms such as chronic inflammation and cellular apoptosis. As the heart continues to employ methods of remodelling and repair to resolve this, a destructive cycle prevails, ultimately leading to deterioration of cardiac function and heart failure [83]. These events are summarised in Figure 2.6 below.

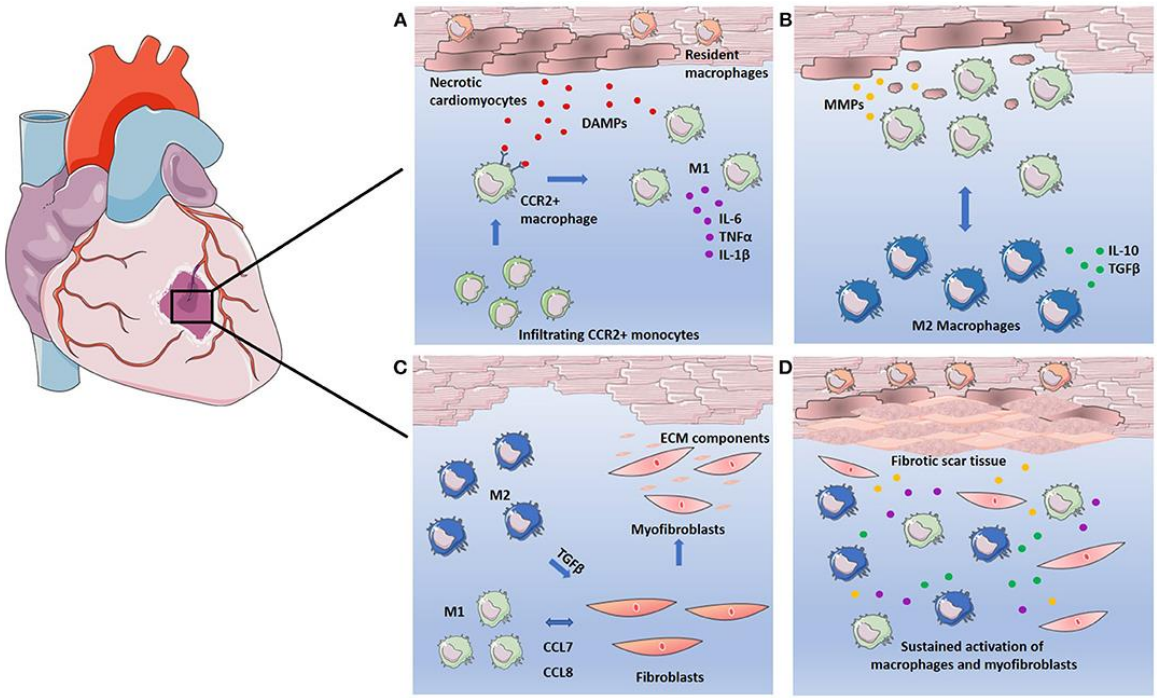

Figure 2-5 – Macrophages in the response to MI.

(**A**) Cardiomyocytes undergo necrosis, releasing DAMPs and attracting CCR2+ circulating monocytes. CCR2+ monocytes differentiate into pro-inflammatory M1 macrophages replacing resident macrophages and secreting high levels of pro-inflammatory cytokines IL-6, TNFα, and IL-1β. (**B**) M1 macrophages clear necrotic cell debris through phagocytosis and induce breakdown of the ECM through secretion of MMPs. Phagocytosis of the necrotic debris causes macrophage polarization to the M2 phenotype. M2 macrophages secrete high levels of anti-inflammatory cytokine IL-10 and growth factor TGFβ. (**C**) Both M1 and M2 macrophages facilitate the fibrotic response. M1 macrophages recruit fibroblasts via CCL7 and CCL8 mediated signalling. M2 macrophages induce fibroblast differentiation into myofibroblasts, which in turn secrete ECM components to facilitate tissue repair. (**D**) Sustained activation of macrophages

leads to continuous secretion of growth factors, pro-inflammatory cytokines, and MMPs. Continued breakdown of ECM as well as overproduction of ECM components by myofibroblasts leads to adverse remodelling of ECM and results in fibrotic scar tissue.

Infiltration of monocyte-derived macrophages to the infarct is a key feature of MI, and can be characterised by stages of macrophage infiltration, and their subsequent actions within the myocardium. Immediately following infarction, resident cardiac macrophages begin to die in response to ischemia, with a complete loss of resident macrophages within the infarct observed in murine models 24 hours post infarction [84]. The resident macrophage population lost in the ischemic region is rapidly replaced by infiltrating monocyte-derived macrophages within 24 hours [84]. Day 1-3 post MI, infiltrating macrophages exhibit a pro-inflammatory M1-like phenotype, driving acute inflammation and facilitating clearance of dead cells. At approximately day 5-7 post MI, these macrophages begin to adopt a reparative M2-like phenotype, working to resolve inflammation and rebuild cardiac tissue [85]. Mouse models of MI have revealed distinct subsets of infiltrating monocyte-derived macrophages, with earlier recruitment of pro-inflammatory $Ly6C^{high}$ macrophages dependent on CCR2/CCL2 signalling, and the later pro-regenerative $Ly6C^{low}$ macrophages recruited via CX3CR1 signalling [86]. One can, therefore, hypothesise that inflammation and resolution is achieved in the myocardium through differential recruitment of macrophages.

It has also recently been demonstrated that infiltrating macrophages in murine mouse models of MI undergo metabolic reprogramming to increase oxidative phosphorylation at approximately day 5 post MI [87]. Increased oxidative phosphorylation in addition to FAO, as previously discussed, is a signature of the M2 phenotype [88] and implies that there is a phenotypic switch from the early pro-inflammatory state to a more pro-regenerative one. Thus, not only is there the possibility of recruitment of separate subsets of macrophages via CCR2 and CXC3R1 dependent signalling, but in addition, there is a switch from the M1 to the M2 phenotype subset based on observed increases of FAO and oxidative phosphorylation. This switch is key in the appropriate resolution of inflammation and progression to a pro-healing state, as highlighted by knockout models of mitochondrial activity. Selective deletion of the mitochondrial Complex 1 protein Ndufs4 in macrophages heightens inflammation, increases mortality, and worsens cardiac function 30 days post MI in mice [89]. As previously mentioned in section 2.4,

accumulation of lactate from glycolytic M1 macrophages, as well as a result of hypoxic regions of the infarcted myocardium may contribute to this M1-M2 transition, as lactylation of histone proteins inside the cell has been shown to promote M2 genes in M1 activated macrophages [51, 53]. In support of this, a study led by Wang et al demonstrated through transcriptome analysis of mice that lactate uptake via MCT1 results in histone lactylation and increases expression of anti-inflammatory gene IL-10 and pro-reparative gene VEGF-A in monocyte-derived macrophages post-MI [90].

Metabolic reprogramming of macrophages can also be promoted through efferocytosis [91]. In addition to necrosis, cardiomyocytes can also undergo programmed "active" cell death, apoptosis, exposing phosphatidylserine (PtdSer) to the cell surface as an "eat me" signal to macrophages [92, 93]. Recognition of this "eat me" signal triggers efferocytosis of the apoptotic cells at the injury site. Efferocytosis in macrophages has been observed to elevate fatty acid synthesis and triggers production of the anti-inflammatory, pro-reparative cytokine TGFβ-1 [94]. However, in circumstances of chronic ischaemia or severe infarction, continuous cardiomyocyte cell death leads to sustained activation of M1 macrophages, which have a diminished efferocytotic capacity [95]. This is heightened in patients suffering from diabetes and obesity whereby underlying chronic inflammation exacerbates the pro-inflammatory response to infarction. In this instance, elevated levels of the pro-inflammatory cytokines, TNF and IL-6, as well as C-reactive protein (CRP) are associated with worse patient outcome [96, 97].

2.7 Damage associated molecular patterns (DAMPs) and the inflammatory response

Research in the field of innate immunity over the last two decade has uncovered novel mechanisms of how immune cells, including macrophages, sense and respond to tissue damage. A well explored avenue in this context is the role of DAMPs as instigators of the inflammatory response. DAMPs are endogenous molecules released from damaged or dying cells, recognised by both immune and non-immune cells via pattern recognition receptors (PRRs). Prolonged presence of DAMPs can lead to persistent inflammation and create further damage in the injured or disease environment. In the context of atherosclerosis and MI, DAMPs have been shown to initiate and maintain the inflammatory response, in particular at advanced stages of atherosclerosis, as well as chronic MI [98, 99].

2.7.1 Atherosclerosis-associated DAMPs

Elevated levels of oxidised LDL, S100 proteins, and cholesterol crystals all have been implicated in the progression and severity of atherosclerosis. Furthermore, each of these established DAMPs have been recognised as drivers of inflammation specifically in macrophages [77, 100, 101]. As previously mentioned, ox-LDL contributes to macrophage-mediated inflammation in atherosclerosis via activation of the NLRP3 inflammasome. Macrophage uptake of ox-LDL involves binding to scavenger receptors such as CD36 [102], which in turn acts in tandem with TLR4/TLR6 signalling to prime the NLRP3 inflammasome, ultimately leading to production of IL-1β [100]. Inflammasome activation, however, typically requires two signals to drive secretion of IL-1β. First, a priming signal, is required to drive expression of inactive pro-IL1β, and secondly, an activation signal which is required for the assembly of the NLRP3 inflammasome complex, which in turn activates caspase-1 leading to the cleavage of pro-IL-1β into its mature and active form. A schematic summary of this mechanism is provided in figure 2.7 below. It is now well established that the uptake of oxidised lipids in macrophages results in the formation and deposition of cholesterol crystals, which can serve as this second signal to activate the NLRP3 inflammasome complex [100].

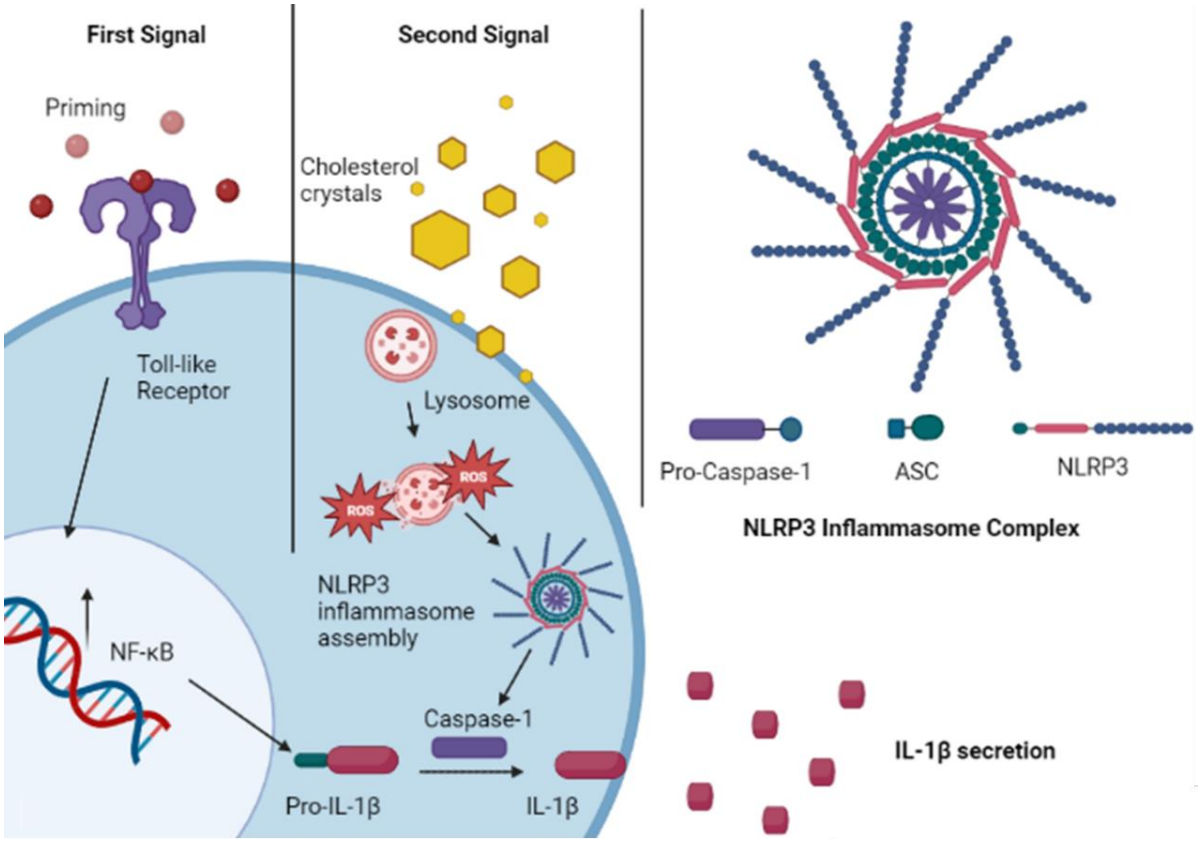

Figure 2-6 - Schematic summary of cholesterol crystal induced NLRP3 inflammasome activation.

Activation of the NLRP3 inflammasome requires two signals in order to secrete IL-1β. Signal 1, typically carried out by PAMPs such as LPS, or DAMPS such as oxidised LDL (oxLDL), stimulates the NF-κB pathway to produce pro-IL-1β and NLRP3 expression. Signal 2 may be carried out by an array of stimuli such as ATP and DAMPs including cholesterol crystals. Phagocytosis of such DAMPs triggers the rupturing of cell lysosomes. This results in the release of ROS, which causes oligomerized NLRP3 to assemble with ASC and pro-caspase 1. Activation of caspase-1 permits the cleavage of pro-IL-1β into IL- 1β, which is then secreted from the cell.

Cholesterol crystals themselves play a significant role in atherogenesis and plaque destabilisation. Evidence for the role of cholesterol crystals in inflammation initiated from studies concerning the ACAT system as a potential therapeutic target for atherosclerosis. Knockout models of ACAT1, thought to improve atherosclerotic lesions, only worsened the condition. It was discovered that diminishing the ACAT system led to significant accumulation of extracellular cholesterol crystals, accompanied by a substantial inflammatory response [103]. As a result of these findings, cholesterol crystals have become elevated in status, from mere biomarkers of atherosclerosis to

explicit mediators of the disease. Targeting cholesterol crystal mediated responses holds great potential as a novel therapy for atherosclerosis. However, while the role of these disease particulates in activating the inflammasome has been well established, there remains little to no reports regarding the impact of cholesterol crystals specifically on macrophage polarisation.

Members of the S100 protein family are now also considered DAMPs, which upon tissue damage/cell stress, are secreted from macrophages [104, 105]. These proteins are present in atherosclerotic plaques where they have been shown to advance atherogenesis and prolong injury via stimulation of TLR4 [106]. Furthermore, it has been reported that increased plasma levels of the S100A8/9 heterodimer correlate with the severity of cardiovascular disease [107]. Increased levels of S100A8 and S100A9 have been identified in unstable regions of atherosclerotic plaques meanwhile elevated levels of S100A9 correlate with increased numbers of macrophages but low smooth muscle cell (SMC) counts and collagen [108]. This suggests a role for S100 proteins in fibrous cap thinning and plaque rupture. Analysis of plaques also reveals high levels of S100A8 and S100A9 to correlate with elevated expression of IL-6 and IL-8 [108]. As well as S100A8/9, other reports have implicated S100A12 in atherosclerosis. Patients presenting with symptoms of CVD express high levels of S100A12, compared to healthy controls [106]. These collective studies highlight the role of S100 proteins as both biomarkers of atherosclerosis, as well as potential therapeutic targets, thus making them a topic of interest for further studies.

2.7.2 MI-associated DAMPs

Necrotic cells in the infarcted myocardium release a milieu of cellular components that can act as instigators of the inflammatory response. Nuclear proteins such as High-Mobility Box-1 (HMGB-1), nuclear and mitochondrial DNA (mtDNA), and ECM fragments all serve as ligands to PRRs on both resident cells of the myocardium as well as infiltrating immune cells [99].

HMGB-1, also known as amphoterin, is released from dying cells, either passively or actively and can activate macrophages via binding to TLR2 and TLR4 [109]. Delivery of recombinant HMGB-1 to cardiac cells results in increased levels of TNF and IL-6, increased infarct size (IS), and increased ischemia/reperfusion injury (IRI) [110]. Elevated

levels of the protein are also observed in patients of MI and correlate with adverse cardiac events and worse prognosis [111]. Studies from murine models of MI suggest the damage driven by HMGB-1 is based on the combined effect with circulating mitochondrial DNA (mtDNA) [112]. Like HMGB-1, mtDNA is released from dying cells, and can promote the inflammatory response via interactions with TLR9, RAGE, and NLRP3 inflammatory pathways [113]. Significant correlations have been observed between elevated levels of mtDNA and TNF and IL-6 in rat models of MI, while inhibition of this DAMP through pre-treatments with the antioxidant, epigallocatechin-3-gallate, results in cardioprotective effects following IRI [114]. Based on the collective evidence, there is no doubt that DAMPs have become relevant therapeutic targets for the treatment of MI, atherosclerosis and heart failure, however much is still to be learned regarding the precise mechanism underlying DAMP-induced cell activation in the myocardium.

2.8 Targeting inflammation in CVD

The traditional strategies for combatting atherosclerosis focus on lowering lipids in the blood through administration of drugs such as statins. Statins combat the effects of hypercholesterolemia via inhibition of 3-hydroxy-3-methylglutaric coenzyme A (HMGCoA), a key enzyme of the cholesterol biosynthesis pathway. As a result, levels of plasma cholesterol and circulating LDLs are significantly lowered, leading to significant plaque regression and improved outcome for patients [115, 116]. More recent discussions regarding the success of statins suggest that its beneficial effects stretch beyond the modulation of lipid metabolism, to also include anti-inflammatory effects [117]. It was found that patients administered statins showed reduced levels of CRP, independent of LDL levels [118], as well as a decrease in levels of circulating inflammatory cells [119]. Meanwhile, *in vitro* studies have demonstrated that statins can inhibit activation of NF-κB, as well as production of TNF, IL-6, and IL-1β [120, 121].

Given these observations, as well as our deeper understanding of atherosclerosis as a chronic inflammatory disease, more current studies have begun to focus on modulating the inflammatory environment within the lesion, as well as macrophage related responses. For example, several clinical trials have been carried out targeting mediators of macrophage inflammation, including cytokines such as TNF, IL-1β, as well as

chemokines including CCR2 [12-15] The CANTOS trial, which involved over 10,000 patients treated with the IL-1β inhibitor, Canakinumab, demonstrated that patients receiving treatment had a 25% reduced risk of CVD [13]. Targeting IL-1β also reduced the risk of new MI events in patients with previous history of infarction, however, no significant reduction in risk of cardiovascular death or overall mortality was observed [13]. Similarly, patients treated with the TNF inhibitors etanercept, methotrexate and infliximab also showed 30% reduced risk of the CVD [15].

Despite clinical studies in MI patients remaining limited, strategies aimed at targeting dysregulated immune responses have been explored as treatment options for heart failure post MI. Early trials involved the use of general immunosuppressants based on the hypothesis that nonspecific inflammation following MI is unfavourable [122]. Such trials included a broad range of candidates that are considered the gold standard of immunosuppression such as corticosteroids, methotrexate and cyclosporin A to name but a few. However, their use in the context of cardiac treatment has yielded conflicting results. A review of clinical trials dating 1964 to 1989 reported that while corticosteroids appear to reduce mortality rates compared to placebo treatments, overall, they do not provide a significant cardio-protective effect [122]. Methotrexate, a well-established immunosuppressive routinely used for the treatment of rheumatoid arthritis, has also produced conflicting results with one trial reporting a reduction in TNF and IL-6 together with an increase in IL-10 [123], while others reported no beneficial effects, and instead worsening of left ventricle ejection fraction following treatment [124, 125]. Cyclosporin A has also been considered for post MI treatment given its ability to inhibit the mitochondrial permeability transition pore and therefore prevent necrotic cell death [126]. However, no improvement of infarct size or mortality was observed in patients in a 3 day follow up [127].

While the lack of success for these drug trials may be attributed to short follow up periods and small sample numbers, it may also be that non-specific suppression of inflammation is insufficient to alleviate the adverse effects associated with infarction and more targeted approaches are required. IL-1β, for example, has proved to be a promising candidate to target due to elevated levels of the cytokine associated with poor prognosis in MI patients. Numerous pre-clinical studies have reported that

inhibition of this cytokine results in reduced inflammation and remodelling in mice post infarction [128, 129]. Anakinra, an established antagonist for the IL-1β receptor; has been assessed in multiple pilot studies for efficacy in reducing left ventricular remodelling in patients [128, 130, 131]. Antagonising IL-1β in the above studies appears to blunt the acute inflammatory response exhibited post-infarction with an increase in pro-inflammatory marker C Reactive Protein (CRP), observed following discontinuation of treatment. While the results of the 2010 study demonstrated an overall improvement in left ventricular remodelling, the small sample size proved limiting in their results. A larger study conducted in 2015 failed to show any improvement in remodelling compared to placebo treatment [131].

Clinical trials targeting TNF have also been conducted. In patients with acute MI, treatment with etanercept, a high affinity TNF receptor antagonist, resulted in reduced levels of IL-6 and lower neutrophil counts, however, no improvements in ventricular dilation or cardiac function were observed [15]. Furthermore, in patients with chronic heart failure, trials involving anti-TNF treatment were terminated prematurely due to lack of benefit [14]. Despite encouraging preclinical results from *in vivo* models, targeting single cytokines alone may not be enough to counteract the complex pathophysiology associated with heart failure, and instead, targeting the source of inflammation may represent a more viable approach.

2.8.1 Targeting macrophages

Targeting macrophage infiltration to combat inflammation is not an entirely new concept, however many studies have failed to show a clear efficacy *in vivo*. Previous work using small molecule inhibitors to target the migration of $CCR2^{+}$ macrophages, while showing a promising *in vitro* result, have failed to overcome challenges *in vivo* due to lack of tissue selectivity for the CCR2 receptor as well as poor potency in administered treatments [12]. Advances in short interfering RNA (siRNA) technology, including improved specificity of targeting sequences, as well as new methods of delivery, have opened the door to novel therapies to treat inflammation and heart failure. For example, siRNA targeting of the cell adhesion molecules intercellular adhesion molecule 1/2 (ICAM1/2), vascular cell adhesion molecule (VCAM) and E and P selectins have been

shown to reduce inflammation and infarct size in a murine model of MI; ultimately preserving left ventricle ejection fraction and improving recovery after infarction [132].

While this study emphasizes that a multi-targeted strategy may be necessary, targeting the CCR2 receptor alone has also yielded promising results with two separate studies demonstrating that siRNA-mediated targeting of the CCR2 receptor significantly reduces infarct size in mouse models [17, 18]. Specifically, siRNA targeting the CCR2 receptor 1-hour post-infarction (induced by coronary ligation) resulted in a 34% reduction in infarct size/area-at-risk at 24 hours post siRNA delivery [17]. A similar study resulted in a reduction in expression of pro-inflammatory cytokines, IL-6, IL-1β, and TNF at day 4 post infarction, while levels of IL-10 appeared to increase [18]. At three weeks post infarction, a significant reduction of ventricular remodelling was observed compared to untreated mice [18]. These results not only strongly implicate macrophages in the aetiology of heart failure, but also demonstrate the ability to diminish their effects through single molecule targeting, which if tissue specific, may represent a viable option for future therapy. Targeting the CCR2 receptor proves particularly advantageous compared to pre-existing immunosuppressive treatments as the strategy does not affect the resident homeostatic macrophages present within the myocardium, nor does it hinder clearance of necrotic matter in the infarct. To improve siRNA delivery, nanoparticles and scaffolds are being extensively explored. In particular, scaffolds can enable a controlled rate of delivery through interactions with the siRNA and designated target, as well as timed degradation of the scaffold itself [133, 134]. Scaffolds can also be placed directly at the intended location of therapy. This proves optimal for MI treatment whereby timing of inflammatory resolution is critical. Premature intervention of the inflammatory response may hinder wound repair, whereas a delayed response could fail to prevent adverse cardiac remodelling and heart failure [135].

2.9 Models of myocardial infarction and heart failure

Much of what we have learned regarding inflammation in heart failure derives from animal models of infarction. Such models employ techniques to mimic that of MI with ligation-induced MI in small rodents amongst the most commonly used, in addition to the use of cryoprobes to create lesions on the epicardial surface. Studies of cryo-lesions have revealed that macrophages may secrete factors which promote cardiomyocyte

proliferation given that a high abundance of macrophages precedes and coincides with the occurrence of cardiomyocyte proliferation post injury. Conversely, proliferation ceases as macrophages numbers decrease [136]. Furthermore, depletion of macrophages via administration of clodronate-containing liposomes attenuates injury repair within the myocardium [137]. Given that all macrophages capable of phagocytosing the liposomes underwent apoptosis, it still remains to be determined which subset of macrophages promotes repair in this model.

Knockout studies have largely been used to elucidate the role of specific cytokines in MI-associated inflammation. For example, IL-6 or TNF deficient mice exhibit improved cardiac function post ligation when compared to wild-type mice [138, 139]. While these studies have proven constructive in delineating the impact of the inflammatory response post MI, the caveat, as always with animal models, is the disparity between animal studies and human clinical trials. Furthermore, much of these studies fail to examine the pathological interactions which drive heart failure at a simpler cellular level, given that there are still considerable gaps in our knowledge of macrophage interactions in the myocardium. Not to mention in general the additional cost and energy requirements associated with development and maintenance of animal models. The quantity of energy consumed by animal research facilities are nearly two fold of standard laboratories, due to the numerous needs of animals such as barrier protection from outside pathogens, indoor air quality, lighting, and the requirement for power intensive equipment in research [140]. Given the call for reduced energy consumption in today's climate, alternatives to animal models are largely welcomed. Thus, tissue engineering is being increasingly explored to build human cardiac models ranging from cell-based models to fully functioning organoids.

2.10 Tissue Engineering

Tissue engineering was defined in the early 90s as an "interdisciplinary field which applies the principles of engineering and life sciences toward the development of biological substitutes that restore, maintain, or improve tissue function" [141]. The successful generation of tissue engineering constructs requires three crucial components; a relevant selection of cells, biomaterial scaffolds, and the presence of appropriate biochemical and biophysical cues to recreate viable tissue. This combination

is denoted in literature as the tissue engineering triad [142]. While tissue engineering strategies were initially developed to induce tissue-specific regeneration processes, thus overcoming the drawbacks of organ transplant failure, more recent approaches have been proposed to develop *in vitro* human models of pathological tissues and organs.

2.11 iPSC-derived cardiomyocytes and disease modelling.

Stable differentiation of induced pluripotent stem cell (iPSC)-derived cardiomyocytes has provided a reliable resource of cells for cardiac tissue engineering, allowing the field to evolve from simple collagen-based hydrogels seeded with primary rat CMs, to more complex larger scale structures [143, 144]. iPSC-CMs have attracted attention as experimental models as they are readily available, and can be maintained *in vitro* for weeks, up to months. This is a significant advantage compared to isolated primary human myocytes, which rapidly dedifferentiate after only a few days of *in vitro* culture [145]. Already the application of iPSC-CMs has been observed in cardiotoxicity drug models, as a testing platform for chemotherapy drugs previously linked with adverse responses in the heart [146]. However, use of iPSC-CMs is not without its limitations. One of the most significant hurdles associated with iPSC-CMs is their immaturity, both structurally and functionally [147]. The profile of iPSC-CMs is known to be the same as that of prenatal CMs, with regard to structure, gene expression, ion channel density, and Ca2+ kinetics. In contrast to human mature CMs, immature CMs do not have anisotropic, rod-like shaped, ordered myofibrils, contractile cytoskeletons, T-tubules, nuclei with abundant DNA, junctions and elevated calcium signalling [148]. These discrepancies in form and function are a significant disadvantage when attempting to replicate native tissue. To overcome this limitation, different approaches have been employed including prolonged culture *in vitro* [149], co-culture with non-CMs [150], three-dimensional culture methods [151-153], and electrical and mechanical stimulation [153, 154].

2.12 Bioelectricity and engineering applications

In particular, significant developments have been made in the application of electrical stimulation (ES) *in vitro*. Some of the earliest studies demonstrating the benefits of *in vitro* ES or pacing of CMs date back to the late 1990s, where embryonic chick CMs, or neonatal rat CMs were subjected to electrical field (EF) stimulation over varied time

courses [143, 155]. In each of these studies, ES resulted in enhanced electrophysiological maturation of the cells (immature CMs undergo spontaneous contraction, whereas mature adult CMs lose their automaticity, responding to depolarisation of neighbouring cells). Similar observations were observed using iPSC-CMs, where again, varied pacing strategies resulted in improved contractility of cells, increased calcium handling and reduced proliferation rates [156]. Changes in electrophysiology can be monitored not only through imaging and patch clamp analysis, but through altered gene expression of structural genes, as well as ion handling channels [157]. Increased expression of the potassium channel protein, KCNH2, and the calcium channel protein, ITPR3, as well as a decrease in expression of potassium/sodium ion channel HCN4 are all indicators of the mature adult CM phenotype [153, 157]. Arguably, one of the most successful techniques of electrical pacing was developed by Ronald-Bouchard *et al*., involving a ramped ES scheme. This strategy, termed "intensity training" involved electrical stimulation of cells, with an increase in frequency from 2 Hz to 6 Hz over two weeks [153]. In comparison to "fixed rate" stimulation, this ramped strategy resulted in enhanced ultrastructure organisation and improved calcium handling of iPSC-CMs. It is interesting to note that the pacing regimes in this study were found to be most effective with early-stage iPSC-CMs, i.e., those that begin spontaneously beating at day 12 post-differentiation, highlighting the plasticity of early stage differentiated cells, rather than those in long term culture.

The benefits of external ES are also observed beyond cardiac tissue engineering, as electrical signalling has been found to be critical for numerous biological processes including tissue repair and wound healing [158]. In the skin endogenous electrical potentials are sustained by active Na+/K+ pumps in the epidermis [159]. During incidence of injury, ion leakage occurs across the wounded cells, generating an EF, which largely dictates the wound healing response. The endogenous EF is responsible for promoting migration of keratinocytes and fibroblasts to the site of the wound, in addition to activating fibroblasts to a "pro-healing" phenotype [160]. Disruption of this endogenous EF severely impairs tissue repair, as observed in rat models of skin injury [161]. Delivery of external EF stimulation to skin wounds has been shown to accelerate wound healing, providing a potential application for ES in regenerative medicine [162].

To further this potential, numerous studies have explored the impact of ES on additional cell types, including MSCs, osteocytes, endothelial cells, and additionally, macrophages. The details of these studies are summarised in Table 2.1 below.

Table 2-1 Summary of published ES studies

Cell Type	ES regime	Results	Reference
Osteoblasts	DC, 50, 100, 200 μA for 4 hours, for 6 days	Increased proliferation, elongation of cells	[163]
Human iPSCs	Biphasic current pulses, 65, 200 mV/mm for 5 min, 1 Hz, 1 ms duration.	Cardiomyocyte differentiation, increased expression of cardiac genes	[164]
Human ESC cell line HES3	Pulsed stimulation, 6.6 V/cm, 1 Hz, and 2 ms pulses for 4 days	Increased expression of cardiac troponin T, cell alignment	[165]
Human Bone marrow MSCs	1.5 or 15 μA/cm2 biphasic current 250/25 μs at 100 Hz for 7 days	Increased proliferation, increased expression of VEGF	[166]
Human dermal fibroblasts	Pulsed stimulation of 100 mV/mm with train of cycles of 10 sec in 1200 sec, or 300 sec / 600 sec for 24 hours	Increased expression of TGFβ-1 and high level of α-smooth muscle actin.	[167]
Human dermal fibroblasts	DC, 50, 100, or 200 mV/ mm for 6 hours	Increased expression of pro-regenerative genes associated with wound healing	[160]
Neonatal rat CMs	Pulsed stimulation, rectangular wave, 5 V/cm, at 1 Hz, 2 ms duration for 5 days.	Increased cell alignment, maturation, and synchronous beating	[168]
iPSC-CMs	Pulsed stimulation, monophasic square wave, 3.5-4 V/cm, 2 ms duration, at 2-6 Hz for 4 weeks.	Induced maturation phenotype, increased cell alignment and organisation, synchronous beating	[153]
HUVECs	DC, 200, 300, 400 mV/cm, 30 min duration for 4 days	Increased viability and adhesion of cells	[169]
HUVECs	DC, 50-300 mV/mm	Increased cell migration, proliferation, and expression of chemokine receptors CCR2, CCR4, associated with wound-healing	[170]
Primary human macrophages	DC, 50 – 450 mV/mm for 2 hours	Increased cell migration, increased phagocytic capacity.	[171]
J774A.1 murine macrophages	DC 100 mV/mm for 1-2 hours	Increased expression of osteogenic markers BMP2, Spp1, reduced expression of TNF following LPS treatment	[172]

Each of these studies highlights the effects of ES as a physical stimulator of cell behaviour, in most cases increasing cell proliferation, or improving organisation and differentiation. It is interesting to note in particular the effects of ES on macrophages, as these findings highlight how macrophage phenotype and function can be shaped not only by biochemical cues, but physical cues also. This is important to consider as macrophages infiltrate various environments where electrical signalling may be a prominent feature, i.e., the myocardium.

2.13 Electroconductive Biomaterials

The observed benefit of ES also provides rationale for the inclusion of electroconductive biomaterials in tissue engineering. In particular, recognition of the electroconductive nature of the myocardium has driven major advances in tissue engineering, moving research from inert biomaterials to those that may mimic the physiological electroconductivity of the heart [173]. Electrically conductive biomaterials can be sub-categorised as either extrinsically or intrinsically conductive. Both categories can be incorporated into tissue engineering due to their ease of processing at low temperatures, both alone and in combination with other materials [173]. Extrinsically conductive materials refer to compounds which have an insulating material surrounding a conductive filler. Examples of such include carbon nanotubes (CNTs) and scaffolds embedded with metallic nanoparticles (NPs) such as silver or gold. The incorporation of CNTs in polymer scaffolds has opened new doors for dynamic scaffold design, enhancing properties such as scaffold strength, flexibility, and biocompatibility, enabling scaffolds to meet the mechanical structures of the native myocardium [174]. When incorporated into gelatin methacryloyl (GelMa) hydrogels, CNTs have been demonstrated to increase the electrophysiological function of the scaffold, with a 3-fold increase in spontaneous beating rates of cardiomyocytes observed when compared to pristine GelMa hydrogels alone [175]. However, widescale employment of CNTs in tissue engineering is limited due to concerns of potential toxicity *in vivo* [176]. Regarding the application of metal NPs, the integration of gold NPs in decellularized matrix has proven to facilitate electrical coupling of cardiomyocytes via organisation of Connexin 43 [177]. Stronger contractile force and greater aligned morphology has been observed in cardiomyocytes

cultured in gold-NP matrix compared to pristine matrix alone [177]. These findings highlight electroconductive materials as highly favourable in cardiac tissue engineering.

Intrinsically conductive materials or intrinsically conductive polymers (ICP) have been widely studied since their initial discovery by Alan J. Heeger, Alan G. MacDiarmid, and Hideki Shirakawa [178]. The polymers themselves are organic conjugated polymers and possess low conductivity, however, this can be enhanced through external doping processes such as chemical treatments (such as oxidation or reduction) [173]. One example of these ICPs is the electroconductive polymer poly(3,4-ethylendioxythiophene): polystyrene sulfonate (PEDOT: PSS). PEDOT itself is a water-soluble polymer, stable at high temperatures [179]. When combined with the secondary dopant, PSS, the compound exhibits both ionic and electroconductive properties [180], making it a prime candidate for the generation of electroconductive biological scaffolds and cardiac tissue engineering. In fact, existing evidence shows that incorporation of PEDOT: PSS in collagen-based hydrogels significantly improves electrical coupling and maturation of neonatal rat CMs, as observed through increased expression of the gap junction protein, Connexin 43, and improved sarcomere organisation [154]. Studies with murine embryonic stem cells (ESCs) have also demonstrated that PEDOT: PSS is a compatible platform for stem cell differentiation to CMs, with increased expression of cardio-myogenesis markers observed in cells seeded onto PEDOT: PSS, both in the presence and absence of electrical stimulation [181]. These results are particularly interesting, as it suggests that the presence of the electroconductive biomaterial, even in the absence of external ES, can facilitate and potentially enhance CM function.

Collectively these findings present PEDOT: PSS as an attractive candidate for use in iPSC-CM tissue engineering constructs. However, much of what we understand regarding the direct effects of this biomaterial, and furthermore, the direct effect of electrical stimulation, is largely limited to cardiomyocytes and fibroblasts. Consideration of additional cell types would be beneficial, as research of *in vitro* cardiac models moves towards the inclusion of multicellular models as discussed below.

2.14 Multicellular models

Studies involving engineered multicellular myocardial tissue emphasise the importance of incorporating multicellular interactions between CMs and non-CMs as intercellular

communication is crucial for the basic development and function of the heart [22]. While studies employing human iPSCs have furthered the field in providing a more clinically relevant model, they can often suffer from a lack of environmental stimuli including interactions with the ECM and non-CM resident cells [182, 183]. The addition of fibroblasts to iPSC-CM cultures was shown to improve cell viability, self-organisation and contractility of CMs [184], while incorporation of endothelial cells resulted in enhanced angiogenesis leading to the formation of vascular structures within the CM organoid [184, 185].

While these studies and more have highlighted that the inclusion of non-CMs shows potential for improving CM maturation and function [186-188], the scope of these studies has yet to extend to all cells residing within the myocardium, including macrophages. However, outside the field of cardiac tissue engineering, numerous studies have investigated the influence of the macrophage secretome in 3D organoid cultures [189]. More recently, this has progressed to the use of human macrophage-enteroid co-culture models [190], human macrophage-squamous cell carcinoma tumour models [190] and incorporation of macrophages into *in vitro* models of skeletal muscle [190]. In each of these examples, the inclusion of macrophages has yielded an organoid system capable of determining the innate immune response to external assault and highlighted the homeostatic role of macrophages in tissue maturation. The inclusion of macrophages in human iPSC-CM culture not only provides the potential to understand macrophage-CM interactions, but also improve tissue engineering strategies, as previous work has shown co-culture of iPSC-CMs with non-CMs enhances maturation and function of CMs [141]. Going forward, the use of multi-cellular models which incorporate macrophages will be of great benefit when assessing pathological changes and new therapeutic approaches in CVD.

2.15 Conclusion

Undoubtedly, inflammation driven by macrophages plays a key role in heart failure. Numerous studies have been discussed in this review which pinpoint macrophages as critical mediators of inflammation in atherosclerosis, as well as the inflammatory response and adverse remodelling following MI. Yet there still remains substantial gaps in our knowledge of the precise role of macrophages, particularly resident macrophages

within the myocardium. It remains to be established which specific subsets of macrophages are precisely responsible for the adverse effects of the inflammatory response, and which are necessary for normal homeostatic function. Knockout models which eliminate specific subsets may bring to light the exact function of resident macrophages, and aid future research in harnessing their protective nature. Additionally, human *in vitro* models may allow us to determine the mechanism behind adverse macrophage function at a simpler cellular level. From these studies, further insight may be gained regarding macrophage communication and interaction within the cardiac environment, thus revealing possible novel targets for future therapies.

Chapter 3：Materials and methods

3.1 Materials

3.1.1 Cell culture

Complete RPMI, or complete DMEM were prepared by supplementing with 10% foetal bovine serum (FBS), 2 mM L-glutamine, 100 U/mL penicillin, and 100 µg/mL streptomycin, which were all purchased from Merck. The concentration of glucose in the RPMI was 11 mM, and the concentration of glucose in the DMEM was 25 mM. Lymphoprep™ is manufactured by Axis-Shield poC. Human recombinant macrophage colony stimulating factor (M-CSF), (IL-4) and IFNγ were purchased from Miltenyi Biotec. The MagniSort™ Human CD14 Positive Selection kit was purchased from Thermo Fisher Scientific. Dulbecco's phosphate buffered saline (PBS) was also purchased from Merck. The HEK-Blue™ human TLR4 assay system was purchased from InvivoGen.

The 11b iPSC cell line (alternative name: DiPS 1016SevA) derived from healthy human male fibroblasts was purchased from the Department of Stem cell and Regenerative biology, Harvard University. GFP-tagged SFCi55 iPSCs derived from healthy human female fibroblasts were kindly provided by Lesley Forrester Research group, University of Edinburgh. mTESR™ basal medium, mTESR™ supplement, and Rho-kinase inhibitor (ROCK inhibitor) Y-27632 were purchased from STEMCELL Technologies. Matrigel© (not growth-factor reduced), StemFlex™ basal media, StemFlex™ supplement, and B-27™ supplement with/without insulin were purchased from Thermo Fisher Scientific. Gsk-pathway inhibitor CHIR99021 and Wnt-pathway inhibitor IWP2 were purchased from Sigma Aldrich. Versene™ was purchased from Biosciences Ltd.

3.1.2 Inhibitors and reagents

For the synthesis of cholesterol crystals, cholesterol derived from sheep wool was purchased in powder-form from Sigma-Aldrich. Ultrapure lipopolysaccharide (LPS) from E. Coli O111:B4 was purchased from Enzo Life Sciences. 2-Deoxyglucose (2-DG) was purchased from Sigma Aldrich. TEPP-46 and 3PO were purchased from Merck. Poly(2,3-dihydrothieno-1,4-dioxin)-poly(styrenesulfonate) (PEDOT: PSS) glycidoxypropyltrimethoxysilane (GOPS), and poly(ethylene glycol) diglycidyl ether (PEGDE) were purchased from Sigma Aldrich.

3.1.3 Western blotting

The protease inhibitor cocktail was purchased from Roche and Phosphatase inhibitor cocktail 3 was purchased from Merck. The western blot antibodies for pro-IL-1β, caspase-3, Hexokinase II (HK2), MFF, DRP-1, and PKM2, as well as AdvanBlock™ were all purchased from Cell Signalling Technology. GLUT1 antibody was purchased from Invitrogen. The antibody for Connexin 43 and Vinculin were purchased from Abcam, and the β-actin antibody, secondary anti-rabbit, and secondary anti-mouse were purchased from Merck. All chemicals used for western blotting buffers and solutions listed in Table 3.1 were purchased from Sigma-Aldrich. Acrylamide was purchased from Fisher scientific. SeeBlue™ Plus2 Pre-Stained Protein Standard was purchased from Invitrogen. Immobilin polyvinylidene difluoride (PVDF) membrane and Enhanced Chemiluminescent (ECL) Horseradish-Peroxidase (HRP) Substrate were purchased from Merck.

Table 3-1 Western blot buffers

Buffer	**Reagents**
1 M Tris-HCL (pH 6.8)	121.4 g Tris, 1 L dH_2O, pH using HCL.
1.5 M Tris-HCL (pH 8.8)	181.71 g Tris, 1 L dH_2O, pH using HCL. 10% SDS 10 g SDS, 100 ml dH_2O. 10% Ammonium Persulfate (APS) 100 mg APS, 10 ml dH_2O
10X Running Buffer (pH8.3)	30.3 g Tris, 144 g Glycine, 10 g SDS, 1 L dH_2O. Dilute 1:10 in dH_2O to use at 1X concentration.
10X Transfer Buffer (pH ~8)	30 g Tris, 144 g Glycine, 1 L dH_2O. Dilute 1:10 in dH_2O to use at 1 X concentration
10X Tris-Buffered Saline with Tween-20 (TBST) (pH 7.6)	24.2 g Tris, 88 g NaCl, 10 ml Tween-20, 990 ml dH_2O. Dilute 1:10 in dH_2O to use at 1X concentration.

3.1.4 Flow cytometry

The DQ-Ovalbumin, FIX & PERM™ Cell Permeabilization Kit, MitoSOX™ red, Fixable Viability Dye eFluor™ 506 and Anti-mouse Ig Comp-Beads were purchased from Invitrogen. The Tissue Dissociation Kit 3 for lifting of iPSC-CMs and iPSCs was purchased from Miltenyi. Fluorochrome-conjugated antibodies were purchased as listed below in Table 3.2.

Table 3-2 Flow cytometry antibodies

Specificity	Fluorochrome	Clone	Supplier
CD14	FITC	HCD14	Invitrogen
CD11b	APC eFluor™ 780	ICRF44	Invitrogen
CD40	eFluor™ 450	5C3	Invitrogen
CD80	PerCP eFluor™ 710	2D10.4	Invitrogen
CD86	PE Cyanine 5	IT2.2	Invitrogen
CD163	PE Cyanine 7	eBioGHI/61 (GHI/61)	Invitrogen
CD206	APC	19.2	Invitrogen
CCR2	Alexa Fluor 647	48607R	R&D
CX3CR1	PE	2A9.1	Invitrogen
CTnT	Vio Blue	REA400	Miltenyi
MLC2a	APC	REA39A	Miltenyi
OCT3/4	eFluor™ 660	EM92	Miltenyi

3.1.5 Polymerase Chain Reaction (PCR)

High-Pure RNA Isolation Kits were purchased from Roche. The High-Capacity cDNA reverse transcription kit, TaqMan™ fast universal PCR Master Mix and TaqMan™ probes for eukaryotic 18S rRNA, human *CXCL9, CXCL10, MRC1, CCL13, S100A8* and *S100A12* were purchased were purchased from Applied Biosystems. The iTaq™ Universal SYBR Green Master Mix was purchased from Bio-Rad. Forward and reverse primers for *GLUT1, HK2, HIF1α, PFKFB3, GAPDH, PKM2, Connexin 43, VEGF, PDGF-β, MMP9* and *B-actin* were purchased from Merck. The primer sequences are detailed in Table 3.3

Table 3-3 Gene primer sequences

Gene	Forward primer sequence	Reverse primer sequence
GLUT1	GAACTCTTCAGCCAGGGTCC	ACCACACAGTTGCTCCACAT
HK2	TTCTTGTCTCAGATTGAGAGTGAC	TTGCAGGATGGCTCGGACTTG
HIF1α	GAAACTTCTGGATGCTGGTGATTT	GCAATTCATCTGTGCTTTCATGTCA
PFKFB3	CCATGAAAGTCCGGAAGCAATG	GCTTTTGACATCTCTCAAGGCAG
GAPDH	ACAGTTGCCATGTAGACC	TTTTTGGTTGAGCACAGG
PKM2	ATGTTGATATGGTGTTTTGCG	ATTTCATCAAACCTCCGAAC
Connexin 43	GGGTTAAGGGAAAGAGCGACC	CCCCATTCGATTTTGTTCTGC
VEGF	AGGGCAGAATCATCACGAAGT	AGGGTCTCGATTGGATGGCA
PDGF-β	GGGCAGGGTTATTTAATATGG	AATCAGGCATCGAGACAG
MMP9	GTACTCGACCTGTACCAGCG	TCAGGGCGAGGACCATAGAG
TGF-β	AACCCACAACGAAATCTATG	CTTTTAACTTGAGCCTCAGC
B-actin	GGACTTCGAGCAAGAGATGG	AGCACTGTGTTGGCGTACAG

3.1.6 Enzyme-linked immunosorbent assay (ELISA)

Human IL-1β, IL-6, IL-8, IL-10 and TNF uncoated ELISA kits were purchased from Invitrogen.

3.1.7 Seahorse XF Assays

The Complete XF assay medium was purchased from Agilent. Oligomycin was purchased from Cayman Chemicals and carbonyl cyanide-p trifluoromethoxyphenylhydrazone (FCCP) from Santa Cruz biotechnology. Rotenone, antimycin A, and 2-deoxy-D-glucose (2-DG) were all purchased from Merck.

3.1.8 Confocal

35 mm μ-dishes for cell plating and imaging were purchased from iBidi. Anti-PKM2 primary antibody was purchased from Cell Signalling Technology. Secondary anti-rabbit antibody conjugated to Alexa 647 fluorochrome was purchased from Abcam. Bovine Serum albumin (BSA) and paraformaldehyde (PFA) were purchased from Sigma Aldrich. MitoTracker™ Red CMXRos was purchased from Life Technologies, and Hoechst stain was purchased from Thermo Fisher.

3.2 Methods

3.2.1 Isolation of PBMCs from human venous blood

Leukocyte-enriched buffy coats (the plasma depleted fraction of anti-coagulated blood from anonymous healthy donors were obtained with permission from the Irish Blood Transfusion Board (IBTS), St. James's Hospital, Dublin. Donors provided informed written consent to the IBTS for their blood to be used for research purposes. Neither sex or age of the donors was disclosed.

Three buffy coats were processed at once. Blood from each pack was diluted 1:2 with sterile PBS and centrifuged (Eppendorf Centrifuge 5810R) at 1250 g for 10 minutes at room temperature, with the brake off. The buffy coat layer containing leukocytes was removed using a Pasteur pipette, diluted in sterile PBS. Donors with an observed high density of leukocytes were excluded from processing to avoid experiments with activated immune cell populations. The diluted leukocytes from the remaining two donors were layered over Lymphoprep™ (20 ml Lymphoprep™ and 25 ml diluted buffy coat per falcon tube). PBMCs were isolated by density-gradient centrifugation (800 g, 20 minutes, at 20°C, with the brake off). The PBMC layer was carefully removed using a Pasteur pipette, washed in sterile PBS and centrifuged for 10 minutes at 650 g. The supernatant was discarded and the PBMC pellet was re-suspended in sterile PBS and centrifuged at 300 g for 10 minutes. The supernatant was discarded, and the pellet was re-suspended in 50 ml of complete RPMI and then counted.

3.2.2 Cell counting

PBMCs in complete RPMI were diluted 1:20 in trypan blue and viable mononuclear cells were counted on a light microscope (Leica DM500) using a haemocytometer (improved Neubauer, Hawksley or Hycor Galsstic slide, Kova). The total number of cells was calculated using the formula

$$Average\ cell\ number\ \times 10^4\ \times trypan\ blue\ dilution\ factor \times volume\ (ml) = total\ cell\ number\ per\ ml$$

3.2.3 Purification of total CD14⁺ monocyte cells by positive selection using magnetic activated cell sorting (MACS).

PBMCs were isolated from blood samples as described in section 3.2.1 and total CD14⁺ monocytes were isolated using the MagniSort™ Human CD14 Positive Selection Kit

according to the manufacturer's protocol. Cells were washed in MACS buffer (49 ml PBS, 1 ml FBS, 200 µl EDTA) and pelleted by centrifugation at 300 g for 5 minutes. The supernatant was completely discarded, and the pellet was re-suspended in MACS buffer at 1 x 10^8 cells/ml in a 12 x 75 mm tube and incubated with anti-CD14 biotin (10 µl per 100 µl cells) for 10 minutes at room temperature. Cells were then washed in 4 ml MACS buffer and pelleted by centrifugation at 300 g for 5 minutes. Supernatant was discarded; cells were re-suspended in their original volume of MACS buffer and incubated with MagniSort™ positive selection beads (15 µl per 100µl cells) for 10 minutes at room temperature. The volume was then adjusted to 2.5 ml and the tube placed inside the magnetic field of a EasySep™ cell sorter magnet (STEMCELL Technology) for 5 minutes. The negative fraction was then poured off by inverting the tube while held inside EasySep™ magnet, and the remaining cells were re-suspended in 2.5 ml MACS buffer. This step was repeated two times and then the positive fraction containing the $CD14^+$ monocytes was re-suspended in complete RPMI and counted.

3.2.4 $CD14^+$ monocyte differentiation and culture of human macrophages

$CD14^+$ monocytes were plated at a concentration of 1 x 10^6 cell/ml in complete RPMI containing M-CSF at a final concentration of 50 ng/ml. $CD14^+/CD11b^+$ macrophages were obtained after 6 days of culture, with replacement of RPMI (containing M-CSF) every 3 days. Purity was analysed on day 6 by assessing the expression of $CD14^+$ and $CD11b^+$ by flow cytometry. Population of $CD14^+$ $CD11b^+$ macrophages was found to be routinely >95% (Figure 3.1).

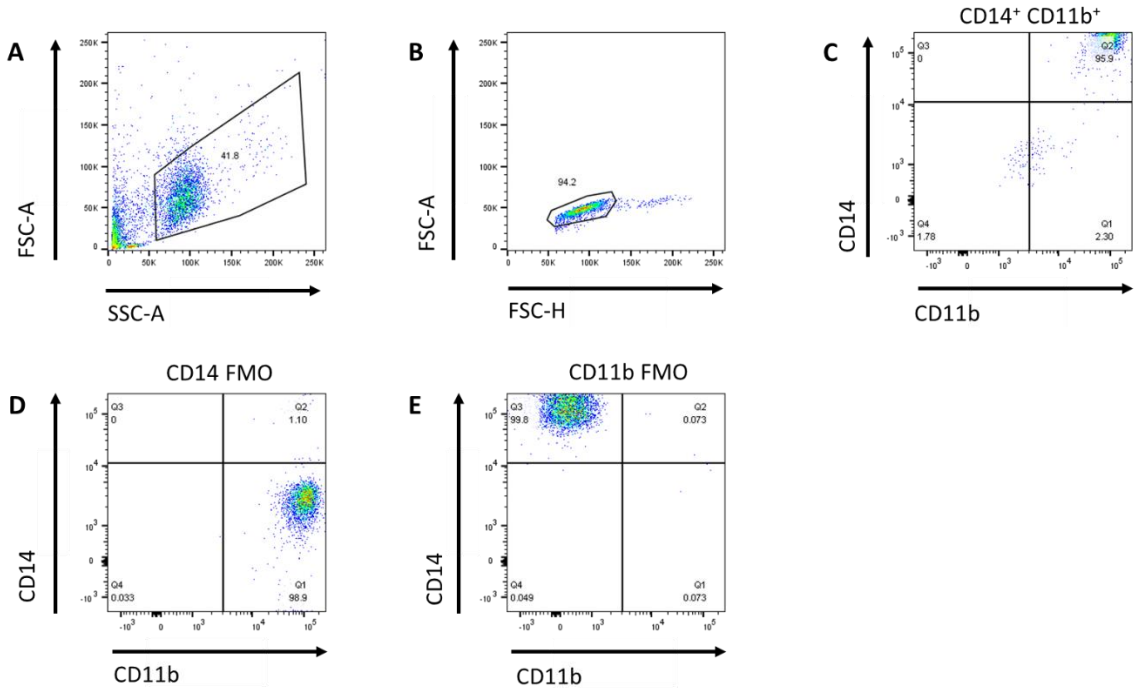

Figure 3-1 – Purity check of primary human macrophages

Primary human monocytes were isolated from PBMCs from healthy human buffy coats through positive selection of surface marker CD14. Monocytes were cultured for 6 days in the presence of M-CSF (50 ng/ml) to differentiate to macrophages. Purity of day 6 macrophages was determined by flow cytometry. (**A-B**) Representative dot plots of gating strategy for single cells. (**C**) Representative dot plot of stained $CD14^+/CD11b^+$ macrophages. (**D-E**) Representative dot plot of CD14/CD11b Fluorescence minus one (FMO) gating strategy.

3.2.5 Macrophage lifting

$CD14^+$ monocytes were plated at a concentration of 1 x 10^6 cell/ml in complete RPMI containing M-CSF at a final concentration of 50 ng/ml in 25cm^3 low adherent flasks (Corning). $CD14^+/CD11b^+$ macrophages were obtained after 6 days of culture, with replacement of RPMI (containing M-CSF) every 3 days. At Day 6, cells were washed with PBS before incubation with pre-warmed Versene™ at 37 °C for 5 minutes. Cells were collected in Versene™ suspension and centrifuged at 300 g for 5 minutes. The resulting pellet was resuspended in complete RPMI and the cells were counted. Purity and viability of macrophages was analysed by flow cytometry (Figure 3.2).

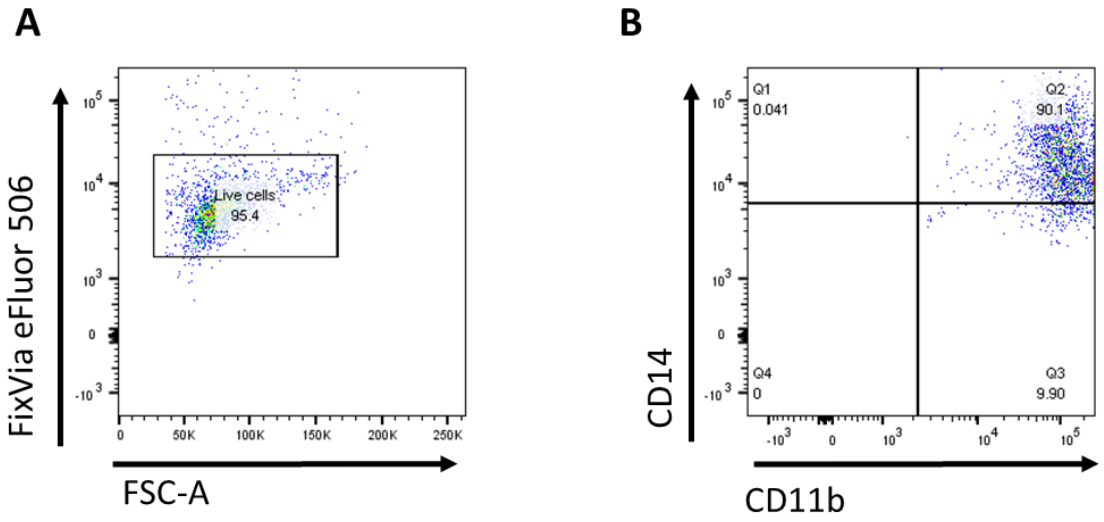

Figure 3-2 – Analysis of macrophage viability and purity following culture in low attachment flasks.

Primary human monocytes (1x10^6 cells/ml) were cultured in low adherence flask for 6 days in the presence of M-CSF (50 ng/ml). Cells were lifted from flasks and stained for viability and macrophages markers. Human monocyte derived macrophages were identified as $CD14^+$ $CD11b^+$ cells. **(A)** Representative dot plot of viable cells gated on using live/dead viability stain. **(B)** Representative dot plot of $CD14^+$ $CD11b^+$ macrophages.

3.2.6 Matrigel© coating

Successful culture and expansion of iPSCs requires the use of tissue culture plates coated with the basement protein matrix gel Matrigel©. Matrigel© (Corning) was prepared at a 1/4 dilution of the manufacturer's recommended concentration. For example, lot. 9280004 recommended dilution is 272 µl of Matrigel© in 25 ml of DMEM/F-12 (STEMCELL Technology), equalling 10.88 µl Matrigel©/ml. The optimal working concentration therefore with 1/4 dilution is 2.7 µl Matrigel©/ml. 2 ml of diluted Matrigel© was added to each well of a 6 well plate. Plates were incubated for a minimum 2 hours before plating of iPSCs. When cells were ready to plate, excess Matrigel© was removed from the well, and replaced with 1 ml of complete mTESR™ media or StemFlex™ media.

3.2.7 iPSC thawing and culture

A cryovial of iPSCs (cell line 11b or GFP tagged cell line SFCi55) was thawed rapidly at 37 °C before resuspension in complete mTESR™ media. Cells were centrifuged at 1200 rpm for 5 minutes. The supernatant was discarded, and the pellet was resuspended in 1 ml of complete mTESR™ or StemFlex™ media. The resuspended cells were added to 1 well of a 6 well Matrigel© coated plate, already containing 1 ml of mTESR™/StemFlex™ media. The final volume in the well was 2 ml. 10 µM of ROCK inhibitor Y-27632 was added to the well to promote cell adherence. 24 hours later, a full media exchange was carried out. Full media exchanges were carried out daily with cells cultured in mTESR™, or every second day with StemFlex™ media, until cells achieved 70-80% confluency. For mass expansion of iPSCs, StemFlex™ media was used in culture. Prior to culture for cardiomyocyte differentiation, cells were switched to mTESR™, media for at least 2 passages, for better monitoring of cell proliferation/density.

3.2.8 iPSC passage

iPSCs were cultured to 70-80% confluency before passaging. Cells were lifted and re-plated at a density of $6x10^5$ cells/ml, or a 1/5 split ratio. Cells in 1 well were washed once with 1 ml of pre-warmed Versene™. 2 ml of Versene™ was then added to the well, and cells were incubated for 6 minutes at room temperature. Versene™ was removed and cells were aspirated off in 1 ml of complete mTESR™/ StemFlex™ media. The 1 ml suspension of cells was collected and diluted to 5 ml with complete mTESR™/ StemFlex™ media. 1 ml of the diluted cell suspension was added to a Matrigel©-coated

well in a 6 well plate, already containing 1 ml of complete mTESR™/ StemFlex™ media. 10µM of ROCK inhibitor was added to each well for 24 hours. After 24 hours, a complete media exchange was carried out and cells were cultured as detailed in 3.2.7 until 70-80% confluency.

3.2.9 iPSC-Cardiomyocyte differentiation

Cardiomyocyte differentiation was carried out using the previously published GiWi protocol [191]. iPSCs were cultured to 70-80% confluency and passaged following the method outlined in section 3.2.8 above. Cells were plated with a 1/5 split ratio for 11b cells, or 1/4 split ratio for SFCi55 cells, in Matrigel© coated 6 well plates. iPSCs were cultured for 3-4 days to reach 90-95% confluency. At Day 0, cells were pre-treated for 1 hour with ROCK inhibitor (10µM) before a full media exchange was carried out. mTESR™ was removed and replaced with RPMI supplemented with B-27™ minus insulin, and 10 µM of Gsk inhibitor, CHIR99021. 23 hours after this exchange, media was replaced again, with RPMI/B-27™ minus insulin. At Day 3, 1 ml of media was removed and replaced with 1 ml of fresh RPMI/B-27™ minus insulin. 5 µM of Wnt inhibitor, IWP2 was added to the well. At Day 5, a full media exchange was carried out with RPMI/B-27™ minus insulin. At Day 7, the media was replaced with RPMI supplemented with B-27™ with insulin. Media exchange with RPMI/B-27™ was carried out every 3 days from day 7. Spontaneous contraction of cardiomyocytes was observed by Day 10. iPSC-CMs were used for experiments between Day 20 and Day 30.

3.2.10 Preparation of PEDOT: PSS films

PEDOT: PSS 1.3 wt.% dispersion in water was mixed with GOPS at a concentration of 3 v/v%. Solutions were vortexed for 30 seconds, sonicated for 30 minutes and filtered with a 0.45 µm PVDF syringe filter to remove aggregates. Indium tin oxide (ITO) coated glass slides (Sigma-Aldrich) were prepared by sonication in consecutive washes of soap (Liquinox, Alconox, Inc), tetrahydrofuran, isopropanol:acetone 2:1 solution, isopropanol and distilled water. Slides were then dried in an oven at 110 °C for 20 minutes and surface activated by oxygen plasma treatment (Diener Electronic, Plasma Surface Technology, PICO) at 200 W for 10 minutes. Afterwards, 150 µl of the filtered PEDOT: PSS blend was spin coated on the ITO surfaces at 1500 rpm for 30 seconds using a spin coater (WS-400BX-6nPP/LITE) and dried to remove excess water. Films were dried in the

oven for 2 hours at 140 °C. Prior to cell seeding, PEDOT glass films were sterilised by washing 3 times with 70% ethanol, followed by 3 washes with sterile PBS and 30-minute exposure to UV light. The films were then left to dry for 24 hours before cell seeding.

3.2.11 Preparation of 3D PEDOT: PSS scaffolds and extraction media.

PEDOT: PSS 1.3 wt.% dispersion in water was either mixed with GOPS at a concentration of 3 v/v% or PEGDE at a concentration of 3 w/v%. Solutions were vortexed for 30 seconds, sonicated for 30 minutes and filtered with a 0.45 µm PVDF syringe filter to remove aggregates. Sponge-like porous scaffolds of PEDOT: PSS were achieved through a lyophilisation process. Sponges were produced in standard 96 well tissue culture plates. Samples were lyophilised in a freeze-dryer (FreeZone, Labconco Corporation) applying a protocol of ramp to -40 °C, hold for 60 minutes, ramp to 10 °C at a rate of 1 °C per minute, hold for 18 hours with a vacuum of 0.2 mbar, ramp to 20 °C at a rate of 1 °C per minute, and hold for 2 hours. Samples with GOPS were then subjected to an annealing treatment in a vacuum oven for 1 hour at 140 °C. After annealing, all samples were washed 3-5 times with deionised water before undergoing a second lyophilisation process to fully dry the materials. The scaffolds were then sterilised through multiple washes with 70% ethanol, and 30-minute exposure to UV light. Scaffolds were then rinsed 3 times with sterile PBS. To measure the effect of indirect contact of PEDOT: PSS scaffolds on macrophages, extraction media was generated from the scaffolds. Sterile scaffolds were submerged in complete RPMI media at 37 °C for 48 hours, at a ratio of 10mg of dry scaffold per 1ml of media as outlined in previously published studies [192]. Media without scaffolds was also incubated at 37 °C for 48 hours, denoted as “aged control media” in experiments. After 48 hours, media was removed from the scaffolds for use in macrophage experiments.

3.2.12 Preparation of cholesterol crystals

To prepare cholesterol crystals, cholesterol was dissolved in 95% ethanol at a concentration of 12.5 g/L by heating to a temperature of 60°C. The solution was then filtered through Whatman™ filter paper and allowed to crystalize overnight at room temperature. Crystals were collected through Whatman™ paper and subsequently autoclaved. The crystals were then ground using a sterile pestle and mortar, and a size

no larger than 40 µm was ensured by passing through a cell strainer. The crystals were then dissolved in serum free RPMI prior to use.

3.2.13 Preparation of bioreactor and delivery of electrical stimulation

Electrical stimulation experiments were carried out using custom-built bioreactor system previously optimized in the Monaghan lab [193] (Figure 3.3).

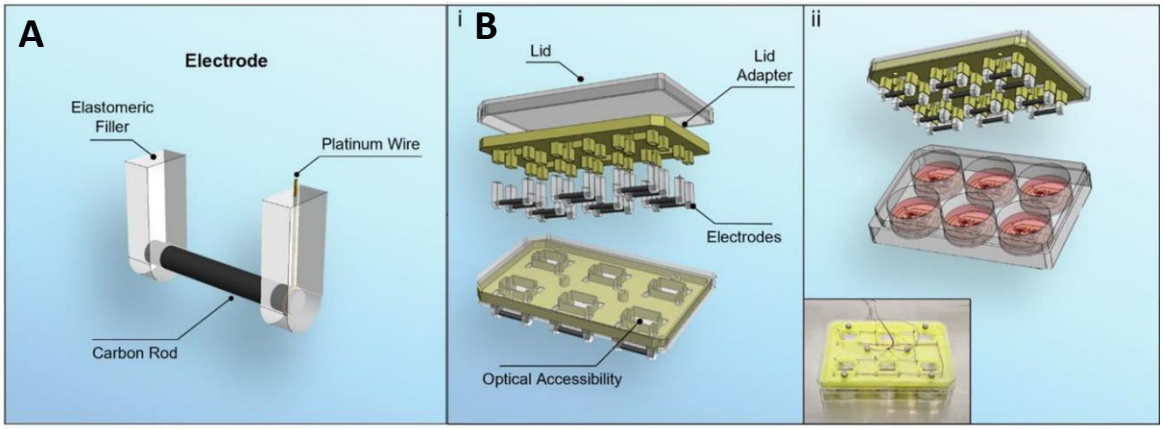

Figure 3-3 – Schematic representation of custom built bioreactor for electrical stimulation of cells. Figure adapted from Solazzo and Monaghan 2022.

(**A**) Carbon rods used as electrodes for delivery of electrical stimulation. (**B**) Overview of the electrical pacing bioreactor. (i) Exploded and collapsed views of the individual components of the electrical pacing bioreactor. (ii) Schematic and picture of the custom-made cell culture pacing setup.

To sterilize the bioreactor lid, carbon rods of the reactor lid were submerged in 70% ethanol for 5 minutes. This was repeated with deionized water to remove ethanol from the rods, and finally the lid was subjected to 30 minutes of UV exposure. Primary human macrophages were seeded at a density of 1 x10^6 cells/ml in a 6 well plate fitted for the bioreactor. The bioreactor was powered using the RS PRO Arbitrary Waveform generator and the signal measured using the RS PRO RSDS 1052 DL oscilloscope. Cells were stimulated for 1 hour with a regime consisting of a biphasic pulse of 2 ms, ±2.5V, with 1 Hz frequency. This regime has been previously implemented in the pacing of cardiomyocytes *in vitro* and resembles the electrical properties native to the myocardium *in vivo* [168, 194]. Prior to initiating stimulation, the volume of media in each well was increased to 4 ml to allow complete submergence of the carbon rods. A

whole media exchange was performed after stimulation. Cells were assessed immediately after stimulation or else left to rest for 24 hours.

3.2.14 Flow Cytometry

3.2.14.1 Cell viability and extracellular staining

For staining of cells with fluorochrome-conjugated antibodies against extracellular markers, cells were harvested and washed in PBS. Cells were stained for viability by incubation with FixVia efluor™ 506 (diluted 1:1000) in 50 µl PBS for 15 minutes at room temperature. After which, cells were washed in PBS and centrifuged at 300 g for 5 minutes. The supernatant was discarded, and cells were incubated with FC Block™ (diluted 1:100) in 50 µl at room temperature for 15 minutes. Cells were washed again in PBS and centrifuged at 300 g for 5 minutes. The supernatant was discarded, and cells were stained for relevant surface markers by incubation with fluorochrome-conjugated antibodies for 15 minutes at room temperature protected from light. Following extracellular staining, cells were washed in PBS and centrifuged at 300 g for 5 minutes. Cells were then fixed with 2% paraformaldehyde (PFA) for 15 minutes at room temperature, protected from light. Cells were washed in PBS, centrifuged at 300 g for 5 minutes, and resuspended in 300 µl of FACs buffer (1% BSA in PBS). Cell samples were stored at 4 °C, protected from light, until acquisition.

3.2.14.2 Intracellular staining for iPSCs and iPSC-CMs

iPSCs were washed twice with PBS, lifted from the wells using Versene™ and resuspended in FACs tubes. Cells were centrifuged at 300 g for 5 minutes. Cells were fixed with 50 µl Fix & Perm™ solution A for 15 minutes at room temperature, protected from light. Cells were washed and stained for the intracellular pluripotency marker Oct3/4 (1/100 dilution) in 50 µl Fix & Perm™ solution B (permeabilisation buffer) for 15 minutes at room temperature in the dark. Cells were washed in PBS and resuspended in PBS for acquisition.

iPSC-CMs were harvested at day 20 with the Tissue Dissociation Kit 3, as per manufacturer's instructions. Cells were fixed with 50 µl Fix & Perm™ solution A for 15 minutes at room temperature, protected from light. Cells were washed and stained for intracellular markers CTnt and MLC2a (1/100 dilution) in 50 µl Fix & Perm™ solution B

(permeabilisation buffer) for 15 minutes at room temperature in the dark. Cells were washed in PBS and resuspended in PBS for acquisition.

3.2.14.3 DQ-Ovalbumin assay

For assessment of cell capacity for antigen uptake, cells were incubated with fresh media containing DQ-Ova (500 ng/ml) for 20 minutes at 37 °C, before transferring to 4 °C for a further 10 minutes incubation to stop the uptake of the model antigen. Cells were then washed in PBS, centrifuged at 300 g for 5 minutes, resuspended in PBS and acquired immediately. Unstained cells (cells given fresh media containing no DQ-Ova) were used as a gating control for DQ-Ova positive cells.

3.2.14.4 MitoSox™ assay

For assessment of mitochondrial ROS, cells were incubated with fresh media containing MitoSox™ red (5 µM) for 30 minutes at 37 °C. Cells were washed in PBS, centrifuged at 300 g for 5 minutes. For cholesterol crystal experiments, cells were incubated with CD14 antibody following MitoSox™ staining, to identify cell populations amongst cholesterol crystal particulates. Cells were incubated with the fluorochrome-conjugated antibody for 15 minutes at room temperature protected from light, washed with PBS, and centrifuged at 300 g for 5 minutes. Cells were resuspended in PBS and acquired immediately.

3.2.15 Endotoxin assay

HEK-Blue™ human TLR4 cells were plated at a density of 5 x 10^5 cells/ml in complete DMEM with 1x selection media, as per manufacturer's instructions. As a positive control, cells were treated in triplicate with serial dilutions of LPS, ranging from 100ng/ml to 0.1ng/ml for 24 hours. Untreated cells were left as a blank control. Cells were treated in triplicate with cholesterol crystals (two separate batches, Batch A and Batch B), PEDOT extraction media, or RPMI/B-27™ media for 24 hours. 20 µl of cell supernatant was taken from each well and incubated with 180 µl of HEK-Blue™ detection medium for 15 minutes at 37 °C. Absorbance values were acquired at 650 nm.

3.2.16 Cell viability and metabolic activity

3.2.16.1 Alamar Blue™

Cells were incubated with 10% Alamar Blue™ for 3 hours until an observed colour change from blue to vivid pink. Absorbance was read at 570 nm and 600 nm. Cell viability/metabolic activity of treated cells was determined using the equation outlined below, where O1 is the molar extinction coefficient (E) of oxidised Alamar Blue™ at 570 nm (80586 a.u.), O2 is the E of oxidised Alamar Blue™ at 600 nm (117216 a.u.), A1 is the absorbance of treated wells at 570 nm, A2 is the absorbance of treated wells at 600 nm, P1 is the absorbance of untreated control wells at 570 nm, and P2 is the absorbance of untreated control wells at 600 nm.

$$\frac{(O2\ x\ A1) - (O1\ x\ A2)}{(O2\ x\ P1) - (O1\ x\ P2)}\ X\ 100$$

3.2.16.2 Neutral red assay

Cells were incubated with 10% neutral red solution (N-2889, TOX4 kit, Sigma) for 2 hours. After incubation media is removed and cells were rinsed with Neutral red assay fixative (N-4270, TOX4 kit). The fixative solution was removed, and cells were solubilized using neutral red assay solubilisation solution (N-4395) equal to the original volume of media per well. The cell plate was placed on a shaker at room temperature for 10 minutes before absorbance was measured at 540 nm. Background absorbance was also measured at 690 nm. Cell viability was determined relative to untreated cells using the equation outlined below where B1 is the absorbance of treated cells at 540 nm, B2 is the absorbance of treated cells at 690 nm, A1 is the absorbance of untreated control cells at 540 nm, and A2 is the absorbance of untreated control cells at 690 nm.

$$\left(\frac{(B1 - B2)}{(A1 - A2)}\right) x100$$

3.2.17 SDS-PAGE, Gel staining and Western blot

3.2.17.1 Sample preparation

For blotting of metabolic proteins GLUT1, HK2, PKM2, and apoptosis marker Caspase 3, cells were lysed by the addition of 100 µl per 1 x 10^6 cells of RIPA buffer containing 1% phosphatase inhibitor cocktail 3 to each well. The samples were then centrifuged at

16,300 g for 5 minutes and lysates were transferred to a new microcentrifuge tube. Samples were stored at -20 °C until use.

For blotting of mitochondrial proteins MFF, and DRP-1, as well as gap junction protein Connexin 43, and pro-IL1β, the following protocol outlined by Cell Signalling Technology was implemented. Cells were lysed in 1X Laemmli buffer (10 µl of 5X Laemmli buffer containing 20% β-mercaptoethanol, in 40 µl de-ionised water) containing 1% phosphatase inhibitor cocktail 3. Cells were transferred to micro-centrifuge tubes and sonicated for 30 seconds to shear DNA and reduce sample viscosity. Samples were then boiled at 100 °C for 5 minutes before being cooled on ice for 5 minutes. Samples were then centrifuged at 16,300 g for 5 minutes. The supernatant containing protein lysate was collected and transferred to fresh microcentrifuge tubes. Samples were stored at -20 °C until use.

3.2.17.2 SDS-PAGE

Samples were prepared for SDS-PAGE by the addition of 5x Laemmli buffer (if not already lysed in 1X Laemmli buffer) in a ratio of 1:5 (5 µl of Laemmli buffer added to 20 µl of each sample) prior to boiling at 100°C for 5 minutes. Samples were cooled on ice before loading into prepared SDS gels.

Depending on the size of the target protein, either 8%, 10%, 12% or 15% polyacrylamide gels were used (see table 3.4 for composition of gels). The gels were submerged in 1X running buffer. 20 µl of samples and 5 µl of pre-stained protein standard were loaded and resolved through the gel at 120 volts (V) for 90 minutes.

Table 3-4 Composition of 2x SDS-Polacrylamide Gels

	8% Resolving Gel	10% Resolving Gel	12% Resolving Gel	15% Resolving Gel	Stacking Gel
30% Acrylamide	4 ml	5 ml	6 ml	7.5 ml	0.67 ml
H_2O	6.9 ml	5.9 ml	4.9 ml	3.4 ml	2.7 ml
1.5M Tris-HCl	3.8 ml	3.8 ml	3.8 ml	3.8 ml	-
1 M Tris -HCl	-	-	-	-	0.5 ml
10% SDS	0.15 ml	0.15 ml	0.15 ml	0.15 ml	40 µl
10% APS	0.15 ml	0.15 ml	0.15 ml	0.15 ml	40 µl
Temed	6 µl	6 µl	6 µl	6 µl	6 µl
Total Volume	15.006 ml	15.006 ml	15.006 ml	15.006 ml	3.956 ml

3.2.17.3 Transfer of proteins onto PVDF membrane

The proteins were transferred onto a PVDF membrane by a wet transfer sandwich. This was prepared in the following order: sponge, filter paper, gel, PVDF membrane, filter paper and sponge. The PVDF membrane was activated by submersion in methanol prior to this. All other components of the transfer sandwich were first submerged in 1X transfer buffer. After ensuring that there were no air bubbles present in the sandwich, the transfer sandwich was placed into the transfer system with the gel on the cathode side and the membrane on the anode side. The proteins were transferred at 200 milliamperes (mA) for 75 minutes.

3.2.17.4 Immunodetection of proteins

Following the transfer, the membrane was incubated in blocking buffer under agitation for 1 hour at room temperature. The blocking buffer and diluent was dependent on the target protein and detection antibodies used (See table 3.5). The membrane was incubated in primary antibody (see Table 3.5) with agitation, overnight at 4°C. The

membrane was washed 5 times for 5 minutes each with 1X TBST prior to incubation in secondary antibody (See table 3.5) for 2 hours at room temperature. The membrane was washed a further 5 times for 5 minutes each and then developed with freshly prepared ECL using Chemi-Luminescent gel documentation system (Bio-rad). The intensity of protein bands was quantified through densitometric analysis using Bio-rad software.

Table 3-5 Dilutions for Western blot antibodies

Blocking agent	Primary Antibody	Dilution	Secondary Antibody	Dilution
5% (w/v) milk in TBST	Anti-pro-IL-1β	1:1000	Anti-Goat	1:2000
AdvanBlock™	Anti-caspase 3	1:1000	Anti-Rabbit	1:2000
AdvanBlock™	Anti-GLUT1	1:1000	Anti-Rabbit	1:2000
5% (w/v) milk in TBST	Anti-Hexokinase II	1:1000	Anti-Rabbit	1:2000
5% (w/v) milk in TBST	Anti-PKM2	1:1000	Anti-Rabbit	1:2000
5% (w/v) milk in TBST	Anti-MFF	1:1000	Anti-Rabbit	1:2000
5% (w/v) milk in TBST	Anti DRP-1	1:1000	Anti-Rabbit	1:2000
AdvanBlock™	Anti-Connexin 43	1:2000	Anti-Rabbit	1:10,000
5% (w/v) milk in TBST	Anti-Vinculin	1:2000	Anti-Mouse	1:4000
-	Anti-β-actin-peroxidase	1:50,000	-	-

3.2.18 Polymerase Chain Reaction (PCR)

3.2.18.1 RNA extraction

Supernatants were removed and cells were washed once with PBS before the addition of 400 µl of lysis/-binding buffer and 200 µl of PBS per well. From this point only filtered pipette tips were used. The lysates were transferred to a High Pure Filter Tube that was inserted into a collection tube. Samples were centrifuged at 8,000 g for 15 seconds (Spectrafuge™ 24 D). The flow through liquid was discarded and 90 µl of DNase incubation buffer with 10 µl DNase I was added to each Filter Tube and incubated for 15 minutes at room temperature. 500 µl of Wash Buffer I was then added to the Filter Tubes which were centrifuged at 8,000 g for 15 seconds. The flow-through liquid was discarded and 500 µl of Wash Buffer II was added to the Filter Tubes which were centrifuged again at 8,000 g for 15 seconds. The flow-through liquid was discarded and a further 200 µl of Wash Buffer II was added to Filter Tubes and centrifuged at 13,000 g for 2 minutes. The Collection Tubes were discarded, and the Filter Tubes were placed into sterile, RNase-free 1.5 ml microcentrifuge tubes. 50 µl of Elution Buffer was added to the filter tubes and centrifuged at 8,000 x g for 1 minute. The concentration of eluted RNA in each sample was determined using a NanoDrop 2000c UV-Vis Spectrophotometer and then equalised by the addition of Elution Buffer, where necessary.

3.2.18.2 cDNA synthesis

cDNA synthesis was then carried out using the High-capacity cDNA reverse transcription kit (Applied Biosystems). A 2X Reverse Transcription (RT) master mix was prepared with the components in Table 3.6.

Table 3-6 Components and volumes required for 2X RT Master Mix

Component	Volume added (per sample)
10X RT Buffer	2 µl
25X dNTP Mix (100mM)	0.8 µl
10X RT Random Primers	2 µl
Multiscribe Reverse Transcriptase	1 µl
Total added (per sample)	5.8 µl

14.2 µl of RNA and 5.8 µl of the 2X RT master mix were added to RNase-free PCR tubes and the reverse transcription (see Table 3.7) was performed using the PTC-200 Peltier Thermal Cycler.

Table 3-7 cDNA Reverse Transcription Reaction

	Step 1	Step 2	Step 3	Step 4
Temperature (°C)	23	37	85	4
Time (Minutes)	10	120	5	Indefinitely

3.2.19 Real-time PCR

Two protocols were used for analysis of gene expression by real-time PCR, Taqman™ (3.2.19.1) and iTaq™ Universal SYBR Green (3.2.19.2).

3.2.19.1 TaqMan protocol:

Having synthesized and equalised cDNA transcripts from primary human macrophages, real-time PCR was carried out on transcripts using the TaqMan™ fast universal PCR Master Mix (Applied Biosystems) and predesigned TaqMan™ gene expression probes. Samples were made up as detailed in Table 3.8, into a 96-well PCR microplate. The PCR reaction is detailed in Table 3.9

Table 3-8 Components and volumes required for qPCR reaction

Component	Volume added (per sample)
18S rRNA	0.5 µl
Target Probe	0.5 µl
TaqMan™ Universal PCR Master Mix	4.5 µl
cDNA sample	4.5 µl
Total Volume	10 µl

The qPCR reaction (Table 3.9) was performed using the BioRad CFX Touch Real-Time PCR detection System. For each sample, mRNA concentration was normalized using the expression of housekeeping 18S ribosomal RNA and gene expression, relative to untreated samples, was determined using the $2^{-\Delta\Delta Ct}$ algorithm.

Table 3-9 Thermal cycling parameters for Taqman™ real-time PCR

	Step 1	Step 2	Step 3	Step 4	Step 5
Temperature (°C)	95	95	60	Plate Read	Go to Step 2
Time (Seconds)	20	3	30	-	X 39

3.2.19.2 iTaq™ Universal SYBR Green protocol:

Real-time PCR was carried out on primary human macrophages cDNA transcripts using the iTaq™ Universal SYBR Green Supermix and oligonucleotide primers (See table 3.3 for primer sequences). Reactions were made up, as detailed in Table 3.10, into a 96-well PCR microplate. The PCR reaction is detailed in Table 3.11.

Table 3-10 Components and volumes required for iTaq™ Universal SYBR Green reaction

Component	Volume added (per sample)
Forward primer	0.5 µl
Reverse primer	0.5 µl
RNase free water	4 µl
iTaq™ Universal SYBR Green	4 µl
cDNA sample	1 µl
Total Volume	10 µl

Table 3-11 Thermal cycling parameters for iTaq Universal SYBR Green real-time PCR

	Step 1	Step 2	Step 3	Step 4	Step 5	Step 6
Temperature (°C)	95	95	60	Plate Read	72	Go to Step 2
Time (Seconds)	10 (mins)	15	30	-	30	X 40

The real-time PCR reactions (detailed in Table 3.11) were performed using the BioRad CFX Touch Real-Time PCR detection system. For each sample, mRNA concentration was normalised using the crossing threshold of the housekeeping gene Beta-actin. Gene expression, relative to untreated samples, was determined using the $2^{-\Delta\Delta Ct}$ algorithm.

3.2.20 Measurement of cytokine production by Enzyme-linked Immunosorbent Assay (ELISA)

3.2.20.1 Sample preparation

Supernatants were harvested from treated cells and the concentrations of various cytokines were quantified using the Invitrogen kits.

3.2.20.2 Measurement of cytokine release by ELISA

The concentrations of human IL-1β, TNF, IL-6, IL-8, and IL-10 were quantified by ELISA, according to the manufacturer's protocol. 30 µl of capture antibody diluted in coating buffer was applied to high-binding 96-well plates (Greiner Bio-one). Plates were incubated overnight at 4°C, capture antibody was removed, and non-specific binding sites were blocked with appropriate blocking solution (1X assay diluent) for 1 hour at room temperature. After blocking, plates were washed in ELISA wash buffer solution, dried, and supernatant samples were loaded into wells in triplicates either neat or diluted in assay diluent. A standard curve of serially diluted recombinant cytokine standard was also loaded onto the plates in triplicate. Blank wells, containing assay diluents only, were included on each plate to allow the subtraction of background absorbance from each sample. Samples were incubated overnight at 4°C. After washing, 75 µl detection antibody was added to each well and incubated for 2 hours at room temperature. Plates were washed and horseradish-peroxidase (HRP) conjugated to streptavidin was applied to wells and then incubated for 30 minutes in the dark. Wells were thoroughly washed and 75 µl of the substrate tetramethylbenzidine (TMB) was added to each well. The enzyme-mediated colour reaction was protected from light while developing and stopped with the addition of 37.5 µl of 1M H_2SO_4. The optical density (OD) of the colour was determined by measuring the absorbance at 450 nm using a microtiter plate reader. A standard curve was generated using the serially diluted protein standards and used to determine the concentration of cytokine in the supernatant.

3.2.21 Metabolic analysis by FLIM

Two-photon excited NAD(P)H- Fluorescence Lifetime Imaging Microscopy (FLIM) was used to measure the levels of free and protein-bound NADH within cells and was performed on a custom multiphoton system. A titanium:sapphire laser (Chameleon, Coherent®) was used for multiphoton excitation. A water-immersion 25x objective (Olympus, 1.05NA) was utilised on an upright (Olympus BX61WI) laser scanning microscope. Two-photon excitation of nicotinamide adenine dinucleotide phosphate (NAD(P)H) fluorescence was performed with 760 nm excitation wavelength. A 455/90 nm bandpass filter was used to isolate NAD(P)H fluorescence signal. 512x512 pixel

images were acquired with a pixel dwell time of 3.81 µs and 30-second collection time. A PicoHarp 300 TCSPC system operating in the time-tagged mode coupled with a PMA hybrid detector (PicoQuanT GmbH) was used for fluorescence decay measurements yielding 256 time bins per pixel. At least three images for each model were acquired. Afterwards, regions of interest (ROI) were selected, and the NAD(P)H fluorescence decay was analysed.

For the NAD(P)H fluorescence decay analysis, an overall decay curve was generated by the contribution of all pixels in the ROI area. Afterwards, it was fitted with a double exponential decay curve (Equation (1):

$$I(t) = \alpha_1 e^{-\frac{t}{\tau_1}} + \alpha_2 e^{-\frac{t}{\tau_2}} + c$$

I(t) represents the fluorescence intensity at time (t) after laser excitation. α_1 and α_2 represent the fraction of the overall signal comprised of a short and long lifetime component, respectively. τ_1 and τ_2 are the long and short lifetime components, respectively. C corresponds to background light. X^2 is calculated to evaluate the goodness of multi-exponential fit to the raw fluorescence decay data—the lowest χ^2 values were considered in this study.

For NAD(P)H, a two-component fit was used to differentiate between the free (τ_1) and protein-bound (τ_2) NAD(P)H. The average lifetime (τavg) of NAD(P)H for each pixel is calculated by a weighted average of both the free and bound lifetime contributions (Equation (2):

$$\tau_{avg} = \frac{(\alpha_1 \times \tau_1) + (\alpha_2 \times \tau_2)}{(\alpha_1 + \alpha_2)}$$

3.2.22 XF Seahorse assays

Primary human macrophages were cultured from monocytes at 1 x 10^6 cells/ml for 6 days prior to re-seeding at 2 x 10^5 cells/well in a Seahorse 96-well microplate and allowed to rest for 5 hours prior to cell treatments with either LPS or cholesterol crystals. Thirty minutes prior to placement into the XF/XFe analyser, cell culture medium

was replaced with complete XF assay medium (Seahorse Biosciences; supplemented with 10 mM glucose, 1 mM sodium pyruvate, 2 mM l-glutamine, and pH adjusted to 7.4) and incubated in a non-CO_2 incubator at 37 °C. Blank wells (XF assay medium only) were prepared without cells for subtracting the background oxygen consumption rate (OCR) and extracellular acidification rate (ECAR) during analysis. Oligomycin (1 mM), carbonyl cyanide-p-trifluoromethoxyphenylhydrazone (FCCP) (1 mM), rotenone (500 nM), and antimycin A (500 nM) and 2-deoxy-d-glucose (2-DG) (25 mM) were prepared in XF assay medium and loaded into the appropriate injection ports on the cartridge plate and incubated for 10 minutes in a non-CO_2 incubator at 37 °C. OCR and ECAR were measured over time with sequential injections of oligomycin, FCCP, rotenone and antimycin A, and 2-DG. Analysis of results was performed using Wave software (Agilent Technologies). The rates of basal glycolysis, max glycolysis, glycolytic reserve, etc. were calculated as detailed in the manufacturer's protocol (Table 3.12)

Table 3-12 Seahorse calculations

Rate	Calculation
Basal glycolysis	Average ECAR values prior to oligomycin treatment – non-glycolytic ECAR
Non-glycolytic ECAR	Average ECAR values after 2-DG treatment
Max glycolysis	Average ECAR values after oligomycin and before FCCP
Basal respiration	Average OCR values prior to oligomycin treatment – non-mitochondrial OCR
Non mitochondrial OCR	Average OCR values after Rotenone/antimycin A treatment
Max respiration	Average OCR values after FCCP & before Rotenone/antimycin A treatment
Mitochondrial ATP reproduction rate	(OCR_{ATP} *2) * P/O ratio[ǂ]
OCR_{ATP}	Average OCR values prior to oligomycin treatment – non-mitochondrial OCR
Glycolytic ATP production rate	Average PER values before oligomycin -- mitoPER
MitoPER	(Average OCR values before oligomycin – Average OCR values after Rotenone/antimycin A treatment) * CO_2 contribution factor (CCF) [ǂǂ].
Total cellular ATP production rate	GlycoATP production rate + MitoATP production rate

[ǂ] P/O ratio = 2.75 pmol ATP/pmol Oxygen (average number of molecules of ADP phosphorylated to ATP per atom of O reduced by an electron pair flowing through the electron transfer chain according to manufacturer).

[ǂǂ] CCF = 0.61 a.u. (empirically derived value to discount CO_2 contribution to XFe96 Analysers, according to manufacturer).

3.2.23 Confocal Imaging

3.2.23.1 Confocal imaging of PKM2 expression

Following cell treatments, cells were fixed with 4% Paraformaldehyde for 15 minutes at room temperature. Cells were washed 3 times with PBS and permeabilised with 0.1% Triton solution for 15 minutes. Cells were washed 3 times with PBS blocked for 1 hour

with 5% (w/v) BSA in PBS. Cells were then incubated in primary antibody (1:100 dilution, rabbit) overnight at 4 °C. Cells were washed 3 times with PBS and then incubated with secondary antibody, anti-rabbit conjugated to Alexa 647 (1:500) for 1 hour. Cells were counterstained with DAPI to stain the nuclei. Cells were imaged using a Lecia SP8 scanning confocal microscope, and image analysis was performed using Imaris™ software.

3.2.23.2 Confocal Imaging of mitochondria

Following cell treatments, cells were incubated with MitoTracker™ Red CMXRos (50 nM) and Hoechst (to counterstain nuclei) (5 μg/ml) and maintained for 30 minutes at 37 °C in a 5% CO_2 atmosphere. Cells were washed 3 times in cold PBS (to protect cell viability) and resuspended in complete media. Cells were imaged immediately using a Leica SP8 scanning confocal microscope and image analysis to quantify mitochondrial morphology was performed using CellProfiler™.

3.2.24 MSC wound scratch assay

Human Mesenchymal stem cells (MSCs) were seeded onto 6 well plates (5 x 10^5 cells /well) and grown to confluence prior to being serum starved for 16 hours. A single scratch wound was induced through the middle of each well with a sterile pipette tip, cells were washed with media to remove lifted cells and media was replaced fresh serum free media. Cells were subsequently either left in serum free control media or cultured in serum free media from unstimulated or electrically stimulated macrophages for 24 hours. MSC migration across the wound margins from 24 hours was assessed and photographed using a phase-contrast microscope (Olympus 1X83). Semi-quantitative analysis of cell repopulation of the wound was assessed by three blinded observers. Tiff images of the scratch wound assays were taken at × 20 magnification at 0 and 24 hours. The mean number of cells that migrated back into the wound was calculated from 3 individual measurements for each wound at each time point. This process was carried out for all biological repeats. Total numbers of cells were also counted in each group to assess for proliferation.

3.2.25 Statistical analysis

All experiments were performed in at least three healthy donors (defined by N), with 3–4 technical replicates run for each experiment (defined by n) depending on the assay

type. Data was assessed with one-way ANOVA for the analysis of more than two groups, with Dunnett's post-test (against controls) or Tukey's multiple comparisons test, where applicable. Paired t-test was used for analysis of only two groups. All statistical analysis was performed on GraphPad Prism™ 9.00 (GraphPad Software) where p value < 0.05 were deemed significant and denoted by an asterisk. *p≤0.05, **p≤0.01, ***p≤0.001, ****p≤0.0001.

Chapter 4 : Investigation of direct and indirect interactions between primary human macrophages and iPSC-Cardiomyocytes

4.1 Abstract

Heart failure is the leading cause of death worldwide. Recent studies have acknowledged a key role of for the immune response and inflammation in this disease, however, there remains a substantial gap in our knowledge regarding the interaction of the immune response with the heart at a cellular level. The aim of this chapter is to generate a co-culture system which incorporates primary human macrophages with iPSC-derived cardiomyocytes, in order to gain insight to the potential role of macrophages in CM function. Two cell lines of iPSCs (11b and GFP-tagged SFCi55) were expanded and a cardiomyocyte differentiation protocol was successfully optimised. The response of primary human macrophages to cardiomyocytes was investigated indirectly via conditioned media, and directly via co-culture studies. Prior to co-culture experiments, the response of macrophages to CM culture media was assessed. It was found that B-27™ supplement, necessary for the maintenance of iPSC-CMs activates a pro-inflammatory response in primary human macrophages. This effect was reduced in the presence of conditioned media or direct co-culture of macrophages with CMs, suggesting that CMs elicit an anti-inflammatory effect on macrophages. Future work fully elucidating the impact of B-27™ supplement on macrophage phenotype will allow for further investigation of the potential immunomodulatory role for CMs with macrophages.

4.2 Introduction

Heart failure accounts for approximately a third of deaths worldwide every year [19]. Myocardial infarction is credited as the most common form of acute cardiac injury attributing to heart failure and while significant advancements have been made in therapies, mortality and morbidity remain high. Novel therapies, including those which target adverse inflammation show promise in pre-clinical studies, however, seldom succeed in clinical trials [195]. Often this failure is attributed to interspecies differences between humans and animal models of heart failure [196]. This challenge greatly impedes the development of novel therapies for CVD and heart failure and illustrates the need for effective *in vitro* models of the human myocardium.

The development of iPSCs in the early 2000's has made a significant impact in the field of tissue engineering, providing a reliable resource of human cells for varied

applications, including cardiac models [197, 198]. iPSC-CMs in the past have acted as effective models for cardiovascular drug models and toxicity screening [145, 146, 199]. However, iPSC-CMs alone still do not represent the complexity of native heart tissue. Multicellular models are required to truly recapitulate the cell-cell interactions which allow the myocardium to function and furthermore provide iPSC-CMs with the necessary cellular cues to achieve a mature CM phenotype [22, 200]. Indeed, the inclusion of non-CM cells such as fibroblasts and endothelial cells in culture with iPSC-CMs has proven to promote significant maturation of iPSC-CMs *in vitro* [150, 201]. In the context of a disease model, *in vitro* cell models allow us to understand heart function and failure at a simpler molecular level, compared to *in vivo* animal models. Furthermore, the generation of a multicellular model allows us to elucidate cellular mechanisms by which non-CMs support healthy CM function, and moreover how this fails in diseased states. For example, it is well acknowledged that a highly regulated intercellular communication network between CMs, and non-CMs is vital in order to mount an efficient wound-healing response post-infarction [21, 22].

As outlined in chapter 2 of this thesis, macrophages play a major role in the epidemiology of both myocardial infarction and subsequent heart failure, with most of our insight gained from the study of animal models [3, 202, 203]. Yet there still remains a substantial gap in our knowledge as to the precise role of macrophages and different macrophages subsets within the myocardium, and how macrophage mediated responses directly affect cardiomyocytes. Furthermore, while recent reports have elucidated a role for resident macrophages in electrical signalling in the myocardium [70], there is much to be explored regarding the adaptation of recruited blood-derived macrophages to this role, as well as the implication of an induced inflammatory phenotype in these cells. This restricted knowledge represents a considerable limitation in the development of macrophage-targeted treatments of heart failure.

Efforts to generate *in vitro* macrophage-CM models have only emerged very recently in the literature, involving simplified co-culture systems which investigate both direct and indirect cellular communication between CMs and macrophages [204-206]. In a study by Ai *et al*. from 2018, the effects of LPS-treated RAW 264.7 macrophages were assessed with H9c2 rat CM [204]. Using a microfluidic chamber device, it was demonstrated that

secreted factors from LPS-treated macrophages promoted apoptosis of CMs, thus creating a model for inflammation-induced myocardial injury [204]. However, conflicting findings were later observed by Hitscherich *et al*., where the impact of macrophage polarisation on CM function was investigated through a controlled *in vitro* inflammatory model (again using RAW macrophages) [206]. In this study it was found that conditioned media from macrophages did not affect CM apoptosis, as indicated by expression levels of apoptosis-mediators BAX and BCL-2 [206]. An *in vitro* model consisting of primary human cells may help to delineate these contrasting findings, and fully elucidate the impact of macrophages on CM function.

In addition to characterising CM response to blood-derived macrophages, it is of equal importance to understand the influence of CMs on macrophage phenotype, of which there is limited knowledge. Recent work has begun to explore this through conditioned media experiments. For example, Paiva *et al*. highlighted the ability of CMs to activate primary human macrophages indirectly through secretion of extracellular vesicles (EV) [207]. Treatment with CM-derived EV resulted increased phagocytic capacity of RAW macrophages, in addition to increased iNOS expression and NF-κB activation [207]. This response was disrupted in ischemic CMs, highlighting how intercellular signalling is altered in settings of inflammation/injury. Again, while this work represents novel findings, there remains the question of whether these results will translate to human cells.

4.3 Chapter Aims

There is a growing appreciation for the functional role of macrophages in the myocardium, and a clear need to characterise the intercellular interactions between blood-derived macrophages and tissue resident cardiomyocytes. Better understanding of these interactions will pave the way towards the incorporation of macrophages in multicellular *in vitro* cardiac models, and furthermore, the development of macrophage-specific therapeutics for heart failure. The aim of this chapter, therefore, is to generate an *in vitro* model which incorporates both human iPSC-CM and primary human macrophages to study these interactions, both indirectly through conditioned media, and directly via a co-culture system. From this, insight can be gained on the functional role of infiltrating macrophages in the healthy heart.

Furthermore, studies to date have highlighted the potential alteration of macrophage-CM crosstalk under settings of injury or inflammation and have speculated this disruption is a significant contributor to cardiac dysfunction observed post-infarction [207]. Therefore, the second aim of this chapter is to induce an inflammatory response in macrophages and investigate the impact this has on CM-macrophage signalling.

Specific aims:

- To determine the intercellular interactions between iPSC-CMs and primary human macrophages through an indirect, and direct co-culture model.
- To investigate the impact of M1 macrophages on CM-macrophage crosstalk.

4.4 Results

4.4.1 iPSCs can be successfully cultured and differentiated to functioning cardiomyocytes

An important requisite for this chapter was the successful culture of iPSCs, and optimization of a differentiation protocol to beating cardiomyocytes. The 11b cell line of iPSCs, (originating from healthy adult male fibroblasts) and GFP-tagged SFCi55 (originating from healthy female fibroblasts) were expanded in the lab following protocols outlined in sections 3.2.8, and 3.2.9, and in doing so, culture conditions were optimized. Cells were stained for the pluripotency marker OCT3/4 and analysed by flow cytometry to ensure cell pluripotency was maintained throughout culture (Figure 4.1). Differentiation of cardiomyocytes was carried out following the protocol previously published by Lian *et al*. [191]. This protocol required optimisation of treatment timing, as well as identification of the optimal concentration of GSK inhibitor CHIR99021. Table 4.1 below highlights the numerous parameters optimized in this process. Successful differentiation to cardiomyocytes was achieved with both cell lines, yielding a robust population of beating cardiomyocytes. Purity of differentiated cells were assessed using flow cytometry, by expression of cardiac specific markers Cardiac Troponin T (CTnT) and Myosin light chain 2 – atrial (MLC2a). CTnT/MLC2a expression was found to be routinely >75 % (Figure 4.2).

Table 4-1 Optimised parameters of iPSC culture and differentiation to cardiomyocytes

Parameter	Previously reported [191]	11b	SFCi55
Seeding Density	$1x10^6$ cells/ml	1/5 split from 80% confluent well	1/4 split from 80% confluent well
Days of culture preceding Day 0 of differentiation	4	4 (95% Confluency)	3 (95% Confluency)
ROCK inhibitor pre-treatment	None	10 µM for 1 hour prior to CHIR treatment	10 µM for 1 hour prior to CHIR treatment
CHIR concentration	Ranging from 6 µM to 14 µM	10 µM	10 µM
IWP2 concentration	5 µM	5 µM	5 µM

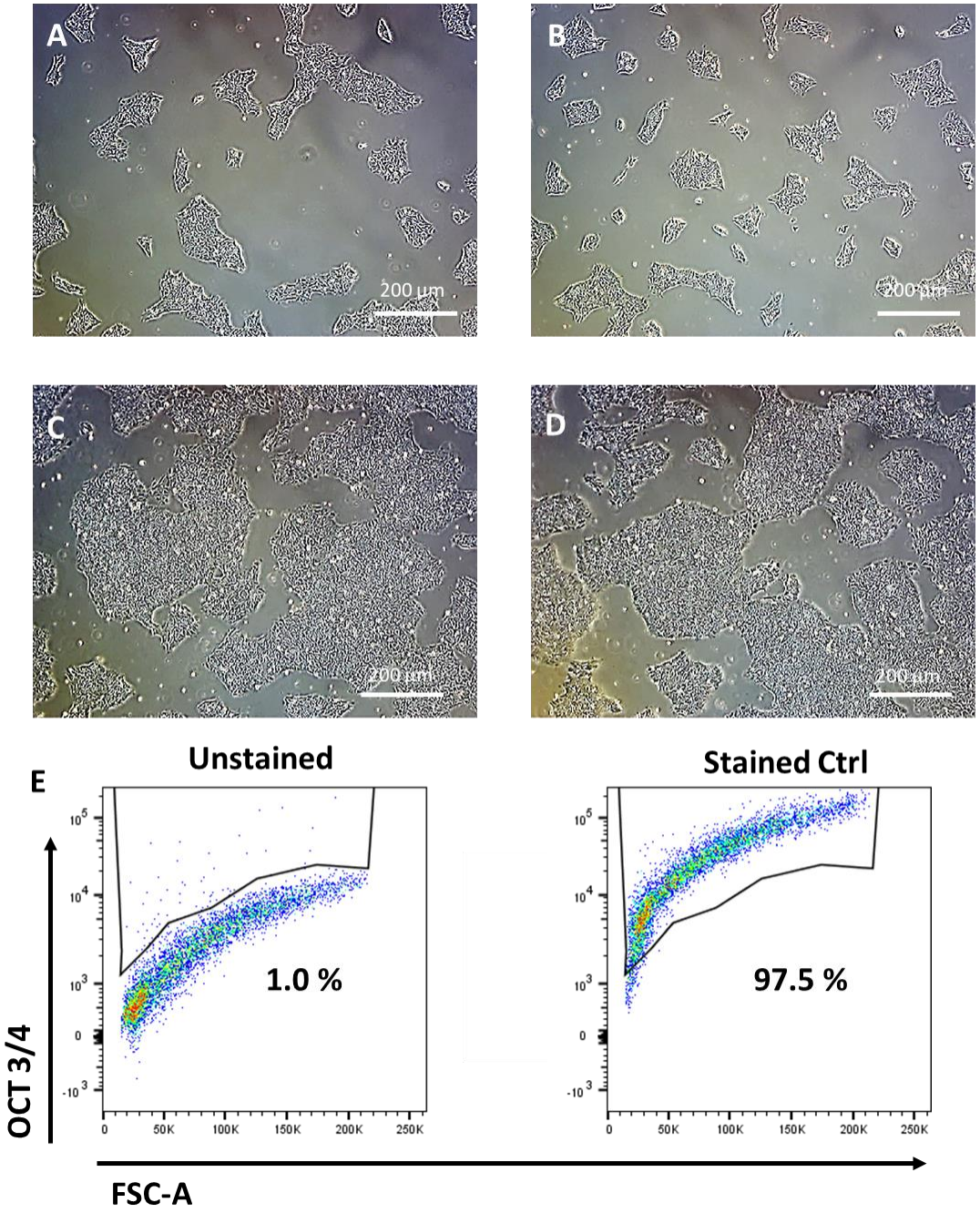

Figure 4-1 – Characterisation of iPSCs

iPSCs were expanded in 6 well plates and assessed for pluripotency by flow cytometry. **(A**) and (**B**) are representative images of cells Day 1 after passage. (**C**) and (**D**) are representative images of cells day 3 after passage. (**E**) Representative flow plots of unstained and stained iPSCs showing expression of pluripotency marker OCT3/4.

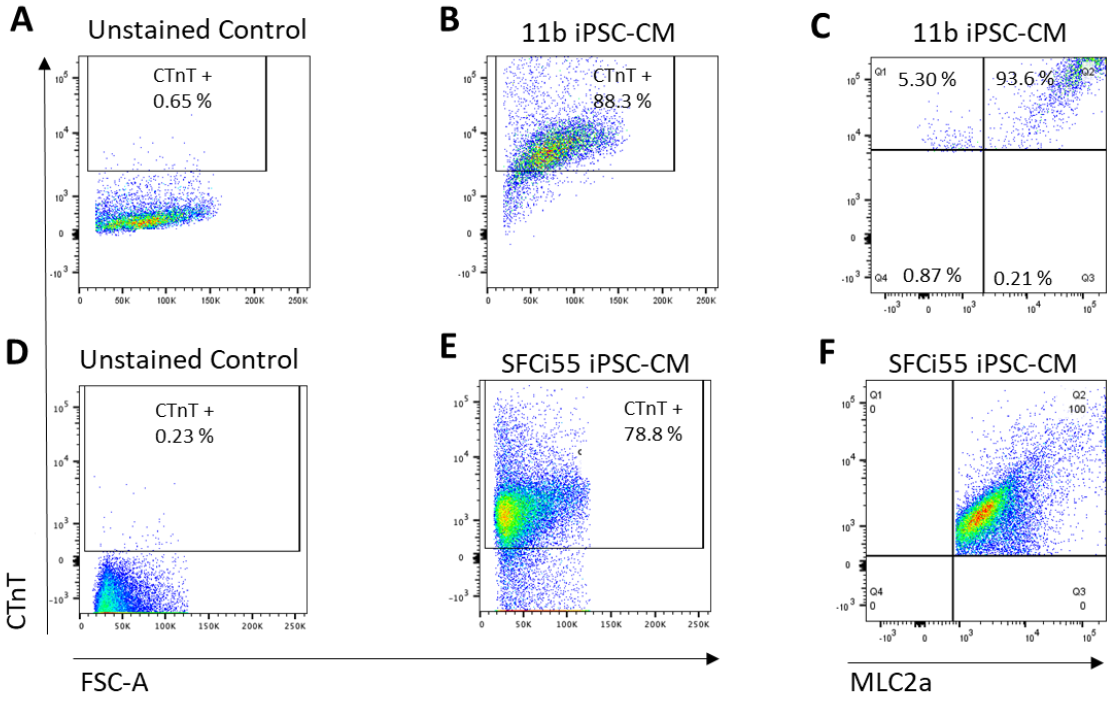

Figure 4-2 – Characterisation of iPSC-CMs

iPSCs were expanded and differentiated to iPSC-CMs using the previously established GiWi protocol. Purity of iPSC-CMs was assessed using flow cytometry. **(A**) Negative unstained control of cardiomyocyte marker Cardiac Troponin (11b cell line). (**B**) iPSC-derived Cardiomyocytes (11b). (**C**) iPSC-derived cardiomyocytes stained for cardiomyocyte markers cardiac troponin T (CTnT) and Myosin light chain atrial (MLC2a) (11b). (**D**) Negative unstained control of cardiomyocyte marker Cardiac Troponin (SFCi55 cell line). (**E**) iPSC-derived Cardiomyocytes (SFCi55). (**F**) iPSC-derived cardiomyocytes stained for cardiomyocyte markers cardiac troponin T (CTnT) and Myosin light chain atrial (MLC2a) (SFCi55).

4.4.2 RPMI supplemented with B-27™ does not impact viability of primary human macrophages

Culture of iPSC-CMs is carried out using standard RPMI media, supplemented with the serum-free supplement B-27™. For future experiments involving conditioned media from CMs and direct co-cultures, it was important to ensure this media supplement did not negatively impact macrophage viability. Primary human macrophages were treated with RPMI/B-27™ media, either with a 50:50 ratio of RPMI/FBS, to RPMI/B-27™ to match conditioned media experiments, or with 100% RPMI/B-27™ to recapitulate co-culture conditions. Cells cultured in 100 % RPMI/FBS were used as an untreated control. Cell viability was assessed after 24 hours by flow cytometry (Figure 4.3). No significant difference in cell viability was detected in comparison to untreated cells, allowing experiments to proceed with RPMI/B-27™ conditioned media.

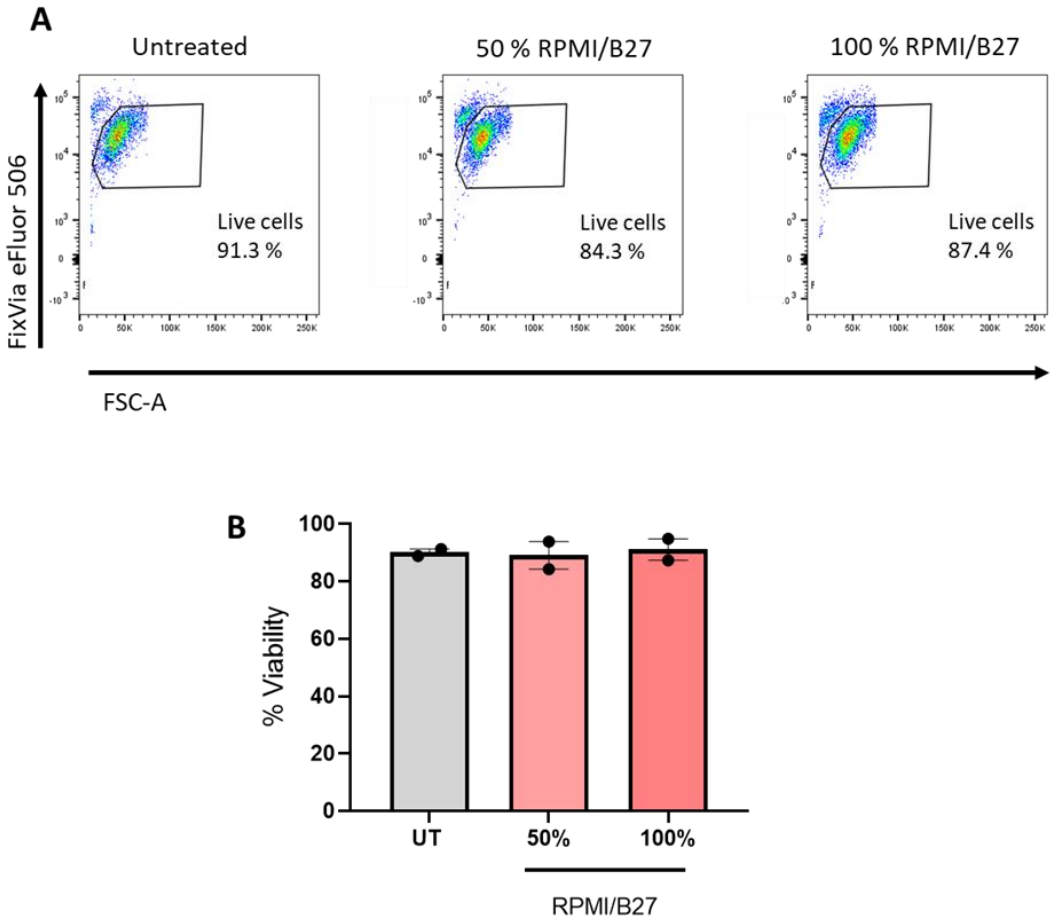

Figure 4-3 – RPMI media supplemented with B-27™ does not impact viability of primary human macrophages.

Primary human macrophages (1 x 10^6 cells/ml) were left untreated (in RPMI with FBS), or treated with 50% RPMI/B-27™ (50% RPMI/FBS) or 100% RPMI/B-27™ for 24 hours. Cells were stained with viability dye FixVia eFluor™ 506 and analysed by flow cytometry. (**A**) Representative flow plots showing viability of untreated, and treated macrophages. (**B**) Bar graph showing pooled data of % viability of untreated and treated cells (N = 2). Data is shown as mean ± SEM and was analysed using One Way Anova with Tukey's post-test.

4.4.3 Conditioned media from iPSC-CMs does not impact viability of primary human macrophages

To begin investigating CM-macrophage interactions, conditioned media experiments were conducted to assess the effect of CM-derived factors on primary human macrophages. Prior to characterising macrophage response, cell viability was first assessed. Primary human macrophages were left untreated, or else treated with RPMI/B-27™ media, or CM-conditioned media for 24 hours. Media treatments were carried out at a 1:1 ratio (50% RPMI/FBS, 50% RPMI/B-27™) to avoid subjecting macrophages to completely spent media. Cells were stained for viability using FixVia eFluor™ 506 and assessed by flow cytometry. Results of this experiment revealed that treatment with CM-conditioned media had no significant effect on macrophage viability, compared to both RPMI/B-27™ media, and RPMI/FBS (Figure 4.4).

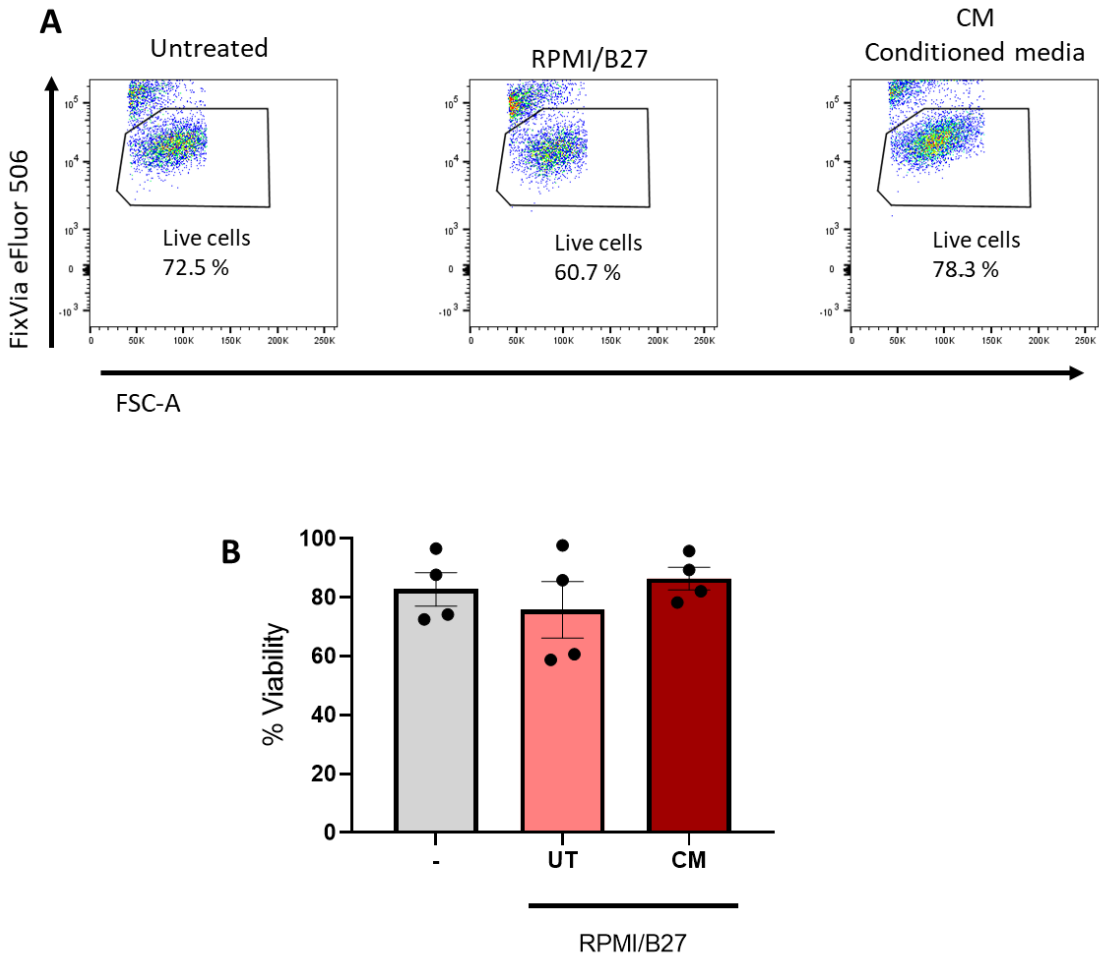

Figure 4-4 – CM-conditioned media does not impact viability of primary human macrophages

Primary human macrophages (1 x 10^6 cells/ml) were left untreated as a negative control (-) or treated with 50% RPMI/B-27™ or 50% CM-conditioned media for 24 hours. Cells were stained with viability dye FixVia eFluor™ 506 and analysed by flow cytometry. (**A**) Representative flow plots showing viability of untreated, and treated macrophages. (**B**) Bar graph shows pooled data of % viability of untreated and treated cells (N = 4). Data is shown as mean ± SEM and was analysed using One Way Anova with Tukey's post-test.

4.4.4 RPMI/B-27™ alone promotes significant cytokine production in primary human macrophages

Having observed no changes in cell viability, macrophage response to conditioned media was next assessed, firstly through assessment of cytokine production. Primary human macrophages were left untreated, or else treated with RPMI/B-27™ or CM-conditioned media for 24 hours. Levels of TNF, IL-6, IL-8 and IL-10 were assessed in cell supernatants by ELISA. It was observed that RPMI/B-27™ alone caused significant production of IL-6 (increase of 2293 pg/ml ± 1478 pg/ml), IL-8 (increase of 30362 pg/ml ± 4308 pg/ml), and IL-10 (increase of 585 pg/ml ± 61.39 pg/ml), but not TNF in primary human macrophages (Figure 4.5). A similar effect was observed in response to conditioned media, although the presence of CM-derived factors appeared to reduce IL-6 and IL-8 production induced by B-27™. Ultimately, the results indicated that B-27™ supplement activates primary human macrophages, highlighting the importance of assessing all culture conditions when generating a co-culture model. Additional experiments were carried out to further characterise this response.

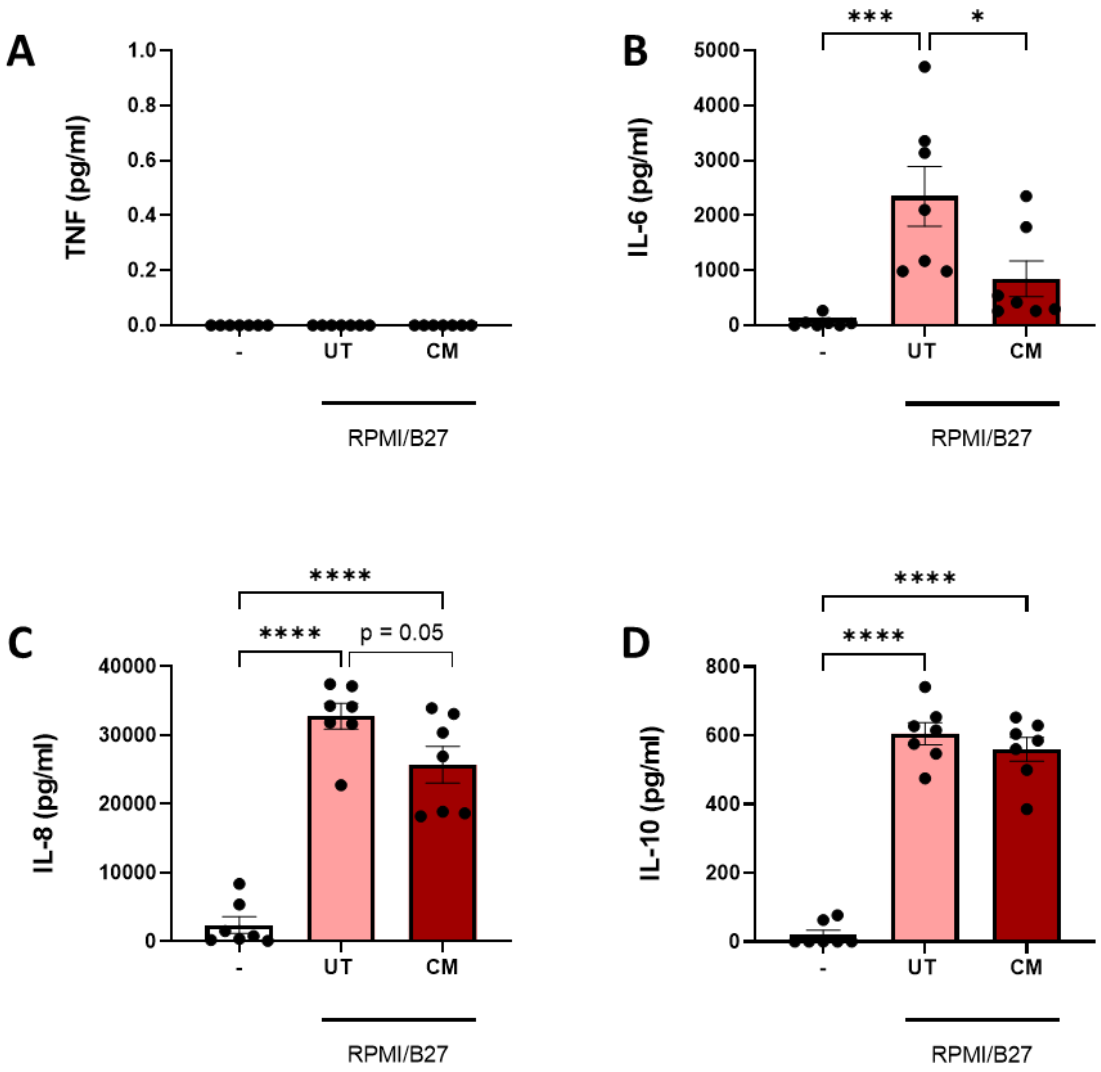

Figure 4-5 – B-27™ supplement drives production of IL-6, IL-8, and IL-10 but not TNF in primary human macrophages.

Primary human macrophages (1 x 10^6 cells/ml) were left untreated as a negative control (-) or treated with 50% RPMI/B-27™ or 50% CM-conditioned media for 24 hours. (**A-D**) Levels of TNF, IL-6, IL-8 and IL-10 were analysed in cell supernatants by ELISA (N = 7, n = 3). Data is shown as mean ± SEM and was analysed using One Way Anova with Tukey's post-test. *p≤0.05, *** ≤0.001, ****p ≤0.0001

4.4.5 RPMI/B-27™-induced cytokine production is not due to endotoxin contamination

Given the significant production of cytokines observed in response to B-27™ supplement, it was important to ensure this effect was not due to endotoxin/LPS contamination using the HEK-Blue™ human TLR4 assay system. These cells stably express the LPS receptor, TLR4, and a secreted alkaline phosphatase (SEAP) reporter gene, the expression of which is under the control of NF-kB. The HEK-Blue™ human TLR4 assay, shows similar levels of sensitivity as the Limulus Amoebocyte Lysate (LAL) assay (the LAL assay is able to detect 0.005 EU/ml LPS, whereas the HEK-Blue™ assay detects 0.01 EU/ml LPS), therefore presenting as a suitable alternative to the LAL assay, which can often be limited by the possibility of test samples directly interacting with LAL reagent, thus interfering with assay results.

HEK-Blue™ TLR4 cells were stimulated with either LPS (0.1-100 ng/ml; positive control), or RPMI/B-27™ media for 24 hours. SEAP expression was then examined by incubating cell supernatants with HEK-Blue™ detection media for 15 minutes and absorbance was monitored at 650 nm. Results indicated that RPMI/B-27™ media did not contain endotoxins (Figure 4.6).

For further confirmation that RPMI/B-27™ was free of contamination, the RPMI/B-27™ media was also filtered through a sterile syringe filter (0.22 µm pore size) before treatment with macrophages. Primary human macrophages were left untreated, or else treated with RPMI/B-27™ (unfiltered and filtered) for 24 hours. Levels of cytokine in cell supernatant were assessed by ELISA. To ensure that B-27™ itself did not cause non-specific binding in the ELISA, thus creating a false positive signal, media that had not been in contact with cells (i.e. directly from the media bottle) was also tested as a cell-free control.

Results of this experiment demonstrated that cell-free media alone did not cause a positive signal for IL-6, IL-8, or IL-10 production (Figure 4.7). Therefore, the observed production of cytokine by ELISA was derived from B-27-treated macrophages, and not a result of non-specific binding of the media supplement in the assay. Furthermore, sterile filtering the media prior to cell treatments had no effect on B-27™-induced cytokine production. These findings taken together with the results of the endotoxin assay

indicate that B-27™ alone directly promotes cytokine and chemokine production in primary human macrophages.

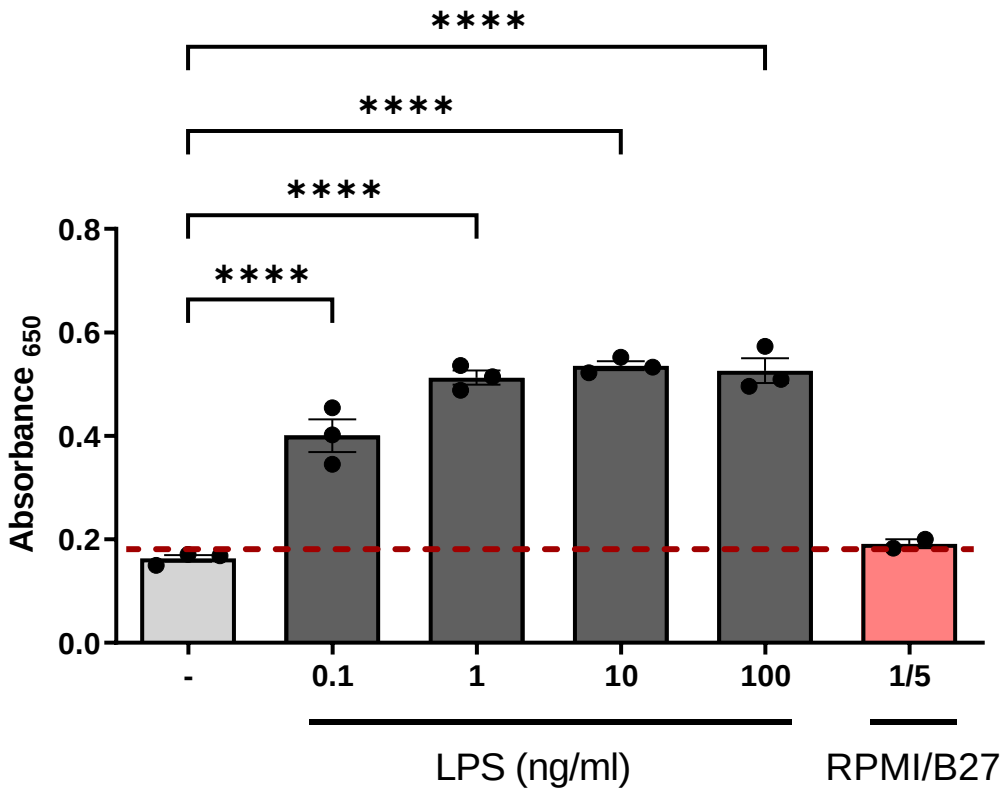

Figure 4-6 – RPMI/B-27™ is free of endotoxin contaminants

HEK-blue cells (5 x 10^5 cells/ ml) were left either untreated as a negative control (-), stimulated with LPS (0.1-100 ng/ml) (as a positive control) or stimulated with RPMI/B-27™ (1:5 dilution) for 24 hours. The expression of SEAP was measured by absorbance at 650 nm. Data is representative of 2 independent experiments (N = 2, n =3) and represented as mean ± SEM. Data was analysed using One Way ANOVA with Dunnett's post-test. ****p ≤0.0001

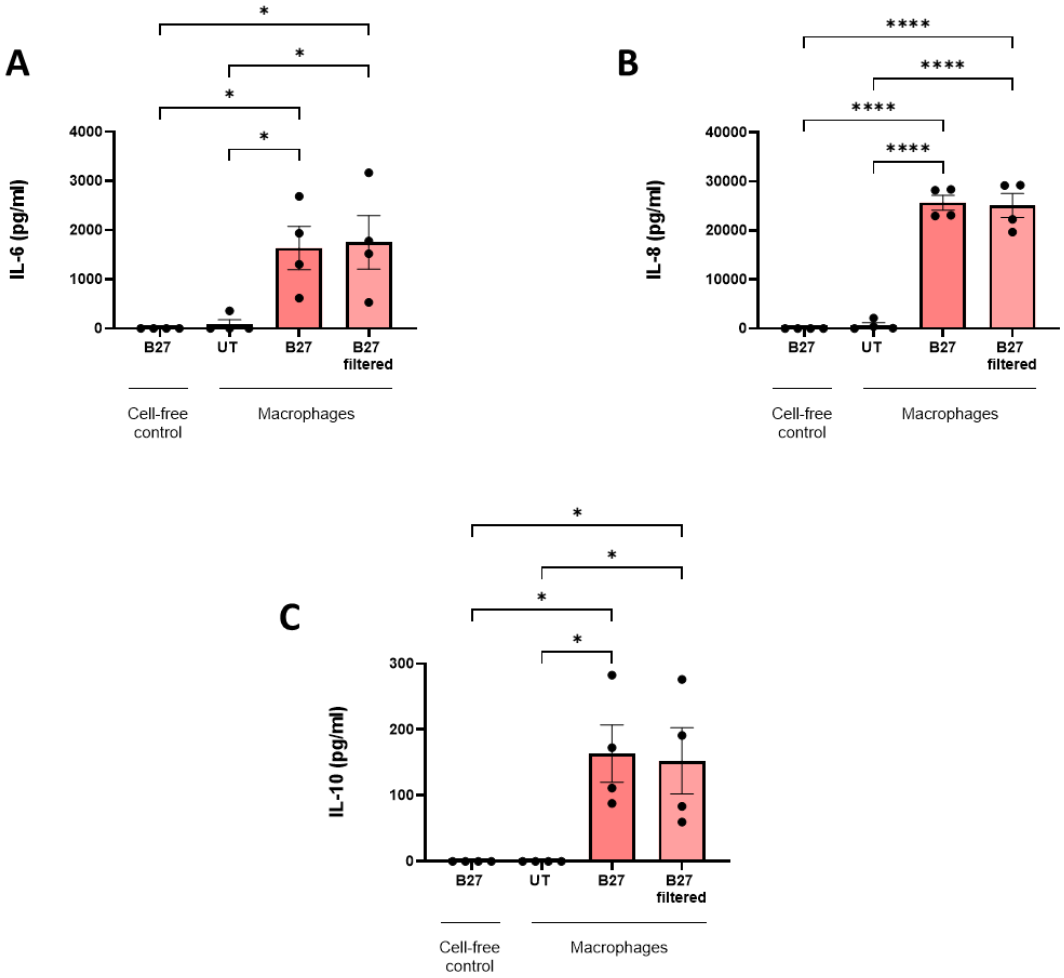

Figure 4-7 – Filtration of RPMI/B-27™ media does not impact B-27™-induced production of cytokines

Primary human macrophages (1 x 10^6 cells/ml) were left untreated as a negative control (UT) or treated with 50% RPMI/B-27™, (unfiltered or filtered) for 24 hours. (**A-C**) Levels of IL-6, IL-8 and IL-10 were analysed in cell supernatants by ELISA (N = 4, n = 3). As a cell-free control, RPMI//B-27™ that had not been in contact with macrophages (i.e., media directly from the bottle) was also assessed by ELISA. Data is shown as mean ± SEM and was analysed using One Way Anova with Tukey's post-test. *p≤0.05, ****p ≤0.0001

4.4.6 Conditioned media from cardiomyocytes, but not RPMI/B-27™, significantly reduces capacity of primary human macrophages to uptake model antigen DQ-Ovalbumin

To further explore the effect of B-27™ supplement on primary human macrophages, it was next of interest to assess cell capacity to process antigens following treatment with either RPMI/B-27™ alone or conditioned media. Activation of macrophages is often accompanied by an alteration to phagocytic capacity. Classically activated macrophages in response to LPS typically exhibit a reduced capacity for phagocytosis and antigen uptake [208], while anti-inflammatory macrophages exhibit an increase in antigen uptake [209]. Given the robust response in cytokine production observed following treatment with B-27™ supplement, it was of interest to investigate whether B-27™ caused any reduction in antigen-uptake capacity or antigen processing, in line with classical activation. Primary human macrophages were left untreated, or else treated with RPMI/B-27™ or CM-conditioned media for 24 hours. Cells were then incubated with model antigen, FITC-conjugated DQ-Ovalbumin (DQ-Ova; 500 ng/mL) and assessed by flow cytometry. Interestingly, CM-conditioned media significantly reduced the antigen-uptake capacity of macrophages (decrease of 42.37% ± 12%), but not RPMI/B-27™ alone (Figure 4.8). This suggests that the CM secretome, and not B-27™ supplement, potentially promotes activation/maturation of primary human macrophages.

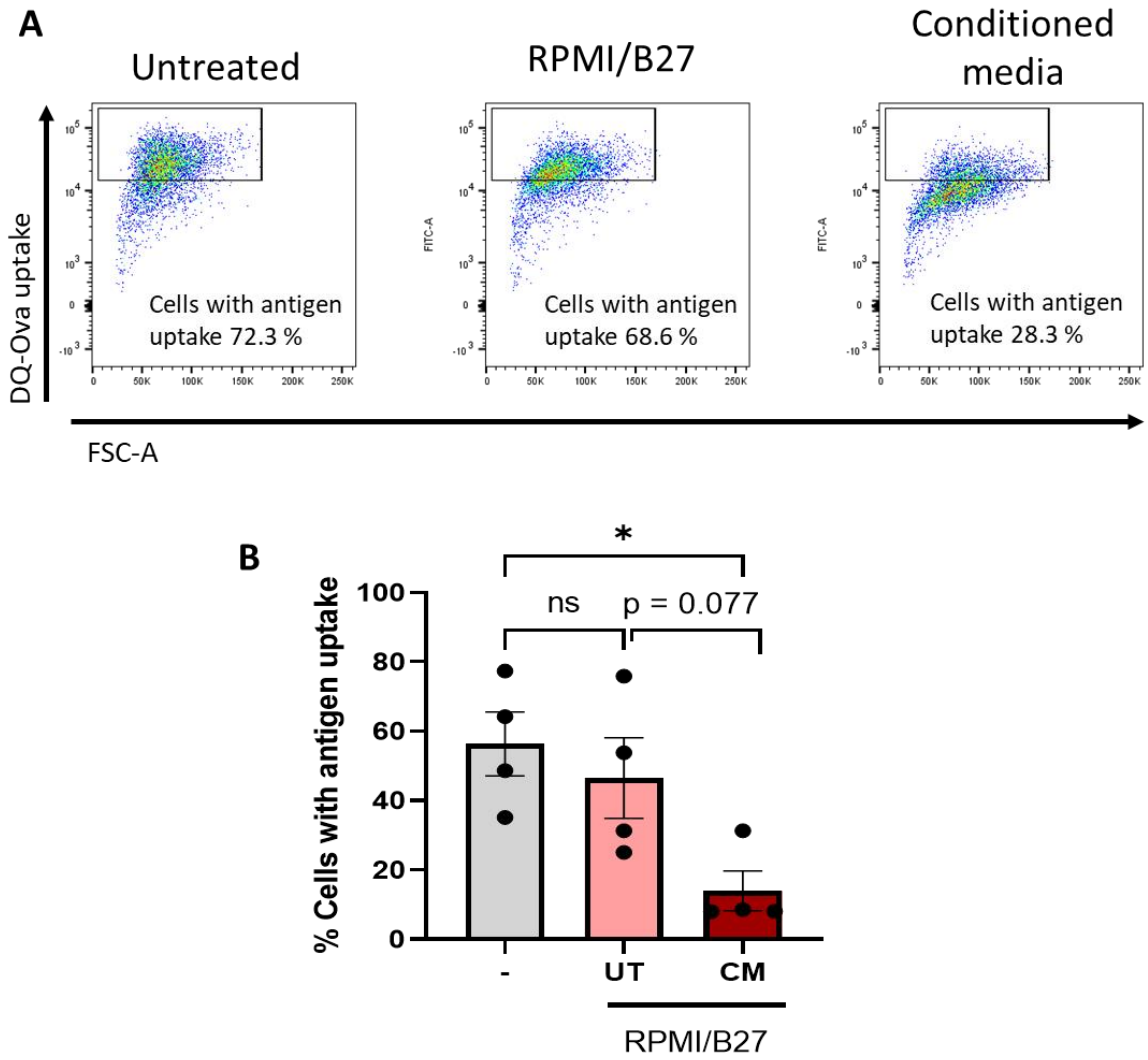

Figure 4-8 – CM-conditioned media reduces the capacity of primary human macrophages to uptake model antigen DQ-Ovalbumin.

Primary human macrophages (1 x 10^6 cells/ml) were left untreated as a negative control (-) or treated with RPMI/B-27™ or CM-conditioned media for 24 hours. Cells were then incubated with model antigen FITC-conjugated DQ-Ovalbumin (500 ng/ml) and analysed by flow cytometry. (**A**) Representative flow plots showing % uptake of DQ-Ova in untreated and treated macrophages. (**B**) Bar graph showing pooled data of % cells with antigen uptake in untreated and treated macrophages (N = 4). Data is shown as mean ± SEM and analysed using One Way Anova with Tukey's post-test. *p≤0.05

4.4.7 RPMI/B-27™ alone does not induce expression of surface maturation markers in primary human macrophages.

To further investigate potential activation of macrophages in response to either RPMI/B-27™ or conditioned media, surface maturation marker expression was next assessed. Primary human macrophages were treated with LPS (100 ng/ml) as a positive control, or RPMI/B-27™ or CM-conditioned media for 24 hours. Expression of M1-associated surface markers CD80, CD86, as well as M2-associated markers CD163, CD206 were assessed by flow cytometry. Median fluorescence intensity (MFI) values for each marker were determined and expressed as a % relative to untreated cells. Results showed no significant increase in expression of any surface markers, in response to either RPMI/B-27™ alone or conditioned media (Figure 4.9).

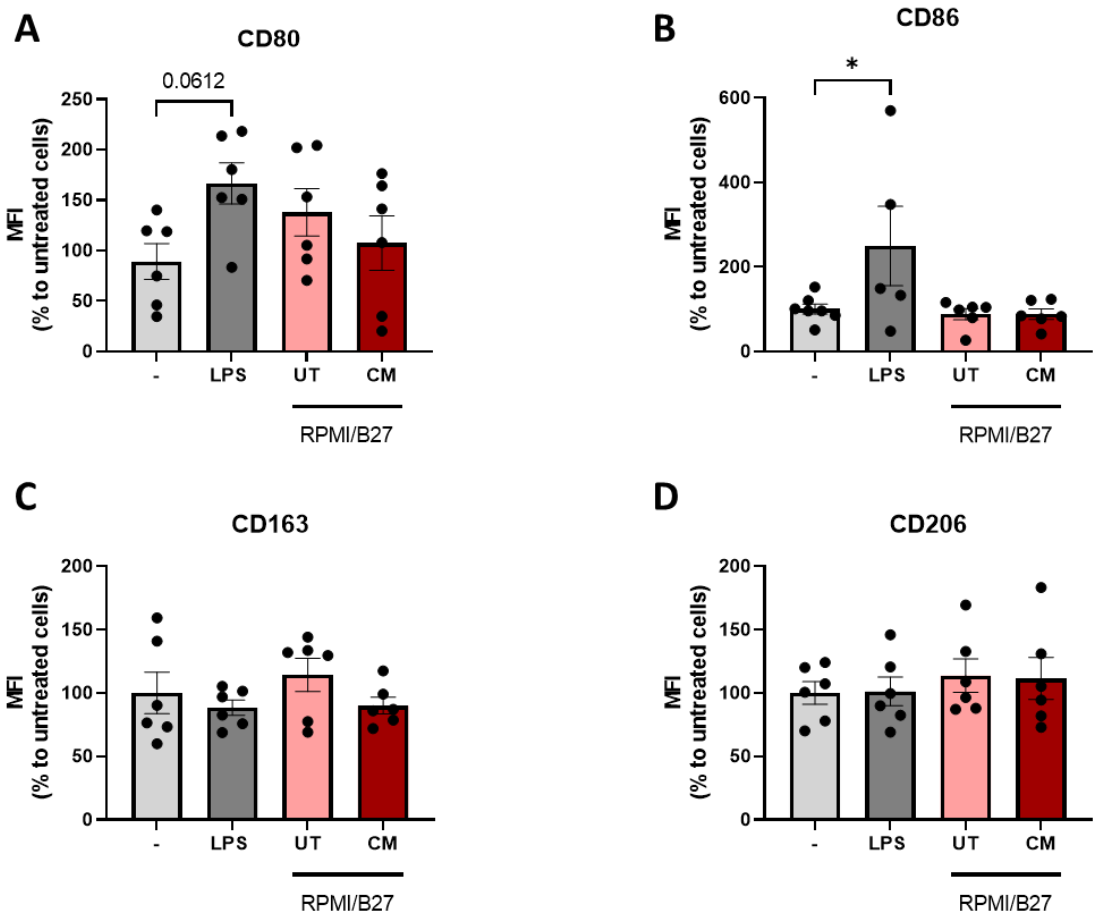

Figure 4-9 – RPMI/B27 does not promote expression of surface maturation markers in primary human macrophages

Primary human macrophages (1 x 10^6 cells/ml) were left untreated as a negative control (-), stimulated with LPS (100 ng/ml) as a positive control, or treated with RPMI/B-27™ or CM-conditioned media for 24 hours. (**A-D**) Expression of CD80, CD86, CD163, and CD206 was assessed by flow cytometry. Bar graphs show pooled data of % of median fluorescence intensity (MFI) of surface markers relative to untreated cells (N = 6). Data is shown as mean ± SEM and analysed using One Way Anova with Tukey's post-test. *p≤0.05

4.4.8 Conditioned media from cardiomyocytes promotes expression of chemokine receptors CCR2 and CX3CR1 in primary human macrophages.

Infiltration of blood-derived monocytes and macrophages into the heart has been shown to be mediated through CCR2-CCL2 signalling [210]. It was of interest to investigate if secreted factors from cardiomyocytes played any role in the recruitment of macrophages. Furthermore, having observed potential activation of macrophages by B-27™ alone, it was also of interest to investigate if this media supplement would also alter expression of the chemokine receptor. Primary human macrophages were left untreated, or else treated with RPMI/B-27™ or CM-conditioned media for 24 hours. Expression of CCR2 was then assessed using flow cytometry. A significant increase in expression of CCR2 was observed in macrophages in response to conditioned media (65.41% ± 36.18%), but not RPMI/B-27™ alone (Figure 4.10 A,C). Studies from mouse models have demonstrated that in addition to CCR2, macrophages can be recruited into the heart via CX3CR1-mediated signalling [86]. Therefore, expression of CX3CR1 was also assessed in response to conditioned media. Similar to results observed with CCR2, an increase in CX3CR1 expression was observed in response to conditioned media (123.2% ± 88.81%), but not RPMI/B-27™ alone (Figure 4.10 B,D). These findings indicate that cardiomyocytes, even under conditions of homeostasis, secrete chemotactic factors to recruit blood-derived macrophages.

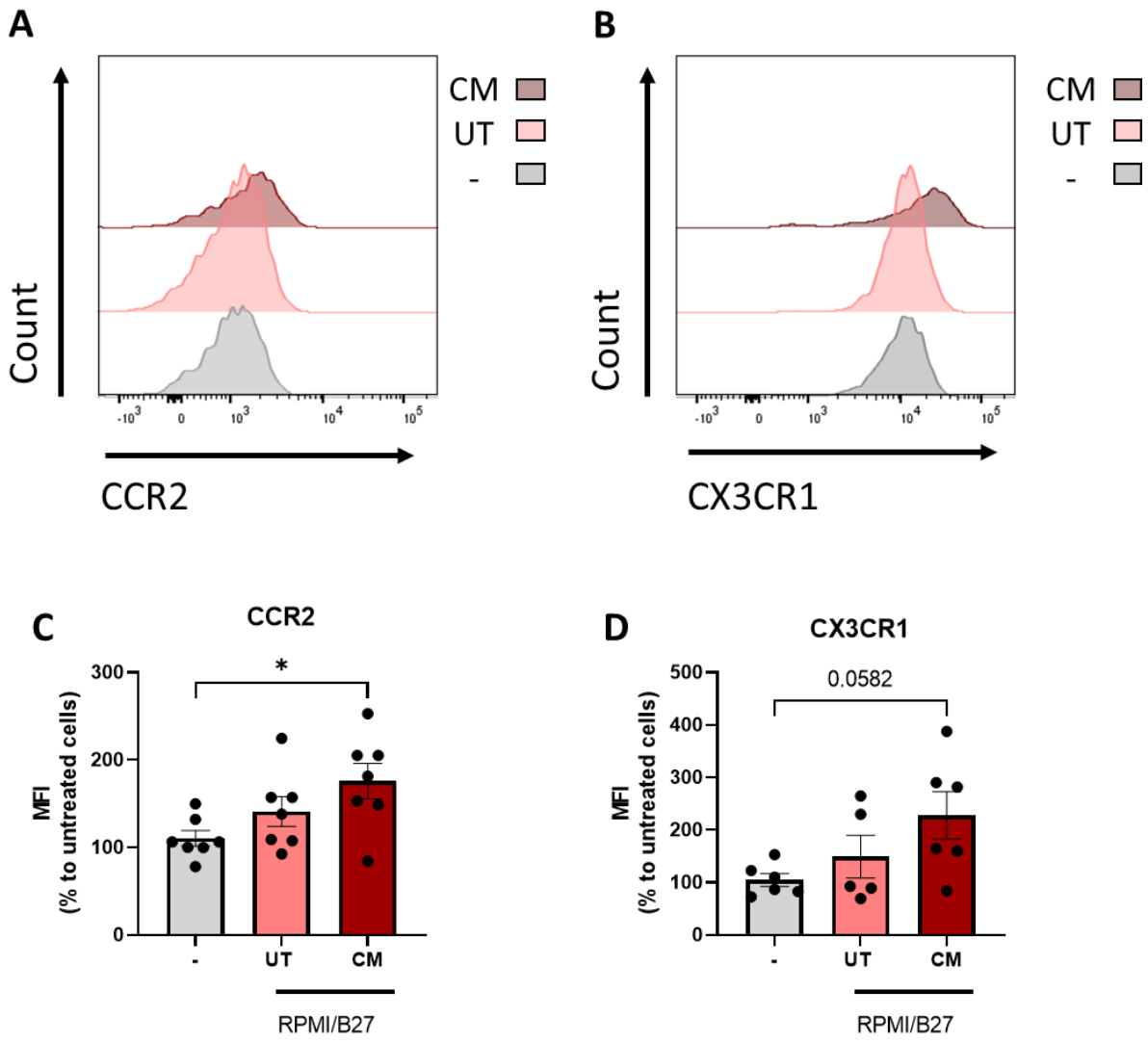

Figure 4-10 – CM-conditioned media promotes expression of chemokine receptors CCR2 and CX3CR1 in primary human macrophages

Primary human macrophages (1 x 10^6 cells/ml) were left untreated as a negative control (-) or treated with RPMI/B-27™ or CM-conditioned media for 24 hours. Expression of CCR2 and CX3CR1 were assessed by flow cytometry (N = 6-7). (**A-B**) Representative histogram showing MFI of CCR2 and CX3CR1 in untreated and treated macrophages. (**C-D**) Bar graphs showing pooled data of % MFI relative to untreated cells. Data is shown as mean ± SEM and analysed using One Way Anova with Tukey's post-test. *p≤0.05

4.4.9 RPMI/B-27™ alone promotes expression of gap junction protein Connexin 43 in primary human macrophages

It is uncertain whether blood-derived macrophages upon infiltration to the myocardium adopt the functional role of tissue resident cells in electrical coupling. To begin exploring this, it was of interest to investigate if CM-secreted factors showed any effect on macrophage expression of gap junction protein, Connexin 43. However, given the observed activation of cells from B-27™ alone, it was important to ensure that any potential alterations to Connexin 43 expression were due to CM-secreted factors and not media alone. Primary human macrophages were left untreated, or else treated with RPMI/B-27™ or CM-conditioned media for 24 hours. Cells were lysed and protein expression of Connexin 43 was assessed by western blot (Figure 4.11). It was observed that RPMI/B-27™ alone showed increased expression of Connexin 43 (0.6104 fold change increase ± 0.2361 relative to untreated), approaching significant difference compared to untreated cells (p value = 0.0721), suggesting that B-27™ may skew any further experiments investigating Connexin 43 mediated signalling.

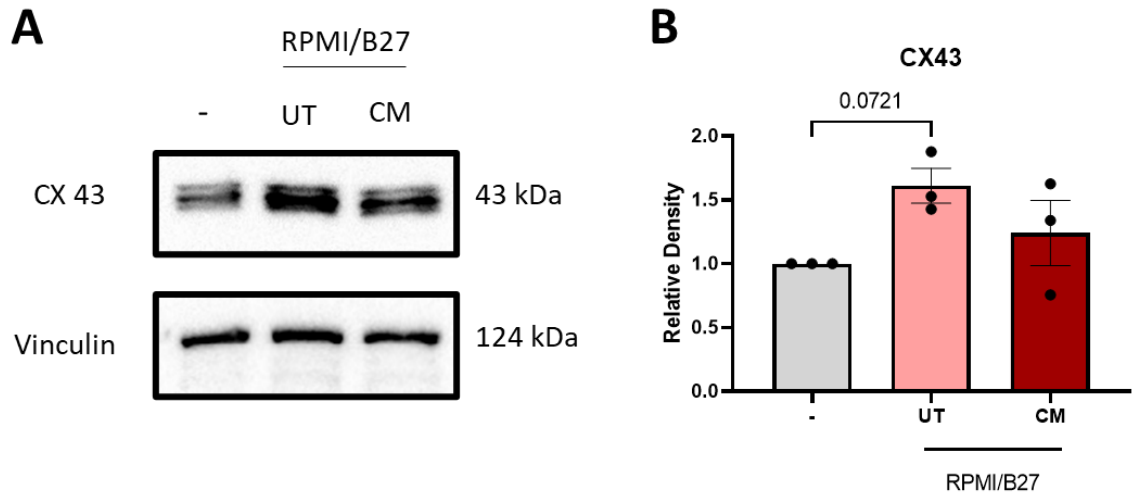

Figure 4-11 – RPMI/B-27™ alone promotes increased expression of gap junction protein Connexin 43.

Primary human macrophages (1 x 10^6 cells/ml) were left untreated as a negative control (-) or treated with RPMI/B-27™ or CM-conditioned media for 24 hours. Expression of Connexin 43 (CX 43) protein was assessed by western blot. (**A**) Representative western blot of untreated, and treated macrophages with RPMI/B27 alone or CM-conditioned media. (**B**) Densitometric analysis of western blots (N = 3) using Biorad software. Bar graphs illustrate the mean ± SEM increase in protein expression relative to untreated control and normalised to vinculin housekeeping protein. Data was analysed using One Way ANOVA and Tukey's post-test.

4.4.10 B-27™-induced cytokine production is reduced in macrophages co-cultured with iPSC-CMs

Findings from B-27™-treated macrophages thus far demonstrated that the supplement promotes robust production of cytokines IL-6, IL-10, and chemokine IL-8, as well as increased expression of Connexin 43. It was of interest to investigate if this response occurred in direct co-cultures of iPSC-CM and primary human macrophages. Primary human macrophages were cultured at a ratio of 1:5 with iPSC-CMs (2 x 10^5 macrophages: 1 x 10^6 CM) for 24 hours. Macrophages were also plated in RPMI/B-27™ media (absent of iPSC-CMs) as a control for B-27-mediated cytokine production. Additionally, as iPSC-CMs in the co-culture group require Matrigel©, macrophages were plated in RPMI/B-27™ media (absent of iPSC-CMs) in Matrigel-coated plates as a further control, to ensure any effects observed in the co-culture, were a result of cell-cell interactions, and not due to presence of Matrigel© proteins.

Levels of IL-6, IL-8, and IL-10 were analysed in cell supernatants by ELISA. Interestingly, results of this experiment reveal that direct co-culture of macrophages and iPSC-CMs significantly reduced B-27™-induced production of IL-6 (decrease of 1951 pg/ml ± 695 pg/ml) and IL-8 (decrease of 12651 pg/ml ± 2002 pg/ml) (Figure 4.12 A-B). No significant difference was observed in levels of B-27™-induced IL-10 (Figure 4.12 C). These results are similar to the observed effect of conditioned media from CMs and suggest that CMs potentially elicit an immunomodulatory effect on primary human macrophages. However, due to the adverse response driven by B-27™ alone, this cannot be taken as an accurate representation of physiological interactions *in vivo*.

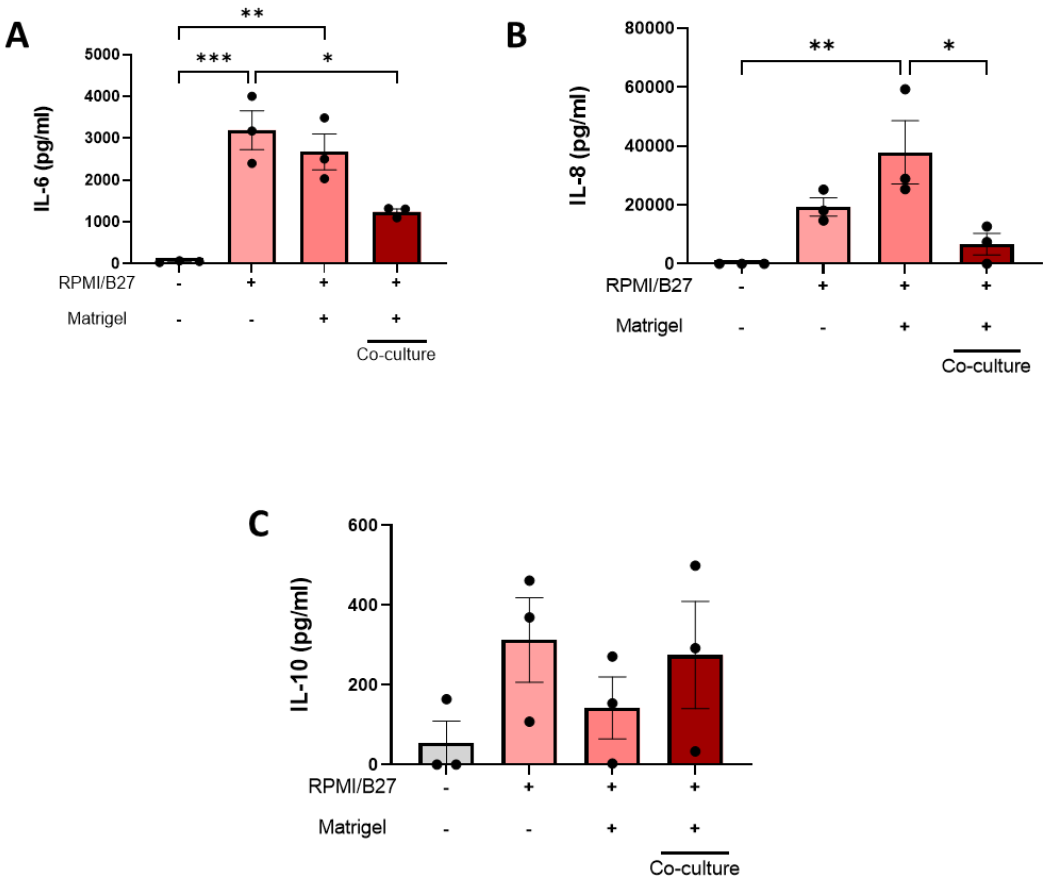

Figure 4-12 – Direct co-culture of primary human macrophages with iPSC-CMs reduces IL-6 and IL-8 production, but not IL-10 in primary human macrophages.

Primary human macrophages were cultured at a ratio of 1:5 with iPSC-CMs (2 x 10^5 macrophages: 1 x 10^6 CM) for 24 hours. As additional controls, primary human macrophages (1 x 10^5 cells/ml) were cultured in 100% RPMI/FBS, or 100% RPMI/B-27™ in the presence/absence of Matrigel©. (**A-C**) Levels of IL-6, IL-8 and IL-10 were assessed in cell supernatants by ELISA (N = 3, n = 3). Data is shown as mean ± SEM and analysed using One Way Anova with Tukey's post-test. *p≤0.05, **p≤0.01, ***p ≤0.001

4.5 Discussion

The established role of macrophages in both the functioning and failing heart has led many researchers to deem these cells prime therapeutic targets in combatting CVD and heart failure. However, many questions surrounding macrophage function in the heart need to be answered before macrophage-specific strategies can be translated to human trials. The aim of this study was to investigate interactions between primary human macrophages and iPSC-CMs, to elucidate the potential role of blood-derived macrophages in CM maintenance and function, and how this is altered under inflammatory settings. An important requisite for this study was to assess the impact of CM maintenance media on primary human macrophages, to ensure any effects observed from either direct or indirect co-culture was specifically a result of CM derived factors. This led to the identification of B-27™ supplement as a potential limiting factor in the study of macrophage-CM interactions. It was observed that the media supplement B-27™ promoted activation of primary human macrophages, indicated by significant production of cytokines IL-6, IL-10, and chemokine IL-8. Not only does this response interfere with investigations of macrophage-CM interactions under homeostatic conditions, but these findings also render the second aim of this study (investigating the impact of M1 macrophages) redundant, given the robust inflammatory cytokine response induced by media supplement alone.

Previous work in neural cell models led by Haenseler *et al*. have acknowledged the unfavourable side-effects of B-27™ supplement, attributing the effects to the presence of corticosterone, superoxide dismutase (SOD), and catalase [211]. Indeed, low doses of corticosterone have proven to exert a stimulatory effect in macrophages, resulting in pro-inflammatory cytokine production [212]. As a result of these findings, B-27™ supplement has been omitted from cultures of microglia and neurons, so as not to compromise microglia function [211]. While this strategy was initially considered in my own study of macrophage-CM culture, ultimately it was deemed unfeasible without a suitable supplement alternative which could maintain healthy CM and macrophage function. Serum-free culture of iPSC-CMs is known to induce hypertrophy of cells, thus disrupting healthy cellular function [213]. Furthermore, serum-free conditions have been known to promote cellular stress in macrophages [214]. Culture with RPMI/FBS is

also not a viable option, as hypertrophic effects in iPSC-CMs have also been observed as a result of culture with FBS [213].

The adverse response induced by B-27™ supplement in macrophages presents a challenge in deciphering cell response to CM secreted factors. For example, in addition to promoting significant cytokine production, B-27™ supplement also induced increased expression of Connexin-43 in primary human macrophages. This signifies that any attempt to gain insight to potential CM-derived factors which may promote Connexin-43 in macrophages, will be masked by B-27™-mediated expression. It is possible that further attempts to characterise macrophage response in either direct co-culture or in response to CM-conditioned media may be also overshadowed by B-27™-mediated effects.

Additionally, CMs are known to be highly receptive to cytokine signalling [215]. IL-6 treatment in rat CMs has been shown to decrease Ca^{2+} flux and contractility of cells, ultimately compromising CM function [216]. Treatment of H9c2 rat CMs with either IL-6 or IL-8 has also been shown to impact contractility of cells, as indicated by alteration to cell cytoskeleton [217]. Additionally, treatment with either IL-6 and IL-8 causes a disruption to CM mitochondrial metabolism, with an observed increase in mitochondrial ROS production [217]. The effect of B-27™ alone on macrophages therefore can have significant impact on CM function in a co-culture model, preventing the assessment of CMs in a "healthy" state. Furthermore, it has been previously reported that activation of macrophages can cause de-differentiation of ESC-CMs, as indicated by reduced expression of cardiac-related genes [205]. Therefore, maintaining homeostasis of macrophages is an important factor to retain differentiation of stem-cell derived CMs in cardiac models.

Of the few existing studies concerning *in vitro* macrophage-CM interactions, there are none which acknowledge the negative impact of B-27™ supplement. The work of Hitscherich *et al*., and Ai *et al*. involved murine cells cultured with FBS supplemented media [204, 206]. Human cell work by Almeida *et al*. involved only EVs extracted from CM conditioned media, and not the media itself. The work of Wrona *et al*. involves co-culture of primary human macrophages in B-27™ supplemented media with ESC-CMs, however fails to include a control of M0 macrophages in media alone as a comparison

for other treatment groups [205]. Furthermore, the data presented in that study shows fold change of cytokine production, and not quantitative values. Most recently, a 2021 published study, led by Yang *et al*., involved the generation of a co-culture of human iPSC-macrophages and iPSC-CMs, as a disease model for COVID-19 infection [218]. Interestingly, data from this study shows iPSC-macrophages to produce similar levels of IL-6 in the presence of B-27™ to that observed in my own work. This result however is not discussed in the study, but more-so used as a basal level of cytokine production compared to incidence of viral infection. The paper fails to show basal levels of cytokine without the presence of either CM or CM maintenance media. Additionally, the scope of this study did not extend beyond investigating cell death in response to viral infection, therefore the impact of macrophages alone on CM function, and furthermore any apparent effect of B-27™ were not investigated.

No significant change in macrophage surface marker expression, or antigen processing was observed in response to B-27™. Surface markers CD80 and CD86 are involved in antigen presentation to the adaptive immune system, acting as co-stimulatory molecules during the antigen presentation process, interacting with CD28 and CD40L receptors on T cells. Therefore, increased expression is typically associated with classical activation of macrophages, as they encounter pathogens and mature in preparation for activation of the adaptive immune response. B-27™ does not promote any increased expression of these co-stimulatory molecules, suggesting the induced response by the supplement in macrophages cannot be simply defined as classical activation. Future work which investigates the classical M1 phenotype at the gene level would perhaps allow further insight to the effects of B-27™. Furthermore, this would allow us to investigate whether B-27™ is indeed driving a pro-inflammatory response in primary human macrophages, or simply triggering cytokine release via activation of secretory pathways. While the latter may be unlikely given previous evidence showing low doses of corticosterone to promote pro-inflammatory cytokine expression at both the mRNA and protein level in murine macrophages [219], this is worthy of investigation in primary human macrophages to gain further understanding of the impact of B-27™ supplement on macrophage function.

Despite the adverse reaction to B-27™ supplement, a notable response was still observed in CM-media treated macrophages. Levels of both IL-6 and IL-8 production were decreased in response to CM-conditioned media, when compared to RPMI/B-27™ media treatment. A similar effect was observed in the co-culture model, where again a significant decrease was observed in both levels of IL-6 and IL-8 in macrophages cultured directly with CMs, compared to macrophages in RPMI/B-27™ media alone. Matrigel© coated plates were implemented as an additional control for these co-culture experiments, to ensure that the observed reduction in cytokine levels was a result of CM-mediated interactions and not the presence of ECM-related proteins. Matrigel© matrix is a solubilized basement membrane preparation extracted from the Engelbreth-Holm-Swarm (EHS) mouse sarcoma. The matrix preparation is comprised of numerous ECM proteins including Laminin, Collagen IV, heparan sulfate proteoglycans, entactin/nidogen, and a number of growth factors, necessary for the attachment and differentiation of iPSCs. It was observed that the presence of Matrigel© alone in the absence of iPSC-CMs caused no significant reduction in B-27™-mediated cytokine levels. This affirmed that the observed reduction in levels of both IL-6 and IL-8 was due to the presence of iPSC-CMs and not Matrigel© in macrophage-CM co-cultures.

It could be argued that this response is due to CMs metabolising the B-27™ supplement, therefore leaving minimal amounts available in conditioned media or co-culture conditions to activate macrophages. However, neither conditioned media nor co-culture conditions decreased IL-10 production in macrophages, suggesting that CMs elicit an anti-inflammatory effect on macrophages, causing a subsequent reduction in pro-inflammatory cytokine production. It is known that tissue resident macrophages typically adopt an anti-inflammatory M2 phenotype in the heart, holding a significant role in the dampening of local tissue inflammation, as well as maintaining tissue homeostasis [220]. In addition to the observed reduction in pro-inflammatory cytokine production, CM-conditioned media was also observed to promote expression of chemokine receptors CCR2 and CX3CR1. The latter in particular is typically associated with alternatively activated macrophages, with $CX3CR1^{+}$ cells co-localised to tissue regions populated by M2 macrophages [221]. In the heart, CX3CR1 macrophages are responsible for the later stages of tissue repair post-MI, as well the secretion of anti-

inflammatory factors such as IL-10 [86]. Based on the preliminary findings of this study, it is possible that secreted factors from CMs contribute towards this M2-like phenotype in macrophages, although further investigation is required to confirm this, ideally under B-27™-free conditions. Previous work involving murine RAW macrophages and H9c2 CMs revealed an immunomodulatory function in CMs via the release of exosomes [207]. It is possible that a similar mechanism may occur between iPSC-CMs and primary human macrophages, given the observed reduction in pro-inflammatory cytokines as a result of CM-conditioned media treatment. Future work involving the detection and subsequent characterisation of potential exosomes in conditioned media may give way to a potential therapeutic strategy, utilising CM-derived factors as anti-inflammatory therapies.

Ultimately, findings from this chapter have highlighted an important consideration for future co-culture models, in that the successful generation of any multicellular model requires careful consideration of each necessary factor which facilitates cell maintenance. B-27™ supplement, while essential for CM maintenance, is a pro-inflammatory stimulant for primary human macrophages, thus presenting a potential limitation to investigations of macrophage-CM interactions. In the absence of a suitable alternative media supplement, future work fully characterising macrophage phenotype in the presence of B-27™ supplement may allow us to overcome this limitation. This is worthy of future investigation, given the potential immunomodulatory effect elicited by CM-derived factors on primary human macrophages.

Chapter 5 : Investigating the impact of cholesterol crystals on macrophage polarisation and metabolism

This chapter has been peer reviewed and published in O'Rourke SA, Neto NGB, Devilly E, Shanley LC, Fitzgerald HK, Monaghan MG, Dunne A. Cholesterol crystals drive metabolic reprogramming and M1 macrophage polarisation in primary human macrophages. Atherosclerosis. 2022 Jul;352:35-45. doi: 10.1016/j.atherosclerosis.2022.05.015. Epub 2022 May 25. PMID: 35667162.

5.1 Abstract

Atherosclerosis is the leading cause of MI, and a major cause of mortality in developed countries. While the disease was once thought to be a result of hyperlipidaemia, research across the last decade has redefined the condition as a chronic inflammatory disease, with macrophages as established mediators. Additionally, metabolic reprogramming of innate immune cells is emerging as a key player in the progression of atherosclerosis, where high rates of glycolysis correlate with plaque instability. This study aimed to investigate if cholesterol crystals, which are a key atherosclerosis-associated DAMP, alter immune cell metabolism and whether this, in turn, impacts on macrophage phenotype and function. Primary human macrophages were treated with cholesterol crystals and expression of M1 (*CXCL9, CXCL10*) and M2-associated (*MRC1, CCL13*) macrophage markers, alarmins, and inflammatory cytokines were assessed either by real-time PCR or ELISA. Cholesterol crystal-induced changes in glycolytic markers were determined using real-time PCR and western blotting, while changes in cellular respiration and mitochondrial dynamics were examined via Seahorse XF analysis, Fluorescence Lifetime Imaging Microscopy (FLIM) and confocal microscopy. Treatment of macrophages with cholesterol crystals upregulated mRNA levels of *CXCL9* and *CXCL10*, while concomitantly downregulating expression of *MRC1* and *CCL13*. Cholesterol crystal-treated macrophages also exhibited a significant shift in metabolism to favour glycolysis, accompanied by the expression of key glycolytic markers *GLUT1, HK2, HIF1α, GAPDH* and *PFKFB3*. Furthermore, these effects were shown to be mediated upstream by the glycolytic enzyme, PKM2, with direct inhibition of glycolysis or PKM2 nuclear localisation leading to a significant reduction in cholesterol crystal-induced inflammatory readouts. This study not only provides further insight into how atherosclerosis-associated DAMPs impact on immune cell function, but also highlights metabolic reprogramming as a potential therapeutic target for cholesterol crystal-related inflammation.

5.2 Introduction

Atherosclerosis is a chronic inflammatory disease and one of the leading causes of myocardial infarction [222]. Analysis of plaques in murine models of the disease show a heterogenous population of both M1 and M2 macrophages, however, as the disease progresses, the population of M2 macrophages becomes depleted, leaving a dominant

pro-inflammatory phenotype [73, 223, 224]. As discussed below, this phenotype is also accompanied by a significant shift in cellular metabolism. Indeed it is now well accepted that upon activation, macrophages undergo a metabolic switch to favour glycolysis over oxidative phosphorylation in order to meet the energy demands of a rapid inflammatory response [88]. This is similar to the Warburg effect observed in cancer cells and results in an accumulation of ROS, degradative enzymes and pro-inflammatory mediators [225]. In LPS-stimulated macrophages, increased glycolysis is accompanied by increased glucose uptake and enhanced expression of the glucose transporter, GLUT1 [226], as well as increased expression of the transcription factor, HIF1α, which facilitates the upregulation of pro-inflammatory cytokines such as IL-1. [50]. This response is principally regulated by an isoform of pyruvate kinase called PKM2 which exists in both an enzymatically active and inactive state [227]. The enzymatically active form of the protein exists as a tetramer that remains in the cytosol of the cell while the enzymatically inactive isoform exists as either a monomer or dimer that can translocate to the nucleus and induce transcription of HIF1α and other proglycolytic enzymes [228]. These events are required for the macrophage response to infection and tissue injury, however, when dysregulated through sustained inflammatory signalling, they can contribute to chronic inflammatory diseases [50, 229, 230].

There is now substantial evidence demonstrating an association between increased glycolysis and plaque instability and rupture during atherosclerosis. Metabolomic studies have revealed increased expression of glycolytic genes to correlate with increased plaque vulnerability and inflammation [231]. Furthermore, elevated uptake of glucose and glycolytic flux has been identified in atherosclerotic plaques, and this is accompanied by increased expression of HIF1α [232]. Dysfunction or damage to the mitochondria is a further consequence of increased glycolysis caused by the accumulation of ROS [233]. This in turn can cause oxidation of low-density lipids, further exacerbating the condition [234]. Considering this emerging correlation between plaque progression and altered immunometabolism, it is plausible that modulation of immune cell metabolism, and subsequent immune cell function, may be a novel strategy to treat the inflammatory component of atherosclerosis.

5.3 Aims

An assortment of environmental cues within the atherosclerotic plaque can contribute to the pro-inflammatory phenotype of macrophages observed. Cholesterol crystals, found at both early and advanced stages of atherosclerosis have been reported to drive inflammation in both human and murine macrophages through activation of the NLRP3 inflammasome [75, 235]. This is supported by studies demonstrating that silencing of NLRP3 in ApoE knockout mice, improves plaque stability and ameliorates disease [236]. A recent study led by Mahon *et al*., demonstrated that basic calcium phosphate (BCP) crystals, which are inflammatory disease-associated particulates associated with osteoarthritis, can polarize macrophages towards an M1 phenotype and are also capable of driving a metabolic switch favouring glycolysis [43]. Similar effects were observed with gout-associated, uric acids crystals, suggesting that the inflammatory effects of these particulates extend beyond activation of the inflammasome [237]. It is therefore of interest to investigate if cholesterol crystals exhibit a similar response by altering macrophage metabolism, subsequently driving an M1 phenotype in primary human macrophages. Furthermore, if these potential alterations to macrophage metabolism represent a potential therapeutic target to combat inflammation in atherosclerosis.

Specific aims:

- To determine if cholesterol crystals alter the immune-metabolic phenotype of primary human macrophages.
- To establish an upstream mechanism of cholesterol crystal-mediated inflammation, for potential therapeutic intervention in atherosclerosis.

5.4 Results

5.4.1 In-house generated cholesterol crystals are endotoxin free.

Prior to assessing the effect of cholesterol crystals (CHCs) on primary human macrophages, it was important to ensure the batches of crystals synthesised in the laboratory (Figure 5.1) were free of endotoxin/LPS using the HEK-Blue™ TLR4 assay system. HEK-Blue™ TLR4 cells were stimulated with either LPS (0.1-100 ng/ml; positive control) or a standard dose of cholesterol crystals used in published studies [235] (Batch A or Batch B; 500 µg/ml) for 24 hours. SEAP expression was then examined by incubating cell supernatants with HEK-Blue™ detection media for 15 minutes and absorbance was monitored at 650 nm. Results indicate that both batches of crystals were free of contaminating LPS (Figure 5.2).

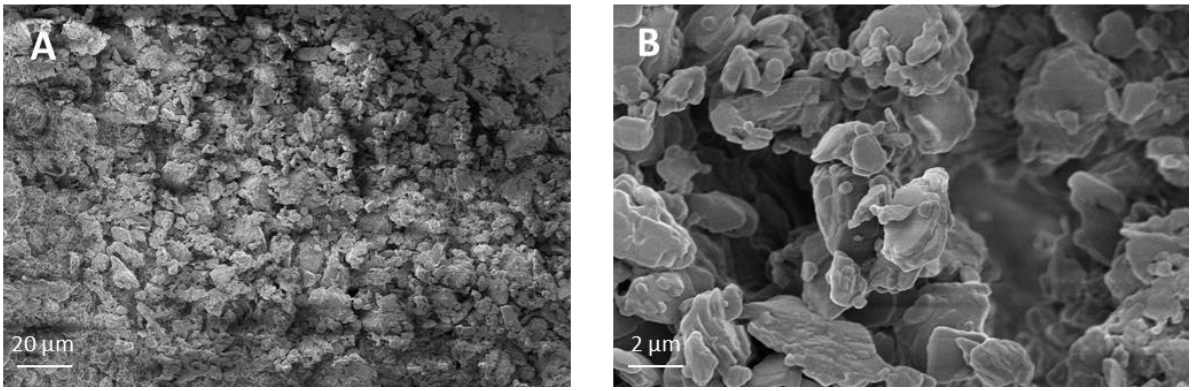

Figure 5-1 - SEM imaging of cholesterol crystals. Images acquired by Dr. Kian Eicholz

SEM image of cholesterol crystals taken at (**A**) 500 X magnification and (**B**) 5000 X magnification.

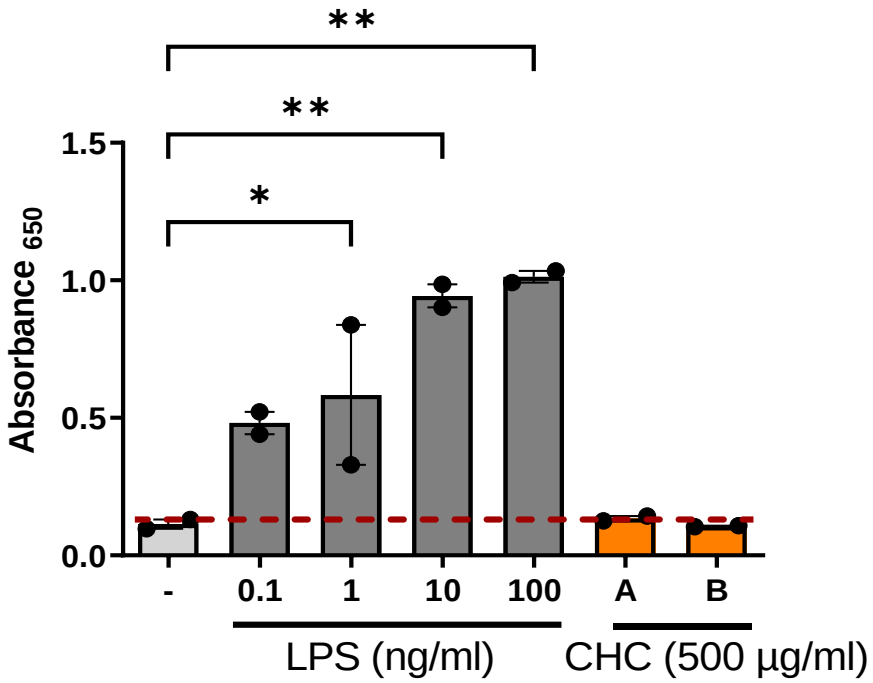

Figure 5-2 – Cholesterol crystals are free of endotoxin contaminants

HEK-blue™ cells (5 x 10^5 cells/ml) were left either untreated, stimulated with LPS (0.1-100 ng/ml) (as a positive control) or stimulated with cholesterol crystals (CHC) (Batch A or B) for 24 hours. The expression of SEAP was measured by absorbance at 650 nm (N =2, n =2). Data is represented as mean ± SEM and analysed by One Way ANOVA with Dunnett's post-test. *p≤0.05, **p ≤0.01

5.4.2 Cholesterol crystals are non-toxic to primary human macrophages.

Prior to examining the immune response of primary human macrophages to cholesterol crystals, the impact of cholesterol crystals on cell viability was assessed firstly by Alamar Blue™ assay, and secondly through a neutral red-based assay. For the Alamar Blue™ assay, primary human macrophages were treated with cholesterol crystals (500 μg/ml) for 24 hours followed by incubation with 10% Alamar Blue™ solution for 1 hour. Spectrophotometric analysis (570 nm/600 nm) indicated that cholesterol crystals did not reduce the viability of macrophages compared to untreated control cells (Figure 5.3 A). For the neutral-red assay, primary human macrophages were treated with cholesterol crystals (500 μg/ml) for 24 hours. Additionally, macrophages were treated with Triton-X 100 (0.5%) for 1 hour as a positive control. Spectrophotometric analysis (540 nm/690 nm) showed cell viability of cholesterol crystal treated macrophages to be significantly higher than Triton-treated cells, and comparable to that of untreated control cells (Figure 5.3 B). Additionally, caspase-3 cleavage was investigated by western blot as a measure of apoptosis. To assess this, primary human macrophages were treated with cholesterol crystals (500 μg/ml) for 6 and 24 hours, or staurosporine (1 μg/ml) for 6 hours as a positive control. Significant cleavage of caspase-3 was observed in response to staurosporine (15.42 fold change ± 8.21), but not cholesterol crystals at either 6 or 24 hours (Figure 5.3 C-D). Collectively these results demonstrated that cholesterol crystals are well tolerated by primary human macrophages.

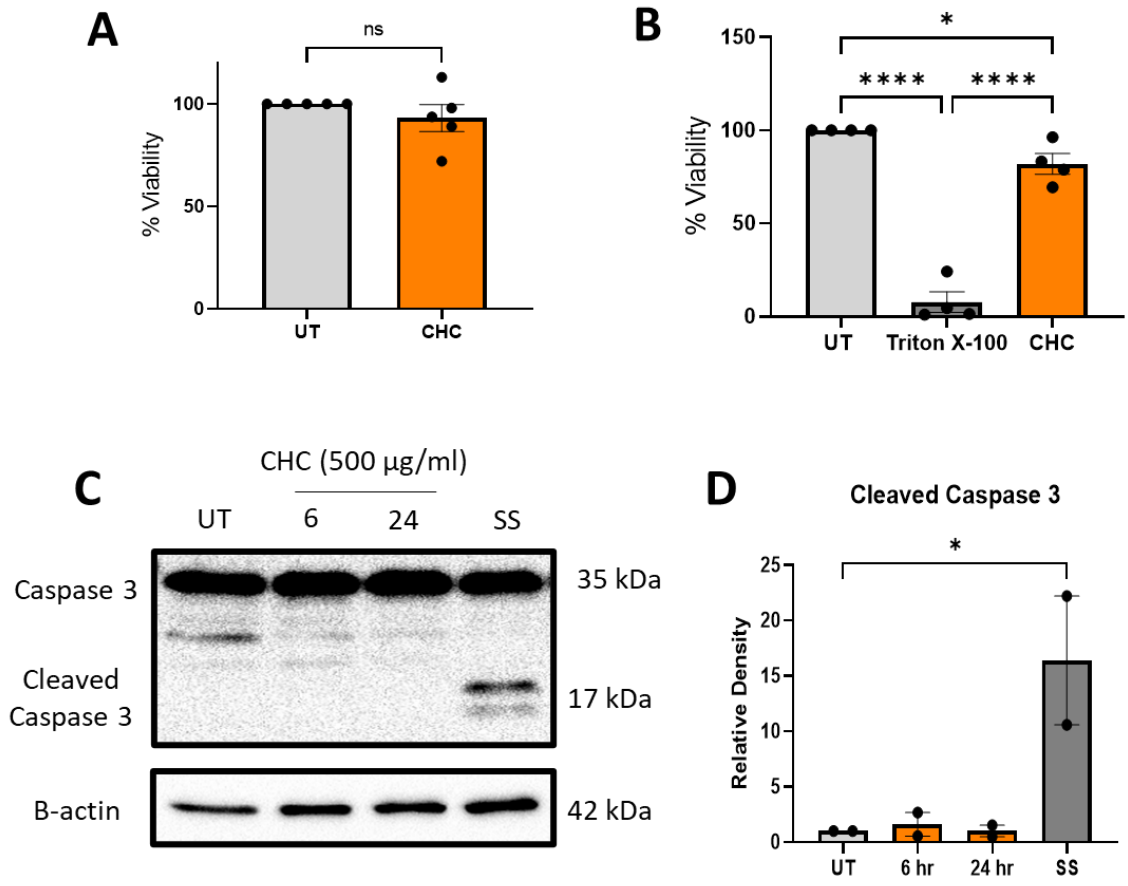

Figure 5-3 – Cholesterol crystals do not impact the viability of primary human macrophages.

Primary human macrophages (1 x 10^6 cells/ml) were left untreated or stimulated with cholesterol crystals (500 µg/ml) for 24 hours. (**A**) Cell viability assessed by the Alamar Blue™ assay. Cells were incubated with 10% Alamar Blue™ solution for 1 hour and absorbance of cell media was assessed at 570 nm and 600 nm. % Viability of cells expressed relative to untreated cells (UT) (N =5, n =3). (**B**) Cell viability assessed through a neutral red-based assay. Cells were incubated with 10% Neutral red solution for 2 hours and absorbance of cell media was assessed at 540 nm and 690 nm. % Viability of cells expressed relative to untreated cells (UT) (N =4, n =2). (**C**) Representative western blot demonstrating cleavage of caspase 3. Primary human macrophages were treated with cholesterol crystals (500 µg/ml) for 6 and 24 hours, or staurosporine (SS) (1 µg/ml) as a positive control. (**D**) Densitometric analysis of cleaved caspase 3 western blot using Biorad software. Bar graphs depict expression of cleaved Caspase 3 protein relative to control cells and normalized to B-actin housekeeping protein (N =2). All data is shown as mean ± SEM. Alamar Blue™ assay was analysed using paired t-test. Neutral red assay was analysed using One Way Anova with Tukey's post-test. Densitometry analysis of caspase 3 was analysed using One Way Anova with Dunnett's post-test. *p≤0.05,

5.4.3 Cholesterol crystals activate the inflammasome in LPS-primed primary human macrophages.

Having established that cholesterol crystals were indeed endotoxin free and non-toxic to primary human macrophages, it was necessary to ensure that the in-house synthesised crystals performed as expected from the literature. As discussed previously, cholesterol crystals are capable of activating the NLRP3 inflammasome to drive the secretion of mature IL-1β [75, 77, 235]. For this to occur, two signals are required. Cells are first primed to stimulate production of pro-ILβ. This can be mediated, for example, by stimulation of TLR4 with LPS. The second signal causes NLRP3 inflammasome assembly and activates caspase-1, which results in the secretion of mature IL-1β. To assess this, primary human macrophages were treated with LPS (100 ng/ml) or cholesterol crystals (250 μg/ml, 500 μg/ml) alone or were pre-treated with LPS for 2 hours, prior to cholesterol crystal stimulation for 6 and 24 hours. As expected, LPS stimulation induced expression of the pro-inflammatory cytokine, pro-IL-1β as assessed by western blot (6.571 fold change ± 2.290), however there was no induction upon treatment with either dose of cholesterol crystals (Figure 5.4 A-B). Furthermore, and in agreement with previous literature, cholesterol crystals alone had no effect on mature IL-1β secretion, while LPS-primed, cholesterol crystal-treated macrophages showed significantly elevated levels of IL-1β (Increase of 754 pg/ml ± 479 pg/ml) relative to untreated cells) (Figure 5.4 C).

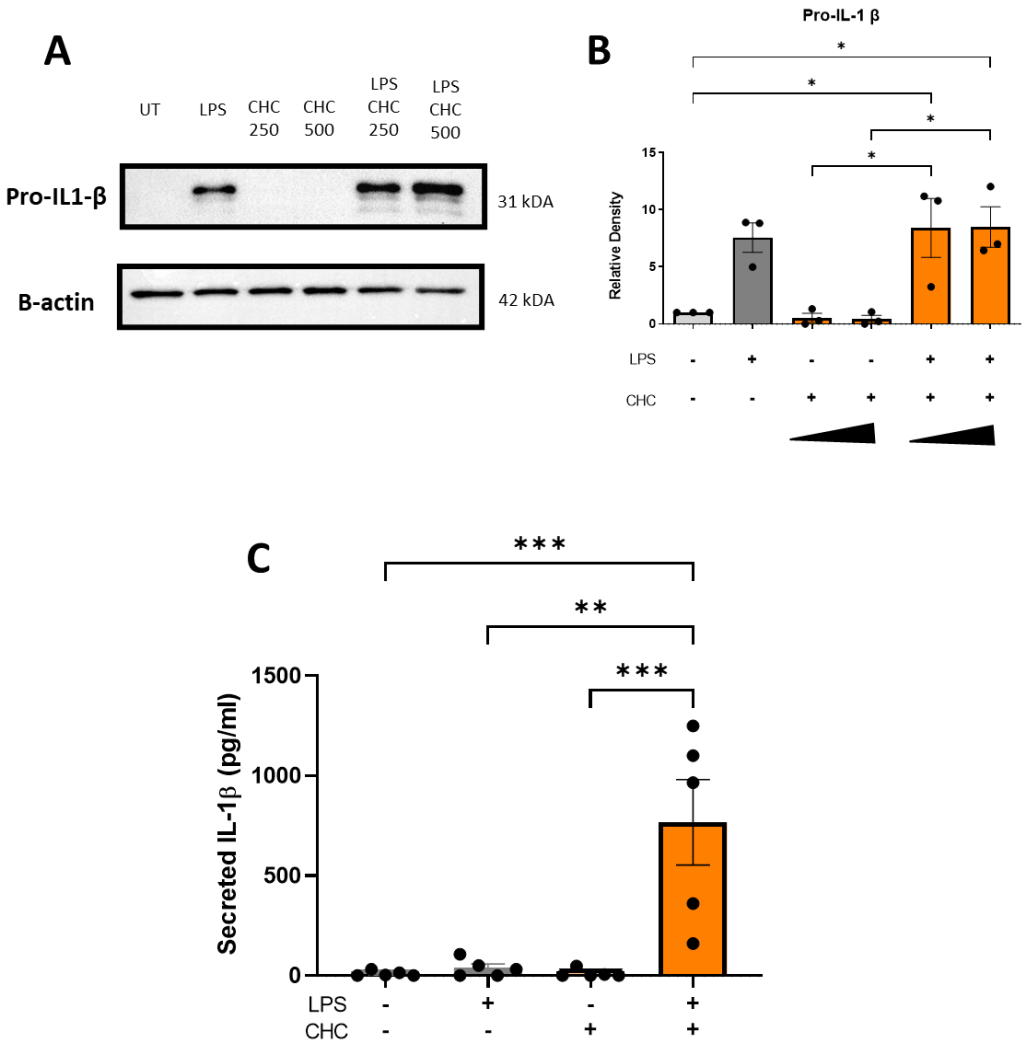

Figure 5-4 - Cholesterol crystals activate the inflammasome and cause secretion of mature IL-1β.

Primary human macrophages (1 x 10^6 cells/ml) were stimulated with LPS (100 ng/ml) alone, cholesterol crystals (500 µg/ml) alone, or else pre-treated with LPS for 2 hours prior to CHC stimulation for 24 hours. Expression of pro-IL-1β were assessed by Western blot (N =3). Secreted IL-1β in cell supernatants was assessed through ELISA (N =5, n =3). (**A**) Representative Western blot showing expression of pro-IL-1β in response to treatments. (**B**) Bar graph showing densitometric analysis of pro-IL-1β blot normalised to house-keeping protein B-actin and relative to untreated cells. (**C**) Bar graph showing secretion of IL-1β. All data is represented as mean ± SEM and was analysed using One Way Anova with Tukey's post-test. *p≤0.05, **p≤0.01 *** ≤0.001

5.4.4 Cholesterol crystals drive expression of M1-associated genes and DAMPs, while simultaneously downregulating expression of M2-associated genes.

Having confirmed that the in-house generated cholesterol crystals successfully activate the inflammasome in primary human macrophages, the next objective was to examine the impact of the crystals on macrophage polarisation. Primary human macrophages were treated with cholesterol crystals (500 µg/ml) for 6 hours and mRNA levels of the M1 associated genes, *CXCL9, CXCL10*, and M2 associated genes *MRC1* and *CCL13* were measured by real-time PCR analysis. In comparison to untreated samples, increased expression of both *CXCL9* and *CXCL10* was observed upon cholesterol crystal treatment (341.5 fold change ± 212.2, and 359.9 fold change ± 239.2 respectively) (Figure 5.5 A-B). Conversely, a significant reduction in expression of the M2 associated genes, *MRC1* (0.77 fold change ± 0.22) and *CCL13* (0.77 fold change ± 0.08), was observed in cholesterol crystal treated cells when compared to the untreated control group (Figure 5.5 C-D). The associated changes in expression of all four genes suggests that cholesterol crystals promote M1 polarisation of primary human macrophages. mRNA levels of the damage-associated molecules, *S100A8* and *S100A12*, were also assessed in response to cholesterol crystal treatment. There was a significant increase in expression of both genes in comparison to untreated cells (13.19 fold change ± 8.51, 14.7 fold change ± 6.35 respectively) (Figure 5.6 A-B), further supporting the inflammatory properties of atherosclerosis-associated cholesterol crystals.

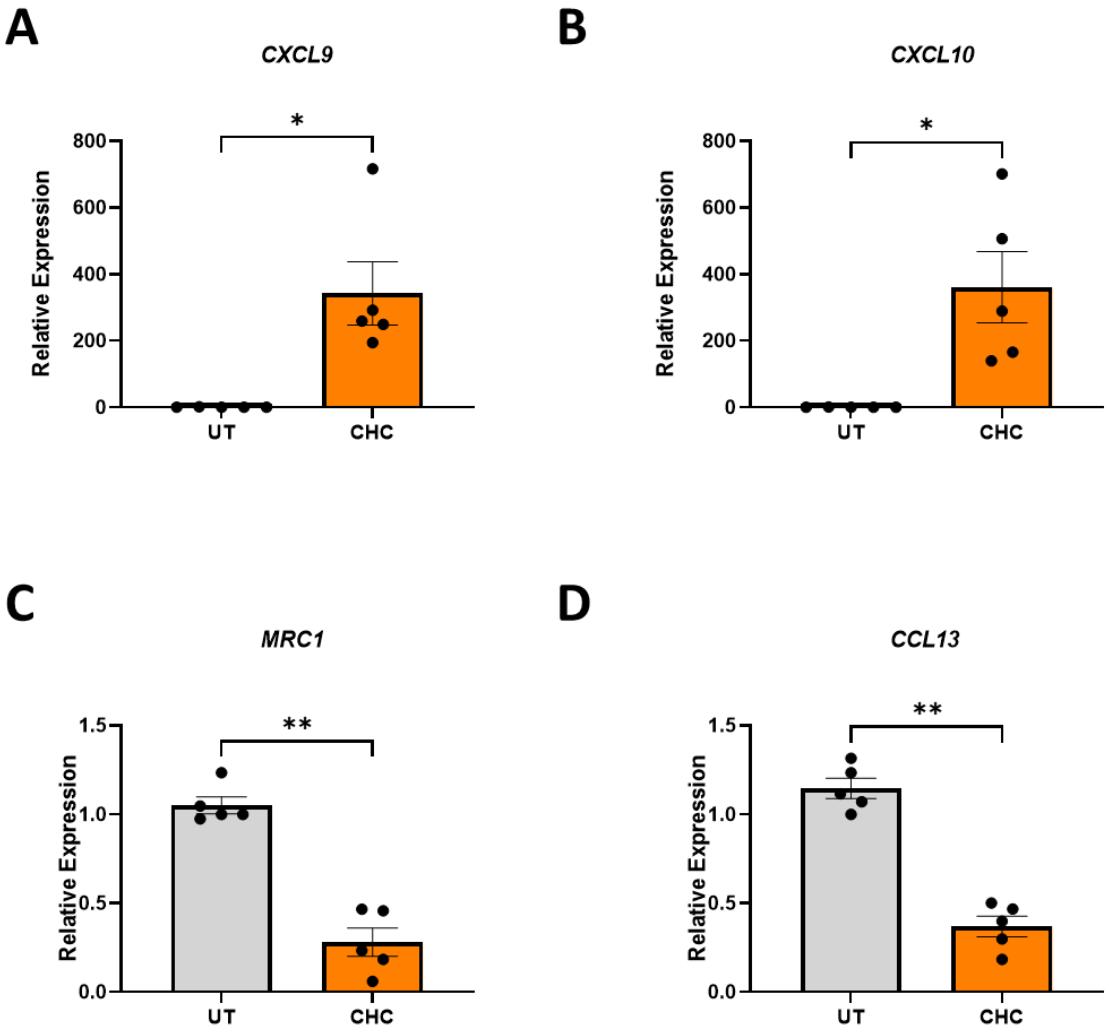

Figure 5-5 – Cholesterol crystals drive M1 polarisation in primary human macrophages.

Primary human macrophages (1 x 10^6 cells/ml) were stimulated with cholesterol crystals (500 µg/ml) for 6 hours. (**A-D**) mRNA expression of *CXCL9*, *CXCL10*, *MRC1*, and *CCL13* was analysed by real-time PCR (N= 5, n = 3). All data is represented as mean ± SEM. and was analysed using paired t-test. *p≤0.05, **p≤0.01

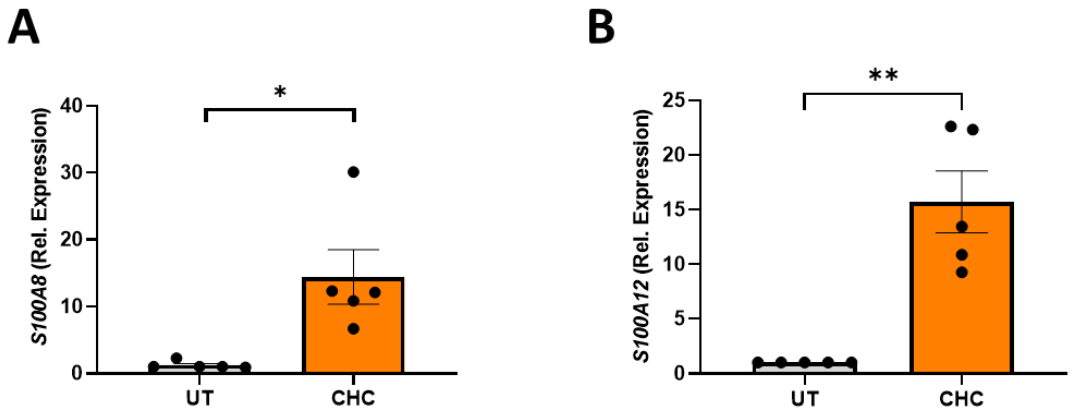

Figure 5-6 – Cholesterol crystals drive DAMP expression in primary human macrophages

Primary human macrophages (1 x 10^6 cells/ml) were stimulated with cholesterol crystals (500 µg/ml) for 6 hours. (**A-B**) mRNA expression of S100A8 and S100A12 was analysed by real-time PCR (N= 5, n = 3). All data is represented as mean ± SEM. and was analysed using paired t-test. *p≤0.05, **p≤0.01

.

5.4.5 Cholesterol crystals drive IL-8 production in primary human macrophages.

Having established that cholesterol crystals induce a pro-inflammatory M1 phenotype in primary macrophages, the next objective was to assess the impact of the crystals on pro-inflammatory cytokine and chemokine production in un-primed macrophages. Primary human macrophages were stimulated with cholesterol crystals (500 µg/ml) or the positive control, LPS (100 ng/ml) for 24 hours and the concentration of TNF, IL-6 and IL-8 in cell supernatants was quantified by ELISA. Treatment with the crystals had no effect on TNF and IL-6 production, however, production of the chemokine, IL-8, was significantly increased (Increase of 9605 pg/ml ± 2004 pg/ml) when compared to untreated samples (Figure 5.7).

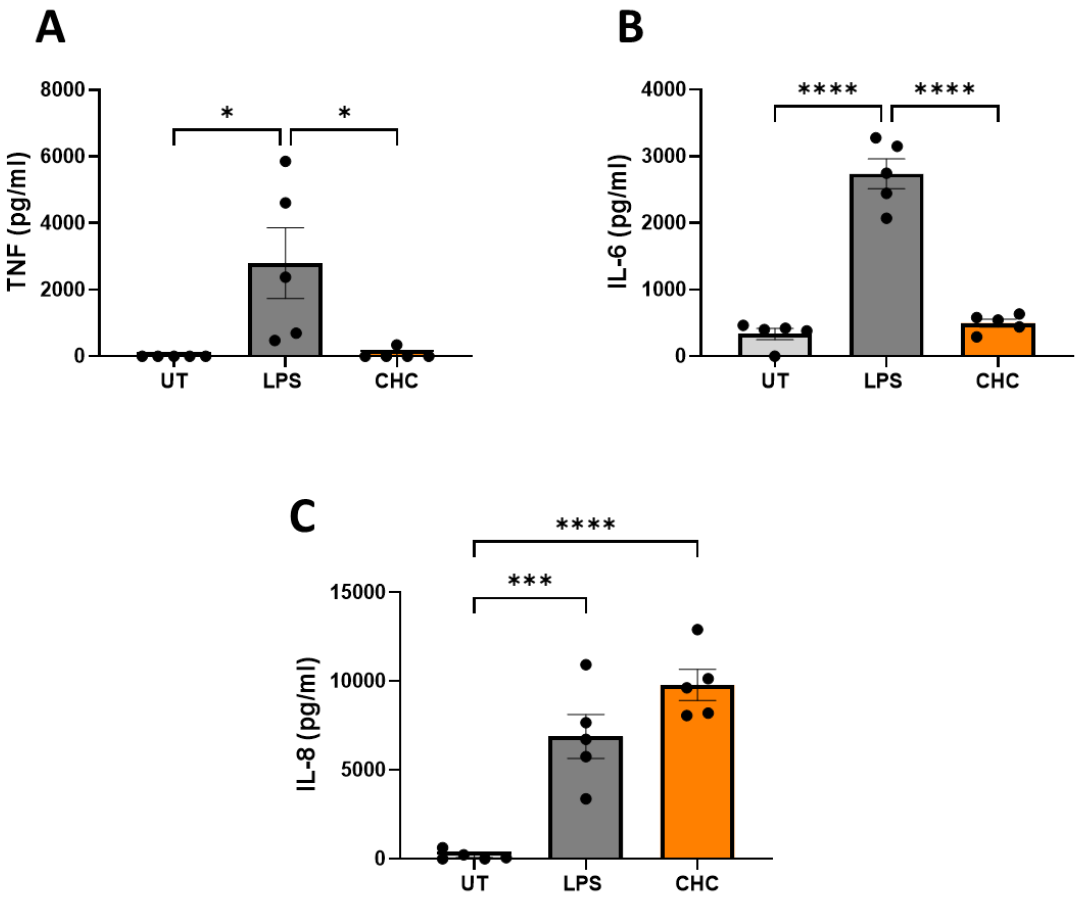

Figure 5-7 Cholesterol crystals drive production of IL-8, but not TNF or IL-6 in primary human macrophages.

Primary human macrophages (1 x 10^6 cells/ml) were stimulated with cholesterol crystals (500 µg/ml) for 24 hours. (**A-C**) TNF, IL-6 and IL-8 cytokine production in cell supernatants was analysed by ELISA (N = 5, n = 3). All data is represented as mean ± SEM. Data was analysed using one-way ANOVA with Tukey's post-test. *p≤0.05, *** ≤0.001, ****p ≤0.0001

5.4.6 Cholesterol crystals drive expression of surrogate markers of glycolysis

A number of studies have confirmed that a metabolic switch to glycolysis is accompanied by M1 macrophage polarisation, increased glucose uptake, and enhanced expression of glycolytic enzymes [88, 238, 239]. This is also observed in human atherosclerotic plaques, whereby pro-inflammatory, pro-atherogenic macrophages typically exhibit enhanced glycolysis [231]. In light of this, it was next aimed to investigate if cholesterol crystals were capable of altering macrophage metabolism *in vitro*.

Primary human macrophages were stimulated with cholesterol crystals for 1, 3, 6 and 24 hours. Expression of the key glycolytic markers, *GLUT1, HK2, GAPDH, HIF1α* and *PFKFB3* were assessed by real-time PCR, while western blotting was used to assess expression of GLUT1 and HK2 at the protein level. Cholesterol crystal stimulation significantly upregulated expression of all five glycolytic markers at the mRNA level (Figure 5.8 A-E). Furthermore, GLUT1 and HK2 were upregulated at the protein level in response to cholesterol crystal treatment, with densitometric analysis revealing maximal expression 24 hours post crystal treatment (2.442 fold change ± 0.6839 for GLUT1, 2.681 fold change ± 1.368 for HK2) (Figure 5.9).

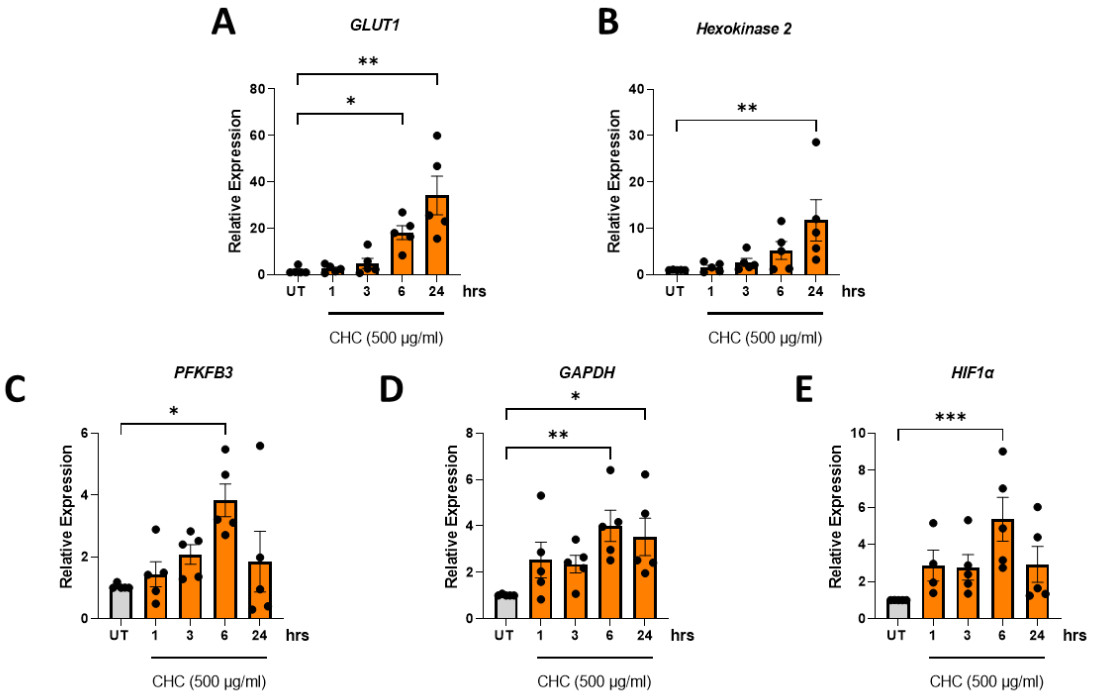

Figure 5-8 – Cholesterol crystals drive expression of glycolytic genes in primary human macrophages.

Primary human macrophages (1 x 10^6 cells/ml) were treated with cholesterol crystals (500 µg/ml) for 1, 3, 6 and 24 hours. (**A-E**) mRNA expression of *GLUT1, HK2, PFKFB3, GAPDH*, and *HIF1α* was analysed by real-time PCR (N= 5, n = 3). All data is represented as mean ± SEM and analysed using One Way ANOVA with Dunnett's post-test. *p≤0.05, **p≤0.01, *** ≤0.001

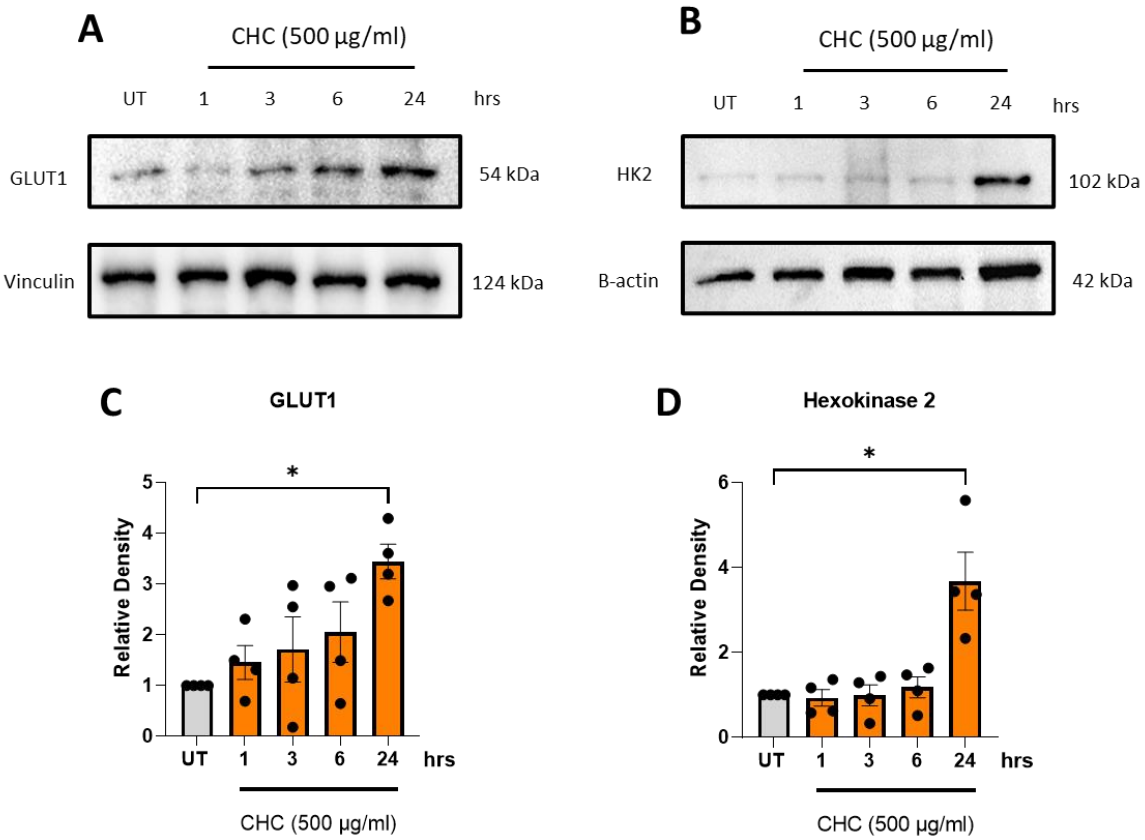

Figure 5-9 – Cholesterol crystals drive protein expression of glycolytic markers in primary human macrophages.

Primary human macrophages (1 x 10^6 cells/ml) were stimulated with cholesterol crystals (500 µg/ml) for an extended time course of 1, 3, 6 and 24 hours. (**A-B**) Representative western blots demonstrating expression of GLUT1 and HK2 in response to cholesterol crystals over time. (**C-D**) Densitometric analysis of western blots (N = 4) using Biorad software. Bar graphs illustrate the mean ± SEM increase in protein expression relative to untreated control and normalised to either vinculin or β-actin housekeeping protein. All data was analysed using One Way ANOVA with Dunnett's post-test. *p≤0.05

5.4.7 Primary human macrophages temporally alter cell metabolism in response to LPS.

In order to gain further insight into the metabolic changes induced by cholesterol crystals in primary human macrophages, the oxygen consumption rate (OCR) and extracellular acidification rate (ECAR), reflecting oxidative phosphorylation and glycolysis, respectively, were next assessed using the Seahorse XF96 Bioanalyser. Prior to conducting these experiments with cholesterol crystals, macrophages were first treated with LPS to investigate the optimal time points for experimental analysis. It is well established that macrophages exhibit a metabolic shift in response to LPS, favouring glycolysis over oxidative respiration [38]. In murine macrophages, LPS treatment results in elevated rates of glycolysis with minimal changes to cellular respiration, with this response sustained at 24 hours [240]. However, in primary human macrophages, changes in cell metabolism appear more temporal, peaking at early time points of 1-6 hours post stimulation [43]. To investigate this in my own work, primary human macrophages were treated with LPS (100 ng/ml) for 1, 3, 6 and 24 hours, and analysed with the Seahorse XFe96 Bioanalyser, following the addition of oligomycin (1 mM); an inhibitor of mitochondrial complex V, FCCP (1 mM); a mitochondrial uncoupler, rotenone (500 nM) and antimycin A (500 nM); which are inhibitors of the mitochondrial complexes I & III, respectively, and 2-DG (25 mM); an inhibitor of glycolysis. Results of this experiment demonstrate that primary human macrophages increase the rate of basal and maximum glycolysis in response to LPS, with an observed peak 1 hour post-treatment (increase of 22.49 mpH/min ± 8.5 in basal glycolysis, increase of 34.28 mpH/min ± 4.87 in max glycolysis compared to untreated cells) (Figure 5.10). No significant changes in oxidative phosphorylation were observed in response to LPS treatments (Figure 5.11). Based on these results, the same time course of 1,3, 6 and 24 hours was utilised in subsequent experiments with cholesterol crystals.

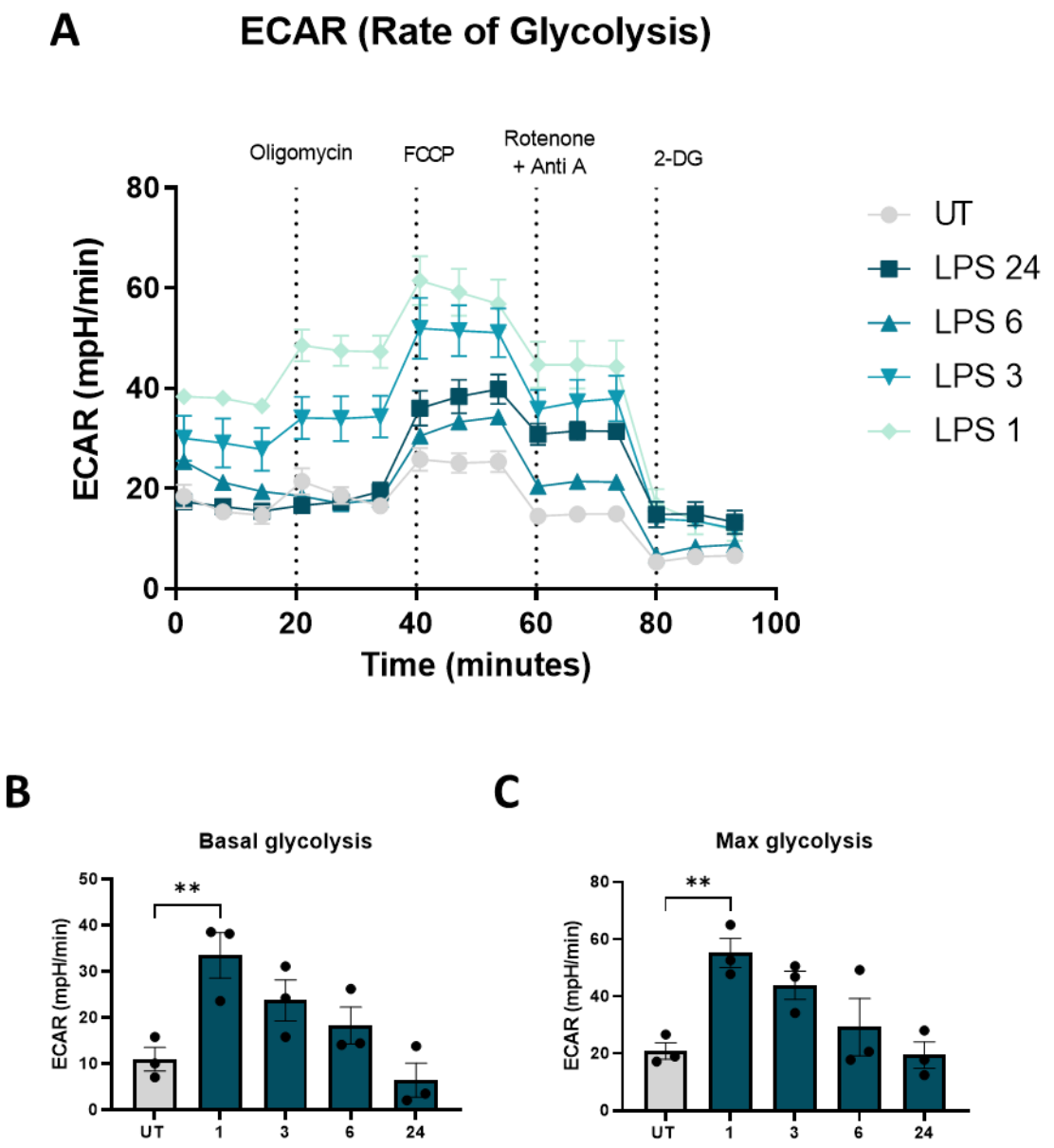

Figure 5-10 – Primary human macrophages temporally increase rates of glycolysis in response to LPS stimulation.

Primary human macrophages (1 x 10^6 cells/ml) were stimulated with LPS (100 ng/ml) for an extended time course of 1, 3, 6 and 24 hours. (**A**) Representative glycolysis (ECAR) Seahorse bioenergetics profiles before and after injections of oligomycin (1mM), FCCP (1mM), antimycin A (500 nM)/Rotenone (500 nM), and 2-DG (25 mM) post stimulation with LPS. (**B-C**) Bar graphs demonstrating basal glycolysis and max glycolysis. All data is represented as mean ± SEM (N = 3, n =4) Data was analysed using RM One Way ANOVA with Dunnett's Test. **p≤0.01

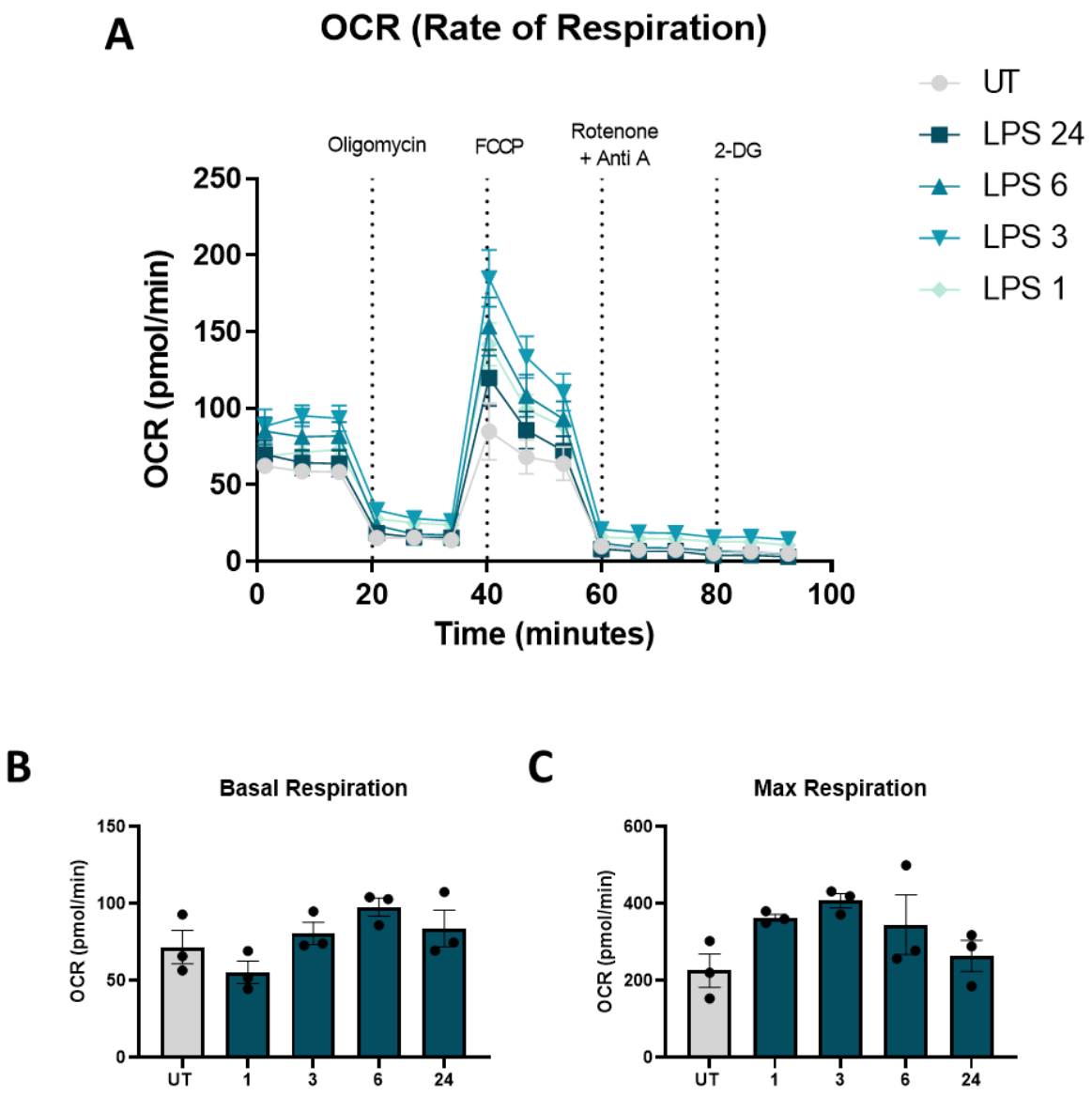

Figure 5-11 – Rates of respiration of primary human macrophages in response to LPS stimulation.

Primary human macrophages (1 x 10^6 cells/ml) were stimulated with LPS (100 ng/ml) for an extended time course of 1, 3, 6 and 24 hours. (**A**) Representative respiration (OCR) Seahorse bioenergetics profiles before and after injections of oligomycin (1mM), FCCP (1mM), antimycin A (500 nM) / Rotenone (500 nM), and 2-DG (25 mM) post stimulation with LPS. (**B-C**) Bar graphs demonstrating basal respiration and max respiration, (**D**) respiratory reserve. All data is represented as mean ± SEM (N = 3, n =4) Data was analysed using RM One Way ANOVA with Dunnett's Test.

5.4.8 Cholesterol crystals alter macrophage metabolism to favour glycolysis.

Having observed the changes in metabolism in primary macrophages in response to LPS stimulation, it was next aimed to investigate if a similar response occurs as a result of cholesterol crystal treatment. Primary human macrophages were treated with cholesterol crystals (500 μg/ml) for 1, 3, 6 and 24 hours, and OCR, ECAR and ATP production were assessed using the Seahorse XFe96 Bioanalyser. Indeed, similar to the results obtained with LPS-treated macrophages, a temporal increase in glycolysis was observed in cholesterol crystal-treated macrophages with both basal and maximum rates of glycolysis showing an observed peak at 6 hours (Increase of 16.45 mpH/min ± 4.4 in basal glycolysis, increase of 20.93 mpH/min ± 8.4 in max glycolysis, relative to untreated cells) (Figure 5.12 A-C). Typically, at the end stage of glycolysis, pyruvate is converted to acetyl coA, to feed into the TCA cycle during oxidative phosphorylation, thus an increase in aerobic glycolysis is accompanied by an increase in respiration/oxidative phosphorylation. However, in response to cholesterol crystal treatments, an increase in respiration is only observed at 1 hour (increase of 120.1 pmol/min ± 91.11 relative to untreated cells) (Figure 5.13 A-C), suggesting the cell primarily favours anaerobic glycolysis as its key energy source. This was indeed reflected in the overall ECAR:OCR rate, which demonstrates a preference towards glycolysis that is significant at 6 hours (Figure 5.14 A). In support of this, there was also an observed increase in the production of glycolysis-derived ATP versus mitochondrial derived ATP (Figure 5.14 B).

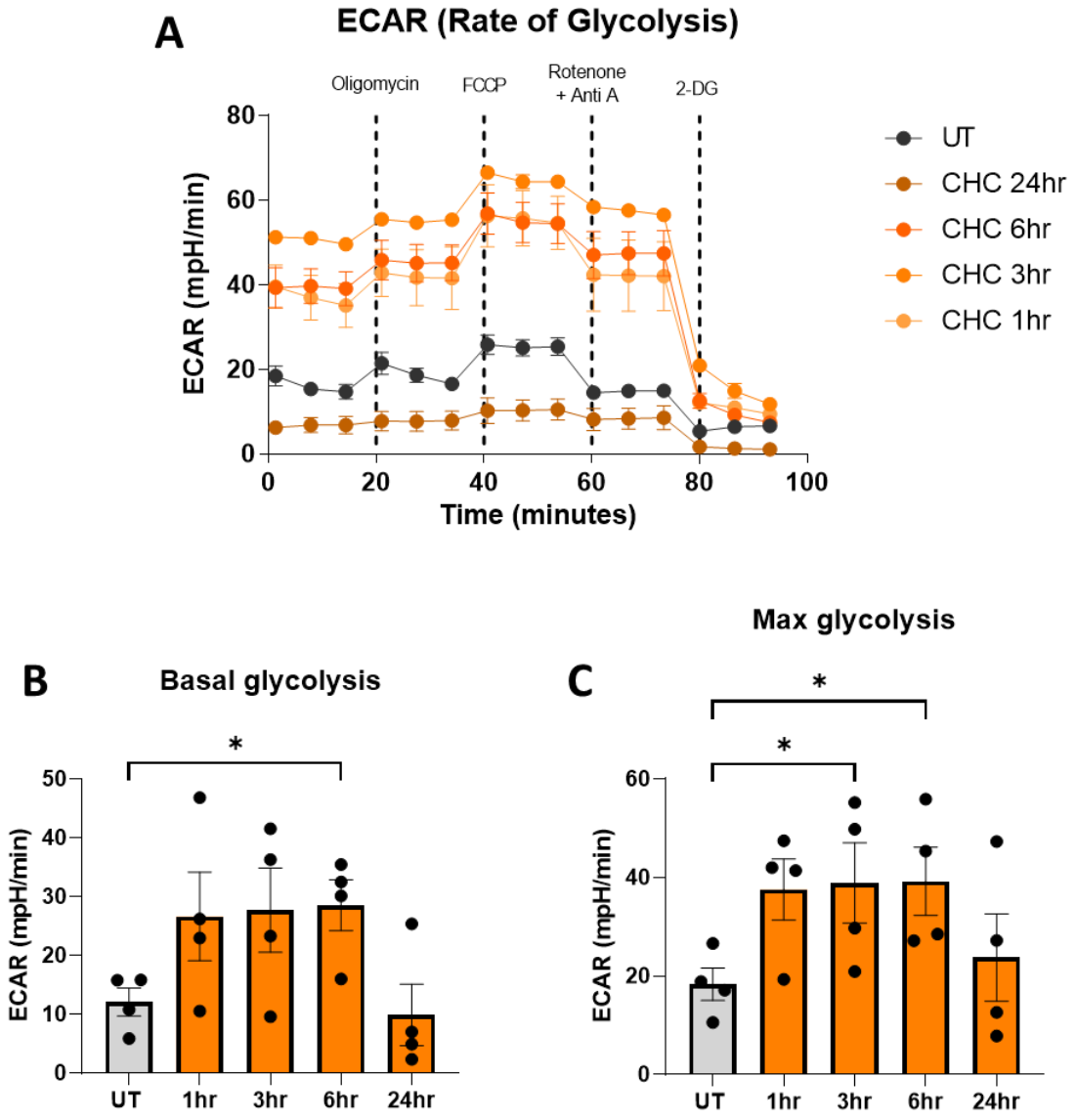

Figure 5-12 Cholesterol crystals increase rates of glycolysis in primary human macrophages.

Primary human macrophages (1 x 10^6 cells/ml) were stimulated with cholesterol crystals (500 µg/ml) for an extended time course of 1, 3, 6 and 24 hours. (**A**) Representative glycolysis (ECAR) Seahorse bioenergetics profiles before and after injections of oligomycin (1mM), FCCP (1mM), antimycin A (500 nM)/Rotenone (500 nM), and 2-DG (25 mM) post stimulation with cholesterol crystals. (**B-C**) Bar graphs demonstrating basal glycolysis and max glycolysis. Data is represented as mean ± SEM (N = 4, n =4). Data was analysed using RM One Way ANOVA with Dunnett's Test. *p≤0.05

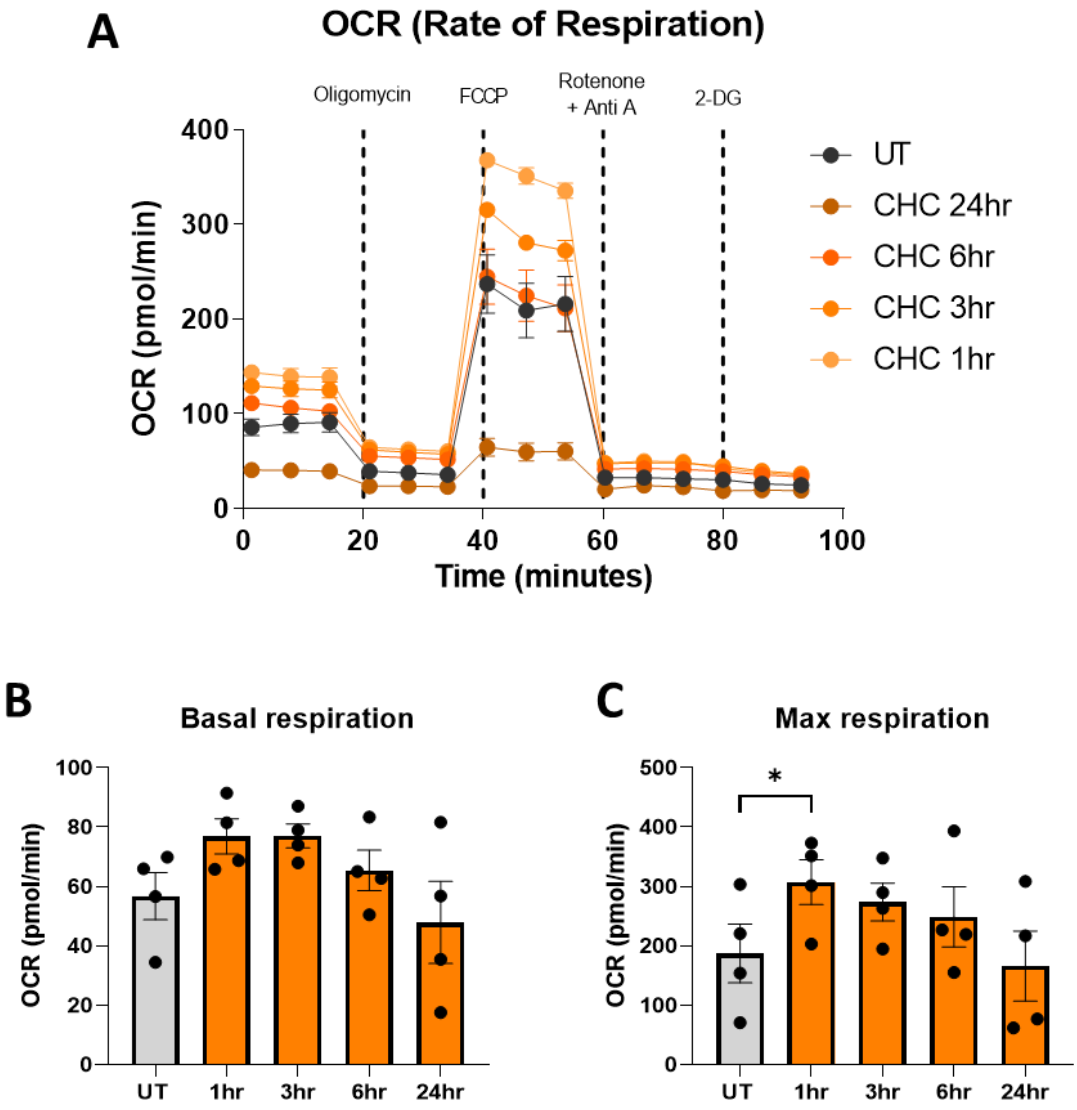

Figure 5-13 – Cholesterol crystals temporally increase rates of respiration in primary human macrophages.

Primary human macrophages (1 x 10^6 cells/ml) were stimulated with cholesterol crystals (500 µg/ml) for an extended time course of 1, 3, 6 and 24 hours. (A) Representative respiration (OCR) Seahorse bioenergetics profiles before and after injections of oligomycin (1mM), FCCP (1mM), antimycin A (500 nM)/Rotenone (500 nM), and 2-DG (25 mM) post stimulation with cholesterol crystals (500 µg/ml). (**B-C**) Bar graphs demonstrating basal glycolysis and max glycolysis. Data is represented as mean ± SEM (N = 4, n =4). Data was analysed using RM One Way ANOVA with Dunnett's Test. *p≤0.05

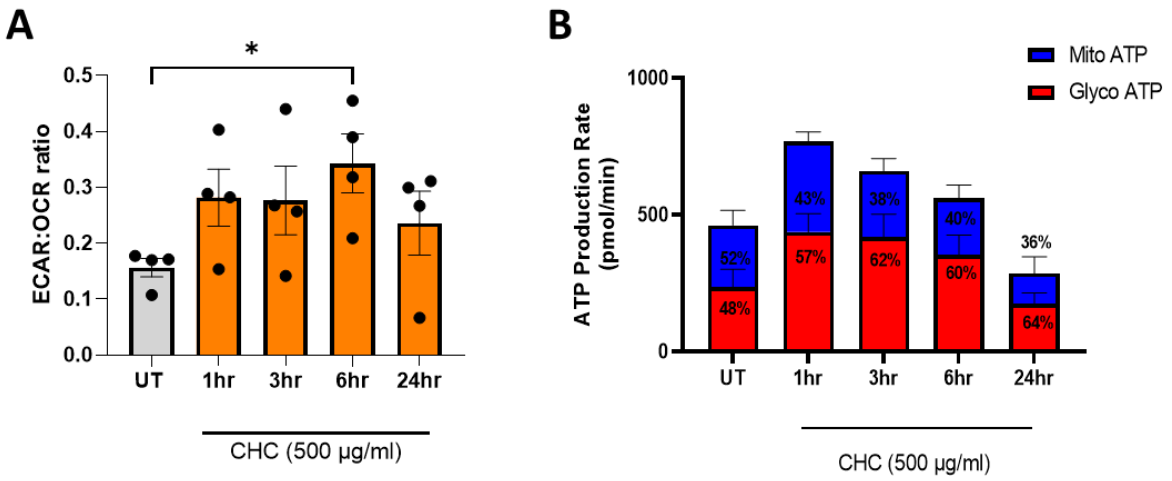

Figure 5-14 – Cholesterol crystals promote metabolic reprogramming to favour glycolysis.

Primary human macrophages (1 x 10^6 cells/ml) were stimulated with cholesterol crystals (500 µg/ml) for an extended time course of 1, 3, 6 and 24 hours. Bar graphs demonstrating (**A**) ratio of basal glycolysis (ECAR): basal respiration (OCR) and (**B**) ATP production rate in macrophages post cholesterol crystal stimulation. All data is represented as mean ± SEM (N = 4, n =4). Data was analysed using RM One Way ANOVA with Dunnett's Test. *p≤0.05

5.4.9 Cholesterol crystals promote a glycolytic profile in primary human macrophages.

To further validate findings from the Seahorse XF assay, primary human macrophages were treated with cholesterol crystals (500 μg/ml) over a 24 hour time course and imaged by fluorescence lifetime imaging microscopy (FLIM), whereby intracellular levels of NADH can be measured. Free NADH is associated with glycolysis, while the bound form of the co-factor is associated with oxidative phosphorylation [241]. The two forms of NADH can be distinguished from one another based on their distinct lifetimes upon fluorescence excitation. The ratio of bound NADH/Free NADH in the cell is then used to profile metabolic shifts in response to various stimuli, both qualitatively and quantitatively. Bound and free NADH levels were first assessed in untreated cells to establish a basal metabolic profile. Following cholesterol crystal treatment, FLIM analysis revealed a significant increase of free NADH at the 6 hour time point, represented by a significant decrease in the average lifetime of excitation of NADH (τavg) (Decrease of 0.12 ns ± 0.048 compared to untreated cells) (Figure 5.15 A-C) A trend in decreasing τavg, albeit not significant, was also observed at 24 hours post treatment (decrease of 0.064 ns ± 0.05) (Figure 5.15 D). These results suggest that macrophages exhibit a temporary shift in metabolism in response to cholesterol crystal treatment, primarily favouring glycolysis as a source of energy.

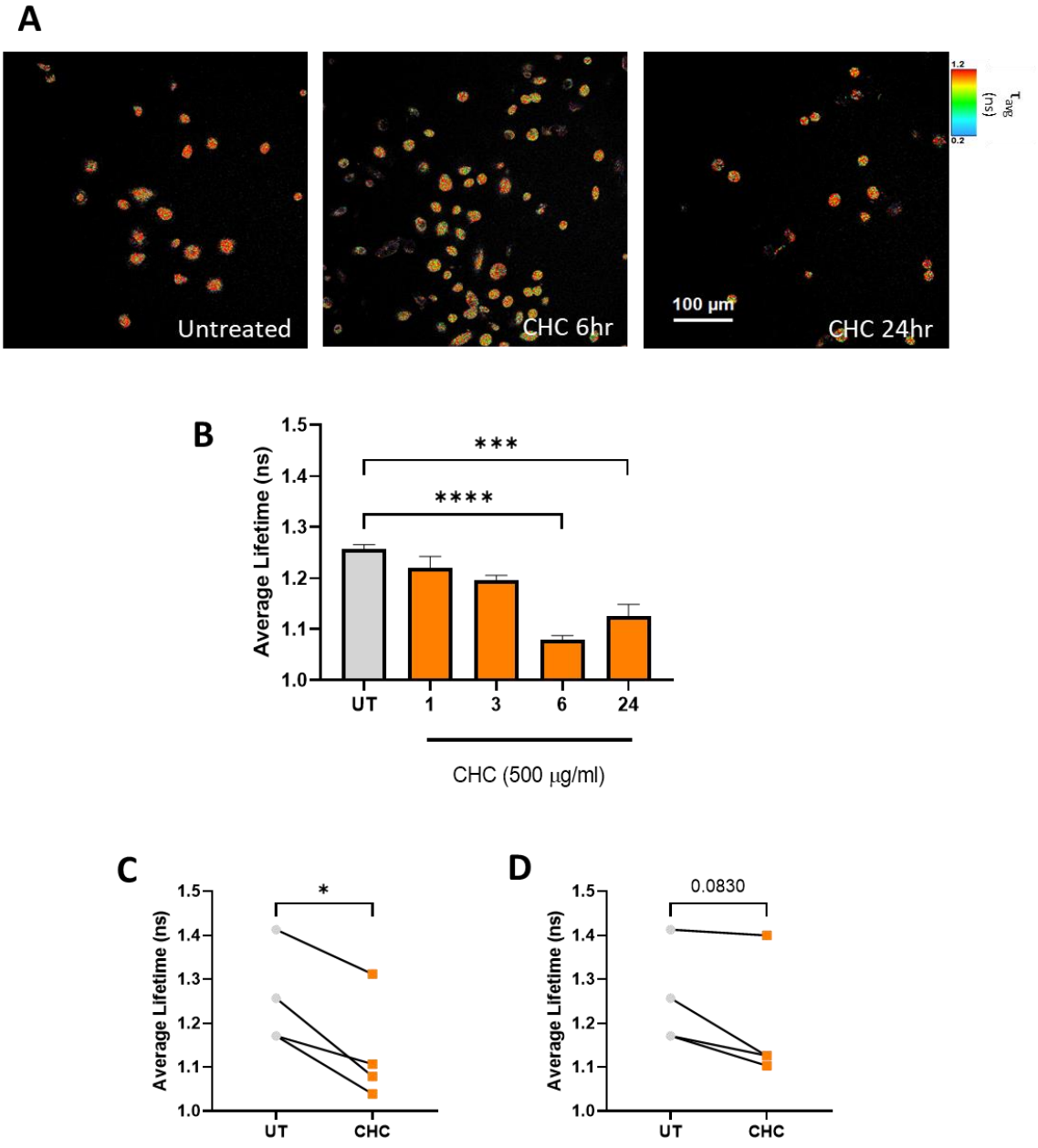

Figure 5-15 – Cholesterol crystals promote a glycolytic profile in primary human macrophages.

Primary human macrophages (1 x 10^6/ml) were stimulated with cholesterol crystals (500 µg/ml) for 1, 3, 6 and 24 hours. Intracellular NADH levels were analysed through Fluorescence Lifetime Imaging Microscopy. (**A**) FLIM images of untreated, and treated macrophages at 6 and 24 hours. (**B**) Representative time course of cholesterol crystal stimulation. Shifts in the ratio of bound: free NADH are represented by decreases of average lifetime (ns) of NADH where a decrease of average lifetime is indicative of increased glycolysis. Pooled data shows decrease of NADH average lifetime in response to cholesterol crystals at 6 (**C**) and 24 hours (D). All data is shown as mean ± SEM. Representative time course was analysed using One Way ANOVA with Dunnett's test. Pooled data was analysed using paired t-test. *p≤0.05, *** ≤0.001, ****p ≤0.0001

5.4.10 Cholesterol crystals drive mitochondrial fission in primary human macrophages

Metabolic reprogramming of LPS-stimulated macrophages is accompanied by changes in mitochondrial dynamics and morphology [242]. This shift favours mitochondrial fission, which is characterised by individual spherical mitochondria. These changes were assessed in primary human macrophages treated with cholesterol crystals at 6 and 24 hours using confocal microscopy. Following cholesterol crystal treatment, macrophages were stained with MitoTracker™ to highlight mitochondrial morphology (shown in red) and counterstained with Hoechst for nuclear staining (shown in blue). In comparison to untreated cells, macrophages exhibited a significant decrease in mitochondrial elongation and a significant increase in sphericity at both 6 hours and 24 hours post crystal treatment, as represented by decreases in eccentricity and aspect ratio of the mitochondria (Figure 5.16). This suggests that the cells are undergoing mitochondrial fission in response to cholesterol crystal treatment.

To further validate these results, macrophages were treated with cholesterol crystals for 6 and 24 hours and expression of mitochondrial fission regulatory proteins mitochondrial fission factor (MFF) and Drp-1 [243] were assessed by western blotting. MFF is recruited to the surface of mitochondria and acts as a further recruiter/receptor site binder for Drp-1. Once at the site of the mitochondria, Drp-1 forms an oligomer, inducing fragmentation/fission of the mitochondria. A significant increase in expression of both proteins was observed in response to cholesterol crystals, at both 6 and 24 hours in comparison to untreated cells (Figure 5.17). This result, combined with findings from image analysis of the mitochondria, indicates that cholesterol crystals promote mitochondrial fission in macrophages, which is in agreement with the glycolytic profile observed using both Seahorse and FLIM analysis.

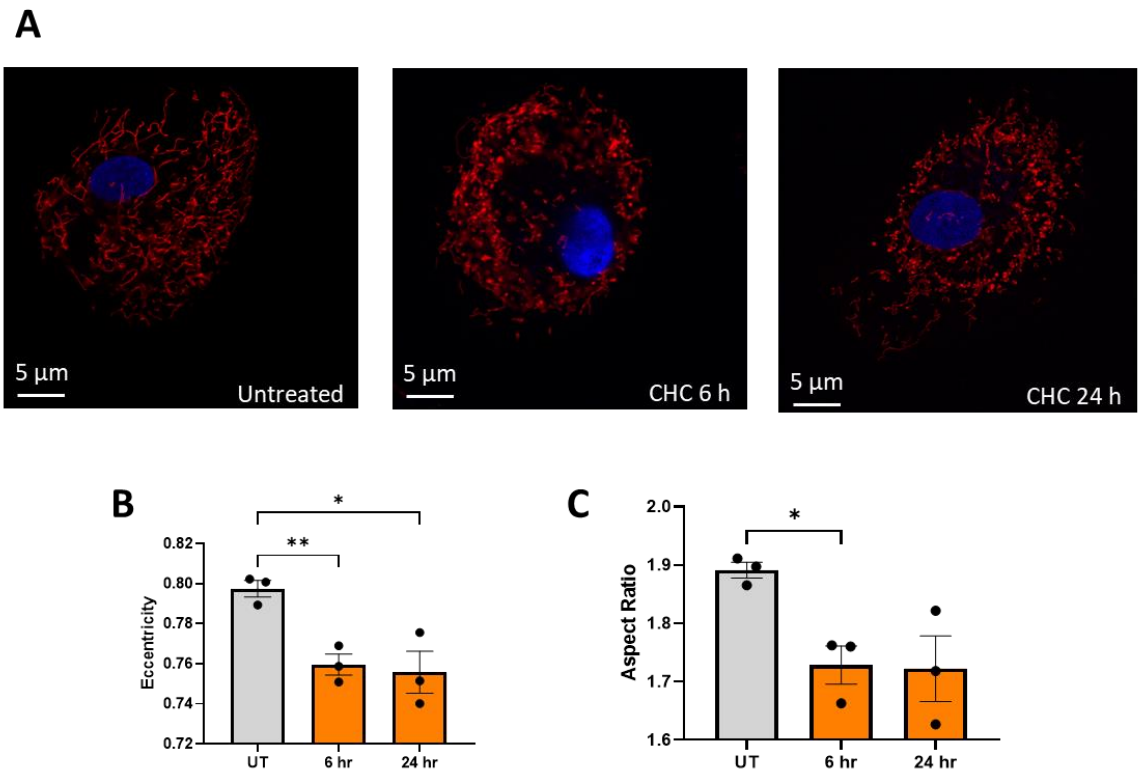

Figure 5-16 – Cholesterol crystals promote mitochondrial fission in primary human macrophages.

Primary human macrophages (1 x 10^6/ml) were stimulated with cholesterol crystals (500 µg/ml) for 6 and 24 hours. Cells were stained with Mitotracker (red) to assess mitochondrial morphology in response to cholesterol crystal treatments. Cells were counterstained with Hoechst (blue) to show nuclei. Cells were imaged using a Leica SP8 scanning confocal microscope. (**A**) Representative images of untreated and cholesterol crystal stimulated macrophages at 6 and 24 hours. (**B-C**) Shape parameters of mitochondria were quantified using Cell Profiler software (N = 3, n = 15). Data was analysed using one-way ANOVA with Dunnett's test. *p≤0.05, **p≤0.01

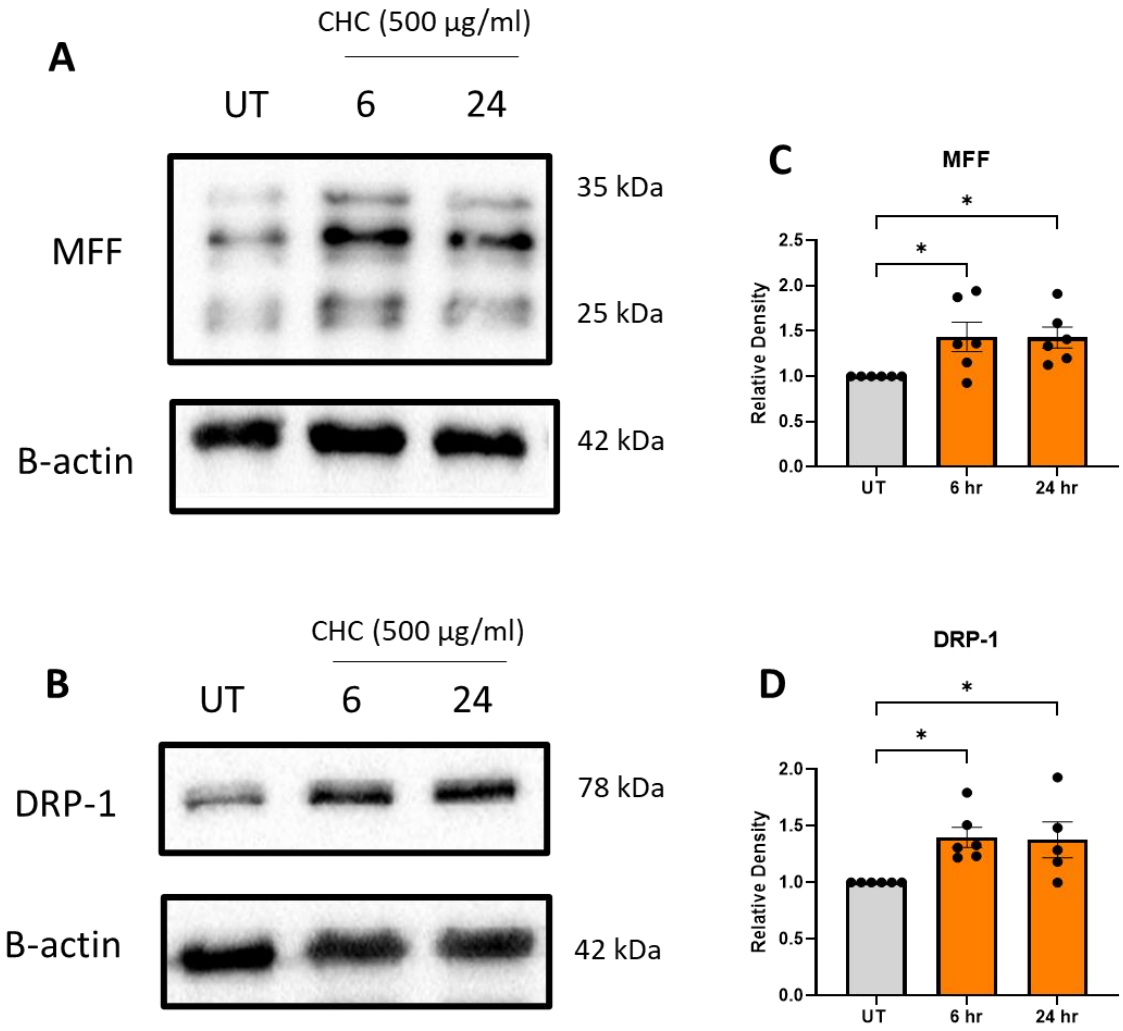

Figure 5-17 – Cholesterol crystals drive expression of mitochondrial regulatory proteins in primary human macrophages.

Primary human macrophages (1 x 10^6 cells/ml) were stimulated with cholesterol crystals (500 µg/ml) for 6 and 24 hours. (**A-B**) Representative western blots demonstrating expression of MFF and DRP-1 in response to cholesterol crystals. (**C-D**) Densitometric analysis of western blots (N = 5) using Biorad software. Bar graphs illustrate the mean ± SEM increase in protein expression relative to untreated control and normalised to B-actin housekeeping protein. All data was analysed using One Way ANOVA with Dunnett's post-test. *p≤0.05

5.4.11 Cholesterol crystals drive mitochondrial ROS production in primary human macrophages.

Given the significant changes in mitochondrial dynamics in cholesterol crystal treated macrophages, it was next investigated whether cholesterol crystals caused mitochondrial stress or dysfunction, as indicated by production of mitochondrial ROS. Furthermore, mitochondrial ROS production is known to occur in metabolically reprogrammed macrophages and is also a feature of atherosclerotic plaques [244]. Primary human macrophages were treated with cholesterol crystals (500 μg/ml) for 6 or 24 hours, prior to incubation with MitoSOX™ Red. MitoSOX™ Red reagent permeates live cells, where it selectively targets the mitochondria. Upon contact with ROS in the mitochondria, the reagent rapidly oxidises, generating a fluorescent product, that can be detected using flow cytometry. In response to cholesterol crystal treatment, a significant increase in median fluorescence intensity (MFI) of MitoSOX™ stained cells was observed relative to untreated cells at both 6 and 24 hours (55.4 % ± 14.35 at 6 hours, 82.57 % ± 30.49 at 24 hours), indicating robust production of mitochondrial ROS (Figure 5.18).

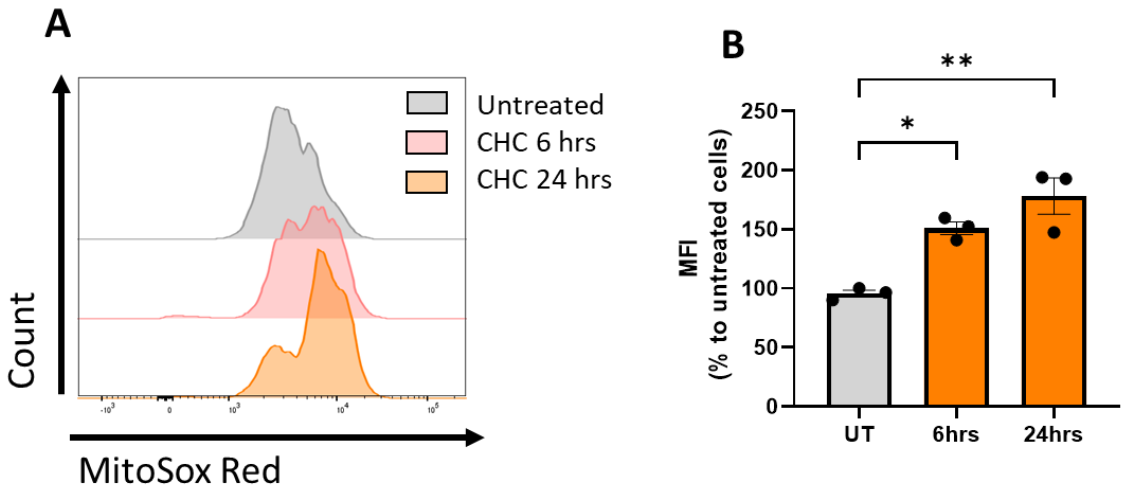

Figure 5-18 – Cholesterol crystals drive mitochondrial ROS production in primary human macrophages.

Primary human macrophages (1 x 10^6 cells/ml) were stimulated with cholesterol crystals (500 µg/ml) for 6 and 24 hours. Cells were stained with MitoSox™ Red to assess mitochondrial ROS production and analysed by flow cytometry. (**A**) Representative histogram demonstrating median fluorescence intensity (MFI) of MitoSox™ in untreated and cholesterol crystal treated cells. (**B**) Bar graph illustrates the mean ± SEM increase in MFI relative to untreated control (N = 3) Data was analysed using One Way ANOVA with Dunnett's post-test. *p≤0.05, **p≤0.01

5.4.12 Inhibition of glycolysis with 2-DG attenuates M1 polarisation and DAMP expression in primary human macrophages.

Having established that cholesterol crystals promote a significant shift in metabolism to favour glycolysis, it was next aimed to investigate if direct inhibition of glycolysis would have any impact on the inflammatory phenotype induced by cholesterol crystals. 2-deoxyglucose (2-DG) acts as an analogue of glucose, competing for interaction with HK2. However, the structure of 2-DG renders conversion to glucose-6-phosphate impossible, thus inhibiting further activity in the glycolytic pathway.

Macrophage viability was first assessed in response to treatment with 2-DG, to ensure that any reduction in inflammatory response observed was a result of glycolysis inhibition, and not reduced cell viability. Primary human macrophages were treated with previously published doses of 2-DG (25 mM) [43] for 24 hours and cell viability was measured by flow cytometry. No significant difference in the percentage of live cells was observed in 2-DG treated macrophages compared to the untreated control ($p > 0.9999$) (Figure 5.19). Macrophages were then pre-treated with 2-DG for 30 minutes prior to cholesterol crystal stimulation. Expression of the M1 genes, *CXCL9*, *CXCL10* and the DAMPs, *S100A8* and *S100A12*, were measured at 6 hours by real time PCR. Production of IL-8 was measured by ELISA after 24 hours. A significant reduction in expression of M1 genes and DAMPs was observed in macrophages pre-treated with 2-DG in comparison to cholesterol crystal treatment alone (Figure 5.20). IL-8 production was also significantly reduced in the presence of 2-DG (Figure 5.21).

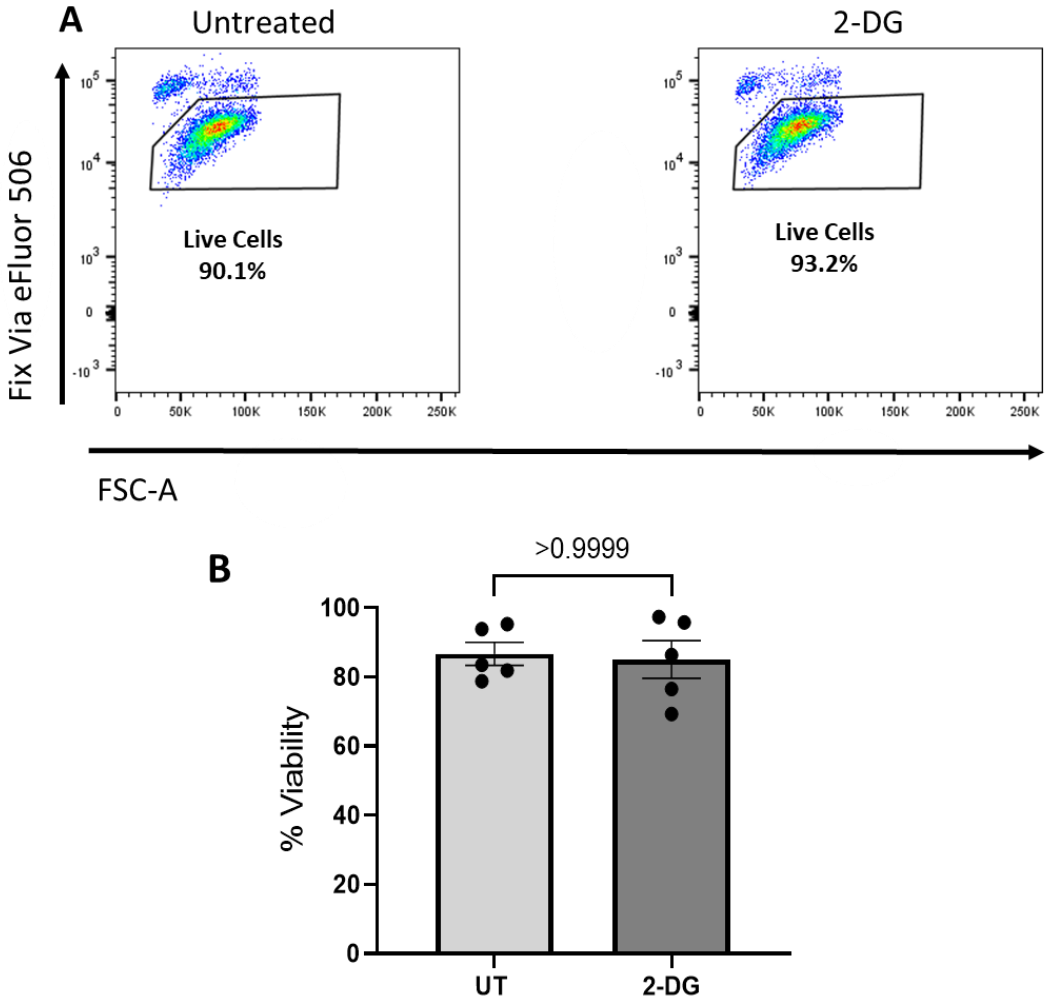

Figure 5-19 - Glycolytic inhibitor 2-DG does not impact viability of primary human macrophages.

Primary human macrophages (1 x 10^6 cells/ml) were treated with 2-DG (25 mM) for 24 hours. Cells were stained with FixVia eFluor™ 506 to assess cell viability and analysed by flow cytometry. (**A**) Representative flow plots demonstrating cell viability in untreated, and 2-DG treated cells. (**B**) Bar graph shows pooled data of % viability of untreated and treated cells (N = 5). Data is shown as mean ± SEM and was analysed using paired t-test.

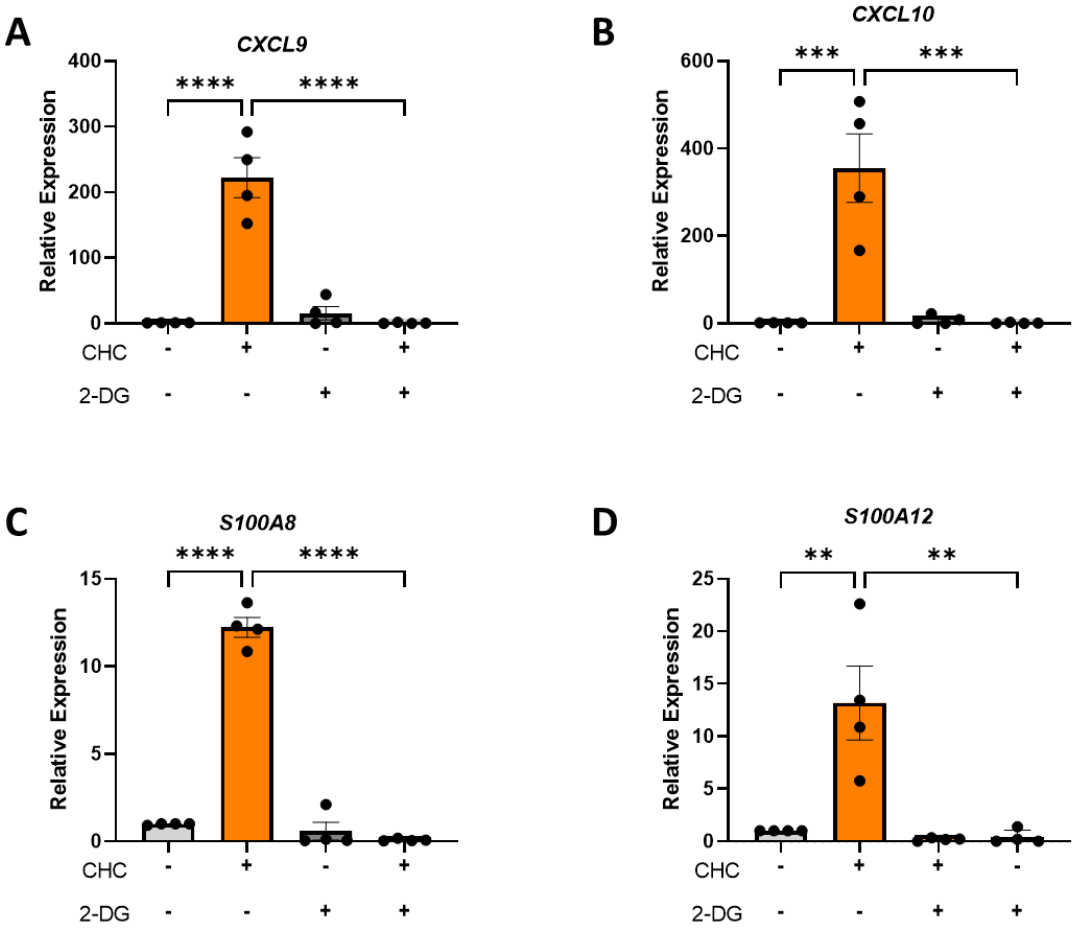

Figure 5-20 - CHC-induced macrophage polarization and DAMP expression is attenuated in the presence of the glycolytic inhibitor 2-DG

Primary human macrophages (1 x 10^6 cells/ml) were stimulated with cholesterol crystals (500 µg/ml) for 6 hours in the presence or absence of 2-DG (25 mM). (**A-D**) mRNA expression of *CXCL9, CXCL10, S100A8* and *S100A12* was analysed by real-time PCR (N= 4, n = 3). All data is represented as mean ± SEM and analysed using one-way ANOVA with Tukey's post-test. **p≤0.01, *** ≤0.001, ****p ≤0.0001

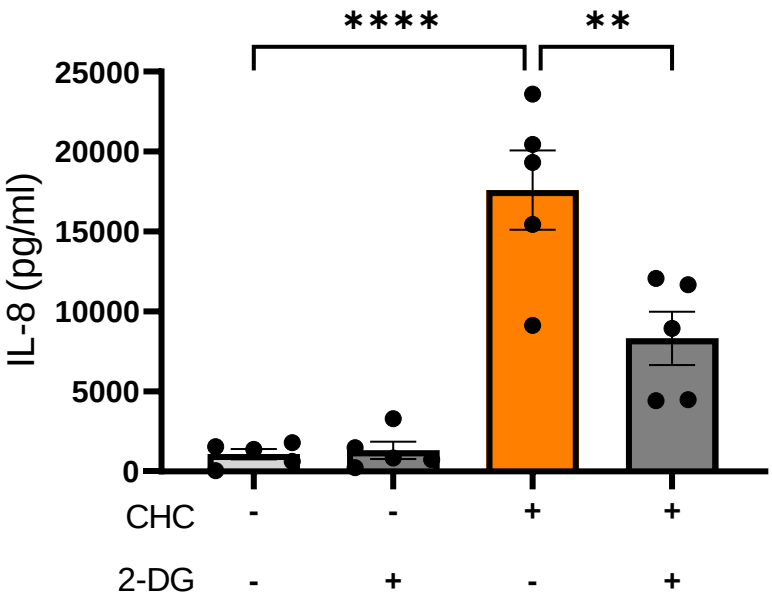

Figure 5-21 - CHC-induced production of IL-8 is abrogated in the presence of the glycolytic inhibitor 2-DG

Primary human macrophages (1 x 10^6 cells/ml) were stimulated with cholesterol crystals (500 µg/ml) for 24 hours in the presence or absence of 2-DG (25 mM). IL-8 cytokine production in cell supernatants was analysed by ELISA (N = 5, n = 3). Data is represented as mean ± SEM and was analysed using one-way ANOVA with Tukey's post-test. **p≤0.01, ****p ≤0.0001

5.4.13 Inhibition of glycolysis with 3PO attenuates M1 polarisation and DAMP expression in primary human macrophages.

An alternative inhibitor of glycolysis (3PO) was used to further confirm the interplay between glycolysis and cholesterol crystal-induced M1 polarisation. 3PO targets the rate limiting enzyme PFKFB3, which is downstream of HK2. Macrophage viability was first assessed in response to the standard dose of 3PO used in published studies (10 μM) [245]. Cells were treated with 3PO (10 μM) for 24 hours and assessed for viability using flow cytometry. Having observed no significant difference in viability between untreated and 3PO-treated macrophages ($p = 0.7297$) (Figure 5.22), it was next aimed to investigate the impact of 3PO on cholesterol crystal-induced gene expression and IL-8 production. Primary human macrophages were treated with 3PO (10 μM) for 30 minutes prior to cholesterol crystal stimulation. Similar to experiments with 2-DG, a significant reduction in expression of M1 genes and DAMPs was observed in cells pre-treated with 3PO, compared to cholesterol crystal treatment alone, further highlighting the link between cholesterol crystal-induced macrophage metabolism and M1 polarisation (Figure 5.23). IL-8 production was also significantly reduced in the presence of 3PO (Figure 5.24).

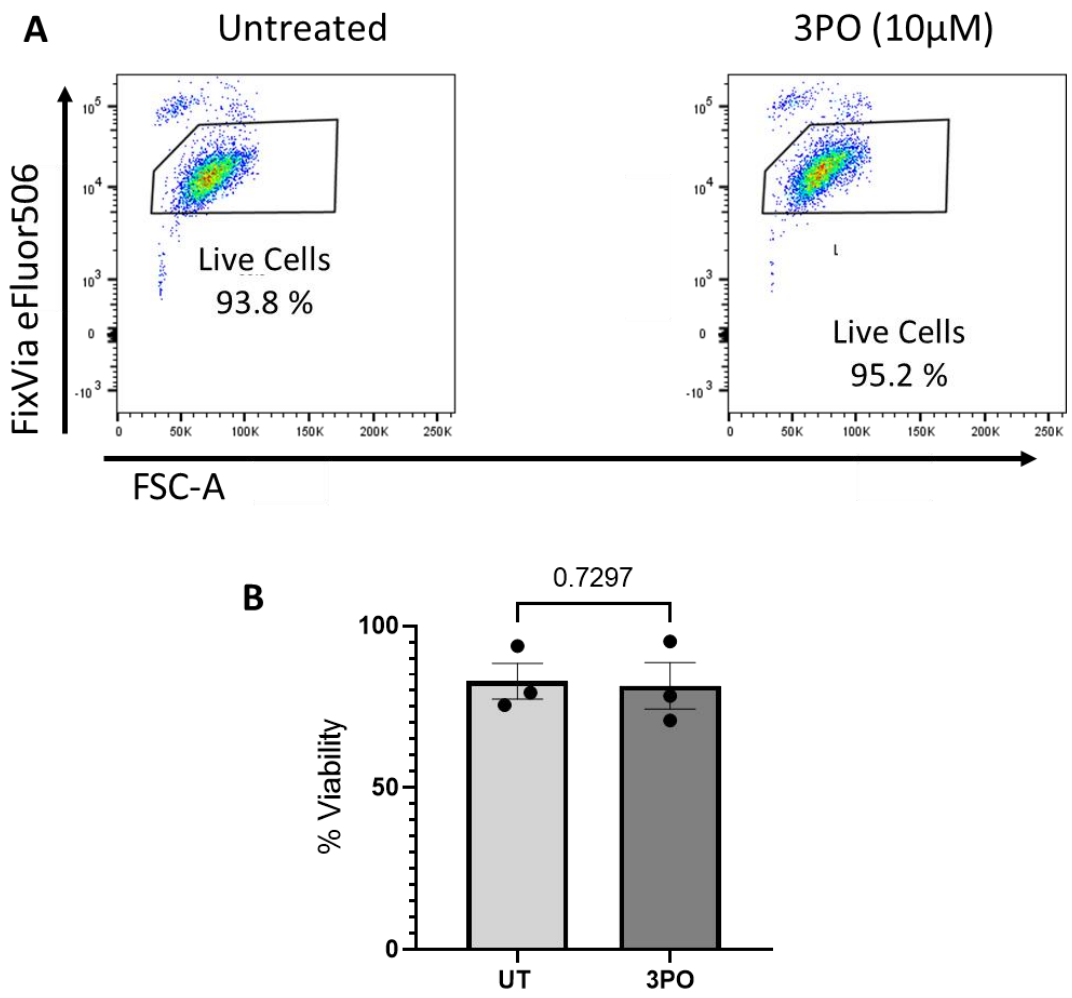

Figure 5-22 – Glycolytic inhibitor 3PO does not impact the viability of primary human macrophages.

Primary human macrophages (1 x 10^6 cells/ml) were treated with 3PO (10 µM) for 24 hours. Cells were stained with FixVia efluor™ 506 to assess cell viability and analysed by flow cytometry. (**A**) Representative flow plots demonstrating cell viability in untreated, and 3PO treated cells. (**B**) Bar graph shows pooled data of % viability of untreated and treated cells (N = 3). Data is shown as mean ± SEM and was analysed using paired t-test.

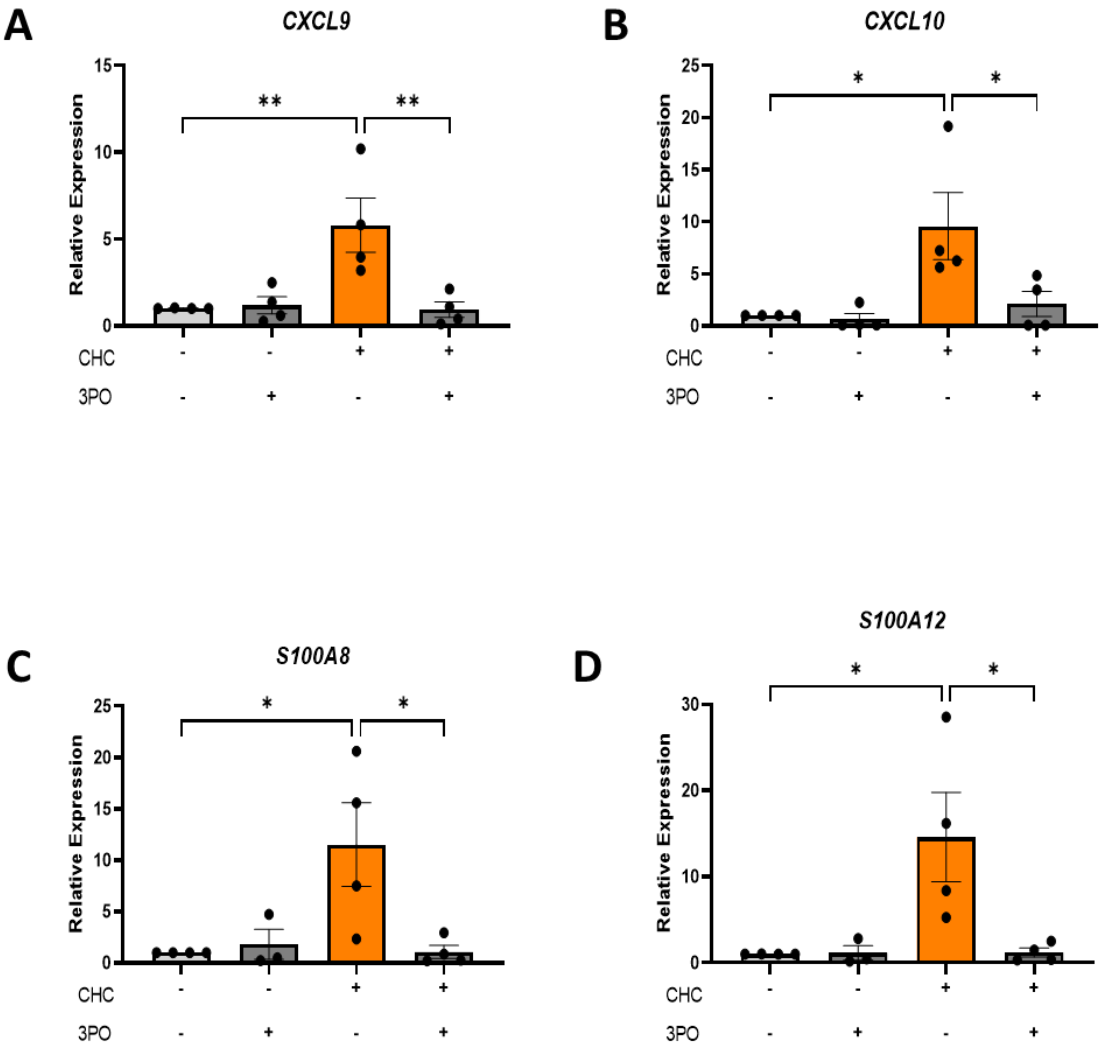

Figure 5-23 - CHC-induced macrophage polarization and DAMP expression is attenuated in the presence of the glycolytic inhibitor 3PO

Primary human macrophages (1 x 10^6 cells/ml) were stimulated with cholesterol crystals (500 µg/ml) for 6 hours in the presence or absence of 3PO (10 µM). (**A-D**) mRNA expression of *CXCL9, CXCL10, S100A8* and *S100A12* was analysed by real-time PCR (N= 4, n = 3). All data is represented as mean ± SEM and analysed using one-way ANOVA with Tukey's post-test. *p≤0.05, **p≤0.01

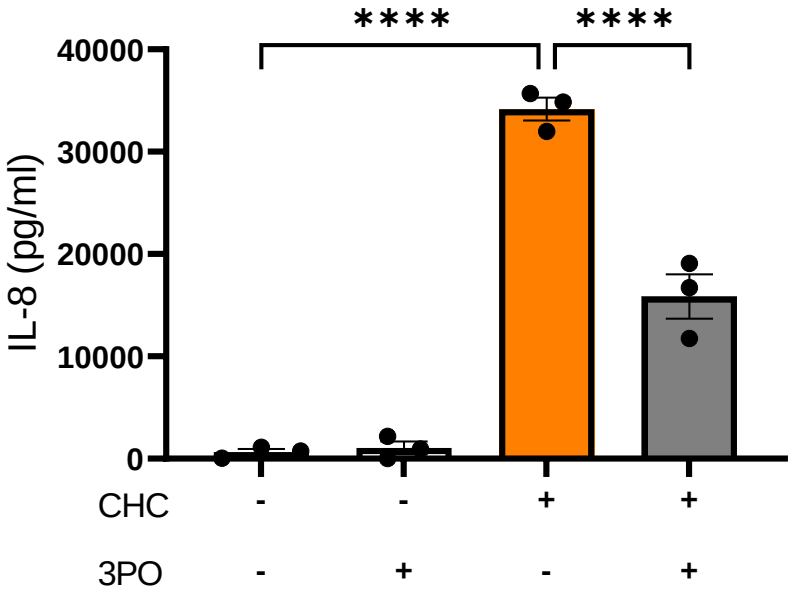

Figure 5-24 - CHC-induced production of IL-8 is abrogated in the presence of the glycolytic inhibitor 3PO

Primary human macrophages (1 x 10^6 cells/ml) were stimulated with CHC (500 µg/ml) for 24 hours in the presence or absence of 3PO (10 µM). IL-8 cytokine production in cell supernatants was analysed by ELISA (N = 3, n = 3). Data is represented as mean ± SEM and was analysed using one-way ANOVA with Tukey's post-test. ****p ≤0.0001

5.4.14 Cholesterol crystals drive expression and nuclear translocation of pyruvate kinase M2 (PKM2).

Having established that inhibition of glycolysis abrogates the inflammatory phenotype of cholesterol crystal treated macrophages, it was next aimed to further understand how this response is regulated. PKM2 has been shown to regulate the expression of key glycolytic proteins and the subsequent production of inflammatory cytokines in LPS-stimulated macrophages [50]. Elevated expression and dimerization of PKM2 in monocytes and macrophages has also been highlighted as a diagnostic marker for atherosclerosis, as well as other cardiovascular and metabolic diseases [246]. Upon activation, PKM2 translocates into the nucleus of the cell, where it promotes transcription of HIF1α and other downstream pro-glycolytic factors. In previous studies with LPS-treated macrophages, nuclear translocation of PKM2 has proven to be essential for metabolic reprogramming and M1 polarisation [50]. Considering this, it was investigated if the elevated level of glycolysis and M1 polarisation seen in cholesterol crystal treated macrophages, was also coupled to increased PKM2 expression and nuclear translocation. mRNA expression of PKM2 was first assessed in macrophages treated with cholesterol crystals for 1, 3, 6 and 24 hours using real-time PCR. Increased PKM2 mRNA expression occurred in a time-dependent manner, with maximal expression observed at the 24 hour time point (5.8 fold change ± 4.39 relative to untreated cells) (Figure 5.25).

Subcellular fractionation of protein lysates was next performed on cholesterol crystal treated macrophages in order to assess the cellular location of PKM2. An increase in PKM2 protein was detected in the nuclear fraction of cholesterol crystal treated cells at 3 and 6 hours, as assessed by western blotting (Figure 5.26 A). These results were further validated using confocal microscopy. Untreated macrophages contained an evenly distributed pattern of cytoplasmic PKM2 (shown in red). However, in macrophages treated with cholesterol crystals at 6 and 24 hours, PKM2 was dispersed in a punctate pattern with observed perinuclear dominance of the protein (Figure 5.26 B). Mean nuclear and cytosolic fluorescence intensities were quantified and compared to yield a nuclear:cytosolic ratio as a relative measure of PKM2 nuclear localisation. A significant increase in the nuclear:cytosolic ratio was observed in cholesterol crystal treated macrophages when compared to untreated macrophages at both time points

(increase of 0.22 a.u. ± 0.11 at 6 hours, increase of 0.19 a.u. ± 0.13 at 24 hours) (Figure 5.26 C-D). This results confirm that PKM2 translocates to the nucleus when macrophages are treated with cholesterol crystals.

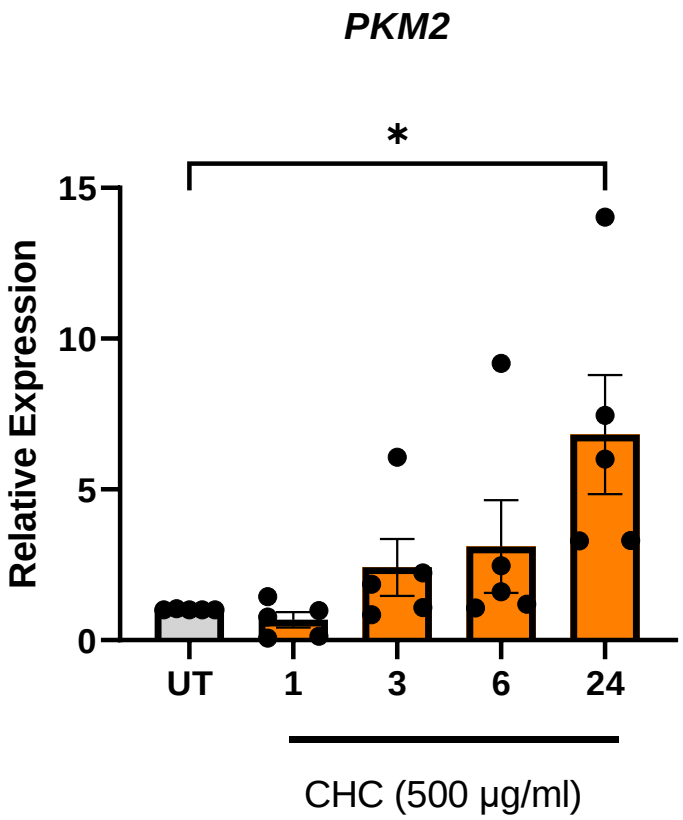

Figure 5-25 - Cholesterol crystals drive mRNA expression of PKM2 in primary human macrophages

Primary human macrophages (1 x 10^6 cells/ml) were stimulated with cholesterol crystals (500 µg/ml) for 1,3, 6 and 24 hours. mRNA expression of *PKM2* was analysed by real time PCR (N = 5, n = 3). Data is represented as mean ± SEM and was analysed using one-way ANOVA with Dunnett's post-test. *p≤0.05

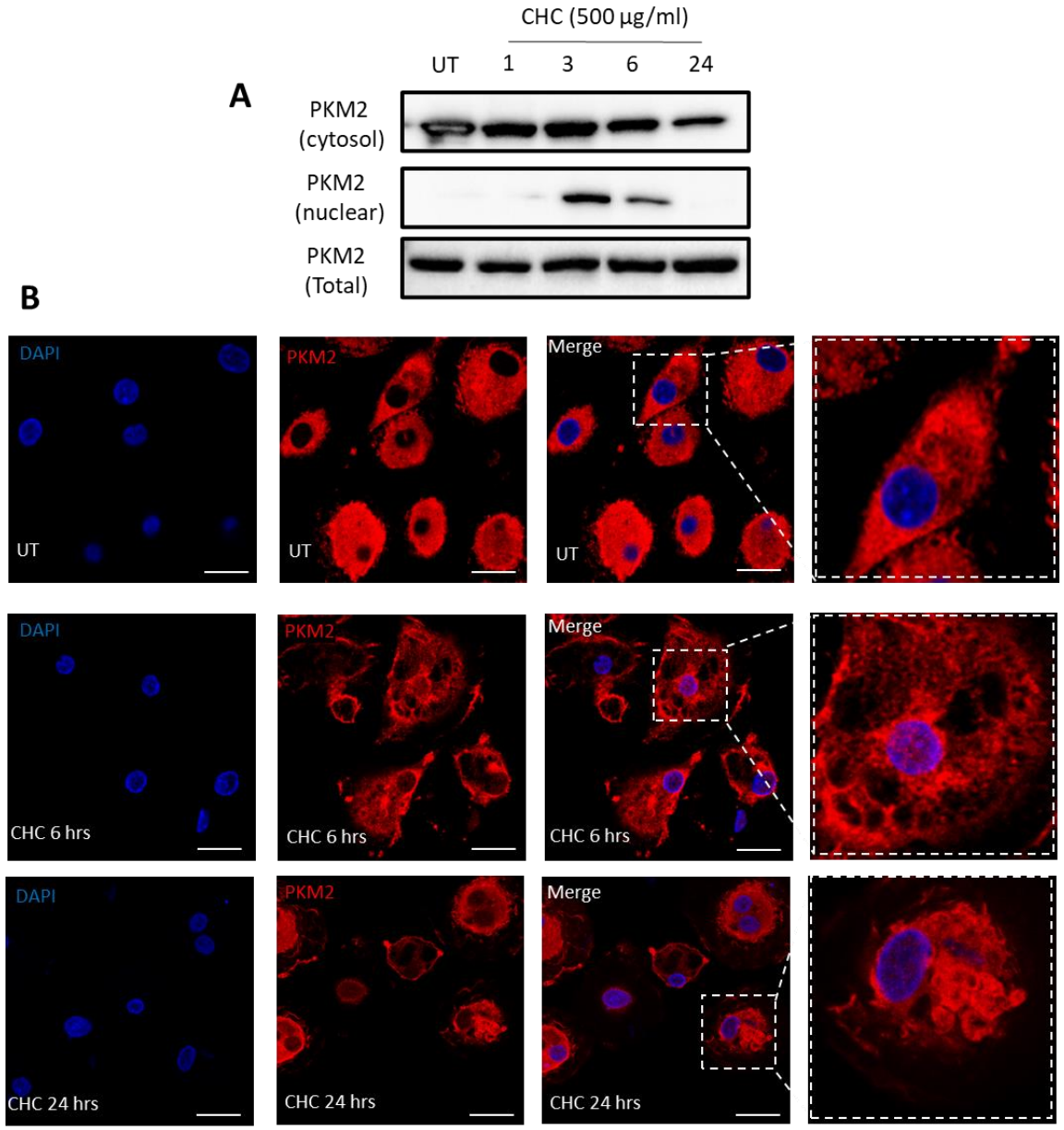
A
CHC (500 µg/ml)
UT
1
3
6
24
PKM2 (cytosol)
PKM2 (nuclear)
PKM2 (Total)
B
DAPI
PKM2
Merge
UT
CHC 6 hrs
CHC 24 hrs
C
Intensity ratio
*
1.0
0.8
0.6
0.4
0.2
0.0
UT
CHC 6 hrs
D
Intensity ratio
*
1.0
0.8
0.6
0.4
0.2
0.0
UT
CHC 24 hrs

Figure 5-26 - Cholesterol crystals drive nuclear translocation of PKM2 in primary human macrophages.

Primary human macrophages (1 x 10^6 cells/ml) were stimulated with cholesterol crystals (500 µg/ml) for 1, 3, 6 and 24 hours. (**A**) Representative western blot showing PKM2 protein in the cytosol and nucleus versus total cell protein expression. (**B**) Representative confocal images of untreated and cholesterol crystal treated cells at 6 and 24 hours. Fluorescence intensity ratio of PKM2 in the nucleus versus the cytoplasm was quantified using Imaris™ software. Bar graphs depict (**C**) untreated versus cholesterol crystal treatment at 6 hours, and (**D**) untreated versus cholesterol crystal treatment at 24 hours. All data is represented as mean ± SEM. PCR data was analysed using one-way ANOVA with Dunnett's post-test, fluorescence intensity ratios were analysed using paired t-test. Scale bar represents 20 µm. *p≤0.05

5.4.15 Cholesterol crystal-induced glycolysis and HIF1α expression is dependent on PKM2 translocation.

Having observed that cholesterol crystals drive translocation of PKM2 into the nucleus, it was of interest to determine if this is coupled to metabolic reprogramming. Treatment with the compound, TEPP-46, results in tetramerization of PKM2 protein in the cytosol, effectively inhibiting translocation of the monomer/dimer form into the nucleus [50, 247]. In a similar fashion to the above experiments involving 2-DG and 3PO, macrophages were first treated with TEPP-46 at a previously published dose (50 µM) for 24 hours [50], to assess viability (Figure 5.27). Having established no significant difference in viability between TEPP-46 treated and untreated macrophages (p = 0.3210), the impact of the PKM2 inhibitor on cholesterol crystal-induced macrophage responses was next investigated.

Macrophages were treated with TEPP-46 (50 µM) for 30 minutes followed by stimulation with cholesterol crystals for 6 hours. ECAR and OCR was assessed using the Seahorse XFe96 Bioanalyser in response to cell treatments. A significant reduction in both basal and max rates of glycolysis were observed in macrophages pre-treated with TEPP-46 when compared to cholesterol crystal treatment alone (Figure 5.28).

Given that the downstream impact of PKM2 nuclear translocation is to drive expression of the transcription factor HIF1α, I investigated the impact of TEPP-46 treatment on cholesterol crystal-induced expression of this protein. Macrophages were pre-treated with TEPP-46 (50 µM) for 30 minutes prior to treatment with cholesterol crystals (500 µg/ml) for 6 hours. mRNA levels of HIF1α were then assessed by real-time PCR. In

agreement with the reduced glycolytic profile observed using Seahorse analysis, pre-treatment with TEPP-46 caused a significant reduction in expression of HIF1α when compared with cholesterol crystal treatment alone (7.45 fold change ± 6.19), as assessed by real-time PCR (Figure 5.29).

Interestingly, the inhibitor appeared to have no impact on cellular respiration (Figure 5.29), as TEPP-46 treatment caused no significant difference in rates of basal or max respiration in cholesterol crystal-treated macrophages ($p = 0.8117$ between treatment groups for basal respiration, $p = 0.2223$ between treatment groups for max respiration). This observation highlights the selective role of the inhibitor in targeting elevated levels of glycolysis, rather than cell metabolism as a whole.

These findings were further validated using FLIM analysis where macrophages pre-treated with TEPP-46 (50 μM) for 30 minutes prior to cholesterol crystal stimulation for 6 hours showed a significant increase in τavg, indicating that the cells are significantly less glycolytic in response to cholesterol crystal treatment when PKM2 translocation is inhibited (Figure 5.31).

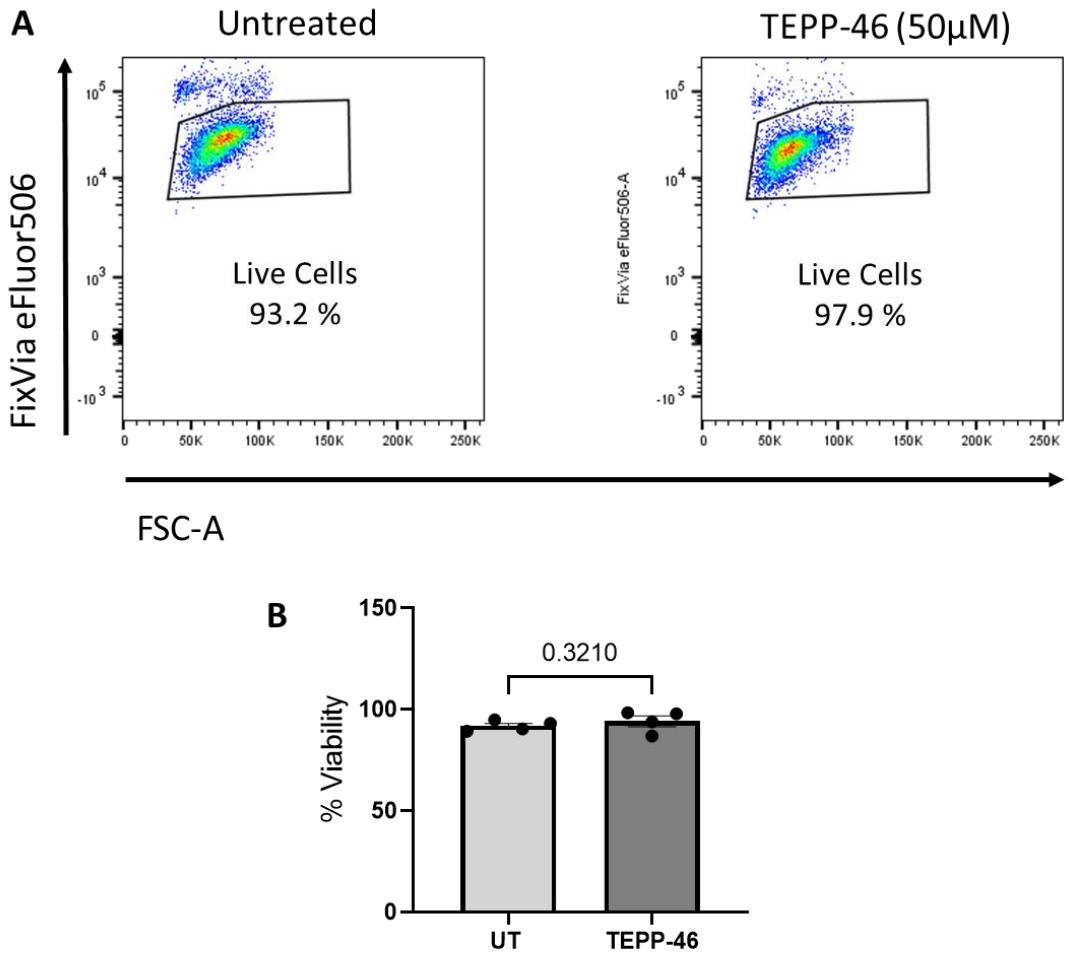

Figure 5-27 - TEPP-46 does not impact viability of primary human macrophages

Primary human macrophages (1 x 10^6 cells/ml) were treated with TEPP-46 (50 µM) for 24 hours. Cells were stained with FixVia eFluor™ 506 to assess cell viability and analysed by flow cytometry. (**A**) Representative flow plots demonstrating cell viability in untreated, and TEPP-46 treated cells. (**B**) Bar graph shows pooled data of % viability of untreated and treated cells (N = 4). Data is shown as mean ± SEM and was analysed using paired t-test.

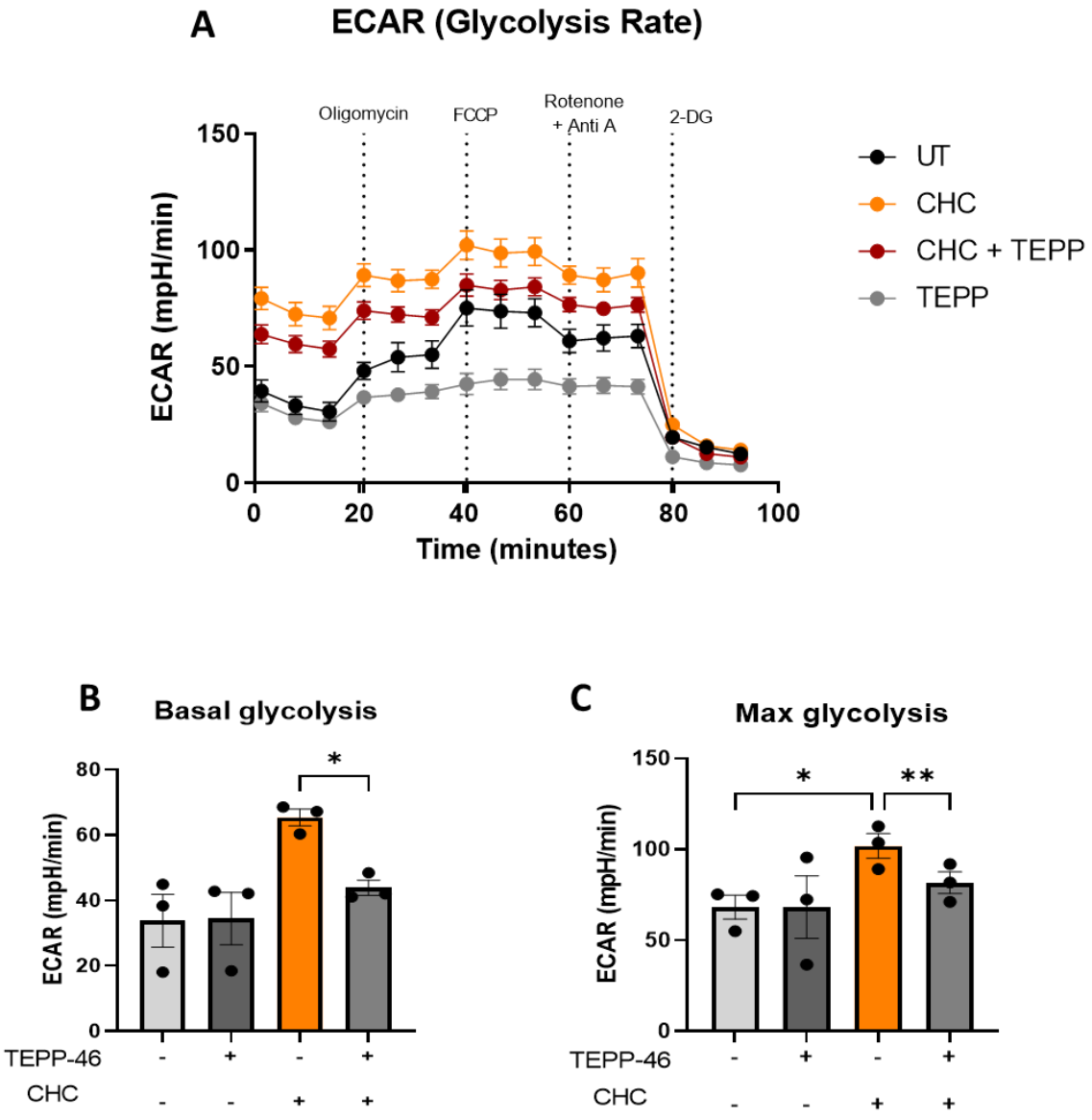

Figure 5-28 -Cholesterol crystal induced metabolic reprogramming is regulated through PKM2.

Primary human macrophages (1 x 10^6 cells/ml) were pre-treated with TEPP-46 (50 µM) prior to treatment with cholesterol crystals (500 µg/ml) for 6 hours. (**A**) Representative glycolysis (ECAR) Seahorse bioenergetics profiles before and after injections of oligomycin (1mM), FCCP (1mM), antimycin A (500 nM)/Rotenone (500 nM), and 2-DG (25 mM) post stimulation with cholesterol crystals (500 µg/ml). (**B-C**) Bar graphs demonstrating basal glycolysis and max glycolysis. Data is represented as mean ± SEM (N = 3, n =4). Data was analysed using RM One Way ANOVA with Tukey's post-test. **p<0.05 *p≤0.01

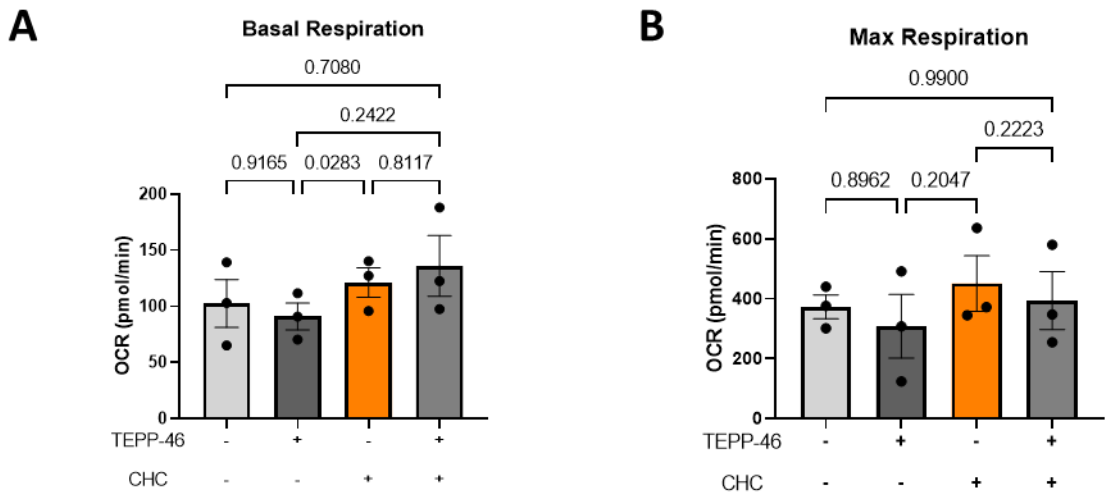

Figure 5-29 - Inhibition of PKM2 activity with TEPP-46 has no impact on macrophage respiration

Primary human macrophages (1 x 10^6 cells/ml) were pre-treated with TEPP-46 (50 µM) prior to treatment with cholesterol crystals (500 µg/ml) for 6 hours. (**A-B**) Bar graphs demonstrating basal respiration and max respiration of cholesterol crystal treated cells in the presence or absence of TEPP-46. Data is represented as mean ± SEM (N = 3, n =4). Data was analysed using RM One Way ANOVA with Tukey's post-test.

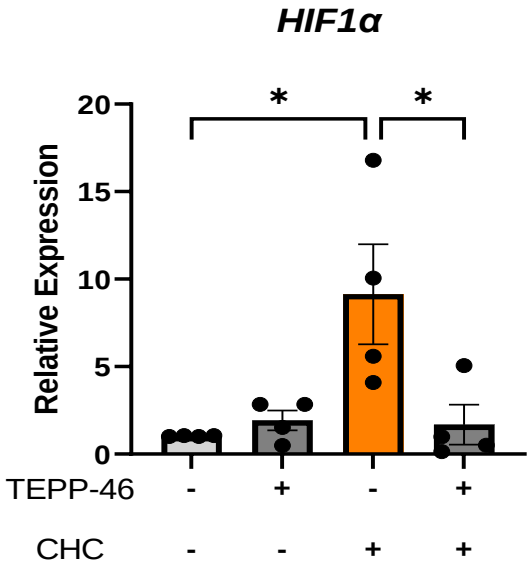

Figure 5-30 - Cholesterol crystal induced HIF1α expression is regulated through PKM2.

Primary human macrophages (1 x 10^6 cells/ml) were pre-treated with TEPP-46 for 30 minutes prior to stimulation with cholesterol crystals (500 µg/ml) for 6 and 24 hours. mRNA expression of *HIF1α* was analysed by real-time PCR (N= 4, n = 3). Data is represented as mean ± SEM and analysed using one-way ANOVA with Tukey's post-test.

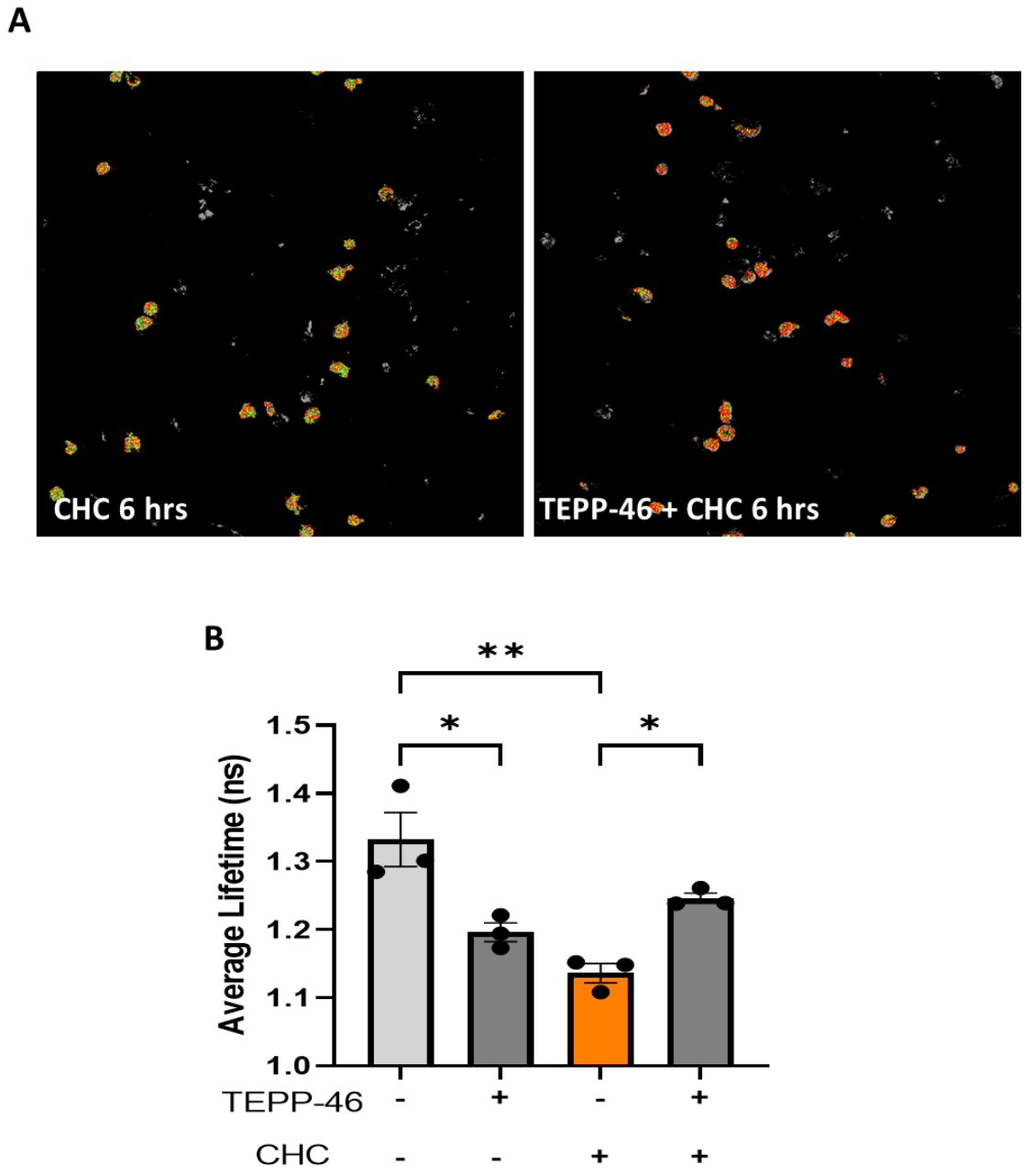

Figure 5-31 - TEPP-46 reduces the glycolytic profile in cholesterol crystal treated macrophages.

Primary human macrophages (1 x 10^6 cells/ml) were pre-treated with TEPP-46 (50 µM) prior to stimulation with cholesterol crystals (500 µg/ml) for 6 hours. Intracellular NADH levels were analysed through Fluorescence Lifetime Imaging Microscopy. (**A**) FLIM images of cholesterol crystal treated macrophages with/without TEPP-46. (**B**) Pooled data shows a significant increase of NADH average lifetime in cells pre-treated with TEPP-46 compared to cholesterol crystal treatment alone. Data is shown as mean ± SEM and analysed using RM One Way ANOVA with Tukey's post-test. *p≤0.05, **p≤0.01

5.4.16 Cholesterol crystal induced mitochondrial fission occurs independent of PKM2 translocation.

Having established that PKM2 translocation was required for the observed shift in macrophage metabolism, it was next aimed to investigate whether alterations to mitochondrial dynamics were also regulated by this protein. To test this, cells were pre-treated with TEPP-46 (50 µM) for 30 minutes before treating with cholesterol crystals for 6 and 24 hours. Cells were then incubated with Mitotracker^{TM} Red to detect mitochondrial morphology (shown in red) and Hoechst nuclear dye (shown in blue). Interestingly, macrophages pre-treated with TEPP-46 prior to stimulation with cholesterol crystals showed no significant difference in mitochondrial morphology, as assessed using confocal imaging, when compared with cholesterol crystal treatment alone (Figure 5.32). This suggests that the events regulating changes in mitochondrial dynamics in response to cholesterol crystals may occur upstream of PKM2 translocation and are worthy of further investigation.

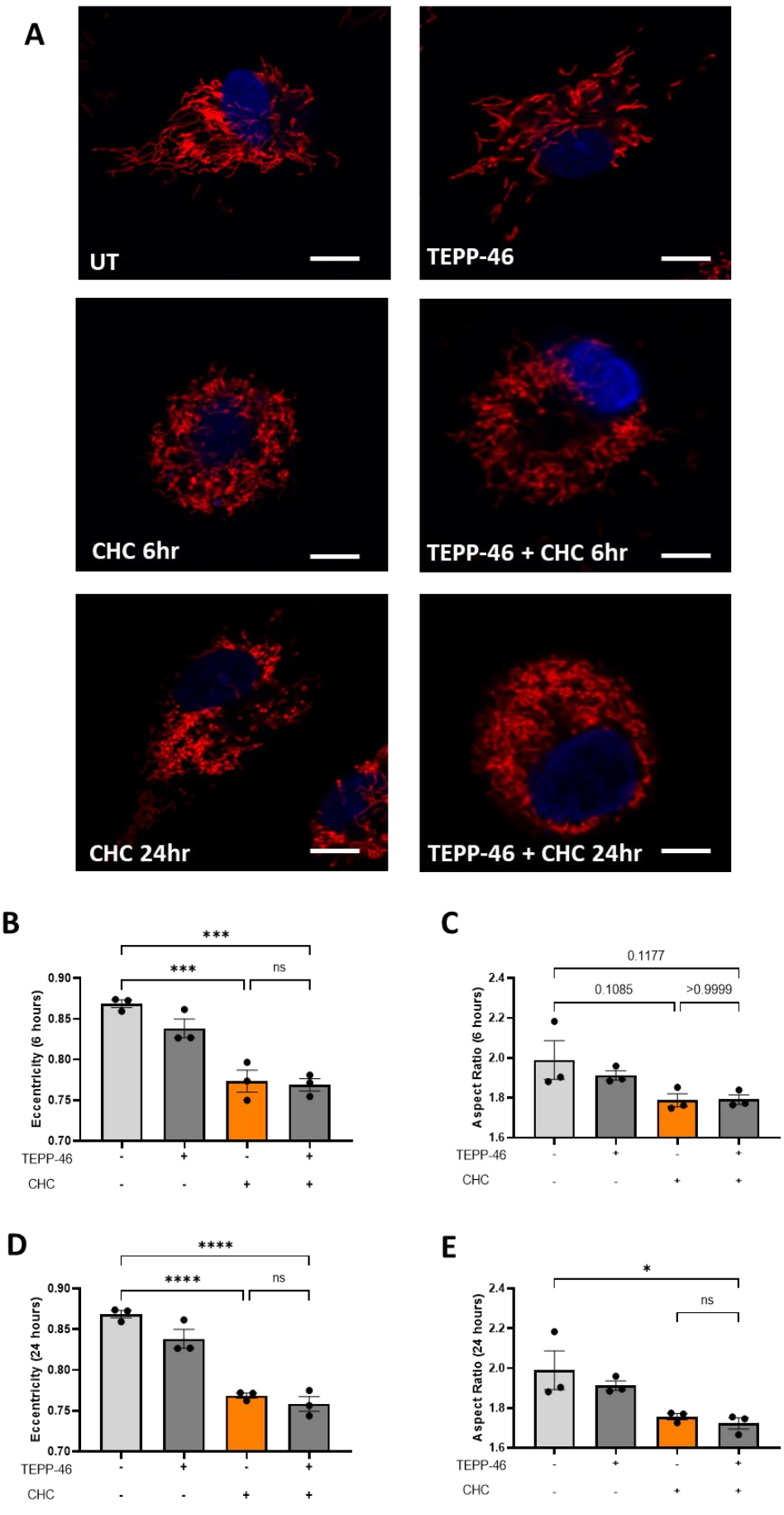
A
UT
TEPP-46
CHC 6hr
TEPP-46 + CHC 6hr
CHC 24hr
TEPP-46 + CHC 24hr
B
***
***
ns
Eccentricity (6 hours)
0.90
0.85
0.80
0.75
0.70
TEPP-46
CHC
C
0.1177
0.1085
>0.9999
Aspect Ratio (6 hours)
2.4
2.2
2.0
1.8
1.6
TEPP-46
CHC
D
****
****
ns
Eccentricity (24 hours)
0.90
0.85
0.80
0.75
0.70
TEPP-46
CHC
E
*
ns
Aspect Ratio (24 hours)
2.4
2.2
2.0
1.8
1.6
TEPP-46
CHC

Figure 5-32 - Cholesterol crystals induced mitochondrial fission is independent of PKM2 activity

Primary human macrophages (1 x 10^6 cells/ml) were pre-treated with TEPP-46 (50 µM) prior to stimulation with cholesterol crystals (500 µg/ml) for 6 and 24 hours. Cells were stained with Mitotracker™ (red) to assess mitochondrial morphology in response to cholesterol crystal treatments. Cells were counterstained with Hoechst (blue) to show nuclei. Cells were imaged using a Leica SP8 scanning confocal microscope. (**A**) Representative images of untreated and cholesterol crystal stimulated macrophages at 6 and 24 hours in the presence or absence of TEPP-46. Scale bar represents 5 µm. (**B-E**) Shape parameters of mitochondria were quantified using Cell Profiler software (N = 3, n = 15). Data was analysed using one-way ANOVA with Tukey's post-test. *p≤0.05, **p≤0.01, *** ≤0.001, ****p ≤0.0001

5.4.17 Inhibition of PKM2 translocation attenuates cholesterol crystal induced M1 polarisation and DAMP expression

Finally, having highlighted PKM2 as a key regulator of metabolic reprogramming of macrophages in response to cholesterol crystals, and having previously established the integral link between glycolysis and M1 polarisation, it was next aimed to explore the impact of TEPP-46 treatment on the inflammatory phenotype induced by these particulates. To test this, cells were pre-treated with TEPP-46 for 30 minutes, prior to treatment with cholesterol crystals for 6 and 24 hours. Pre-treatment of macrophages with TEPP-46 prior to cholesterol crystal stimulation resulted in a significant reduction of M1 and DAMP expression at 6 hours, in a similar fashion to direct inhibition of glycolysis with 2-DG or 3PO (Figure 5.33). A significant reduction of IL-8 was also observed at 24 hours when cells were pre-treated with TEPP-46 (Figure 5.34). Collectively these results highlight a role for PKM2 in cholesterol crystal mediated metabolic reprogramming and inflammation.

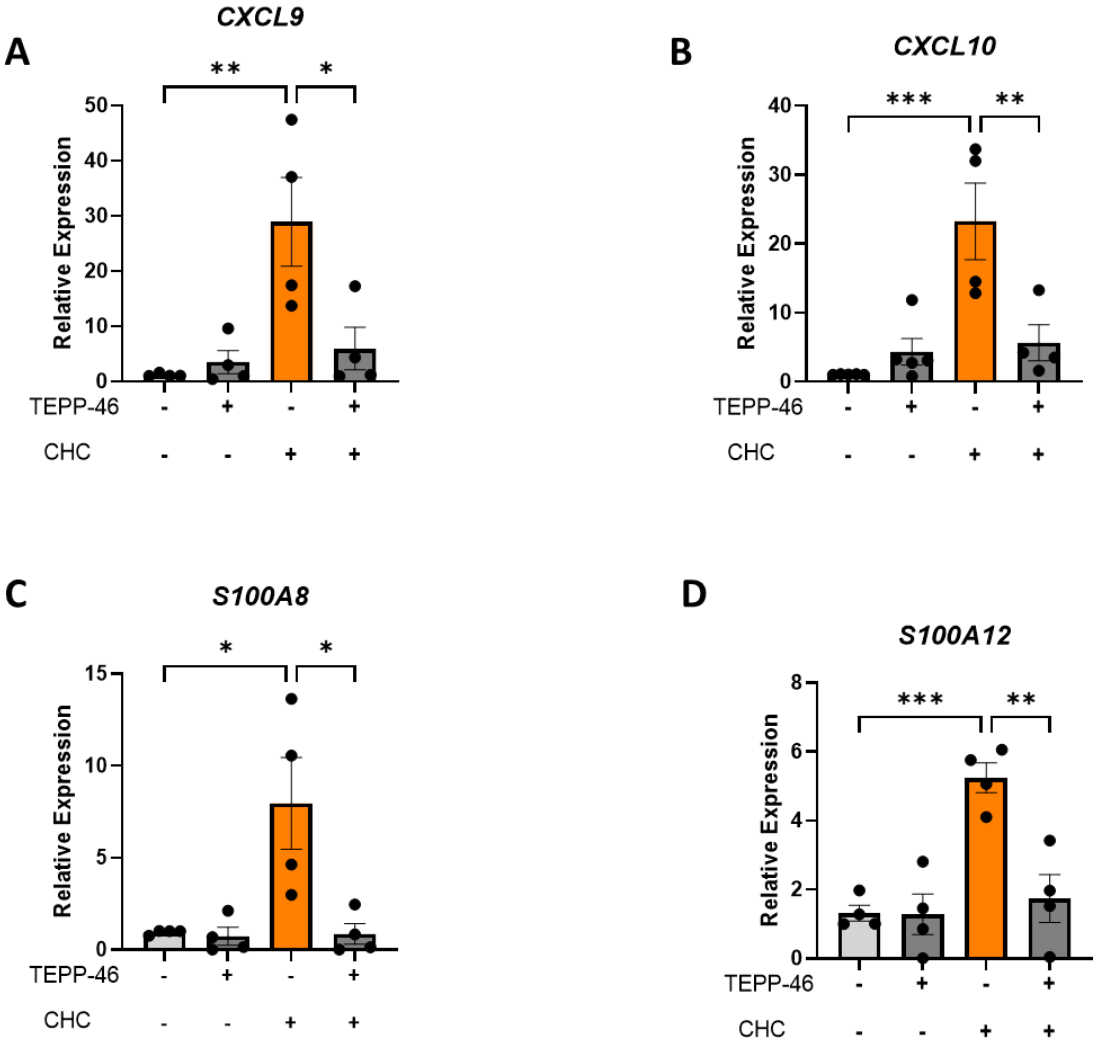

Figure 5-33 -Cholesterol crystal induced macrophage polarization and DAMP expression is regulated through PKM2.

Primary human macrophages (1 x 10^6 cells/ml) were pre-treated with TEPP-46 for 30 minutes prior to stimulation with cholesterol crystals (500 µg/ml) for 6 and 24 hours. (**A-D**) mRNA expression of *CXCL9, CXCL10, S100A8,* and *S100A12* was analysed by real-time PCR (N= 4, n = 3). All data is represented as mean ± SEM. All data was analysed using one-way ANOVA with Tukey's post-test. *p≤0.05, **p≤0.01, *** ≤0.001

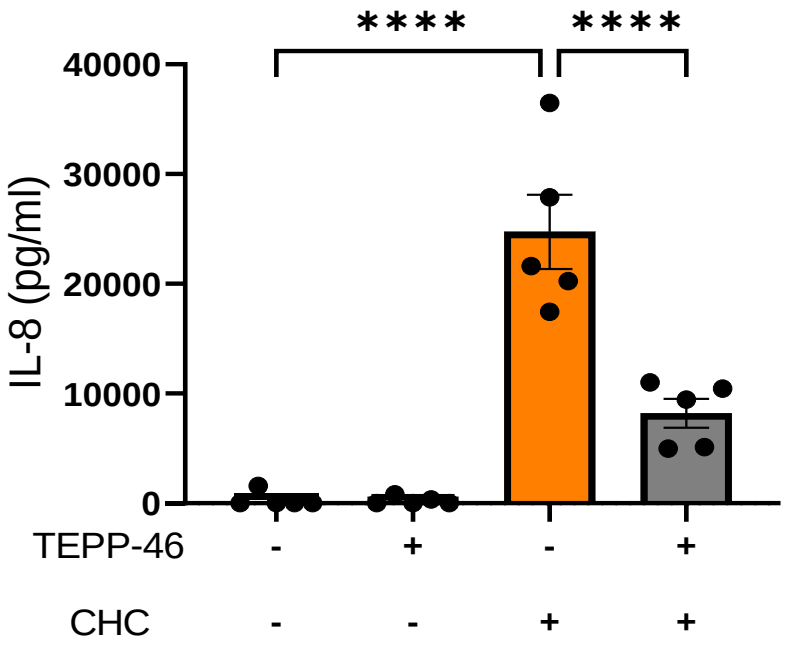

Figure 5-34 - Cholesterol crystal induced IL-8 production is regulated through PKM2.

Primary human macrophages (1 x 10^6 cells/ml) were pre-treated with TEPP-46 for 30 minutes prior to stimulation with cholesterol crystals (500 µg/ml) for 24 hours. IL-8 production was measured by ELISA (N= 5, n = 3). Data is represented as mean ± SEM and analysed using one-way ANOVA with Tukey's post-test. ****p ≤0.0001

5.5 Discussion

It is now well established that metabolic reprogramming of immune cells is linked to an inflammatory phenotype in non-infectious diseases, including rheumatoid arthritis (RA), diabetes and systemic lupus erythematosus (SLE) [248]. Dysregulated immunometabolism has also been observed in atherosclerotic plaques and has been linked to disease progression [40]. While LPS and IFNγ are routinely used *in vitro* as surrogate inducers of metabolic reprogramming, there are few studies examining the role of DAMPs or alarmins in mediating these effects. This study demonstrates for the first time that cholesterol crystals can polarise primary human macrophages towards an M1 pro-inflammatory phenotype and promote a metabolic switch favouring glycolysis. This is accompanied by increased expression of key glycolytic markers and translocation of the metabolic regulator, PKM2, to the nucleus, thus providing a link between cholesterol crystal-induced inflammation and dysregulated bioenergetics.

In addition to having a direct effect on macrophage metabolism and polarisation, cholesterol crystals are known to drive inflammasome activation and IL-1β production in primed cells. It is highly plausible that in an *in vivo* setting, both the crystals and IL-1β are contributing to metabolic reprograming. In support of this, recombinant IL-1β has been shown to increase rates of glycolysis *in vitro* [245], while LPS-primed macrophages deficient for the IL-1R fail to increase glycolysis in response to beta amyloid [245]. While I have demonstrated that the cholesterol crystals can promote metabolic reprogramming in the absence of LPS priming, it is likely that *in vivo* priming signals such as OxLDL coordinate with the crystals to promote changes in macrophage metabolism. Furthermore, it is possible that the crystals cause the release of IL-1α over time (IL-1α is secreted from damaged cells), which likely also promotes glycolysis, similar to IL-1β.

Robust production of IL-8 was also observed in direct response to cholesterol crystal stimulation. Further analysis of the pathway(s) leading to IL-8 production is required, although it may involve a link between oxidative stress and NF-κβ activation. Several reported studies have outlined intracellular ROS production as a key driver of downstream inflammatory responses, specifically through NF- κB activity [249]. Indeed, production of IL- 8 requires the coordinated activation of NF-κB and MAP kinase activation [250]. Activation of NF-κB and JNK pathway results in moderate expression

and transcription of IL-8, while further activation of p38 MAP-kinase causes stabilisation of mRNA and chemokine secretion [251]. Future work involving the use of ROS scavengers such as TEMPOL as well as MAP kinase/NF-kB inhibitors will provide further insight into the production of this chemokine by the crystals.

Multiple studies have outlined a role for elevated glycolysis in atherosclerotic plaques through F- radiolabelled glucose analogue fluorodeoxyglucose positron emission tomography CT (F-FDG-PET/CT). Increased FDG uptake is associated with plaque sites containing an abundance of macrophages, as well as lipid rich necrotic cores [232, 252], while metabolomic studies on human atherosclerotic plaques have shown that increased levels of glycolysis are associated with a decrease in plaque stability [231]. Enhancement of glycolytic flux is likely mediated by HIF1α, as atherosclerotic plaques are characterized by local hypoxic regions [253] which favours HIF1α stabilisation. Furthermore, deletion of HIF1α in macrophages from ApoE deficient mice reduces necroptosis of cells, thereby limiting formation of the necrotic core and stabilizing plaques [254]. However, even in normoxic conditions, HIF1α levels can be elevated, leading to increased cytokine production and enhanced glycolysis [50, 228]. Such effects are observed in LPS-stimulated macrophages, and I have now demonstrated that elevated HIF1α levels are a feature of cholesterol-crystal treated macrophages. This is accompanied by increased expression of the glucose transporter, GLUT1, and HK2; the rate-limiting enzyme in glycolysis. Furthermore, my findings also builds on the existing knowledge of the PKM2-HIF1α signalling axis, first reported in cancer cells [255, 256] and later observed in LPS-stimulated macrophages [50].

PKM2 itself represents a novel therapeutic target to combat cholesterol crystal-induced inflammation, as inhibition of PKM2 nuclear translocation, not only abrogated the enhancement of glycolysis seen with cholesterol crystals, but also resulted in decreased expression of M1 macrophage markers (*CXCL9* and *CXCL10*), the DAMPS *S100A8* and *A12*, and the chemokine, IL-8. Indeed, it has been demonstrated that increased expression and secretion of chemokines in atherosclerosis exacerbates disease [224], while *in vivo* studies exploring chemokine inhibition have resulted in significant plaque regression [257]. For example, neutralisation of CXCL10 in ApoE deficient mice results in a more stable plaque phenotype with increased numbers of smooth muscle cells [258],

while IL-8 has been implicated in plaque destabilization via the downregulation of TIMPs (inhibitors of matrix metalloproteases) [259]. Studies focusing specifically on IL-8 are however limited and given the potent induction of this chemokine by cholesterol crystals, it is worthy of further investigation. In the case of PKM2, this work supports previous studies highlighting a role for PKM2 in monocytes and macrophages from patients with cardiovascular disease, where increased glucose uptake and glycolytic flux were shown to enhance the generation of mitochondrial-derived reactive oxygen species, PKM2 nuclear translocation and proinflammatory cytokine production [246]. Furthermore, inhibiting glycolysis with 2-DG, 3PO, and enforcing PKM2 tetramerization abrogated this pro-inflammatory phenotype.

Targeting dysregulated immunometabolism is now being explored as a treatment option in a number of diseases settings. Inhibition of glycolysis with 2-DG reduces disease severity in murine models of RA and SLE, while inhibition of pyruvate dehydrogenase kinase was shown to protect against EAE, in this case resulting in reduced TH17 cell numbers, whilst simultaneously boosting anti-inflammatory T-regs [260]. A number of anti-inflammatory metabolites such as itaconate have also been shown to have immune modulatory effects *in vivo* [261] and, as with the above-mentioned targets, further *in vivo* study is required to determine if these promising pre-clinical studies will eventually translate to the clinic. Encouragingly, a recently emerged study led by Doddapattar *et al.,* demonstrated that both inhibition of PKM2 translocation, or selective deletion of the protein in macrophages effectively reduced rates of glycolysis, inflammation, and ultimately plaque formation in $LDLR^{-/-}$ murine models [262]. This study effectively validates the results presented herein, in that PKM2 holds a pivotal role in atherogenic inflammation and is a worthy target to combat atherogenic inflammation in the clinic.

In summary, the findings of this chapter show that cholesterol crystals drive M1 polarisation of primary human macrophages. In addition, significant insight was gained to the inner mechanisms by which cholesterol crystals drive this inflammatory response. Not only does this allow cholesterol crystals to be added to the growing list of associated particulates that are capable of altering immune cell metabolism, but the results of this chapter also highlight a potential therapeutic strategy to combat atherosclerosis through

immunometabolism. A schematic summary of these findings is shown below in Figure 5.35

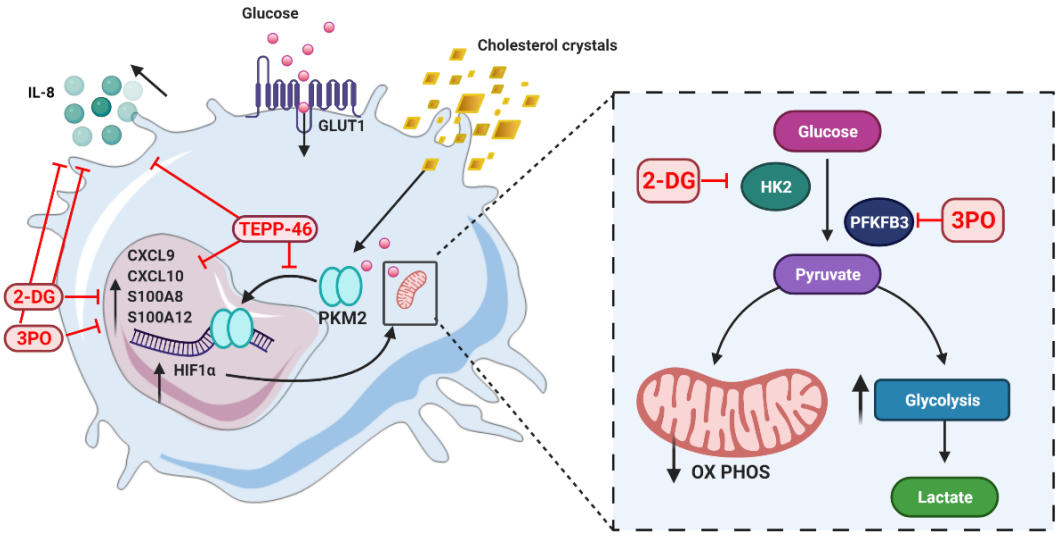

Figure 5-35 - Schematic summary of findings

Cholesterol crystals promote M1 polarisation of primary human macrophages, as indicated by increased expression of M1-associated genes *CXCL9* and *CXCL10,* and DAMPs *S100A8, S100A12*, as well as robust production of pro-inflammatory chemokine IL-8. Cholesterol crystals are also observed to promote significant metabolic reprogramming of primary human macrophages, to favour glycolysis as a primary energy source. Direct inhibition of glycolysis with 2-DG or 3PO, or else indirectly through inhibition of the upstream mediator PKM2 abrogates the inflammatory profile induced by cholesterol crystals.

Chapter 6 : The impact of electric field stimulation on macrophage polarisation and attenuation of stimulated polarisation

6.1 Abstract

Electrical signalling is an important feature of numerous biological processes. Endogenous electric fields (EFs) are critical to nerve signalling in the brain, muscle contraction in the heart, in addition to effective tissue repair across numerous sites in the body following injury. The growing appreciation for bioelectricity has led to the application of electrical stimulation (ES) across various fields of tissue engineering. However there remains little to no knowledge of the impact of ES on the immune response. It has been well established that macrophage responses can be influenced by an assortment of physical cues including mechanical stress and matrix stiffness, yet the impact of ES has not been extensively studied. This study demonstrates that ES plays a role in shaping macrophage polarisation by promoting an anti-inflammatory, pro-regenerative M2 phenotype in primary human macrophages, thus presenting a novel therapeutic strategy across multiple injury and defence microenvironments. Using a custom-built bioreactor system, primary human macrophages were subjected to 1-hour ES, with a regime consisting of a biphasic pulse of 2 ms, ± 2.5 V, with 1 Hz frequency. Increased expression of M2 associated markers, enhanced phagocytic capacity, and expression of angiogenic factors were observed in response to ES. Additionally, ES was shown to limit the pro-inflammatory response of LPS-stimulated macrophages. Finally, conditioned media from ES-macrophages was shown to increase migration of human MSCs in a wound scratch model, indicating the pro-regenerative potential of ES-macrophages.

6.2 Introduction

Much of our previous understanding of factors driving macrophage polarisation concern cytokines and chemokines, as well as pathogen associated molecular patterns (PAMPs) and endogenous DAMPs [5, 263] However, in more recent years, both physical and mechanical signals from the local environment have also been recognised for their ability to modulate macrophage phenotype and behaviour [264]. Factors such as cyclic stress, matrix stiffness and ECM components are capable of shaping macrophage function [103, 265-267]. Much of this knowledge arises from the field of biomaterials, where in many cases, the physical properties of said materials initiates a foreign body response in macrophages, delaying tissue repair and driving the formation of a

detrimental fibrotic capsule [268]. However, much is yet to be explored regarding intrinsic biophysical properties present *in vivo*, and the impact these properties may have on macrophage fate and function. One such property worth exploring in this context is ES.

The study of electrical signalling has become an area of active research, due to a growing appreciation for the influence of endogenous EFs on cellular function [269]. In this context, biological tissues can be credibly regarded as electrical systems, with endogenous EFs modulating a plethora of biological processes including muscle contraction, neurotransmission, wound healing and tissue regeneration [158]. In the brain, electrical signalling is responsible for neural cell communication via the generation of action potentials [270]. In the skin, endogenous EFs are imperative to the tissue repair process in response to injury whereby EFs at the site of an acute wound promote cell migration in order to facilitate repair and regeneration [271]. Manipulation of endogenous EF in rat models highlights the importance of these electrical cues, as pharmacological inhibition of the ion pump Na/K ATPase with ouabain disrupts ion flow, limiting cell division and migration around the wound site, ultimately delaying tissue repair [161]. Further examples of the impact of electrical signalling can additionally be seen in bone tissue, where EFs have proven critical for the differentiation and proliferation of osteogenic progenitor cells [166, 272, 273].

Application of externally sourced electrical stimulation to cells *in vitro* has further highlighted the significant role of electrical cues in tissue repair and wound healing. For example, electrical stimulation has been shown to have a significant effect on dermal fibroblasts, driving the upregulation of TGFβ-1, as well as increased migration of cells into subcutaneous wounds [167]. This “pro-healing” phenotype has been further affirmed by findings from Park *et al.*, whereby electrical stimulation of dermal fibroblasts over 6 hours resulted in selective upregulation of 49 different wound-healing genes [160]. Electrical stimulation has also been found to promote cell proliferation, which addresses a major challenge in tissue injury, that is the loss of competent cells [274]. Preosteoblasts, adult human somatic stem cells, neural stem cells, and human umbilical vein endothelial cells (HUVECs) all exhibit increased proliferation in response to electrical stimulation *in vitro* [169, 275-277], and furthermore, show increased

differentiation and gain of function [278-280]. Based on these findings, electrical stimulation has become increasingly recognised as a valuable tool in the field of regenerative medicine [158, 274, 281].

Macrophages are key mediators of tissue repair, yet information pertaining to macrophage response to ES remains limited. Pre-existing work to date is largely limited to the use of murine cells, or cell lines rather than primary cells [171, 172, 282]. Nevertheless, results of these studies suggest a potential immune-modulatory role for ES in macrophages in line with the pro-reparative effects observed in non-immune cells such as fibroblasts and MSCs [160, 166, 167]. In particular Srirussamee *et al.* demonstrated that delivery of electrical stimulation prior to LPS stimulation resulted in reduced expression of TNF, compared to LPS stimulation alone [172]. Bioelectric modulation of THP-1 macrophages through selective inhibition of ion transporters also generated similar findings. Inhibition of the K+ channel in macrophages using the drug glibenclamide effectively reduced M1 associated gene expression and pro-inflammatory cytokine secretion in LPS/IFNγ-treated cells, while simultaneously enhancing M2-associated gene expression in IL-4/IL-13 treated cells [283]. It is of great interest to investigate if these effects translate to primary human cells.

Characterisation of primary human macrophage responses to electrical stimulation not only allows for better understanding of the role of electrical signalling in tissue repair, but also provides insight to how macrophage phenotype is shaped in environments largely modulated by such a stimulus, i.e., the myocardium. Electrical signalling in the myocardium is initiated by a mass of specialized cells located in the right atrium, known as the sinoatrial (SA) node. The ES generated by the SA node occurs approximately 60-100 times per minute and propagates along the atria toward the atrioventricular (AV) node, causing the atria to contract. Gap junctions between muscle fibres in the heart ensure the action potential generated by the SA and AV nodes is spread throughout the muscle fibre network [173]. Disruption to this signalling pathway can contribute to oxidative stress of resident cardiac cells [284], and at a larger scale extensive remodelling of cardiac tissue [285, 286].

External delivery of ES to cardiomyocytes has proven to have immense benefits towards cell maturation and function. A study led by Radisic *et al*. demonstrated that *in vitro*

stimulation of neonatal rat CMs resulted in improved contractility of cells, as well a more mature cell phenotype, as indicated by increased expression of α-MHC, and a decrease in expression of β-MHC [168]. These results were later reproduced using human iPSC-CMs, showing again that external delivery of ES resulted in a more mature, better functioning CM phenotype, indicated by improved contractility and cell alignment [153]. Such findings have led many researchers to conclude that ES is a necessary biomimetic tool for the successful generation of *in vitro* cardiac models [152, 157, 287], however there are little to no studies addressing the impact of these electrical pacing regimes on non-CMs such as macrophages. Furthermore, while it has been established that tissue resident macrophages in the myocardium facilitate electrical conductivity [70], very little is known regarding the handling of electrical signalling by non-residential macrophages, those which infiltrate the heart upon injury. This raises the question whether ES may influence macrophage phenotype, as these cells enter the myocardium. Implementation of an ES regime similar to those previously used in the pacing of CMs, may allow us to address this question, while also translating the potential immunomodulatory role of ES to human cells.

6.3 Aims

Macrophage phenotype and function is greatly influenced by the surrounding microenvironment. Previously in chapter 5 of this thesis, it was demonstrated how endogenous DAMPs, i.e., disease-associated particulates, alter macrophage phenotype, skewing polarisation towards an M1 profile. It is the aim of this chapter to explore how physical stimuli, i.e., ES may also influence macrophage phenotype, and the implications this has for regenerative medicine, as well as macrophage function in the cardiac environment. Previous work with cell lines has outlined how ES may elicit anti-inflammatory effects on macrophages. It is of interest to investigate this effect in primary human macrophages. This includes investigation of macrophage metabolism as it was demonstrated in chapter 5 of this thesis, that macrophage phenotype and metabolism are integrally linked. Therefore, in addition to investigating the impact of ES on macrophage polarisation, the effect on LPS-induced metabolic reprogramming will also be investigated. Finally having characterised macrophage response to electrical stimulation, it is of interest to explore the therapeutic potential of this response.

Specific Aims:

- To determine if external electrical stimulation alters the phenotype and metabolic profile of primary human macrophages.
- To harness the therapeutic impact of electrical stimulation in macrophage mediated-inflammation and tissue repair

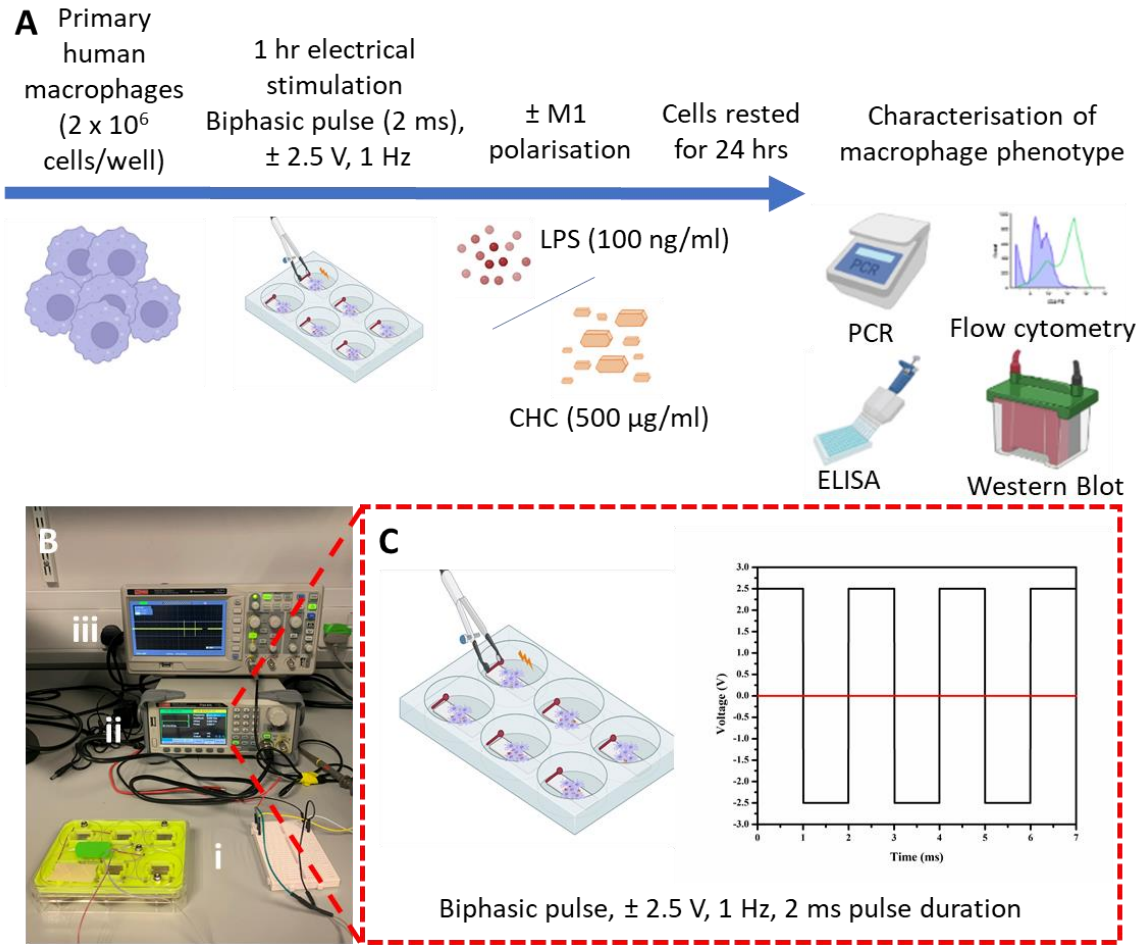

Figure 6-1 - Schematic summary showing experimental methods.

(**A**) Primary human macrophages were plated in the custom-bioreactor (2 x 10^6 cells/well) and stimulated with electrical stimulation (± 2.5 V, 1 Hz, 2 ms) for 1 hour. Following stimulation cells were left to rest or further polarised with either LPS (100 ng/ml) or cholesterol crystals (CHC) (500 µg/ml) for 24 hours. At 24 hours, macrophage phenotype was characterised. Gene expression was assessed by real-time PCR. Protein expression was assessed by flow cytometry and Western blot. Cytokine production was assessed by ELISA. (**B**) Image shows (i) bioreactor plate connected to breadboard, (ii) signal generator, and (iii) oscilloscope. (**C**) Graph showing electrical stimulation regime, showing frequency, amplitude, and wave shape applied to cells.

6.4 Results

6.4.1 Electrical stimulation does not impact macrophage viability and prolongs cell survival *in vitro*

Prior to assessing macrophage response to ES, it was first necessary to ensure the stimulation regime selected was non-toxic to cells. Primary human macrophages were seeded in a 6 well plate, compatible with the custom-built bioreactor established in the Monaghan lab [193], and stimulated for 1 hour with a regime consisting of a biphasic pulse of 2 ms, ± 2.5 V, with 1 Hz frequency. This regime has been previously implemented in the pacing of cardiomyocytes *in vitro* [168] and resembles the electrical properties native to the myocardium [194]. A 1-hour stimulation was selected for cell treatments, as similar pacing durations have been previously used with iPSC-CMs and allowed for preservation of cells, as well as the prevention of excessive production of potentially harmful redox oxygen species [274, 288]. Following stimulation, macrophages were stained for viability with Fix Via eFluor™ 506 and analysed by flow cytometry directly after. No significant difference was detected between unstimulated and ES-cells, indicating the selected regime did not negatively impact cell viability in real-time (Figure 6.2). Furthermore, macrophages left to rest for 24 hours after stimulation showed increased percentage of viability compared to unstimulated cells, suggesting that electrical stimulation provides adequate engagement with macrophages to prolong their survival *in vitro* (Figure 6.3).

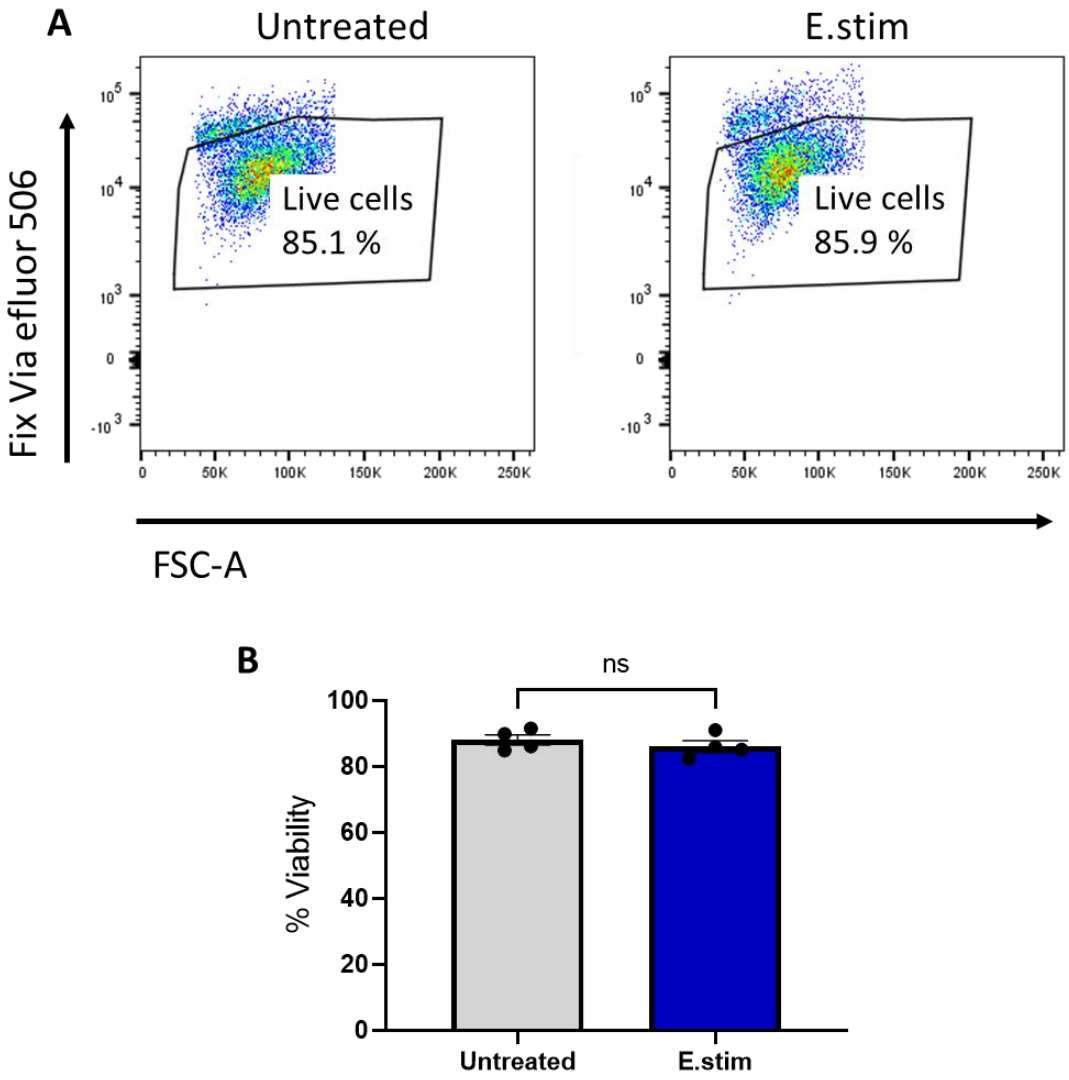

Figure 6-2 - Electrical stimulation does not reduce viability of primary human macrophages

Primary human macrophages (1 x 10^6 cells/ml) were left untreated or stimulated with electrical stimulation (± 2.5 V, 1 Hz, 2 ms) for 1 hour. Cell viability was assessed by flow cytometry using Fix Via eFluor™ 506. (**A**) Representative flow plots showing % Live cells of untreated and electrically stimulated (E. stim) macrophages. (**B**) Bar graph showing pooled data of % viability of untreated and E. stim macrophages of four independent experiments (N = 4). Data is shown as mean ± SEM and analysed using paired t-test.

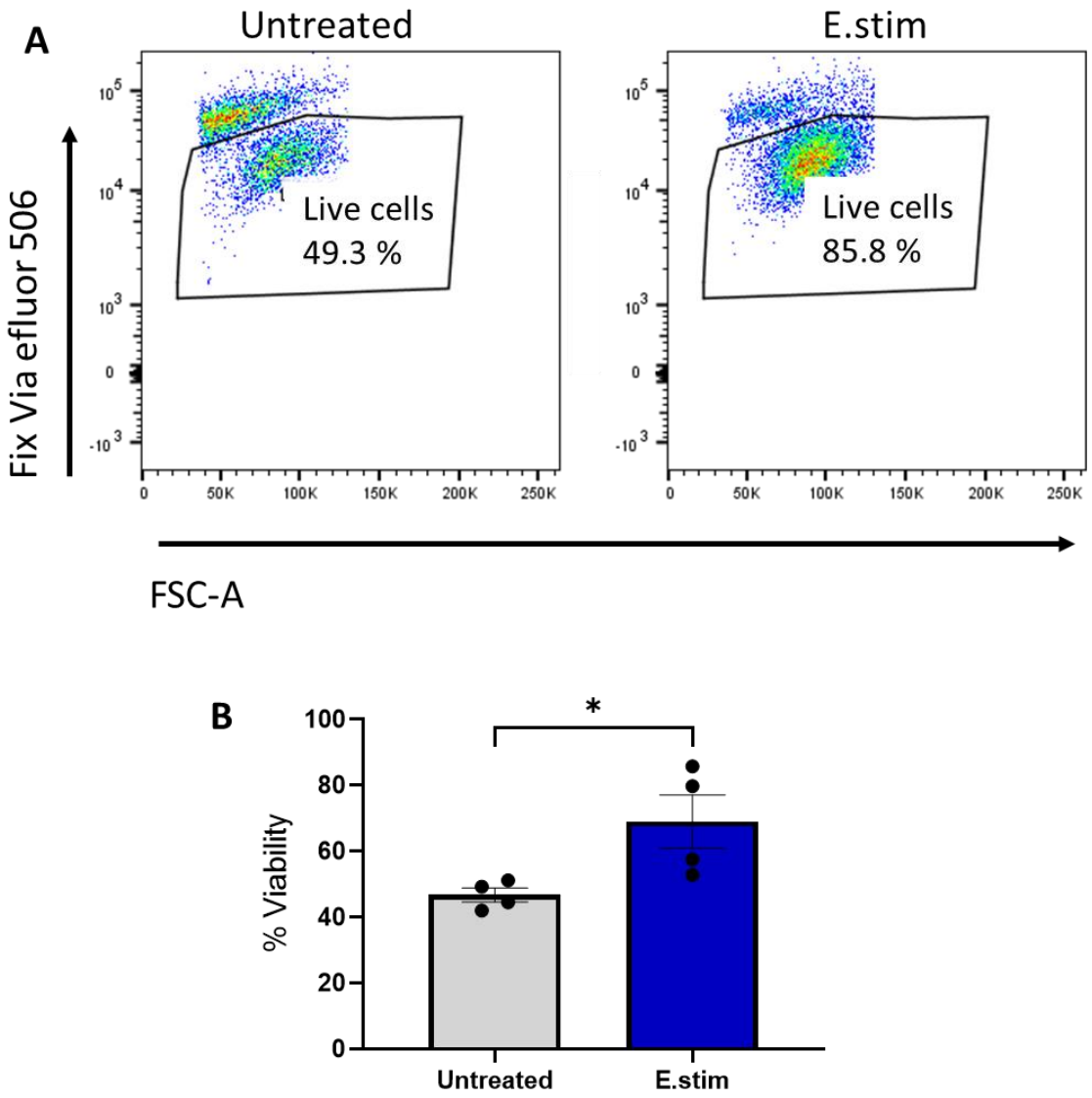

Figure 6-3 - Electrical stimulation improves survival of primary human macrophages

Primary human macrophages (1 x 10^6 cells/ml) were left untreated or stimulated with electrical stimulation (± 2.5 V, 1 Hz, 2 ms) for 1 hour, and left to rest for 24 hours. Cell viability was assessed by flow cytometry using Fix Via eFluor™ 506. (**A**) Representative flow plots showing % live cells of untreated and electrically stimulated (E.stim) macrophages. (**B**) Bar graph showing pooled data of % viability of untreated and E.stim macrophages of four independent experiments (N = 4). Data is shown as mean ± SEM and analysed using paired t-test. *p≤0.05

6.4.2 Electrical stimulation induces expression of chemokine receptor CCR2 in primary human macrophages

Migration of monocytes or macrophages into the myocardium is largely dependent on expression and activation of the chemokine receptor CCR2 [289]. It was of interest to investigate if ES alone could promote CCR2 expression, thus demonstrating how physical factors of the native myocardium may facilitate monocyte/macrophage infiltration/migration. Primary human macrophages were electrically stimulated for 1 hour and left to rest for a further 24 hours, after which surface expression of CCR2 was assessed by flow cytometry. Relative to unstimulated cells, a significant increase of 30.73 % (± 19.23) was observed in CCR2 expression in response to ES (Figure 6.4), suggesting that pulsed ES promotes migratory behaviour of primary human macrophages via the upregulation of chemokine receptors.

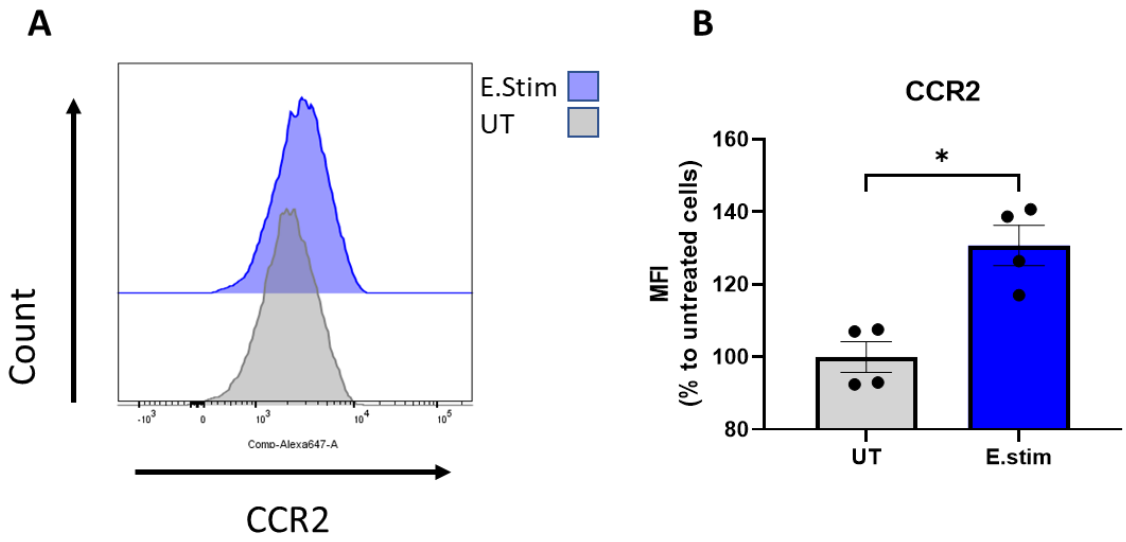

Figure 6-4 - Electrical stimulation increases expression of chemokine receptor CCR2 in primary human macrophages

Primary human macrophages (1 x 10^6 cells/ml) were left untreated or stimulated with electrical stimulation (± 2.5 V, 1 Hz, 2 ms) for 1 hour, and left to rest for 24 hours. Cells were then stained for CCR2 and analysed by flow cytometry. (**A**) Representative histograms showing median fluorescence intensity (MFI) of CCR2 in untreated and electrically stimulated (E.stim) macrophages. (**B**) Bar graph showing pooled data of % MFI relative to untreated cells (N = 4). Data is shown as mean ± SEM and analysed using paired t-test. *p≤0.05

6.4.3 Electrical stimulation promotes expression of gap junction protein Connexin 43 in primary human macrophages.

It has been established that tissue resident macrophages in the heart facilitate electrical conduction via coupling with cardiomyocytes [70]. This coupling is achieved through the formation of gap junctions consisting of the protein Connexin 43 [70]. The significant role of this protein is exemplified by its deletion in cardiac macrophages, which significantly delays atrioventricular conduction murine models of cardiac function [70]. It is unclear what factors modulates expression of Connexin 43 in resident macrophages *in vivo*, however, it is possible that ES may play a role, as it has been shown that external delivery of ES increases expression of the gap junction protein in cardiomyocytes *in vitro* [290]. To investigate if this also occurs in macrophages, primary human macrophages were electrically stimulated for 1 hour. Cells were either assessed immediately for expression of Connexin 43, or else left to rest for 24 hours. Western blot analysis revealed that increased Connexin 43 expression (2.629 fold change ± 3.791) in macrophages occurs immediately following 1 hour stimulation. Analysis of mRNA revealed that expression of Connexin 43 in ES-macrophages is maintained after 24 hours with a fold change increase of 5.11 (± 1.7) relative to untreated cells (Figure 6.5).

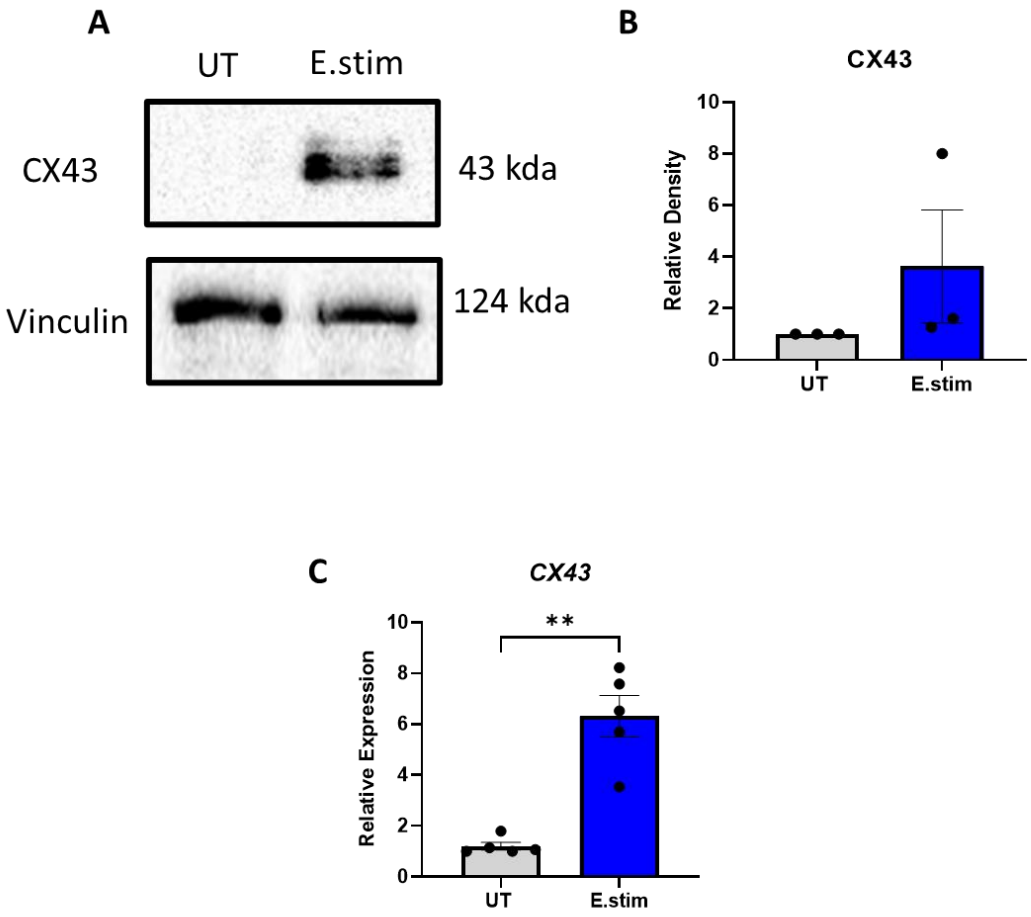

Figure 6-5 - Electrical stimulation induces expression of Connexin 43 in primary human macrophages

Primary human macrophages (1 x 10^6 cells/ml) were left untreated or stimulated with electrical stimulation (± 2.5 V, 1 Hz, 2 ms) for 1 hour. Cells were lysed immediately to assess protein expression of Connexin 43 or else left to rest for 24 hours. At 24 hours, cells were lysed for mRNA analysis by real-time PCR. (**A**) Representative western blots showing expression of Connexin 43 in UT and E.stim cells at 1 hour. (**B**) Densitometric analysis of western blots (N = 3). (**C**) Bar graph showing mRNA expression of *Connexin 43* in electrically stimulated cells (E.stim), relative to untreated cells (UT) at 24 hours (N = 5, n =3). All data is shown as mean ± SEM and analysed using paired t-test. **p≤0.01

6.4.4 Electrical stimulation increases capacity of primary human macrophages to uptake model antigen DQ-Ovalbumin

Both increased survival and heightened CCR2 expression in ES-macrophages suggest that ES activates macrophages, altering their phenotype and function. To further investigate this, phagocytic capacity of macrophages was assessed following ES. As highlighted in chapter 4, classically activated macrophages typically exhibit a reduced capacity for antigen uptake in response to stimulants such as LPS [208], while anti-inflammatory macrophages exhibit an increase in phagocytic capacity and antigen uptake [209]. To investigate the effect of electrical stimulation, the model antigen FITC-conjugated DQ-ovalbumin (DQ-Ova, 500 ng/ml) was used. Primary human macrophages were electrically stimulated for 1 hour and left to rest for 24 hours before treatment with DQ-Ova. Uptake of the model antigen was assessed via flow cytometry. Interestingly, results of this experiment show that ES of macrophages caused a significant increase of 5.88 % (± 4.02) of antigen uptake in macrophages, compared to unstimulated cells (Figure 6.6). These results agree with previously published findings from Hoare *et al*., where macrophages subjected to a continuous EF show increased phagocytic capacity [171], and furthermore suggests that ES potentially promotes an M2 phenotype in primary human macrophages.

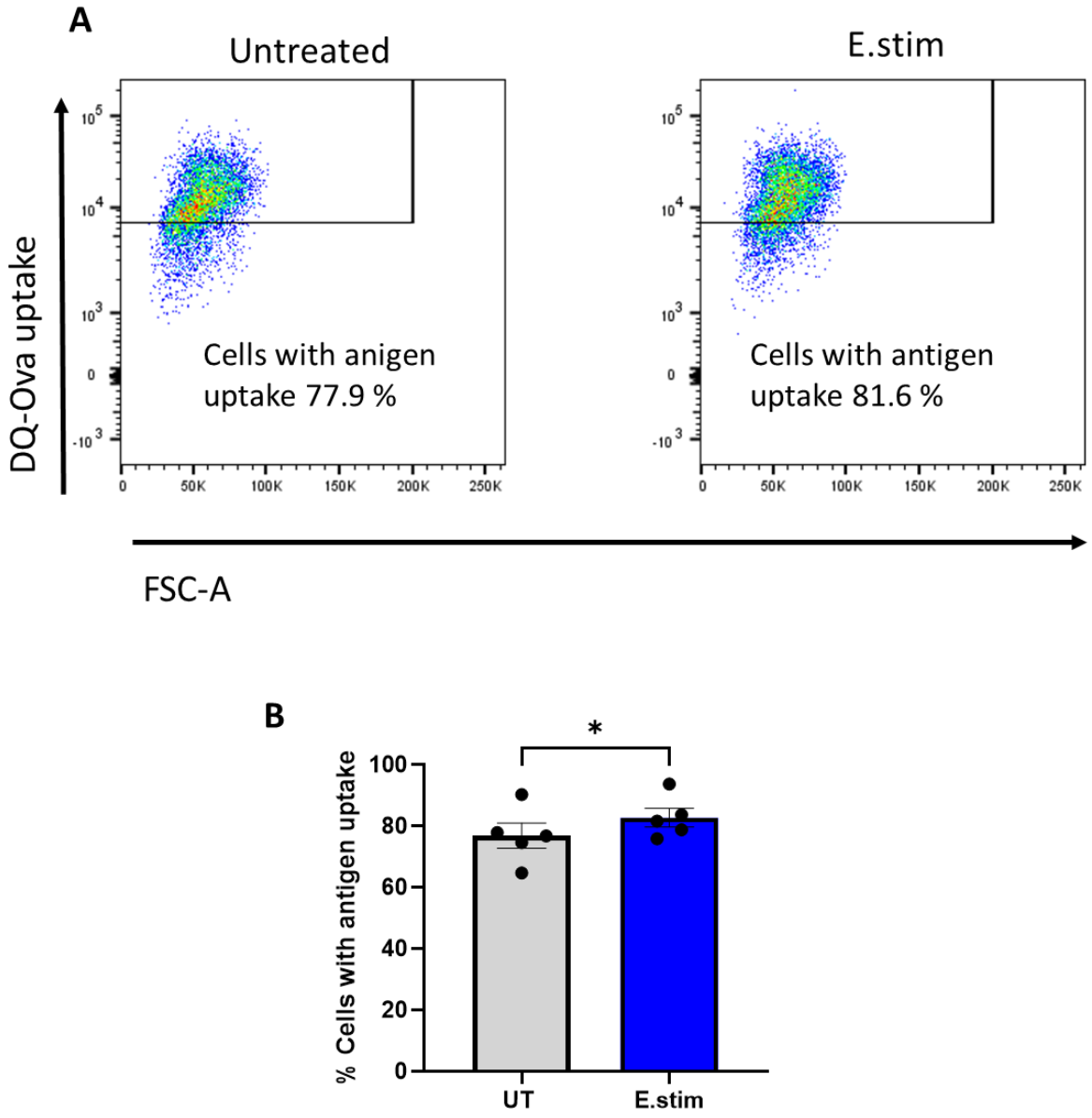

Figure 6-6 - Electrical stimulation increases capacity of primary human macrophages to uptake model antigen DQ-Ovalbumin

Primary human macrophages (1 x 10^6 cells/ml) were left untreated or stimulated with electrical stimulation (± 2.5 V, 1 Hz, 2 ms) for 1 hour, and left to rest for 24 hours. Cells were then incubated with model antigen FITC-conjugated DQ-Ovalbumin (500 ng/ml) and analysed by flow cytometry. (**A**) Representative flow plots showing % cells with antigen uptake in untreated and electrically stimulated (E.stim) macrophages. (**B**) Bar graph showing pooled data of % cells with antigen uptake of untreated and E.stim macrophages of five independent experiments (N = 5). Data is shown as mean ± SEM and analysed using paired t-test. *p≤0.05

6.4.5 Electrical stimulation induces expression of M2-associated genes in primary human macrophages

To further investigate the potential shift in macrophage phenotype in response to ES, mRNA levels of M1-associated genes *CXCL9, CXCL10*, and M2-associated genes *MRC1*, *CCL13* were assessed. Primary human macrophages were stimulated for 1 hour and left to rest for 24 hours. Cells were then lysed and mRNA levels of M1/M2 genes were assessed by real-time PCR. While no significant change was observed in the expression of either *CXCL9* or *CXCL10* (Figure 6.7 A-B), increased expression was observed in both *MRC1* and *CCL13,* with a fold change of 1.57 (± 1.32), and 1.45 (± 1.13) respectively (Figure 6.7 C-D). To further investigate this response, mRNA level of *TGFB-1* (an additional M2 marker) was also assessed. Similar to *MRC1* and *CCL13*, ES induced significant expression of *TGFB-1* with a fold change of 8.66 (± 4.97) relative to untreated cells (Figure 6.7 E). Collectively these findings indicate that ES promotes an M2 phenotype in primary human macrophages.

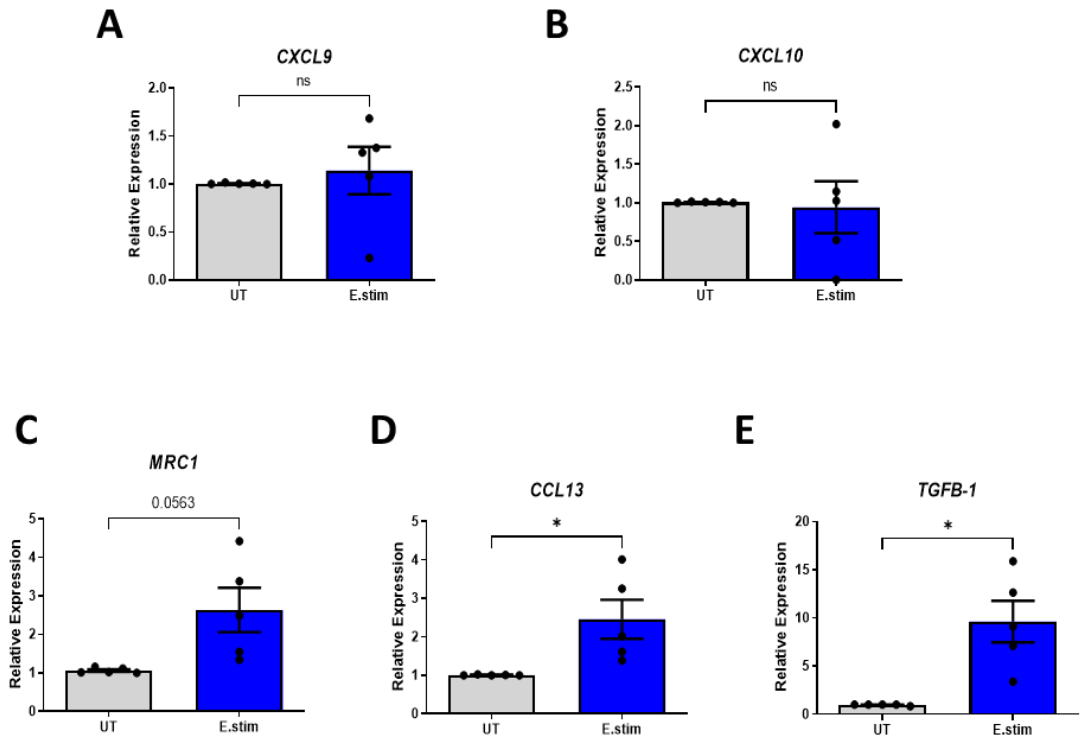

Figure 6-7 - Electrical stimulation induces expression of M2 associated genes in primary human macrophages

Primary human macrophages (1 x 10^6 cells/ml) were left untreated or stimulated with electrical stimulation (± 2.5 V, 1 Hz, 2 ms) for 1 hour and left to rest for 24 hours. (**A-E**) mRNA expression of M1 associated genes *CXCL9, CXCL10*, and M2 associated genes *MRC1, CCL13,* and *TGFB-1* was assessed by real time PCR (N = 5, n = 3). All data is shown as mean ± SEM and analysed using paired t-test. *p≤0.05

6.4.6 Electrical stimulation promotes expression of M2 surface markers in primary human macrophages

Macrophage phenotype can be further assessed through the analysis of surface marker expression by flow cytometry. As highlighted in chapter 4, surface proteins CD40, CD80, and CD86 are maturation markers typically associated with the M1 phenotype [291]. These markers are co-stimulatory molecules during the antigen presentation process, interacting with CD28 and CD40L receptors on T cells. Meanwhile, increased surface expression of CD206 (MRC1) and CD163 are typically associated with an M2 phenotype [36]. In response to ES, macrophages showed a trend towards reduced expression of CD80 (Figure 4.8 B), with no changes detected in CD40 or CD86 (Figure 6.8 A, C). A significant increase in CD206 expression was observed relative to untreated cells (10.23 % ± 2.14) (Figure 6.8 E), in agreement with the results obtained through PCR. A trend towards increased expression was also observed with CD163 (24.2 % ± 22.96), albeit not significant (Figure 6.8 D).

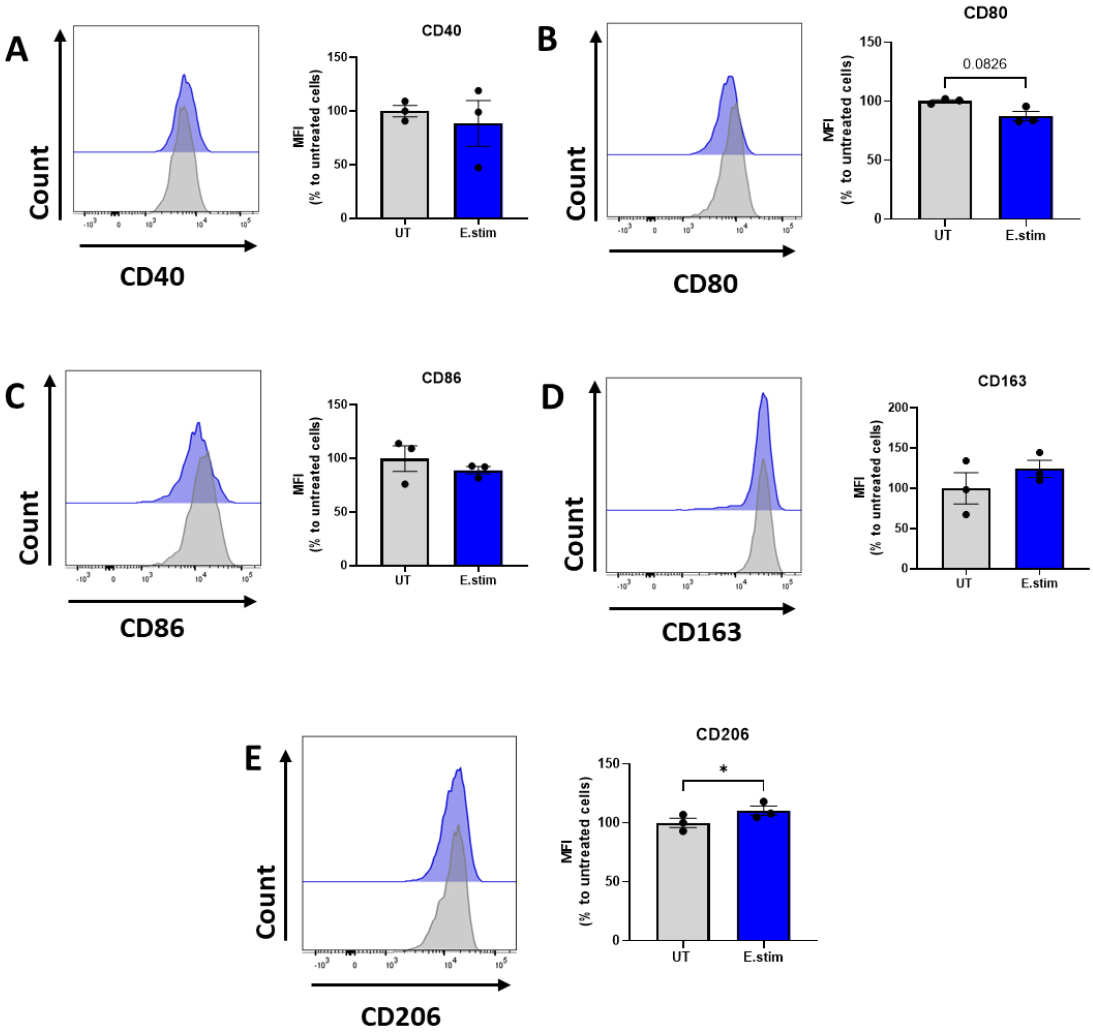

Figure 6-8 - Electrical stimulation increases expression M2 associated surface marker CD206 in primary human macrophages

Primary human macrophages (1 x 10^6 cells/ml) were left untreated or stimulated with electrical stimulation (± 2.5 V, 1 Hz, 2 ms) for 1 hour and left to rest for 24 hours. Cells were stained for CD40, CD80, CD86, CD163, and CD206 and analysed by flow cytometry. (**A-E**) Representative histograms showing MFI of respective surface markers and bar graphs showing pooled data of % MFI relative to untreated cells (N = 3). All data is shown as mean ± SEM and analysed using paired t-test. *p≤0.05

6.4.7 Electrical stimulation does not induce pro/anti-inflammatory cytokine or chemokine production in primary human macrophages

Having observed the significant shift in macrophage polarisation in response to ES, it was next of interest to investigate if ES had any effect on cytokine or chemokine production. It is known that $CCR2^{+}$ cells at sites of tissue injury such as the infarcted myocardium, initiate the inflammatory response through secretion of pro-inflammatory cytokines such as TNF and IL-6 [68], however, M2 macrophages are typically associated with secretion of anti-inflammatory cytokine IL-10 [7]. Primary human macrophages were stimulated for 1 hour and left to rest for 24 hours. Unstimulated cells, and LPS treatment (100 ng/ml) were used as untreated and positive controls respectively for cytokine production. Levels of TNF, IL-6, IL-8 and IL-10 were measured from cell supernatants by ELISA. No significant production of any cytokine was observed in response to ES, compared to both untreated and LPS-treated cells, indicating that ES alone does not induce either pro or anti-inflammatory cytokine production in primary human macrophages (Figure 6.9).

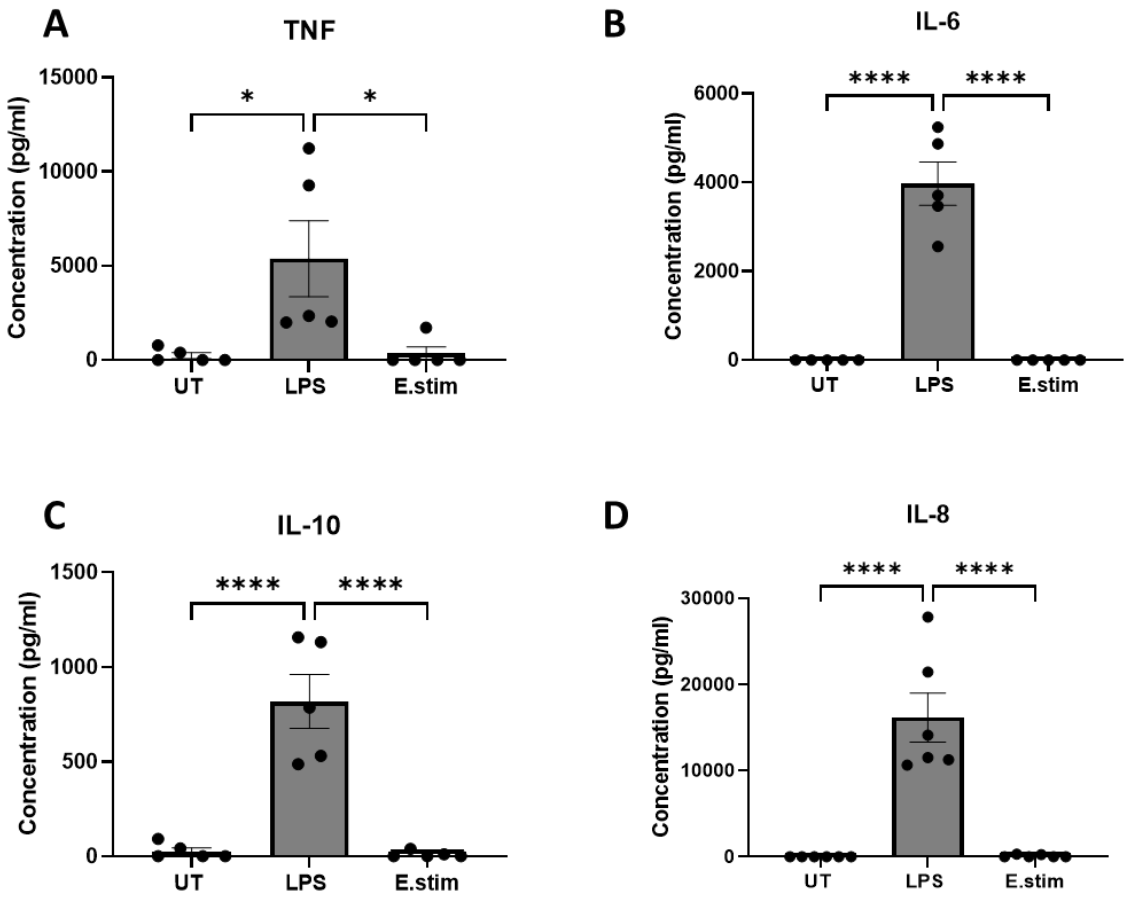

Figure 6-9 - Electrical stimulation does not promote cytokine or chemokine production in primary human macrophages

Primary human macrophages (1 x 10^6 cells/ml) were stimulated with electrical stimulation (± 2.5 V, 1 Hz, 2 ms) for 1 hour and left to rest for 24 hours. Unstimulated and LPS treated cells (100 ng/ml) were used as untreated and positive controls. (**A-D**) Levels of TNF, IL-6, IL-8 and IL-10 were assessed in cell supernatants by ELISA (N = 5-6, n = 3). All data is shown as mean ± SEM and analysed using One Way Anova with Tukey's post-test. *p≤0.05, ****p ≤0.0001

6.4.8 Electrical stimulation inhibits LPS-induced M1 polarisation of primary human macrophages

Despite the lack of production of cytokines in ES-macrophages, the collective results obtained from PCR and flow cytometry suggest an immune-modulatory role for ES, skewing macrophages towards an anti-inflammatory M2 phenotype. To investigate this further, macrophages were electrically stimulated and then subsequently challenged with LPS, to investigate if the ES could restrict pro-inflammatory activation of macrophages. Previously published findings have highlighted this potential effect in LPS-treated J774A.1 macrophages [172], therefore it was of interest to investigate if this translated to human cells. Primary human macrophages were electrically stimulated for 1 hour prior to 24-hour treatment with LPS (100 ng/ml) and mRNA level of M1-associated genes *CXCL9* and *CXCL10* were assessed by real time PCR. It was observed that pre-treatment of cells with electrical stimulation prior to LPS stimulation resulted in reduced expression of both *CXCL9* (11.60 fold change ± 5. 57) and *CXCL10* (6.38 fold change ± 2.43), when compared to LPS stimulation alone (Figure 6.10). More-over, pre-treatment of macrophages with ES decreased surface marker expression of CD40, CD80, and CD86 in LPS-treated macrophages (Figure 6.11). Taken together these results suggest that ES inhibits LPS-induced M1 polarisation in primary human macrophages.

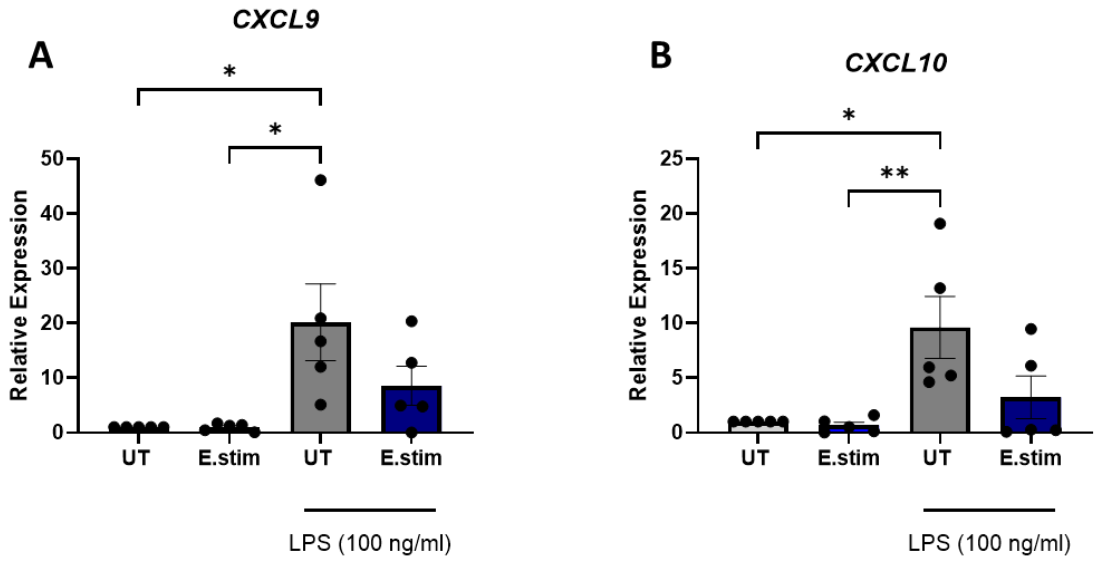

Figure 6-10 - Electrical stimulation reduces expression of M1 associated genes in LPS-stimulated macrophages

Primary human macrophages (1 x 10^6 cells/ml) were stimulated with electrical stimulation (± 2.5 V, 1 Hz, 2 ms) for 1 hour, followed by treatment with LPS (100 ng/ml) for 24 hours. (**A-B**) mRNA expression of *CXCL9* and *CXCL10* was assessed by real time PCR (N = 5, n = 3). Data is shown as mean ± SEM and analysed using One Way Anova with Tukey's post-test. *p≤0.05, **p≤0.01

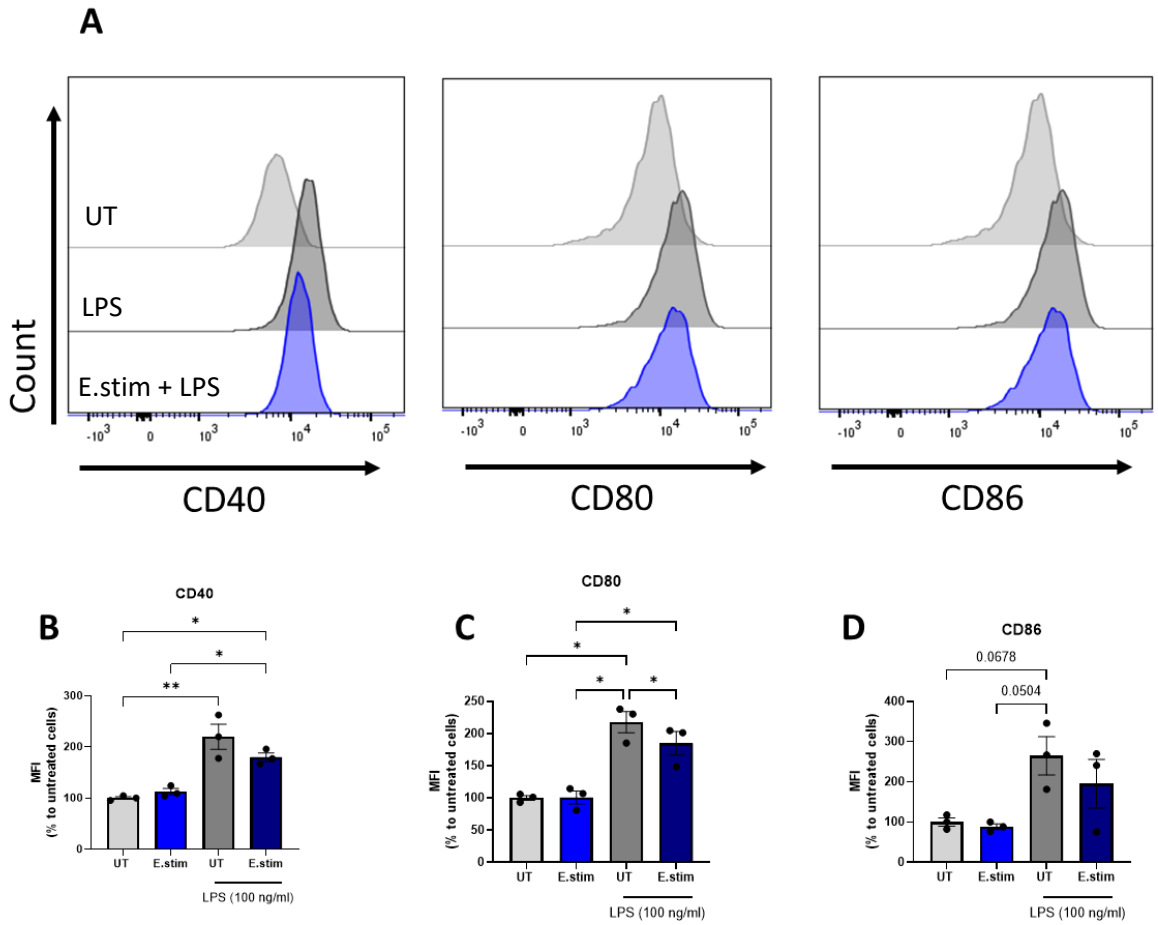

Figure 6-11 - Electrical stimulation reduces expression of M1 associated genes in LPS-stimulated macrophages

Primary human macrophages (1 x 10^6 cells/ml) were stimulated with electrical stimulation (± 2.5 V, 1 Hz, 2 ms) for 1 hour, followed by treatment with LPS (100 ng/ml) for 24 hours. Cells were stained for CD40, CD80, and CD86 and assessed by flow cytometry (N = 3). (**A**) Representative histograms showing median fluorescence intensity of CD40, CD80, CD86 respectively. (**B**) Bar graphs show pooled data of % MFI relative to untreated cells. Data is shown as mean ± SEM and analysed using One Way Anova with Tukey's post-test. *p≤0.05, **p≤0.01

6.4.9 Combined treatment of electrical stimulation and LPS does not impact macrophage viability

Having observed potential inhibition of M1 polarisation in ES-macrophages, it was important to ensure this reduced response was not due to cell death from combined stimulations. Primary human macrophages were pre-treated with electrical stimulation for 1 hour prior to treatment with LPS (100 ng/ml) for 24 hours. Cell viability was assessed at 24 hours by flow cytometry. Flow analysis revealed no difference between LPS-treated macrophages, and ES/LPS treated macrophages (Figure 6.12), indicating that reduced expression of M1 genes and surface markers was due to the immune-modulatory effect of ES.

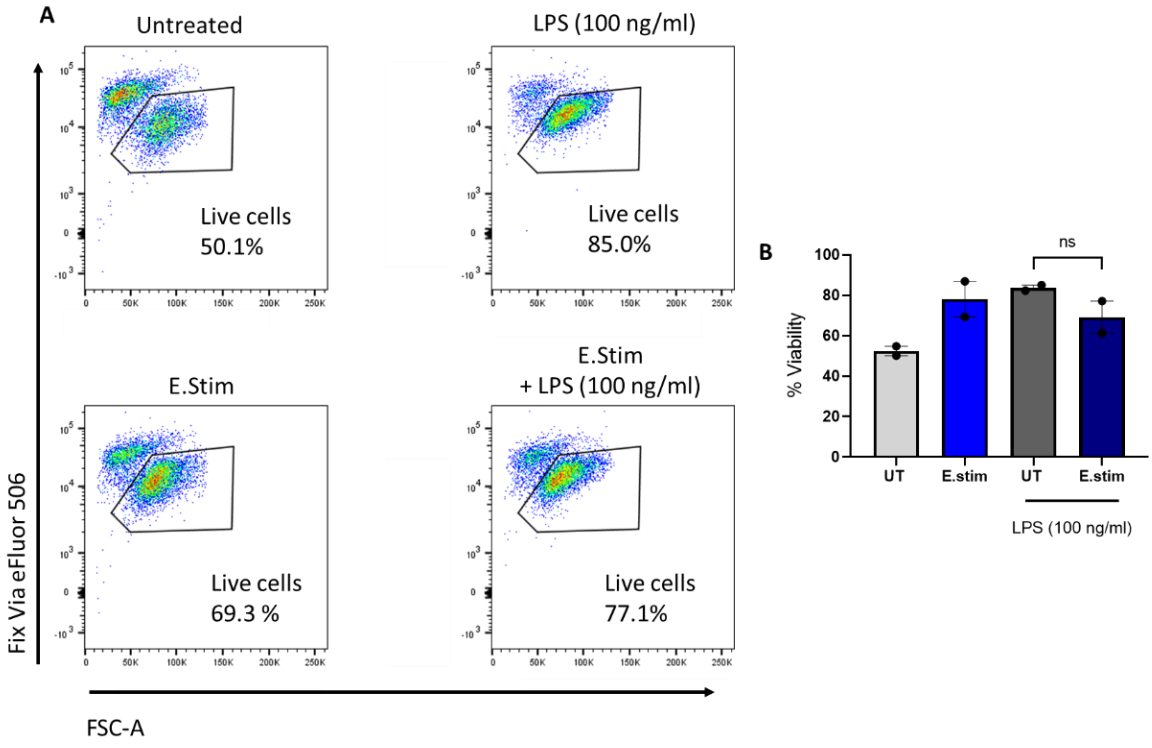

Figure 6-12 - Combined treatment of electrical stimulation and LPS does not reduce viability of primary human macrophages.

Primary human macrophages (1 x 10^6 cells/ml) were stimulated with electrical stimulation (± 2.5 V, 1 Hz, 2 ms) for 1 hour and left to rest or else treated with LPS (100 ng/ml) for 24 hours. Cells were stained with FixVia efluor™ 506 and analysed by flow cytometry. (**A**) Representative dot plots showing viability of untreated and treated macrophages. (**B**) Bar graph showing pooled data of % viability of untreated and treated macrophages (N = 2). Data is shown as mean ± SEM and analysed using One Way Anova with Tukey's post-test.

6.4.10 Electrical stimulation reduces production of IL-6 and IL-8, but not TNF or IL-10 in LPS-treated macrophages

Given that pre-treatment of macrophages with ES effectively reduced expression of both M1 genes and surface maturation markers in LPS-treated macrophages, it was next of interest to investigate any effect on LPS-induced cytokine production. Primary human macrophages were pre-treated with ES for 1 hour prior to treatment with LPS (100 ng/ml) for 24 hours. Levels of TNF, IL-6, IL-8 and IL-10 were assessed from cell supernatants by ELISA. While no change was detected in TNF or IL-10 production (Figure 6.13 A, D), it was observed that pre-treatment with ES significantly reduced both IL-6, and IL-8 production compared to LPS treatment alone, with a decrease of 1663 pg/ml (± 554) and 5685 pg/ml (± 1445) observed respectively (Figure 6.13 B, C). This response indicates that the immune-modulatory effects of ES are cytokine specific, rather than entirely shutting down macrophage function.

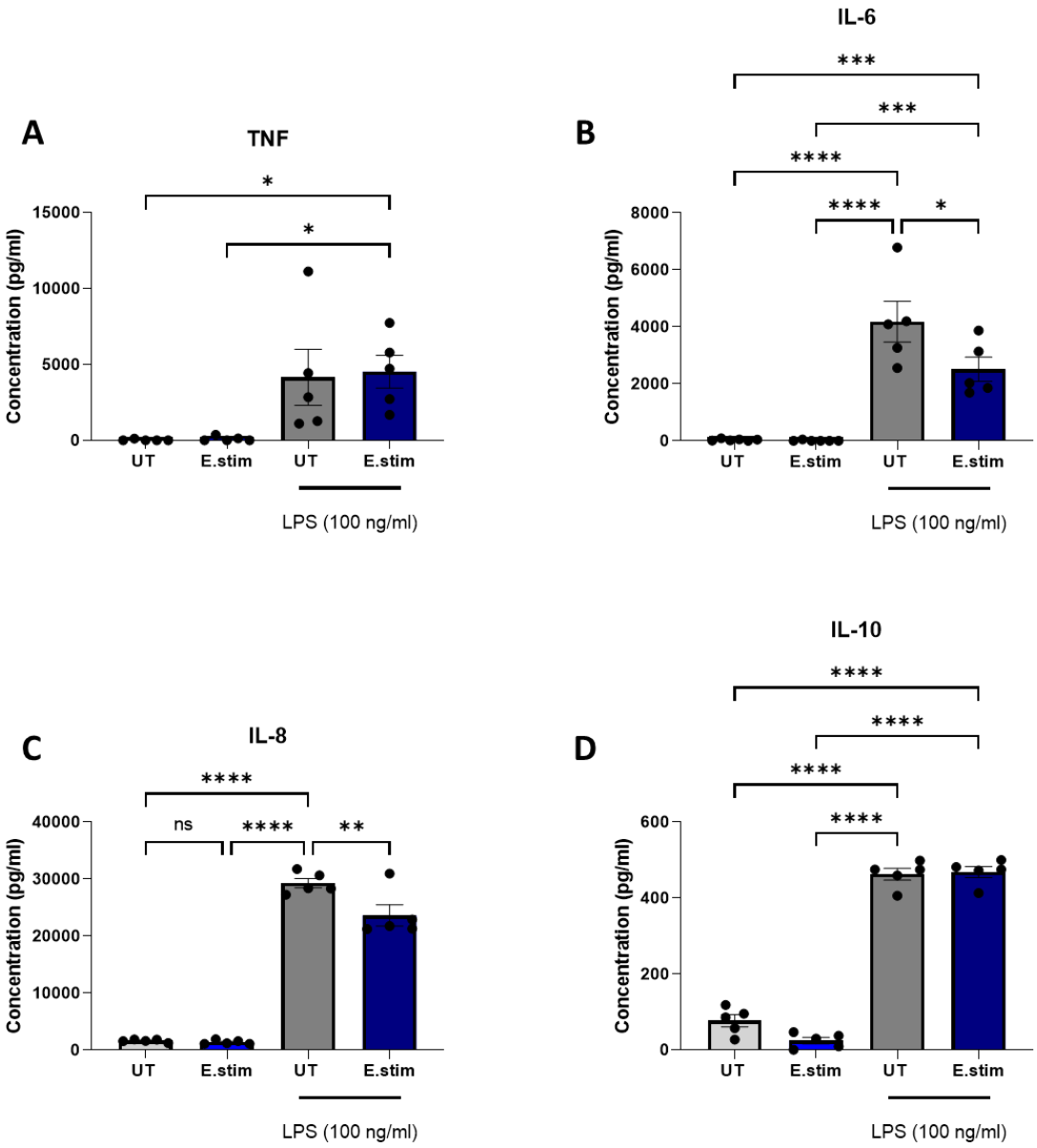

Figure 6-13 -Electrical stimulation reduces production of IL-6 and IL-8, but not TNF or IL-10 in LPS-stimulated macrophages

Primary human macrophages (1 x 10^6 cells/ml) were stimulated with electrical stimulation (± 2.5 V, 1 Hz, 2 ms) for 1 hour, followed by treatment with LPS (100 ng/ml) for 24 hours. (**A-D**) Levels of TNF, IL-6, IL-8 and IL-10 were assessed in cell supernatants by ELISA. Data is shown as mean ± SEM and analysed using One Way Anova with Tukey's post-test. *p≤0.05, **p≤0.01, *** ≤0.001, ****p ≤0.0001

6.4.11 Electrical stimulation inhibits CHC-induced IL-8 production in primary human macrophages

Having observed that ES significantly reduces LPS-induced inflammatory response, it was also of interest to explore potential effects on DAMP-related inflammation, more specifically, cholesterol crystals. Primary human macrophages were pre-treated with ES for 1 hour prior to cholesterol crystal stimulation (500 µg/ml) for 24 hours. Levels of IL-8 were assessed in cell supernatants by ELISA. A significant decrease of 15,864 pg/ml (± 2298) was observed in IL-8 production in cells pre-treated with ES compared to cholesterol crystal treatment alone, indicating that ES modulates not only PAMP-induced inflammatory responses but also those induced by DAMPs (Figure 6.14).

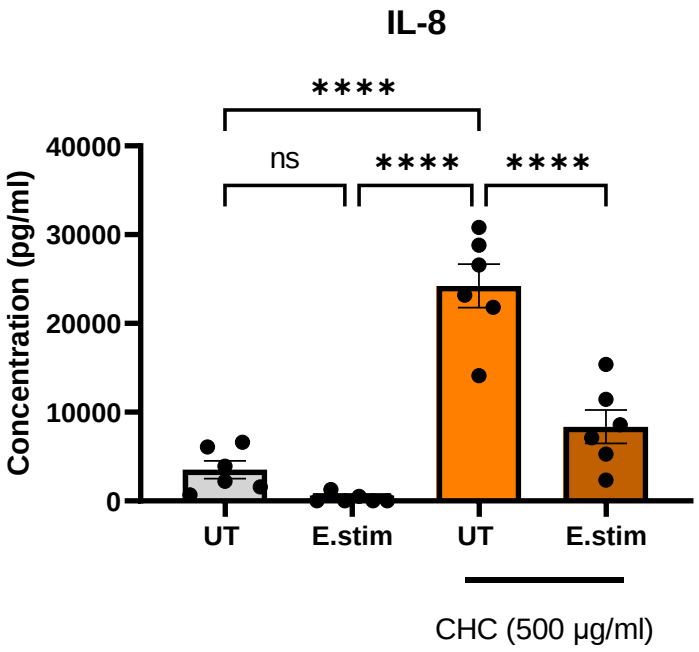

Figure 6-14 -Electrical stimulation reduces production of IL-8 in cholesterol crystal-stimulated macrophages

Primary human macrophages (1 x 10^6 cells/ml) were stimulated with electrical stimulation (± 2.5 V, 1 Hz, 2 ms) for 1 hour, followed by treatment with cholesterol crystals (CHC) (500 µg/ml) for 24 hours. Levels of IL-8 were assessed in cell supernatants by ELISA (N = 6, n =3). Data is shown as mean ± SEM and analysed using One Way Anova with Tukey's post-test. ****p ≤0.0001

6.4.12 Electrical stimulation inhibits LPS-induced metabolic reprogramming of macrophages.

As previously outlined in chapter 2, section 2.4, and further demonstrated in chapter 5, macrophage activation state and metabolism are integrally linked. LPS promotes a metabolic shift in macrophages to favour glycolysis as a dominant source of energy. Without this upregulation of glycolysis, macrophages cannot exert a pro-inflammatory response, as demonstrated through inhibition of the pathway with inhibitors such as 2-DG [292]. Having observed that ES limits the pro-inflammatory response in LPS-treated macrophages, it was next aimed to investigate if ES also inhibits LPS-induced metabolic reprogramming in macrophages. Primary human macrophages were pre-treated with ES for 1 hour prior to treatment with LPS for 24 hours. mRNA levels of key glycolytic markers, *GLUT1, HK2*, and *HIF1α* were assessed by real-time PCR. It was found that pre-treatment with ES significantly reduced expression of both *HK2* (fold change of 4.93 ± 0.84) and *HIF1α* (fold change of 1.87 ± 0.5), with a trend towards reduced expression of *GLUT1* also (fold change of 62.32 ± 36), when compared to LPS treatment alone (Figure 6.15). To further validate these findings, expression of the glycolytic rate limiting enzyme, HK2 was also assessed at the protein level by western blot. Similar to findings with PCR, densitometric analysis showed that pre-treatment of macrophages with ES caused a reduction in expression of HK2, when compared to LPS treatment alone (fold change of 2.495 ± 0.814 (Figure 6.16). Collectively these results indicated that ES effectively disrupts LPS-induced metabolic reprogramming in primary human macrophages.

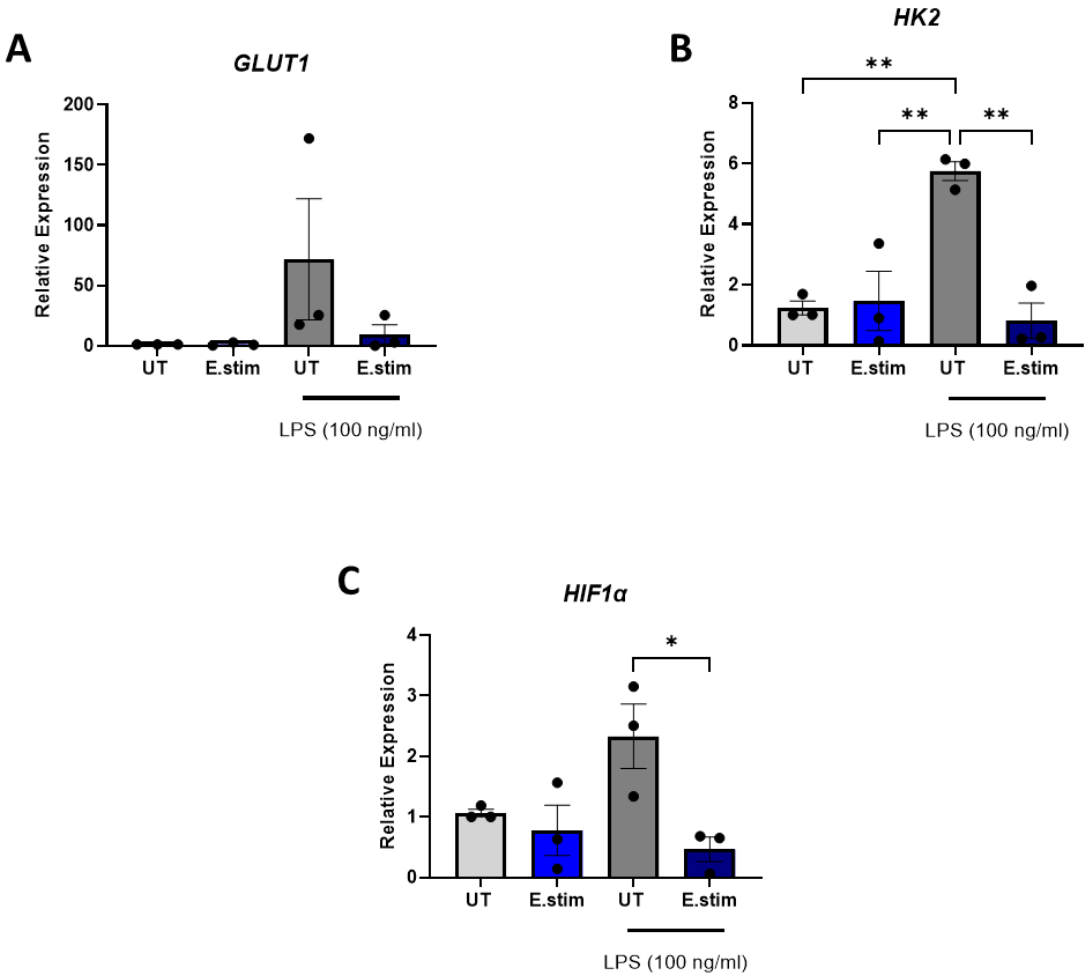

Figure 6-15 - Electrical stimulation inhibits LPS-induced expression of glycolytic markers *GLUT1, HK2,* and *HIF1α*

Primary human macrophages (1 x 10^6 cells/ml) were stimulated with electrical stimulation (± 2.5 V, 1 Hz, 2 ms) for 1 hour, followed by treatment with LPS (100 ng/ml) for 24 hours. (**A-C**) mRNA expression of *GLUT1, HK2,* and *HIF1α* were assessed by real-time PCR (N = 3, n =3). All data is shown as mean ± SEM and analysed using One Way Anova with Tukey's post-test. *p≤0.05, **p≤0.01

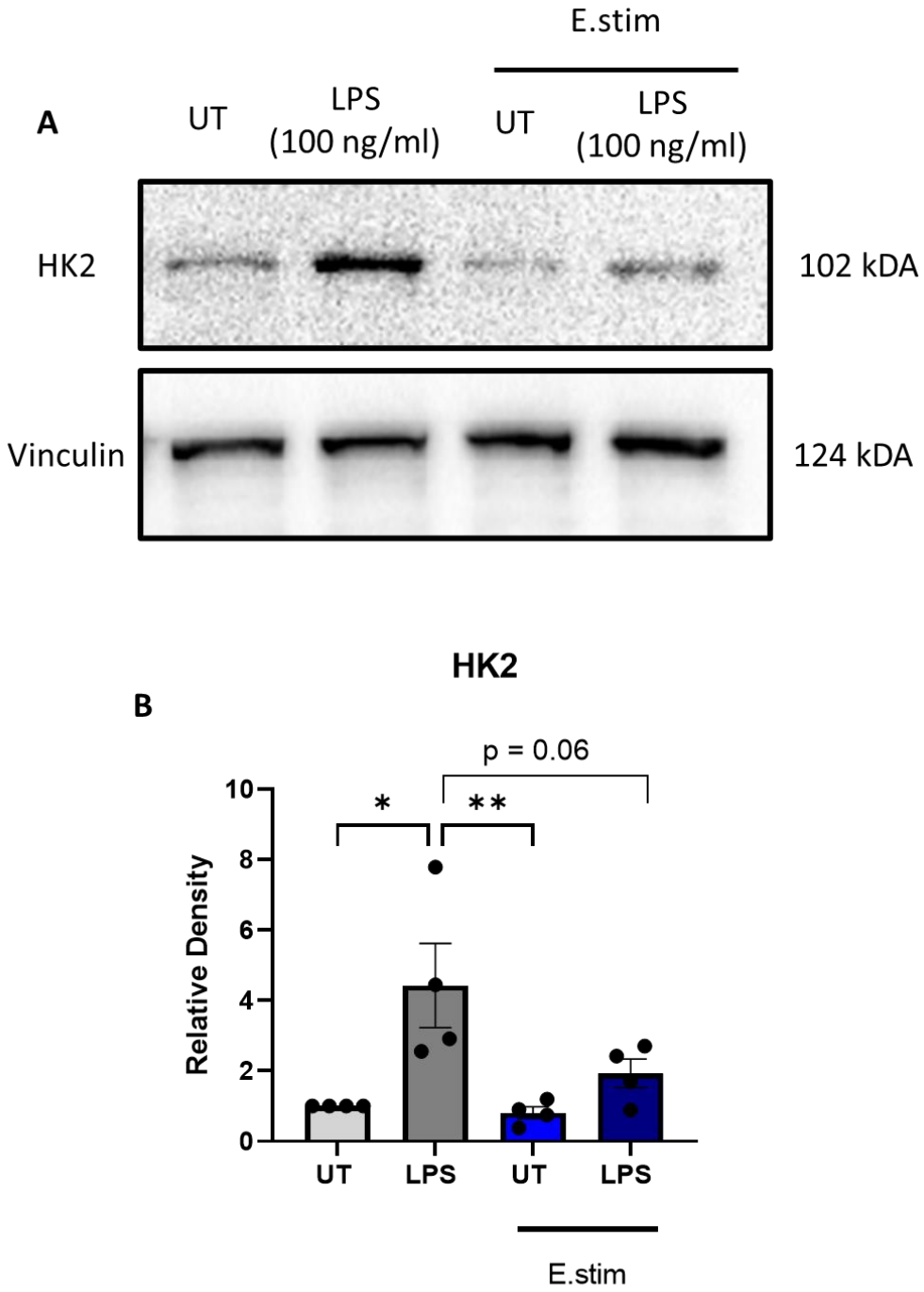

Figure 6-16 - Electrical stimulation inhibits LPS-induced protein expression of HK2

Primary human macrophages (1 x 10^6 cells/ml) were stimulated with electrical stimulation (± 2.5 V, 1 Hz, 2 ms) for 1 hour, followed by treatment with LPS (100 ng/ml) for 24 hours. Protein expression of HK2 was assessed by western blot. (**A**) Representative western blot of HK2 expression in unstimulated and electrically stimulated cells with/without LPS treatment. (**B**) Bar graph showing densitometric analysis of western blots normalised to vinculin house-keeping protein and relative to untreated cells (N = 4). All data is shown as mean ± SEM and analysed using One Way Anova with Tukey's post-test. *p≤0.05, **p≤0.01

6.4.13 Electrical stimulation induces expression of ion channel TRPV4 in primary human macrophages

Previous studies have highlighted that ES triggers Ca^{2+} influx and intracellular mobilisation of the ion in numerous cell types including macrophages [171, 293-295]. Increases in intracellular Ca^{2+} levels have been shown to regulate cytokine production and play a central role in macrophage function [296, 297]. Connexin 43 is known to contribute to Ca^{2+} influx to the cytoplasm of the cell [298], however it is not the sole mediator of calcium transport. An additional key transporter responsible for influx of Ca^{2+} in macrophages is the ion channel TRPV4, which has previously been identified as a mediator of enhanced phagocytosis in LPS-stimulated macrophages [299]. Given the increase in expression of Connexin 43 observed in response to ES, it was of interest to additionally investigate the influence of ES on TRPV4 expression. Primary human macrophages were electrically stimulated for 1 hour and left to rest for 24 hours. mRNA expression of *TRPV4* was assessed at 24 hours by real-time PCR. Increased expression of the ion channel was observed in ES-macrophages with a fold change of 64.68 ± 71.08, relative to untreated cells, suggesting a role for ion channel in the immune-modulatory responses observed as a result of ES (Figure 6.17).

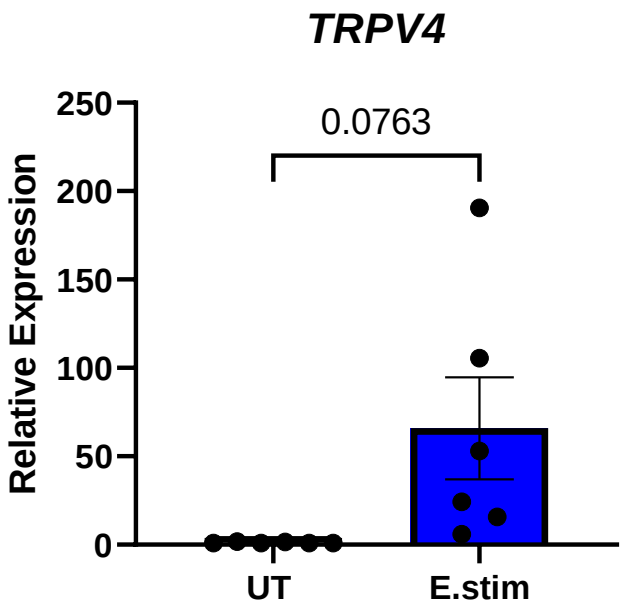

Figure 6-17 - Electrical stimulation induces expression of the ion channel TRPV4 in primary human macrophages.

Primary human macrophages (1 x 10^6 cells/ml) were stimulated with electrical stimulation (± 2.5 V, 1 Hz, 2 ms) for 1 hour, and left to rest for 24 hours. mRNA expression of *TRPV4* was assessed by real-time PCR (N = 6, n = 3). Data is shown as mean ± SEM and analysed by paired t-test.

6.4.14 Electrical stimulation induces expression of angiogenic factors in primary human macrophages

Having established from the findings thus far that ES promotes an anti-inflammatory phenotype in macrophages, it was next aimed to investigate additional macrophage functions associated with the M2 phenotype. It is known from literature that M2 macrophages play a critical role in angiogenesis, secreting pro-angiogenic factors which activate local endothelial cells, thus contributing to wound healing and tissue repair [300]. VEGF, platelet derived growth factor B (PDGF-B) and MMP9 are all growth factors known to have key modulatory roles in endothelial cell proliferation and migration and are produced by M2 macrophages at sites of tissue injury. It was of interest to investigate if ES showed the capacity to induce expression of these factors in primary human macrophages. Primary human macrophages were treated with ES for 1 hour and left to rest for 24 hours. mRNA expression of *VEGF, PDGFB* and *MMP9* were assessed by real-time PCR relative to unstimulated cells (Figure 6.18). A significant increase in expression was observed with *VEGF* (3.87 fold change ± 2.33) and *MMP9* (2.3 fold change ± 0.43), with a trend towards increased expression also in levels of *PDGF-B* (3.28 fold change ± 2.16), indicating that in addition to promoting an M2 phenotype in macrophages, ES also contributes to their pro-angiogenic function.

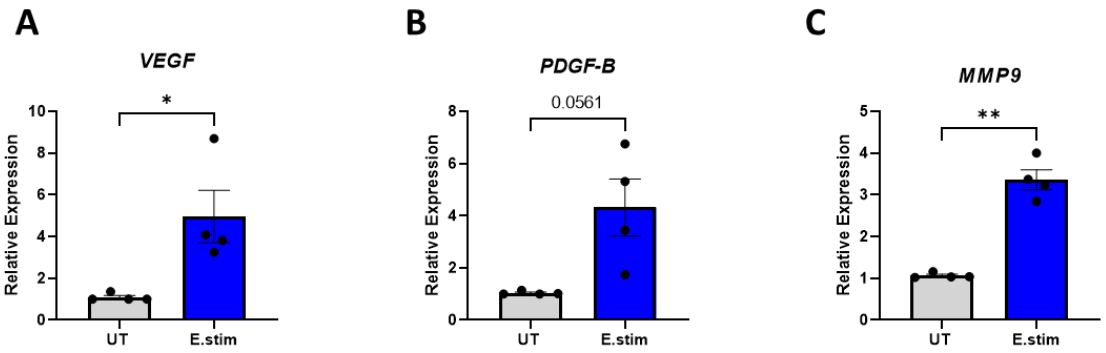

Figure 6-18 -Electrical stimulation induces expression of angiogenic markers VEGF, PDGF, and MMP9 in primary human macrophages

Primary human macrophages (1 x 10^6 cells/ml) were stimulated with electrical stimulation (± 2.5 V, 1 Hz, 2 ms) for 1 hour and left to rest for 24 hours. (**A-C**) mRNA expression of *VEGF, PDGF-B,* and *MMP9* were assessed by real-time PCR (N = 4, n =3). Data is shown as mean ± SEM and analysed using paired t-test. *p≤0.05, **p≤0.01

6.4.15 Conditioned media from electrically stimulated macrophages enhances migration of human MSCs.

To further demonstrate the pro-regenerative/pro-healing capacity of ES-macrophages, the influence of the macrophage secretome on additional non-immune cells (associated with the wound healing process) was investigated. MSCs are multipotent stromal cells capable of differentiating into multiple different tissue lineages including osteoblasts, chondrocytes, myocytes, and adipocytes, and have been increasingly recognised for their active participation in tissue repair [301-303] as well as an autologous source of therapeutic cells [304, 305]. When tissue damage occurs, MSCs either in the immediate vicinity or else derived from the bone marrow are recruited to the site [306]. Studies of conditioned media from M1/M2 polarised macrophages reveal that M2 macrophages promote enhanced migration of MSCs, highlighting their role in MSC recruitment to facilitate tissue repair [307]. To investigate if ES-macrophages elicited similar effects, primary human macrophages were stimulated for 1 hour and supernatants were collected after 24 hours for treatment with human MSCs.

The migratory capacity of the MSCs was assessed using an *in vitro* scratch assay as a model of wound healing [308, 309], where a single scratch was made through a monolayer of MSCs before culture in media alone, or conditioned media (CM) from untreated or electrically stimulated macrophages. MSC migration across the wound margins was then assessed visually at 24 hours and cells migrating into the wound site were counted by blinded individuals. Enhanced migration and repopulation of the wound site was apparent by eye in cells cultured in the ES-macrophage CM group (Figure 6.19 A). Semi-quantitative analysis of cell repopulation at the wound site within 24 hours revealed a significantly higher number of MSCs migrating back across the wound margin (Figure 6.19 C). Importantly there were no differences in the total cell number in each group, eliminating the possibility that the differences observed were due to cell proliferation (Figure 6.19 B). Taken together, these results suggest that secreted factors from electrically stimulated macrophages enhance MSC migratory capacity.

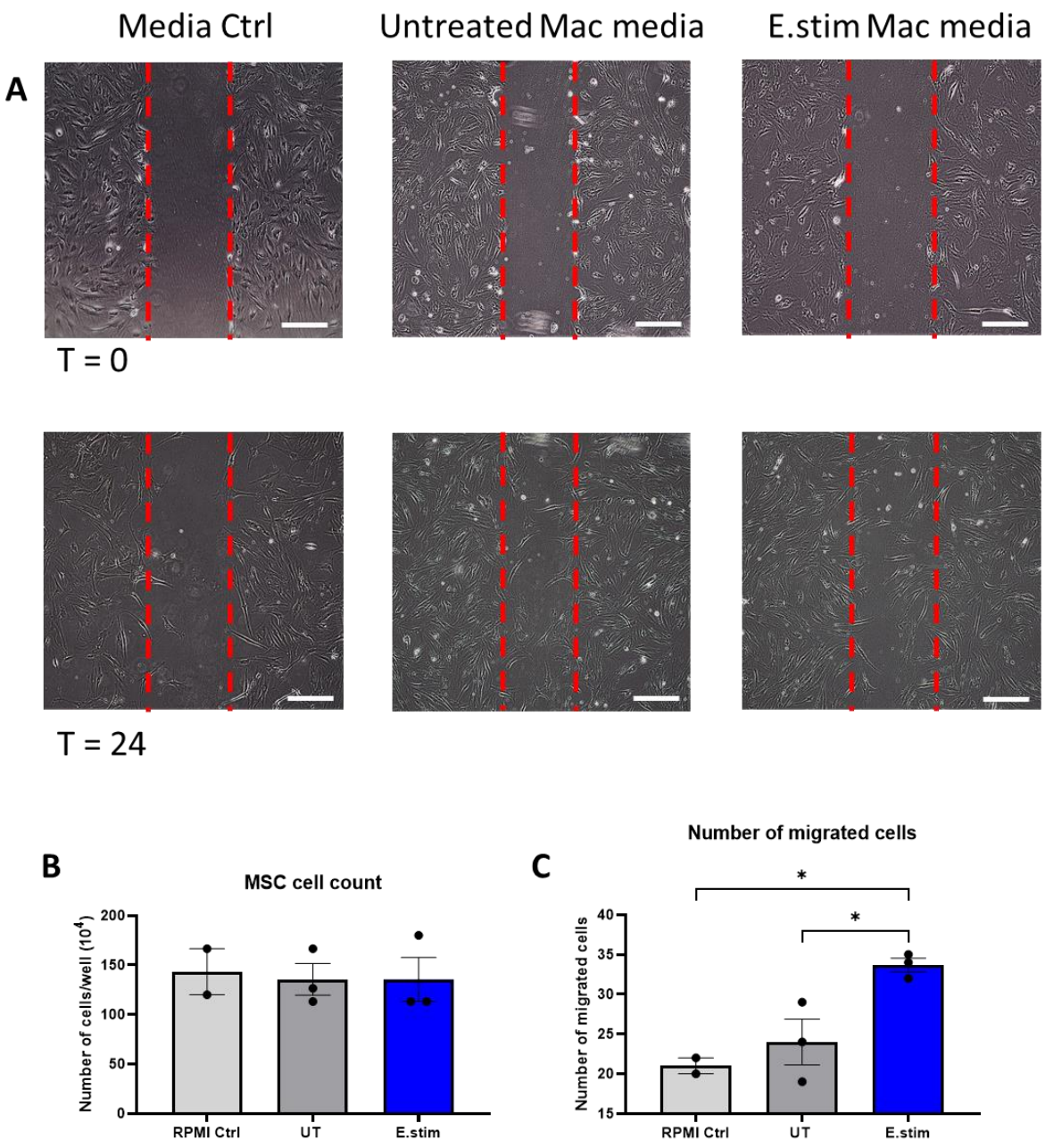

Figure 6-19 -Conditioned media from electrically stimulated macrophages promotes migration of human MSCs

Primary human macrophages (1 x 10^6 cells/ml) were stimulated with electrical stimulation (± 2.5 V, 1 Hz, 2 ms) for 1 hour and left to rest for 24 hours. Cell supernatants were collected and used to treat human MSCs in a wound scratch model. (**A**) Representative images displaying human MSC migration (at time of induced scratch, T=0 and after 24 hours, T=24) following culture in media alone, or conditioned media from untreated or electrically stimulated macrophages. (**B**) Cell count of MSCs after 24 hours of culture in macrophage conditioned media. (**C**) Cells were counted by blinded individuals at pre-determined imaged sites from each healthy donor and a mean value per donor was calculated and plotted. Data (n=3) is represented as mean ± SEM was analysed using one-way ANOVA with Tukey's Post-Test. Scale bar = 100 µm. *p≤0.05

6.5 Discussion

Electrical signalling has long been considered an essential mediator of tissue homeostasis in the body, and imperative to tissue regeneration following incidence of injury [274, 281]. While electrical cues have been extensively studied in cells such as fibroblasts and stem cells [166, 167, 288, 290], there is limited knowledge of the impact on the immune response, more specifically, macrophages, which also play a substantial role in tissue repair [310]. In the context of the heart, it is known that resident macrophages facilitate electrical signalling [70], yet this function is largely unknown in blood-derived macrophages. Given that under circumstances of MI, blood-derived macrophages repopulate the heart, partly replacing the resident cell population [84], characterisation of their response to ES is a worthwhile investigation. Previous studies assessing the impact of electrical stimulation on macrophages were done so in the context of wound healing, where the applied voltage ranged from 30 mV/mm to 150 mV/mm, mimicking the endogenous EF created at the site of wounds [171, 172]. The voltage applied in this study was notably higher (± 2.5 V), with 2 ms pulse duration at a frequency of 1 Hz, as it was set to mimic the conditions found native to the myocardium [194]. These settings have also previously been implemented in the pacing and maturation of CMs *in vitro* as a biomimetic approach to recapitulate the physiological features of the heart [168], and have shown to be highly advantageous for the successful generation of functionally mature iPSC-CMs [287, 290]. The work of this results chapter has furthered the benefits of externally applied ES to non-CMs, revealing that ES promotes an M2 pro-regenerative phenotype in primary human macrophages.

It is worth noting that the external ES applied to macrophages in these experiments, while mimicking stimulation experienced by cardiac cells in vivo, does not truly recapitulate endogenous electrical fields of the heart. This is due in part to the use of 2D monolayer cultures of macrophages. As previously mentioned, the heart is comprised of a complex three-dimensional network of various cells and ECM. Monolayers of cells in vitro have reduced cell-cell interactions compared to 3D structures, which can also limit formation of gap junctions. As a result, propagation of electrical signal is altered compared to that observed in vivo.

Furthermore, there is a noteworthy absence of CMs from these experiments, which in vivo, are present in a 1:5 ratio with macrophages in the heart [311]. Given the significant contribution of CMs to endogenous electrical fields in the heart, it is right to say that the electrical fields applied externally, will differ from physiological electrical fields of the heart. Nevertheless, these monolayer cultures of macrophages alone act as a reliable starting point for basic research elucidating primary human macrophage response to electrical stimulation, of which, there is limited knowledge.

In addition to promoting an M2 phenotype, experimental findings of this chapter also suggest ES may potentially support coupling of cardiomyocytes with blood-derived macrophages, a necessary trait of cardiac resident macrophages *in vivo* [70, 85]. Tissue resident macrophages facilitate electrical conductivity in the myocardium through expression of Connexin 43, allowing gap junctions to be directly formed between resident macrophages and cardiomyocytes. It was previously understood that blood-derived macrophages may also be capable of expressing the gap junction protein [312], however this protein is not ubiquitously expressed by resting macrophages. Pro-inflammatory conditions such as stimulation with LPS and IFNγ have been shown to induce Connexin 43 expression in blood derived macrophages, suggesting a role for gap junction formation in intercellular macrophage communication and function [312]. This study has now demonstrated that electrical stimulation is also capable of inducing expression of the gap junction protein in primary human macrophages.

Previous work from Cox *et al*. has shown that co-culture of RAW 264.7 macrophages with cardiomyocytes can induce Connexin 43 expression in macrophages [313]. Increased expression of Connexin 43 also coincided with raised resting membrane potentials of CMs, thus leading to a more excitatory phenotype. This response was enhanced in IL-10/TGFβ treated macrophages, suggesting that M2 macrophages in particular, are required for effective Connexin 43-mediated coupling with CMs. Findings from my own work suggest that electrical stimulation in the cardiac environment potentially plays a role in promoting this M2 phenotype deemed necessary for effective electrical coupling. It will be of immense interest in future work to investigate coupling of cardiomyocytes with blood-derived macrophages, both in the presence and absence of electrical stimulation. Not only will this highlight the ability of blood-derived

macrophages to facilitate electrical conduction of CMs, which previously has not been identified, but it also may demonstrate the potential of macrophages to improve maturation of iPSC-CM *in vitro* for tissue engineering applications. The benefits of incorporating macrophages in tissue engineering constructs has been previously seen in the study of skeletal muscle, whereby co-culture of macrophages with skeletal muscle cells resulted in improved repair and regeneration following injury [314].

Hoare *et al*. demonstrated in their work that human macrophage migration increases in response to electrical field stimulation of 150 mV/mm [171]. The findings observed in this chapter suggest a similar response, in that ES-treated macrophages exhibit increased expression of chemokine receptor CCR2, suggesting an increase in migration capacity. Chemotaxis of macrophages to sites of injury, i.e. the infarcted myocardium is mediated via monocyte CCR2 signalling, as demonstrated through selective inhibition of the receptor, which results in abrogation of blood-derived macrophages from the heart following infarction [289]. While further experiments are required to validate this result, the observed increase in CCR2 expression suggests that physical factors from the cardiac environment itself, i.e., electrical stimulation facilitate the honing effect of blood-derived macrophages. It will be of interest in future work to investigate the direction of macrophage migration in response to pulsed electrical stimulation, or if similar effects are exerted in monocyte progenitors. Furthermore, if electrical stimulation alone can promote monocyte differentiation towards a mature macrophage phenotype.

Previous studies have demonstrated that external delivery of electrical stimulation results in activation of the PI3K/Akt pathway [315]. These findings also extend to EF-mediated macrophage responses [171]. Hoare *et al*. demonstrated that increased phagocytosis in response to electrical stimulation was accompanied by phosphorylation of both PI3K and Akt, with inhibition of PI3K using LY294002, resulting in a significant reduction in phagocytic capacity of electrically stimulated cells [171]. Future work exploring the role of PI3K/Akt signalling in my own findings would be of great interest, particularly due to the established role of Akt signalling in M2 macrophage polarisation [316]. In particular, activation of Akt may explain the disruption to LPS metabolic reprogramming observed in response to electrical stimulation. Phosphorylation of Akt effectively inhibits activity of the TSC complex, which ultimately inhibits MTORC1

activity, known to mediate “Warburg” glycolysis in macrophages [59]. Therefore, a potential mechanism may be that electrical stimulation activates the PI3K-Akt signalling pathway in macrophages, phosphorylating Akt and consequentially inhibiting Warburg metabolism following LPS stimulation. Further experiments investigating PI3K/Akt activation in electrically stimulated macrophages, as well as direct inhibition of the signalling pathway, may allow us to fully elucidate this mechanism and its potential role in electrically induced M2 polarisation of primary human macrophages.

However, it is worth noting from previous studies that EF-induced effects are not completely abrogated through inhibition of PI3K signalling [171], suggesting this pathway is not the sole mediator of macrophage response to electrical cues. It is plausible that cell response is also driven by intracellular movement of ions, particularly given that increased expression of the Ca^{2+} TRPV4 was observed in response to electrical stimulation. Previous studies have demonstrated that electrical stimulation triggers intracellular mobilisation of Ca^{2+} ions in numerous cell types including macrophages [167, 171, 294, 317]. Modulation of ion transporters has been previously observed to have consequential effects on macrophage phenotype and function, as inhibition of K+ channels reduces pro-inflammatory cytokine production in LPS/IFNγ-treated macrophages [283]. Additionally, inhibition of Ca^{2+} influx can also disrupt macrophage function. Treatment of murine macrophages with SKF-96365, inhibits calcium entry into the cell and, as a result, significantly decreases expression of M2-associated markers CD206 and Arginase-1 in IL-4 stimulated macrophages [297]. However, the effects of calcium influx are more complex than simply driving M2 polarisation, as increases in intracellular Ca^{2+} levels have been observed to play a central role in both pro and anti-inflammatory macrophage function. Indeed, treatment of IFNγ-stimulated macrophages with the same inhibitor SKF-96365 significantly decreases pro-inflammatory cytokine production. Similarly, the role of TRPV4 has been implicated in both pro and anti-inflammatory responses [318, 319]. Future work elucidating precisely how calcium mobilisation regulates the M2 phenotype from electrical stimulation would greatly benefit not only this work, but future tissue engineering studies which aim to harness pro-regenerative macrophages as a therapeutic strategy.

Alterations to macrophage metabolic reprogramming may also be a consequence of calcium influx, which has been recently shown to be linked with macrophage metabolic reprogramming in murine cells [297]. Specifically, mitochondrial respiration, necessary for M2 polarisation of macrophages has been shown to be mediated by the calcium channel Orai1 [297]. Orai1$^{-/-}$ murine macrophages exhibit significantly reduced oxygen consumption rates (OCR), while pharmacological inhibition of the channel results in reduced mitochondrial bioenergetics [233, 296, 297]. Therefore, in addition to exploration of the PI3K/Akt signalling pathway, future work investigating Orai1 may also reveal how electrical stimulation promotes metabolic rewiring of primary human macrophages.

It was of importance in this study not only to investigate the anti-inflammatory effect of electrical stimulation in LPS-activation of macrophages, but additionally the pro-regenerative paracrine function of macrophages following stimulation. An important feature of M2 macrophages is their role in wound-healing through secretion of pro-angiogenic factors as well as chemotactic recruitment of additional pro-healing cell types [320]. This is also observed in the heart, where anti-inflammatory macrophages facilitate tissue healing by activation of local fibroblasts, in addition to the secretion of pro-angiogenic factors [300]. Electrical stimulation was shown to promote significant expression of TGF-B in macrophages, a critical factor involved in the activation of fibroblasts [321]. Moreover, significant expression of pro-angiogenic factors were also observed in electrically stimulated macrophages. Numerous studies have outlined how efforts to stimulate angiogenesis after MI can improve heart recovery, however, the molecular pathway involved in myocardial neovascularisation after ischemia remains unknown. The findings of this study now suggest that endogenous electrical stimulation in the myocardium may play a role in promoting neovascularisation. Already there have been notable effects of external EF stimulation on endothelial cells for the context of wound healing [169, 170]. It would be worthwhile to investigate whether the electrical stimulation regime specifically applied in this study promotes similar pro-angiogenic effects in endothelial cells, again to gain clearer insight to the role of electrophysical signalling in heart function and repair.

The pro-regenerative phenotype of electrically stimulated macrophages was further demonstrated in this study through conditioned media experiments with human MSCs, whereby conditioned media from stimulated macrophages was shown to significantly enhance migration of MSCs in a wound scratch model. This data represents a very interesting finding as it demonstrates the potential benefits of electrical stimulation for additional tissue engineering applications beyond the heart. Migration of MSCs in incidence of bone or cartilage injuries is an important aspect of the healing response, in order to sustain tissue regeneration. However, the chemotactic signals that guide MSCs to these sites have not been extensively studied. It has been observed that MSC-macrophage cross-talk may be involved, as secreted factors from M2 macrophages have been shown to actively recruit MSCs in *in vitro* models, and furthermore, enhance osteogenesis of these cells [307, 309]. Such studies have used soluble factors or bone-mimetic particles to induce M2 polarisation, here we present an alternative strategy, implementing physical stimulus which promotes a similar "pro-healing" secretome in primary macrophages. Already there is evidence to show the regenerative and osteogenic effects of direct electrical stimulation on MSCs, mediated through activation of MAP kinase proteins p38 and ERK1/2, as well as calcium signalling [166]. It is possible that the combined effect of electrically stimulated macrophages may enhance this response. It would be of great interest to further explore this in the future as a novel electrotherapeutic strategy in bone repair.

Interestingly, the activation of MSCs is also being considered as a therapeutic strategy in heart failure [322]. In the cardiovascular system, MSCs can protect the myocardium by reducing the level of inflammation through secretion of anti-inflammatory factors such as PGE2 Interestingly, the activation of MSCs is also being considered as a therapeutic strategy in heart failure [322]. In the cardiovascular system, MSCs can protect the myocardium by reducing the level of inflammation through secretion of anti-inflammatory factors such as PGE2 [323], as well as exosomes which have been shown to inhibit the inflammatory response in macrophages via inhibition of the NF-κB pathway [324]. [325, 326]. MSC transplantation in murine models of MI results in improved cardiac function in mice, correlated with reduced apoptosis of myocardial cells, as well as reduced levels of TNF, IL-6 and IL-1 [325]. MSCs have also been found to

promote proliferation of CMs post-MI [327], as well as inhibiting fibrosis of cardiac tissue [328], which are ideal qualities for cardiovascular repair. However, challenges still remain in pre-clinical studies of MSCs, such as their low rate of migration to the ischemic myocardium, low tissue retention, and low survival rate after transplantation [322]. The observed capacity of M2 macrophages to promote MSC recruitment, as observed previously in the literature, as well as in this study, may represent a novel therapeutic target for future investigations.

In summary, this study has demonstrated that in addition to endogenous DAMPs and chemical factors, electrical stimulation can play a role in shaping macrophage polarisation by promoting an anti-inflammatory, pro-regenerative M2 phenotype in primary human macrophages. While further investigation is required to identify the signalling pathways at work which elicit this cell response, this work has allowed us to shed some light on how homeostasis of macrophages is potentially maintained in the heart. Additionally, this study has presented a novel therapeutic strategy for harnessing anti-inflammatory, pro-regenerative responses across multiple injury and defence microenvironments.

A summary of the results generated in this study, in addition to a proposed mechanism of action is provided in figure 6.20

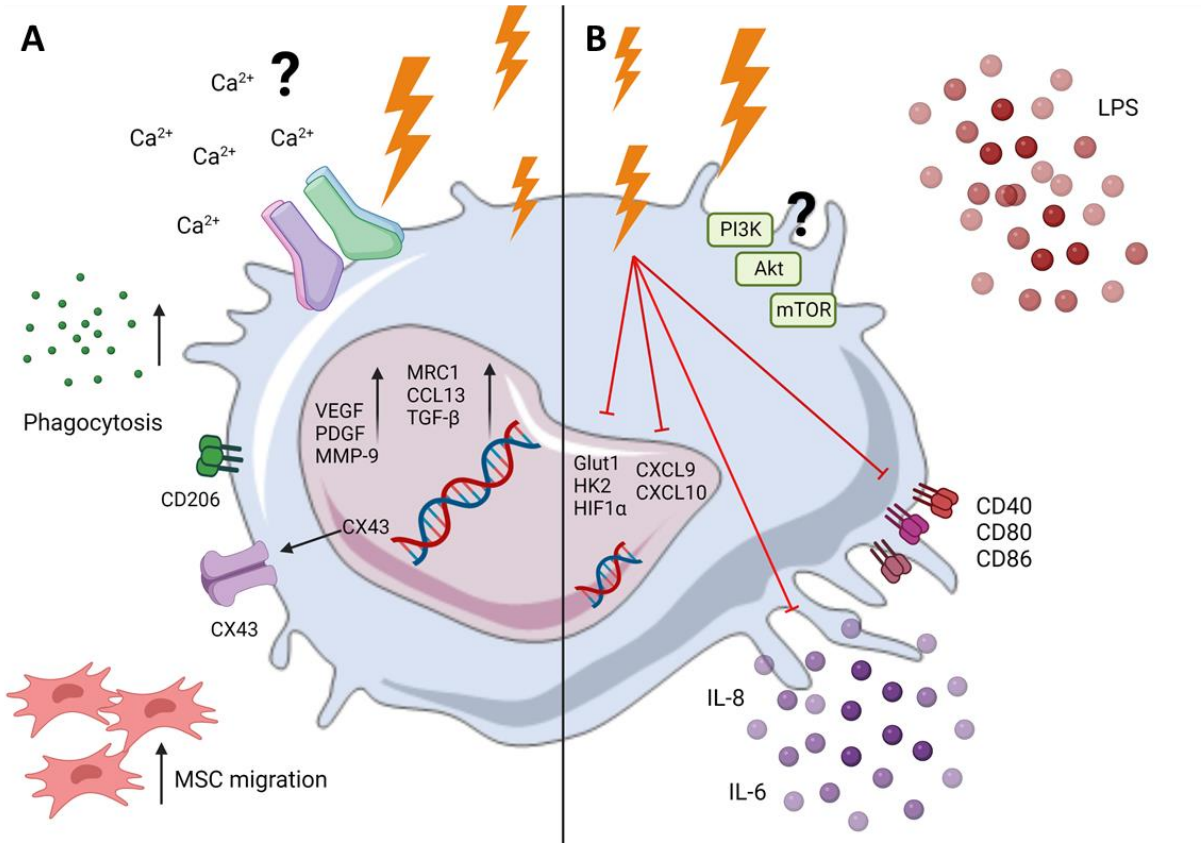

Figure 6-20 - Schematic summary of findings.

(A) Electrical stimulation upregulates expression M2-associated genes MRC1, CCL13, TGF-β, and M2 surface marker CD206. Increased expression of gap junction protein Connexin 43 is also observed at mRNA and protein level. The M2 phenotype is accompanied by an increase in phagocytic capacity, increased expression of angiogenic growth factors and ability to recruit MSCs. This response may potentially be modulated through Calcium ion transport.

(B) Electrical stimulation limits expression of pro-inflammatory markers CXCL9 and CXCL10, in addition to IL-6 and IL-8 production in LPS-stimulated macrophages. Reduced expression of glycolytic markers was also observed, with this potentially modulated through the PI3K-Akt-mTOR signalling axis.

Chapter 7 : Assessment of macrophage response to the electroconductive biomaterial PEDOT: PSS

7.1 Abstract

The growing appreciation for the role of bioelectricity in tissue processes has garnered significant attention towards the use of electroconductive materials in tissue engineering. Electroconductive biomaterials such as PEDOT: PSS have proven beneficial towards the maintenance and function of numerous cell types including CMs, MSCs, osteocytes, and neural cells *in vitro*. Given the observations of chapter 6, in that macrophages are also responsive to electrical stimulation, there is rationale to explore the use of electroconductive materials with macrophage culture. The aim of this chapter, therefore, was to investigate the response of primary human macrophages to PEDOT: PSS, including the assessment of two different cross-linkers GOPS, and PEGDE (which facilitate its fabrication into stable 3D scaffolds). Primary human macrophages were treated with media conditioned with PEDOT: PSS (extraction media), or else seeded directly onto PEDOT: PSS films. It was observed that PEDOT: PSS cross-linked with PEGDE significantly reduced viability of cells, while PEDOT: PSS cross linked with GOPS exerted no such effects. PEDOT: PSS (GOPS) was proven to have no significant impact on macrophage phenotype, either indirectly via extraction media, or directly via seeding on PEDOT: PSS (GOPS) films. Importantly, PEDOT: PSS (GOPS) also did not impede typical macrophage responses to pro-inflammatory stimuli LPS or cholesterol crystals, or the anti-inflammatory cytokine IL-4. These findings indicate that PEDOT: PSS (GOPS) is well tolerated by primary human macrophages, and furthermore, provides useful insight to the potential success of PEDOT: PSS *in vivo*, as macrophages failed to elicit a pro-inflammatory response to either PEDOT: PSS extraction media, or PEDOT: PSS films directly.

7.2 Introduction

The classic paradigm of tissue engineering requires three crucial components; a relevant selection of cells, biomaterial scaffolds, and the presence of appropriate biochemical and biophysical cues to recreate viable tissue [142]. As outlined in chapter 6 of this thesis, electrical signalling is an important physical cue in numerous tissues processes, including wound healing, signal transduction in the brain, and muscle contraction in the heart. Therefore, the use of “smart” electroconductive biomaterials materials (materials that can carry electronic current) has gained increasing interest in the development of *in*

vitro tissue models, as a means of facilitating the necessary electrical cues required for native cell function. This is evident in particular, in the field of cardiac tissue engineering, where the incorporation of electroconductive materials in tissue engineered constructs leads to significant improvements in cell adhesion, organisation and cell-cell coupling of CMs *in vitro* [173]. Furthermore, application of electroconductive biomaterials in stem cell culture has been shown to drive iPSC-CM maturation, addressing the primary limitation of iPSC use in cardiac tissue engineering [154, 329]. Such effects have led to the consideration of electroconductive materials as potential platforms for *in vitro* cardiac models, to better recapitulate the biophysical properties of the native tissue.

Conductive biomaterials can be broadly categorised into two classes, extrinsically conductive polymers, or else intrinsically conductive polymers (also known as conjugated polymers). Extrinsically conductive polymers refer to compounds which have an insulating material surrounding a conductive filler such as gold or silver nanoparticles, graphene, or carbon nanotubes. The addition of these fillers to biomaterial scaffolds has proven very beneficial towards the culture of various cells including osteocytes, dermal fibroblasts, and MSCs [330-333], all of which are known to function via endogenous electrical signalling *in vivo* [160, 166, 280, 293, 294]. The application of conductive polymers in cardiac-related studies has also been investigated, for example hydrogels embedded with gold nano-rods have been shown to increase cell attachment and alignment of neonatal rat CMs when compared to non-conductive hydrogel scaffolds [334]. Incorporation of carbon nanotubes in hydrogels elicits a similar response, with CNT-embedded scaffolds causing high cell retention of neonatal rat CMs, as well as improved cell alignment and function [175].

Intrinsically conductive polymers are organic conjugated polymers that initially possess low conductivity but are subjected to a secondary doping process (for example chemical reactions such as reduction or oxidation) which results in a significant increase in conductivity. The application of conjugated polymers in multiple fields of tissue engineering has been extensively discussed [173, 335, 336]. Polyaniline (PANI) for example have been shown to promote neural differentiation in MSCs [337]. Polypyrrole (PPy) has been used as a coating for non-conductive silk fibroin films, where it was shown to improve cell alignment of ESC-CMs as well as maturation [338]. However, work

with PPy remain limited as it has been shown to elicit cytotoxic effects at high concentrations [339]. PEDOT: PSS is a highly versatile material and has been extensively studied in the area of biosensors [340, 341], actuation [342], and biological scaffolds for neural development and optoelectronic applications [343-345]. PEDOT:PSS has emerged as a prime candidate for cardiac tissue models, given its highly conductive nature, ease of processing, and increased stability relative to other existing polymers [173]. Previous studies of PEDOT: PSS in hydrogels have shown the polymer to enhance maturation of both rat and iPSC derived CMs [154], showing its promise as an *in vitro* biomaterial platform.

One of the many advantages of PEDOT: PSS as a biomaterial is its water solubility, making its manufacture relatively simple compared to alternative conductive materials in the field [346]. However, the caveat of this feature is that PEDOT: PSS requires additional cross-linking in order to stabilise the material for use in aqueous solutions such as *in vitro* cell culture. The cross-linker GOPS has been extensively used for this application, and successfully prevents both dissolution and delamination of PEDOT: PSS films in aqueous solutions [347]. GOPS binds to excess PSS in the polymer but not PEDOT, in a cross-linking reaction between the SO_3^- groups of the excess PSS and the epoxy ring of GOPS. GOPS additionally binds to other GOPS molecules, or else the glass substrate in the case of 2D films, thus explaining its prevention of delamination from coverslips. Unfortunately, this reaction also results in a reduction in the conductivity of PEDOT: PSS, as binding of GOPS to PSS limits movements of ions through the polymer [347]. This trade off in conductivity for stability has led researchers to seek alternative methods to prevent dissolution of PEDOT: PSS. One alternative cross-linker under consideration is poly (ethylene glycol) diglycidyl ether (PEGDE). PEGDE is a water-soluble epoxy resin, previously implemented as a cross-linker of silk fibroin films, and redox hydrogels for biosensors [348, 349]. Previous work led by Solazzo *et al*. et al has demonstrated that PEGDE successfully cross-links PEDOT:PSS at low temperatures, resulting in a stable film, with increased conductivity and hydrophilicity compared to uncross-linked PEDOT: PSS, and PEDOT: PSS (GOPS) [346]. While these findings are promising, future work requires more in-depth characterisation of cell response to the material for further consideration of the material for biological applications.

Many previously established studies assessing the biocompatibility of electroconductive biomaterials, including PEDOT: PSS, are limited to either cell lines, or in the context of cardiac tissue engineering, either rat or iPSC derived CMs. Very little is understood regarding the immune response to these materials.

It is well established that the host immune response, predominantly led by macrophages largely dictate the success of biomaterials *in vivo*. Most well understood in this context, is the ability of macrophages to drive a foreign body response (FBR) to implanted biomaterials, whereby macrophages form foreign body giant cells, promote chronic inflammation, and ultimately drive fibrotic encapsulation of the material [350]. Failure of biomaterials under these circumstances are most often seen in total joint replacements of the hip or knee, where chronic inflammation causes aseptic loosening of implants and necessary revision surgeries [351]. However, incidences of implant failure are also seen in the heart, where bioprosthetic heart valves fail due to chronic inflammation causing calcification and structural degeneration of the implant [352, 353]. As a result, characterisation of the immune response has become a high priority in the field of tissue engineering. Furthermore, numerous studies have now adopted strategies in biomaterial design to manipulate macrophage response towards a more favourable "M2-like" state which facilitates tissue regeneration or repair [354]. Biomaterial properties such as surface topography, chemistry, porosity, and stiffness have all been observed to influence macrophage form and function [350]. Parallel gratings on PCL scaffolds have been shown to create differential macrophage responses, with larger gratings resulting in a reduction of TNF and VEGF secretion in RAW 264.7 macrophages [355]. Altering surface chemistry also provides an immune altering effect, as shown by rat cage implant models. Biomaterials with anionic or hydrophilic surface chemistries showed reduced infiltration of monocytes and macrophages, and a reduction also in apoptotic cells surrounding the implant [356]. With regards to scaffold porosity, smaller pore size favours an M2-like response in macrophages, however larger pore sizes result specifically in pro-angiogenic phenotypes, and improved integration of scaffolds into tissue [357, 358]. As a result, characterisation of the immune response has become a high priority in the field of tissue engineering.

Characterisation of macrophage response to biomaterials is not only helpful as a predictive tool for the survival of materials *in vivo*, but also in the identification of suitable platforms to facilitate macrophage function *in vitro*. It was established in chapter 6 of this thesis that primary human macrophages are indeed responsive to electrical signalling, undergoing polarisation towards an M2 pro-regenerative phenotype. There is therefore strong rationale for the use of electroconductive biomaterials such as PEDOT: PSS in macrophage culture, to further promote the pro-healing effects of electrical stimulation. Furthermore, PEDOT: PSS has been previously shown to enhance function of CMs *in vitro*, therefore there is also rational for the implementation of PEDOT: PSS as a platform for macrophage-CM co-cultures, given that electrical signalling regulates function of both cell types. Prior to this however, characterisation of macrophage response to PEDOT: PSS is crucial.

7.3 Aims

In order to consider PEDOT: PSS as a suitable *in vitro* platform for macrophages, the response of macrophages to the material is required. It is therefore the aim of this chapter to assess the response of primary human macrophages to the electroconductive material PEDOT: PSS. This includes the assessment and comparison of two different cross-linkers of PEDOT: PSS, firstly GOPS which is extensively used in the generation of PEDOT: PSS scaffolds and secondly, PEGDE, which has emerged as a novel alternative cross-linker to address the impedance associated with GOPS cross-linking.

Specific aims:

- Characterise macrophage response to the conductive polymer PEDOT: PSS
- Investigate macrophage response to alternative cross-linker PEGDE

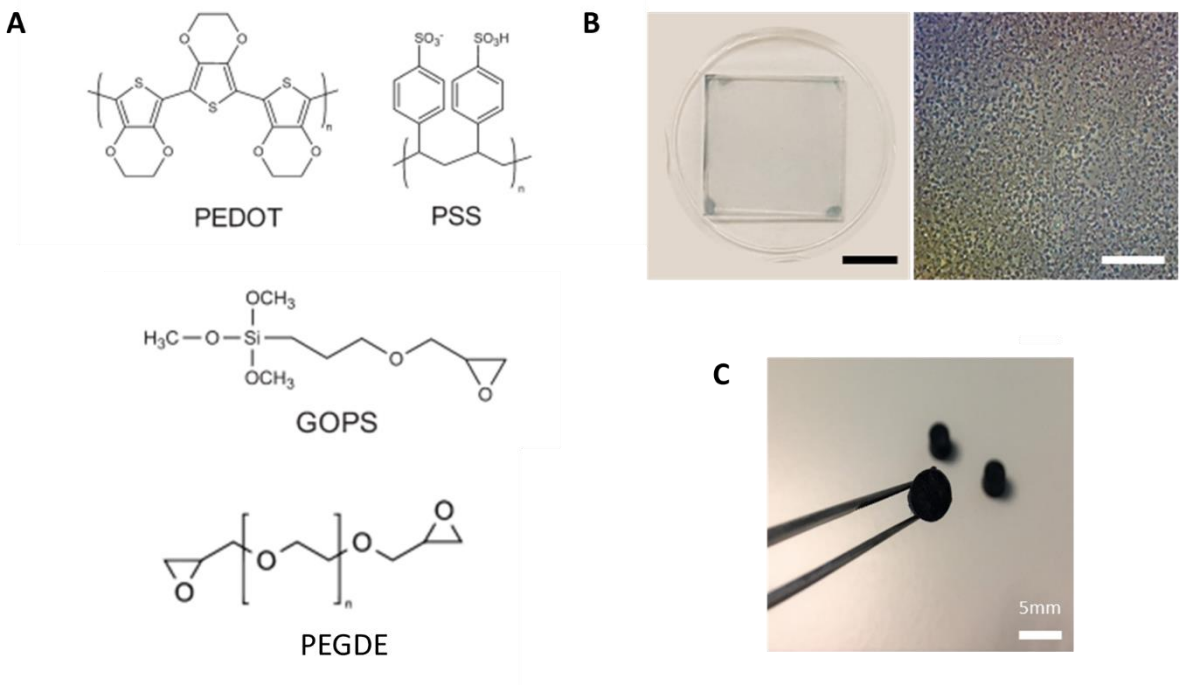

Figure 7-1 – PEDOT: PSS and cross-linkers

(A) Chemical structure of PEDOT, PSS, and crosslinkers GOPS and PEGDE. (B) 2D films of PEDOT: PSS spin coated on glass coverslips. Scale bar represents 1 cm (left) and 50 µm (right). (C) 3D porous scaffolds of PEDOT: PSS.

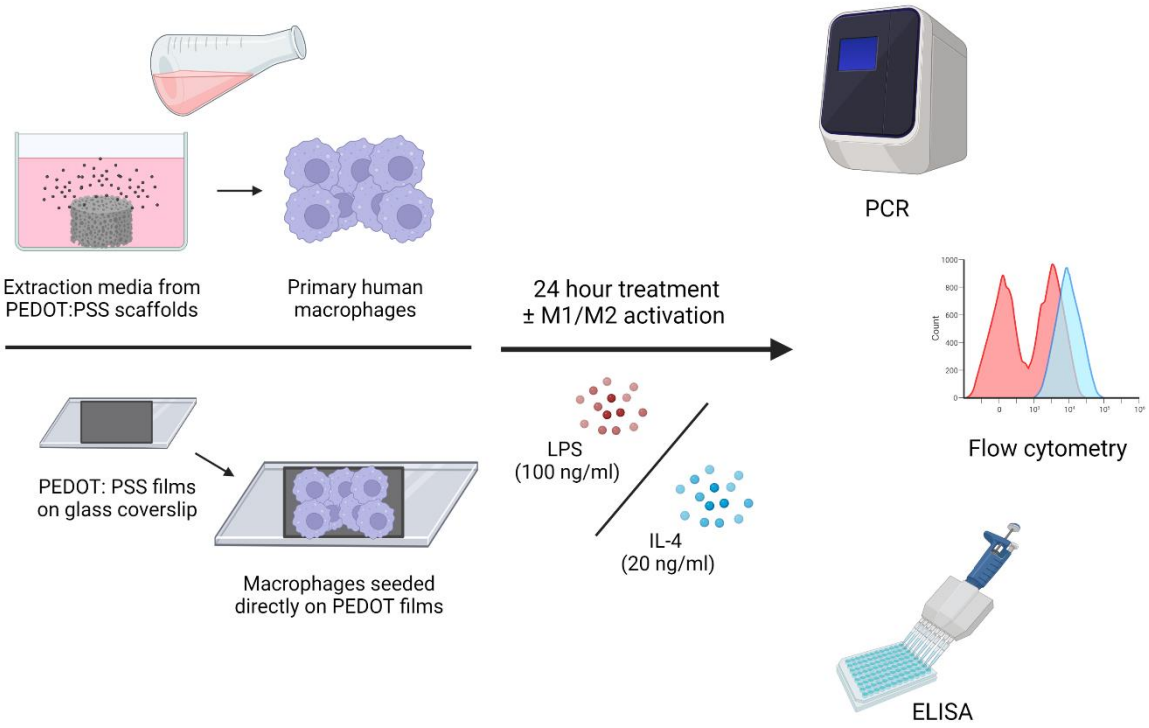

Figure 7-2 – Schematic summary of PEDOT: PSS experiments

Extraction media from PEDOT: PSS scaffolds (either cross-linked with PEGDE or GOPS) were incubated for 48 hours in supplemented RPMI media for 48 hours. Primary human macrophages (1 x 10^6 cells/ml) were treated with PEDOT extraction media, or else directly seeded onto 2D films of PEDOT: PSS for 24 hours. Cells were either treated with PEDOT alone, or else in the presence of either LPS or IL-4 which drive M1 or M2 polarisation respectively. After 24 hours, macrophage response was characterised using real-time PCR, flow cytometry, and ELISA.

7.4 Results

7.4.1 Extraction media from 3D scaffolds of PEDOT: PSS (PEGDE) and PEDOT: PSS (GOPS) is endotoxin-free.

To begin characterising macrophage response to PEDOT: PSS, macrophage viability was first assessed in response to PEDOT: PSS extraction media, assessing two different cross-linkers, GOPS and PEGDE. Cross-linking of PEDOT: PSS is a necessary step to prevent dissolution of the material in aqueous solutions, however, there is existing evidence that implementation of certain cross-linkers, for example, GOPS impedes the conductivity of the material, with the conductivity of PEDOT: PSS (GOPS) shown to range from 0.02-0.1 S/cm [347]. Due to this, there are current efforts to identify alternative cross-linkers for PEDOT: PSS. PEGDE shows potential as one such alternative, previously demonstrating the capacity to successfully cross-link with PEDOT: PSS, and even enhance conductivity of the material [346]. To determine the biocompatibility of PEDOT: PSS, crosslinked with either GOPS or PEGDE, with macrophage culture, PEDOT extraction media was prepared. PEDOT: PSS scaffolds, cross-linked with GOPS or PEGDE were prepared through a lyophilisation process, sterilised, and submerged in complete RPMI media at 37 °C for 48 hour. Complete media incubated at 37 °C for 48 hours without PEDOT scaffolds was implemented as an additional control, termed “Aged media”. This was to ensure any cell response observed was due to the release of material by-products and not from supplement degradation in the media. Before assessing macrophage response to the extraction media, it was first necessary to ensure the prepared media was free of endotoxins/LPS using the HEK-Blue™ TLR4 assay system. HEK-Blue™ TLR4 cells were stimulated with either LPS (0.1-100 ng/ml; positive control), aged media, or extraction media from PEDOT scaffolds (GOPS or PEGDE cross-linked) for 24 hours. SEAP expression was then examined by incubating cell supernatants with HEK-blue™ detection media for 15 minutes and absorbance was monitored at 650 nm. Results indicate that PEDOT extraction media as well as aged media were endotoxin free (Figure 7.3).

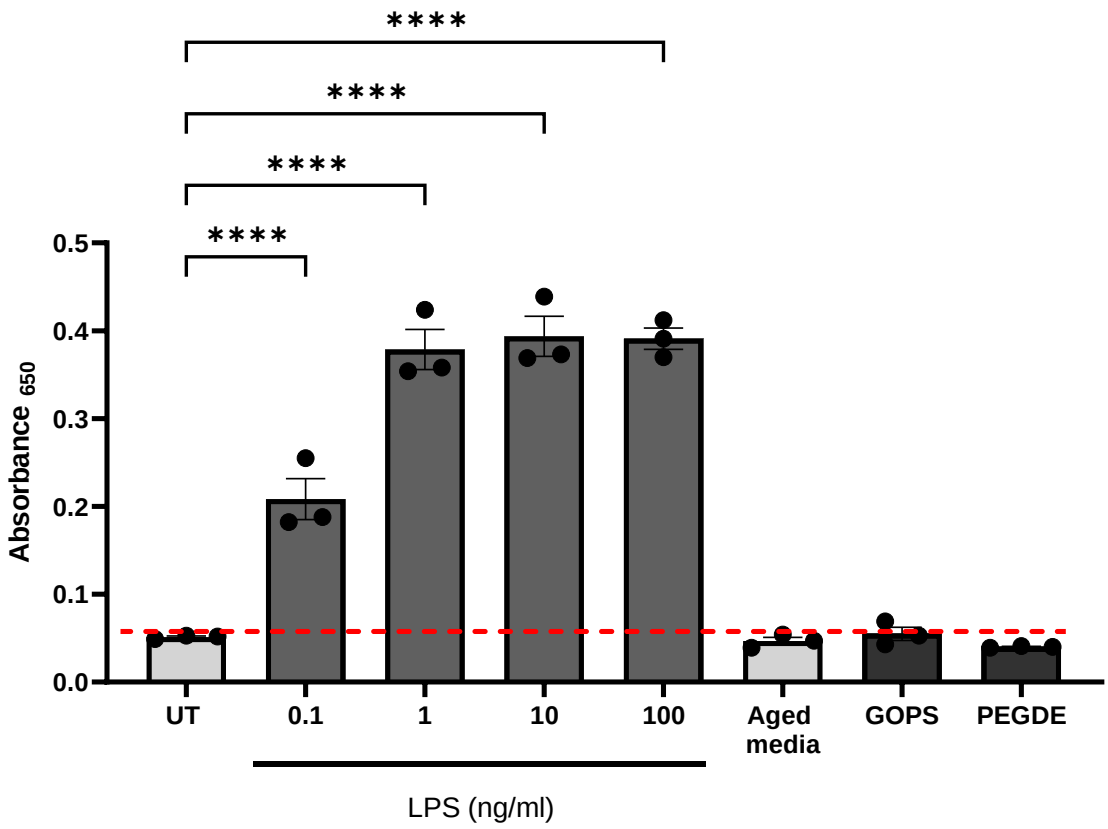

Figure 7-3 – Extraction media from PEDOT: PSS scaffolds are free of endotoxin contaminants.

HEK-blue™ cells (5x 10^5 cells/ml) were left either untreated, stimulated with LPS (0.1-100 ng/ml) (as a positive control) or treated with aged media, or extraction media from PEDOT (GOPS) and PEDOT (PEGDE) scaffolds for 24 hours. The expression of SEAP was measured by absorbance at 650 nm. Data is represented as mean ± SEM and is representative of two independent experiments. Data was analysed using One Way ANOVA with Dunnett's post-test. ****p ≤0.0001

7.4.2 Extraction media from PEDOT: PSS (PEGDE) but not PEDOT: PSS (GOPS) significantly reduces viability of primary human macrophages.

Having ensured the prepared media was endotoxin-free, PEDOT extraction media from both PEDOT: PSS (PEGDE) and PEDOT: PSS (GOPS) scaffolds were next incubated with primary human macrophages for 24 hours. As previously, aged media was implemented as an additional control. Cells were stained for viability using FixVia eFluor™ 506 and analysed by flow cytometry. Flow cytometry analysis revealed that neither aged media, nor PEDOT: PSS (GOPS) extraction media affected macrophage viability. However, a significant decrease of 56.1 % (± 28.93) in viability was observed in response to PEDOT: PSS (PEGDE) extraction media, relative to untreated cells (Figure 7.4). These results suggest that PEGDE is cytotoxic to primary human macrophages, deeming the cross-linker unsuitable for further cell culture experiments. As GOPS showed no such effect on macrophages, further experiments with PEDOT: PSS were carried out exclusively with PEDOT: PSS (GOPS).

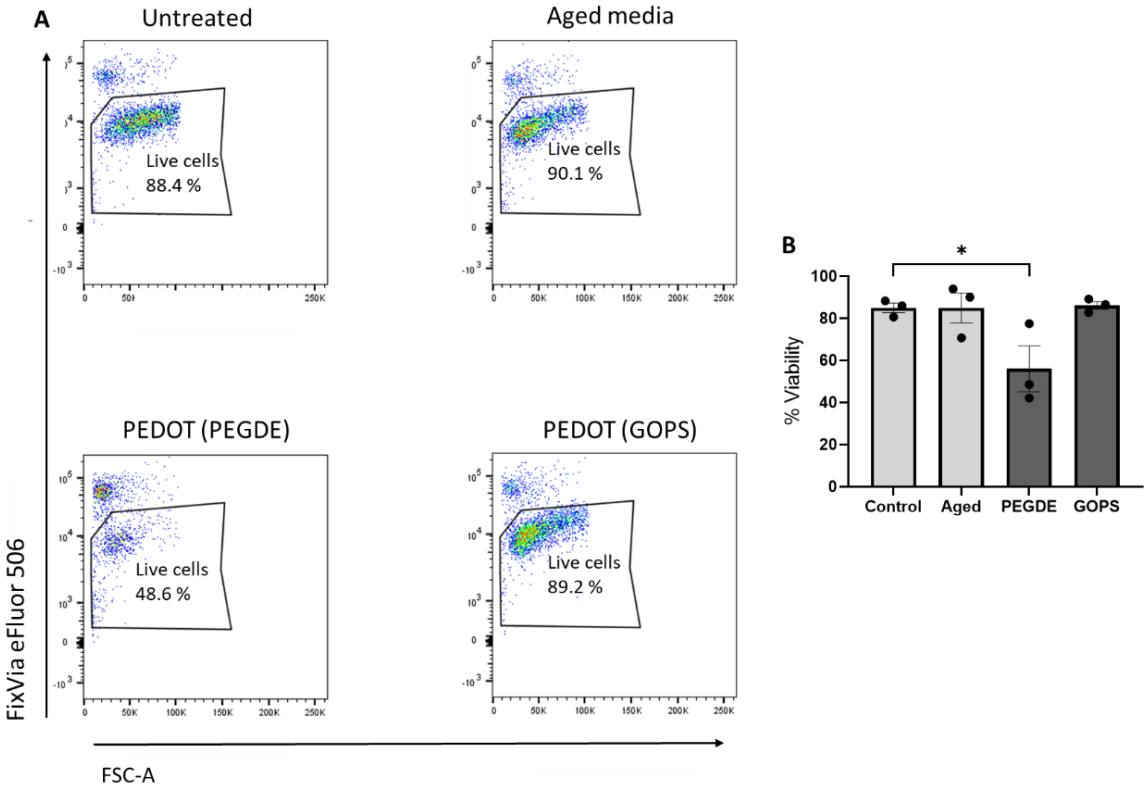

Figure 7-4 - Extraction media from PEDOT: PSS (PEGDE) is cytotoxic to primary human macrophages

Primary human macrophages (1 x 10^6 cells/ml) were left untreated, or treated with aged media, or conditioned media from PEDOT: PSS (GOPS) or PEDOT: PSS (PEGDE) scaffolds for 24 hours. Cells were then stained for viability with FixVia efluor™ 506 and analysed by flow cytometry. (**A**) Representative flow plots showing % live cells of untreated, aged media treated, and PEDOT media treated macrophages. (**B**) Bar graphs showing pooled data of % viability of untreated and treated macrophages (N = 3). Data is shown as mean ± SEM and analysed using One Way ANOVA with Tukey's post-test. *p≤0.05

7.4.3 PEDOT: PSS (GOPS) alone does not induce expression of M1/M2 associated genes in primary human macrophages

Having established that PEDOT: PSS (GOPS) extraction media exhibited no effects on macrophage viability, the direct response of macrophages to GOPS crosslinked PEDOT: PSS films was next assessed. Primary human macrophages were seeded on 2D films of PEDOT: PSS (GOPS) for a period of 24 hours. Macrophages were also seeded on to standard tissue culture plastic (TCP) as a control. mRNA levels of M1 associated genes *CXCL9, CXCL10,* and M2-associated genes *MRC1* and *CCL13* were assessed through real-time PCR relative to untreated control cells (Figure 7.5). No significant difference in expression of the M1-associated gene *CXCL10*, or M2-associated genes *MRC1* and *CCL13* was detected in response to PEDOT: PSS. However, a significant decrease in *CXCL9* expression (0.94 fold change ± 0.48) was observed in macrophages seeded on PEDOT: PSS. This response suggested a potential immuno-modulatory effect from PEDOT: PSS (GOPS) on primary human macrophages and warranted further investigation.

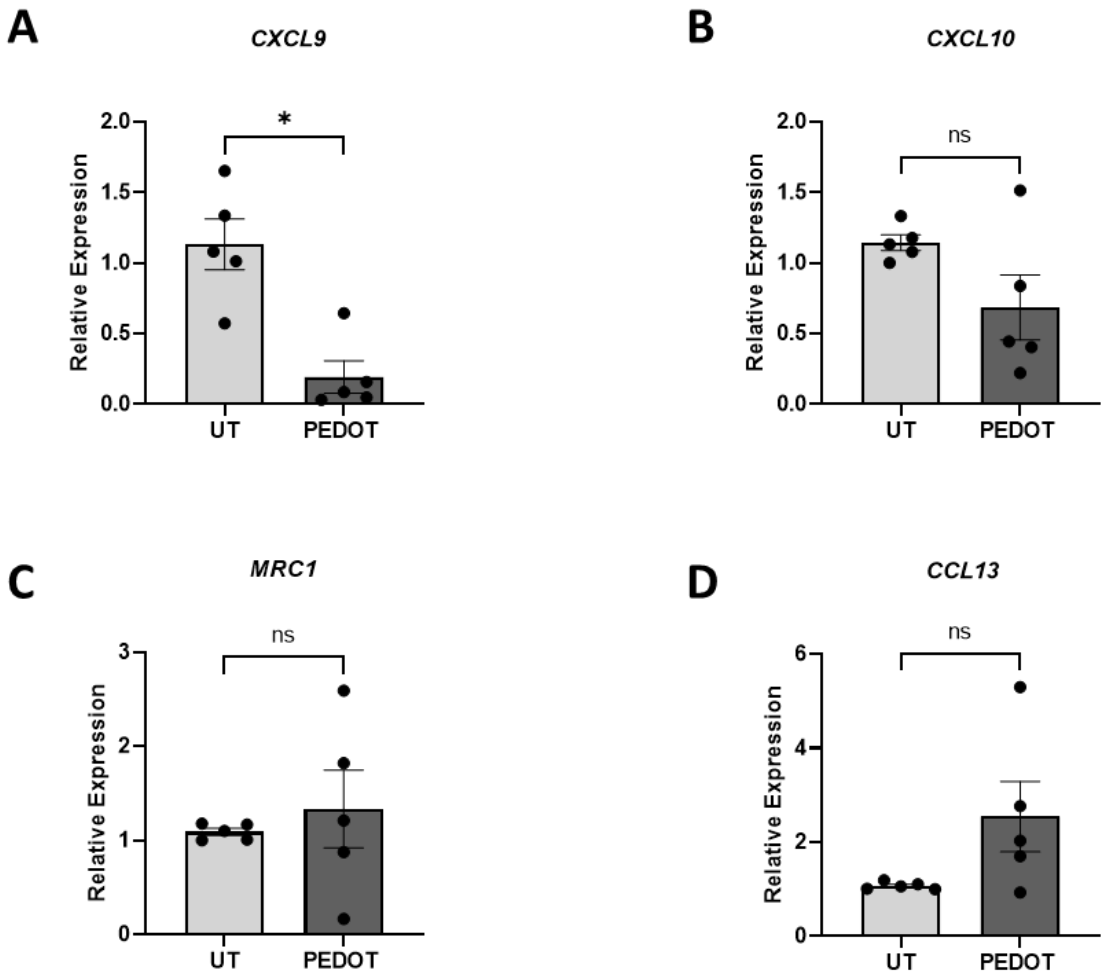

Figure 7-5 - PEDOT: PSS (GOPS) does not drive expression of M1/M2 associated genes

Primary human macrophages (1 x 10^6 cells/ml) were seeded onto PEDOT: PSS (GOPS) films or standard tissue culture plastic (TCP). (**A-D**) mRNA expression of M1 associated genes *CXCL9, CXCL10* and M2 associated genes *MRC1, CCL13* was assessed by real-time PCR (N =5, n = 3). All data is shown as mean ± SEM and analysed using paired t-test. *p≤0.05

7.4.4 PEDOT: PSS (GOPS) alone does not drive production of pro-inflammatory or anti-inflammatory cytokines.

Following from the assessment of M1/M2 gene expression in response to PEDOT: PSS (GOPS), the next aim was to examine cytokine production. Primary human macrophages were seeded onto 2D films of PEDOT: PSS (GOPS) for 24 hours. Cells seeded onto TCP and LPS-stimulated were used as untreated and positive controls. Analysis of cell supernatants via ELISA revealed no significant changes in levels of pro-inflammatory cytokines TNF and IL-6 when compared to macrophages seeded on TCP (Figure 7.6 A, B). Additionally, no significant change was observed in levels of the anti-inflammatory cytokine IL-10 (Figure 7.6 D). A slight increase in IL-8 production was observed from cells seeded onto PEDOT: PSS (5050 pg/ml ± 2903) (Figure 7.6 C), however these results were not significant compared to untreated cells on tissue culture plastic. These results indicate that PEDOT: PSS alone does not drive production of either pro- or anti-inflammatory cytokines.

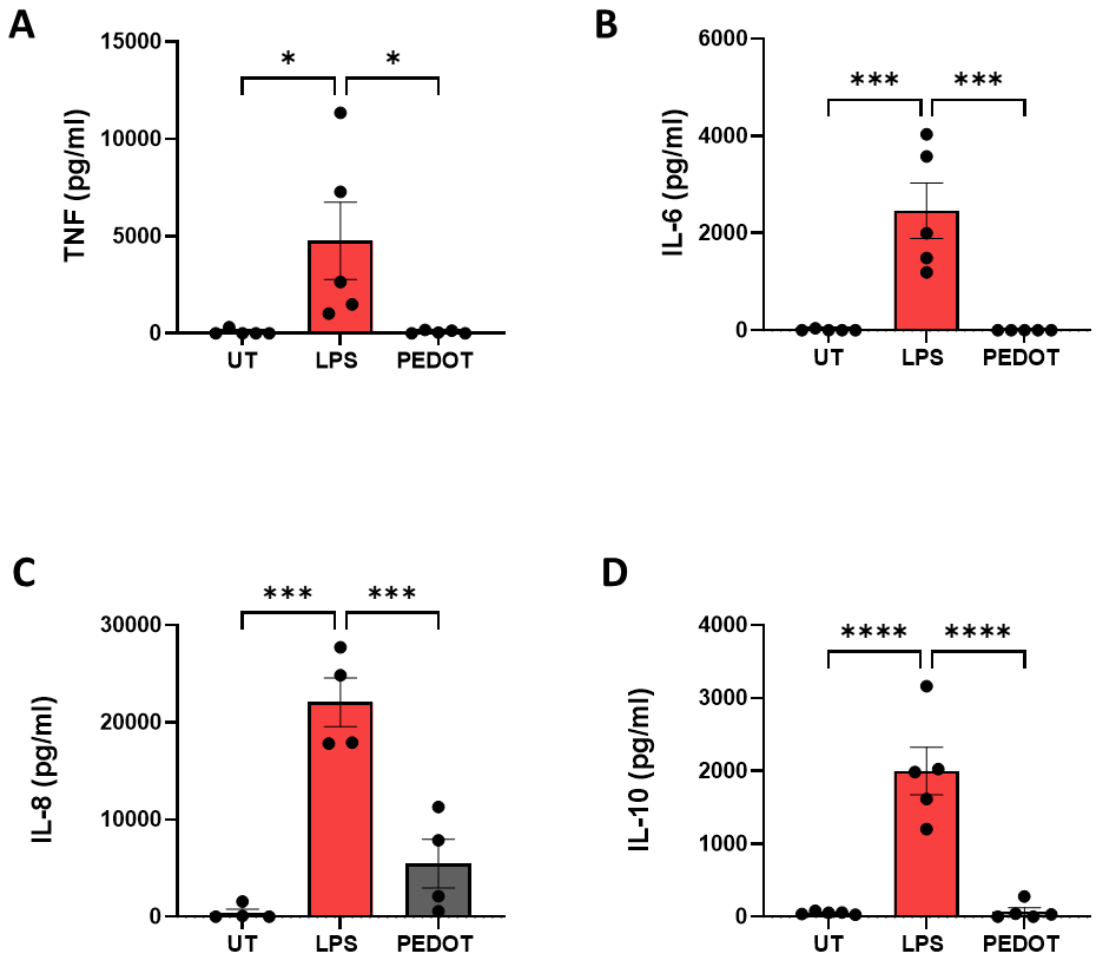

Figure 7-6 - PEDOT: PSS (GOPS) does not drive production of pro/anti-inflammatory cytokines.

Primary human macrophages (1 x 10^6 cells/ml) were seeded onto PEDOT: PSS (GOPS) films or standard tissue culture plastic (TCP). LPS stimulation (100 ng/ml) of macrophages on TCP for 24 hours was used as a positive control. (**A-D**) Levels of TNF, IL-6, IL-8 and IL-10 were assessed in cell supernatants by ELISA (N =5, n = 3). All data is shown as mean ± SEM and analysed using One Way ANOVA with Tukey's post-test. *p≤0.05, *** ≤0.001, ****p ≤0.0001

7.4.5 Primary human macrophages seeded on PEDOT: PSS (GOPS) films exhibit a significant response to TLR4 stimulation

Having established that PEDOT: PSS itself had no major impact on macrophage gene expression or cytokine production, it was next necessary to ensure that the absence of upregulation of M1 associated genes and pro-inflammatory cytokines observed above was not a result of PEDOT: PSS hindering cell response. Primary human macrophages were seeded onto 2D films of PEDOT: PSS (GOPS), and further stimulated with LPS (100 ng/ml) or IL-4 (20 ng/ml) for 24 hours. Supernatants were analysed by ELISA to assess cytokine production. Significant levels of TNF, IL-6, IL-8, and IL-10 were observed in response to LPS stimulation when compared to untreated macrophages on TCP and PEDOT: PSS alone (Figure 7.7). Once again, an increase in IL-8 production was observed in response to PEDOT: PSS alone, however again this was not significant when compared to untreated cells on TCP (Figure 7.7 C). Overall, these results show that primary human macrophages are still capable of exhibiting a significant response to TLR4 stimulant LPS when in direct contact with PEDOT: PSS (GOPS).

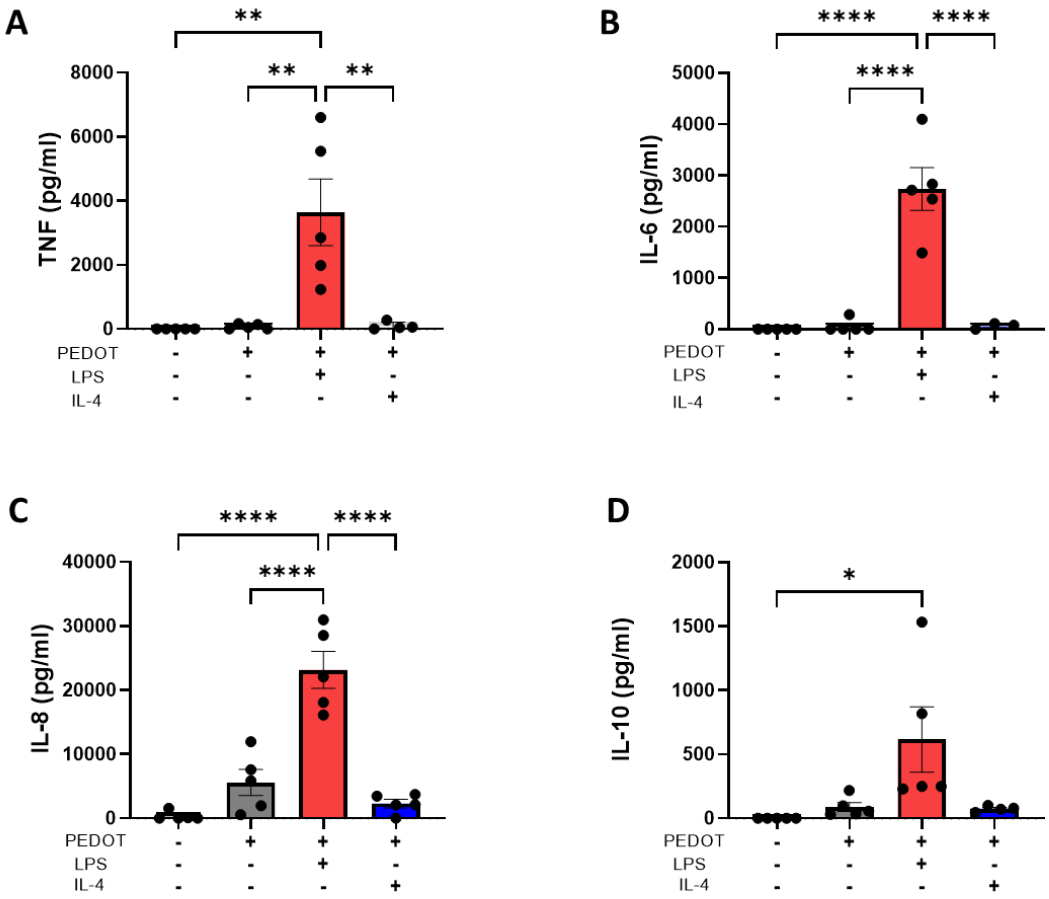

Figure 7-7 - Primary human macrophages seeded on PEDOT: PSS (GOPS) films exhibit a significant response to TLR4 stimulation

Primary human macrophages (1 x 10^6 cells/ml) were seeded onto PEDOT: PSS (GOPS) films or standard tissue culture plastic (TCP) and treated with LPS (100 ng/ml) or IL-4 (20 ng/ml). (A-D) Levels of TNF, IL-6, IL-8 and IL-10 were assessed in cell supernatants by ELISA (N =5, n = 3). All data is shown as mean ± SEM and analysed using One Way ANOVA with Tukey's post-test. *p≤0.05, **p≤0.01, ****p ≤0.0001

7.4.6 Primary human macrophages seeded on PEDOT: PSS (GOPS) films are capable of M1/M2 polarisation in response to either LPS or IL-4.

Having observed that PEDOT: PSS does not impact production of cytokines in response to LPS treatment or IL-4, it was next of interest to examine expression of M1-associated, and M2-associated genes in LPS or IL-4 treated macrophages seeded on PEDOT: PSS. Primary human macrophages were seeded on 2D films of PEDOT: PSS (GOPS) and treated with either LPS (100 ng/ml) or IL-4 (20 ng/ml) for 24 hours. mRNA levels of M1 associated genes *CXCL9* and *CXCL10*, and M2 associated genes *MRC1*, and *CCL13* were assessed through real time PCR. Results demonstrated a significant increase in expression of *CXCL9* (9.6 fold change ± 6.9) and *CXCL10* (11.7 fold change ± 10.53) in response to LPS compared to PEDOT: PSS alone (Figure 7.8 A-B). Additionally, increased expression was observed in levels of both *MRC1* (18.73 fold change ± 20.43) and *CCL13* (106.3 ± 80.18) in IL-4 treated macrophages compared to PEDOT: PSS alone (Figure 7.8 C-D). Collectively these results show that primary human macrophages are still capable of M1/M2 polarisation when in direct contact with PEDOT: PSS (GOPS).

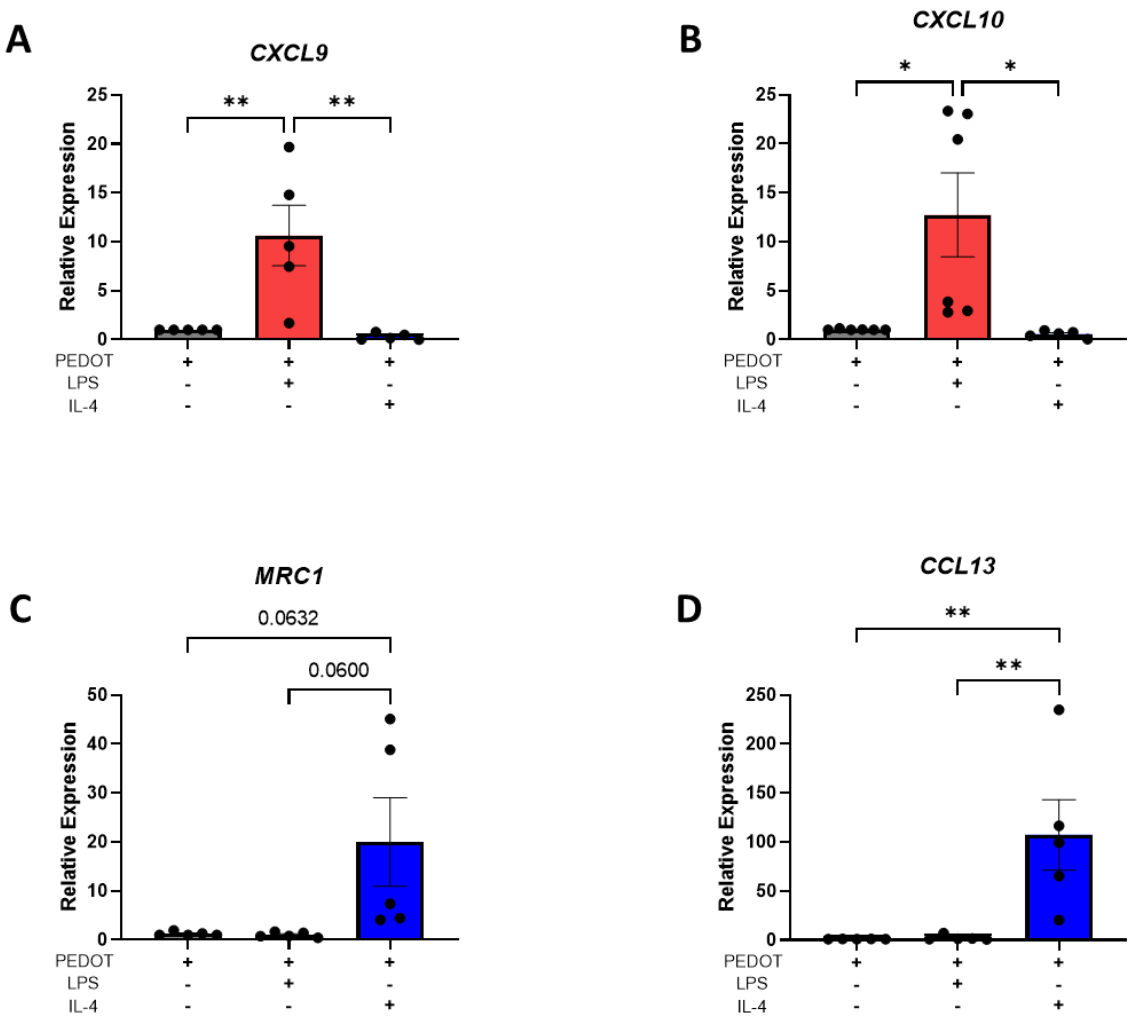

Figure 7-8 Primary human macrophages seeded on PEDOT: PSS (GOPS) films are capable of M1/M2 polarisation in response to either LPS or IL-4

Primary human macrophages (1 x 10^6 cells/ml) were seeded onto PEDOT: PSS (GOPS) films or standard tissue culture plastic (TCP) and treated with LPS (100 ng/ml) or IL-4 (20 ng/ml). (**A-D**) mRNA expression of M1 associated genes *CXCL9, CXCL10* and M2 associated genes *MRC1, CCL13* was assessed by real-time PCR (N =5, n = 3). All data is shown as mean ± SEM and analysed using One Way ANOVA with Tukey's post-test. *p≤0.05, **p≤0.01

7.4.7 PEDOT: PSS (GOPS) extraction media does not affect the capacity of primary human macrophages to process model antigen DQ-Ovalbumin.

Having affirmed that macrophage function and phenotype is not negatively impacted by 2D films of PEDOT: PSS, this study continued the indirect response of macrophages to 3D scaffolds of PEDOT: PSS using PEDOT extraction media. As mentioned in chapter 4, when macrophages undergo activation, they can exhibit either a reduced or increased capacity for antigen uptake and processing, depending on their phenotype. Antigen uptake of cells can therefore act as a functional read-out for macrophage activation and maturation. It was of interest to this study to investigate if potential by-products from PEDOT extraction media were capable reducing the capacity of primary human macrophages to uptake model antigen DQ-Ova, thus indicating if PEDOT: PSS could promote activation/maturation of the cells. Primary human macrophages were treated with PEDOT: PSS (GOPS) extraction media for 24 hours, followed by incubation with FITC-conjugated DQ-Ova (500 ng/mL). Uptake of this model antigen was assessed by flow cytometry. Treatment with PEDOT media caused no significant change to the capacity of macrophages to uptake DQ-ova, in comparison to untreated cells (Figure 7.9), indicating that PEDOT: PSS (GOPS) does not drive activation or maturation of primary human macrophages.

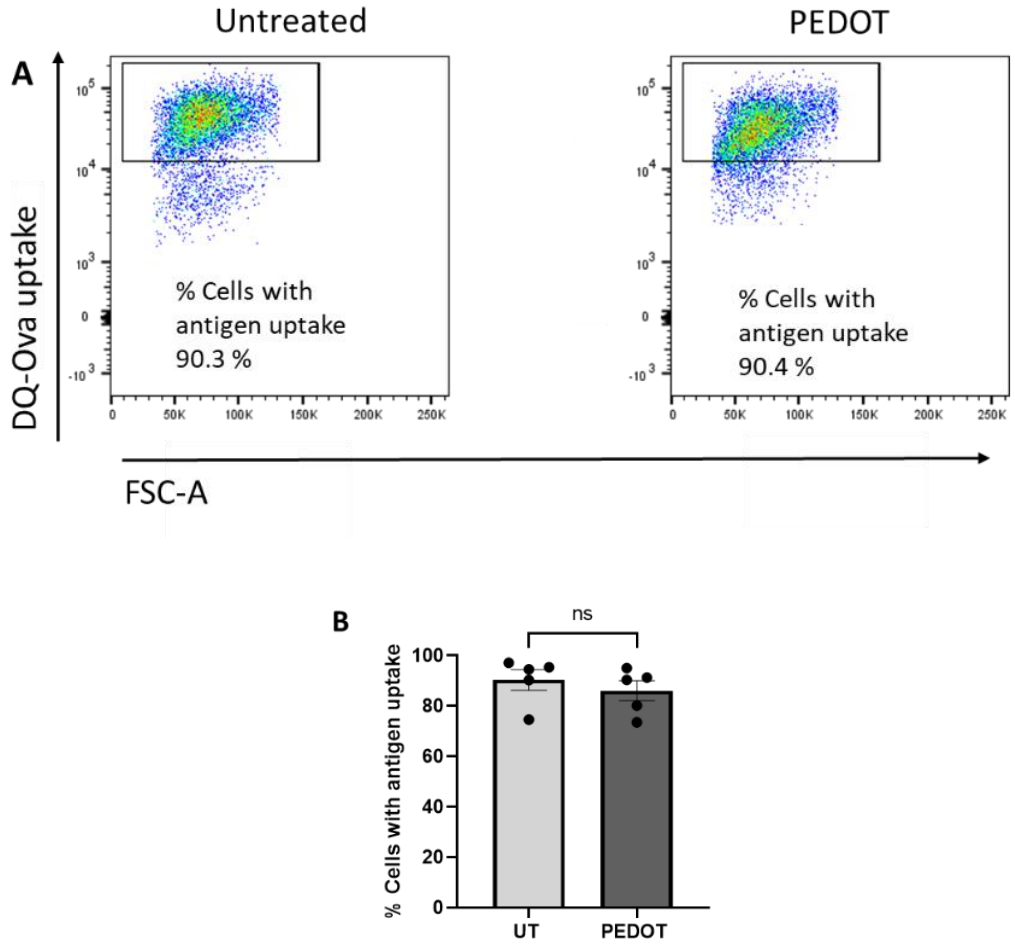

Figure 7-9 -Extraction media from PEDOT: PSS (GOPS) does not alter the capacity of primary human macrophages to uptake model antigen DQ-Ovalbumin

Primary human macrophages (1 x 10^6 cells/ml) were left untreated or treated with conditioned media from PEDOT: PSS (GOPS) scaffolds for 24 hours. Cells were then incubated with FITC-conjugated DQ-ova and analysed by flow cytometry. (**A**) Representative flow plots showing % phagocytosing cells of untreated and PEDOT media treated macrophages. (**B**) Bar graphs showing pooled data of % viability of untreated and treated macrophages (N = 5). Data is shown as mean ± SEM and analysed using paired t-test

7.4.8 PEDOT: PSS (GOPS) extraction media does not induce expression of M1/M2 associated genes in primary human macrophages

To further assess macrophage phenotype in response to PEDOT extraction media, mRNA levels of M1 associated genes *CXCL9, CXCL10*, and M2-associated genes *MRC1* and *CCL13* were assessed. Primary human macrophages were treated with PEDOT: PSS (GOPS) extraction media for 24 hours and mRNA expression was assessed by real time PCR. In contrast to treatment with the PEDOT films, treatment with PEDOT media resulted in no significant change in M1 gene expression (Figure 7.10 A-B), or the expression of M2 gene *CCL13* (Figure 7.10 D). A significant down-regulation in expression of *MRC1* was observed relative to untreated cells (0.93 fold change ± 0.23) (Figure 7.10 C). However, this down regulation was also observed in the aged media control group (0.64 fold change ± 0.36), suggesting this response was an artefact of the incubation period of the media, and not due to by-products from PEDOT media.

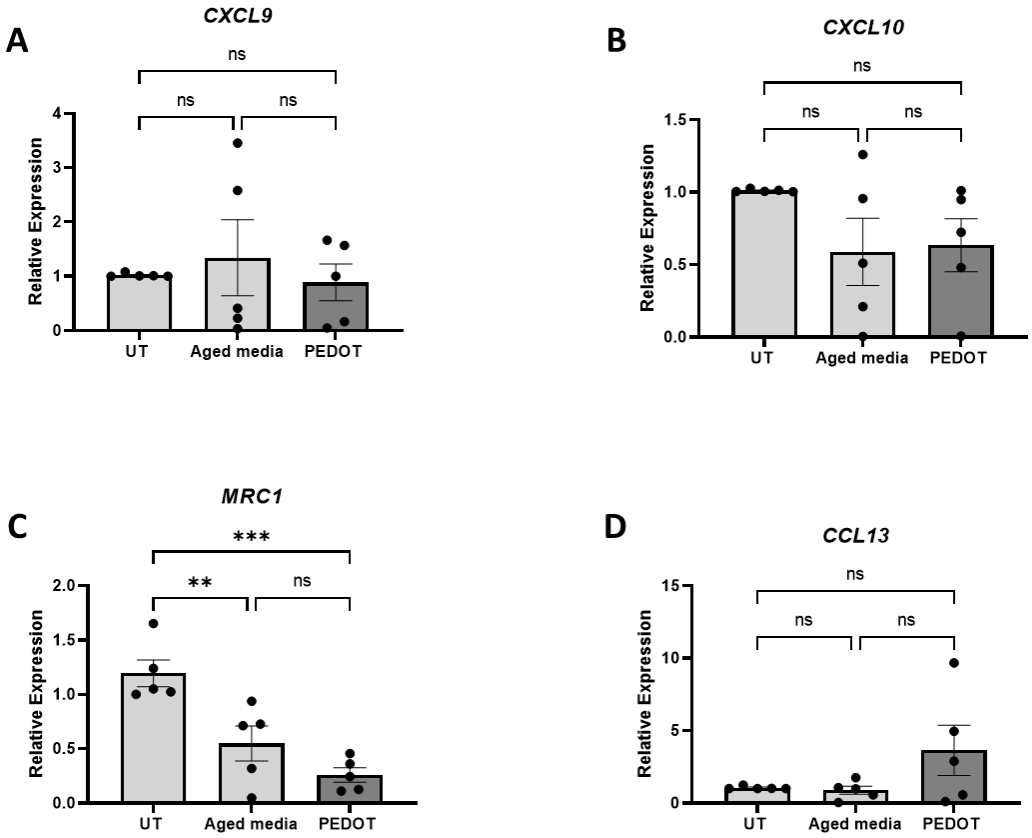

Figure 7-10 - Extraction media from PEDOT: PSS (GOPS) does not drive expression of M1/M2 genes in primary human macrophages

Primary human macrophages (1 x 10^6 cells/ml) were left untreated or treated with either aged media or conditioned media from PEDOT: PSS (GOPS) scaffolds for 24 hours. (**A-D**) mRNA expression of M1 associated genes CXCL9, CXCL10 and M2 associated genes MRC1, CCL13 was assessed by real-time PCR (N =5, n = 3). Data is shown as mean ± SEM and analysed using One Way ANOVA and Tukey's post-test. **p≤0.01, *** ≤0.001

7.4.9 PEDOT: PSS (GOPS) extraction media downregulates expression of surface marker CD86 in primary human macrophages.

To further characterise macrophage phenotype in the presence of PEDOT: PSS, expression of surface maturation markers was next assessed. Primary human macrophages were treated with PEDOT: PSS (GOPS) extraction media for 24 hours after which, expression of maturation markers CD80, CD86, CD163, and CD206 were assessed by flow cytometry. A significant decrease in expression of CD86 (33.69 % ± 9.72) was observed in macrophages treated with PEDOT (GOPS) extraction media, in comparison to both untreated cells, and those treated with aged media (decrease of 40.87 % ± 12.09 (Figure 7.11 B). No difference in expression of CD80, or CD163 was detected (Figure 7.11 A, C). A trend towards increased expression of CD206 was observed (23.97 % ± 28.22), with a significant difference detected between aged media-treated cells and PEDOT media (45.71 % ± 25.38) (Figure 7.11 D). However, this was not significant when compared to untreated cells. Overall, these results suggest that treatment with PEDOT: PSS extraction media does not drive maturation of primary human macrophages, in agreement with the above findings regarding antigen uptake. Furthermore, these results also mirror the response observed with 2D films of GOPS crosslinked PEDOT: PSS, where direct contact with 2D films of PEDOT resulted in selective downregulation of the M1-associated gene *CXCL9*, but no other distinct changes.

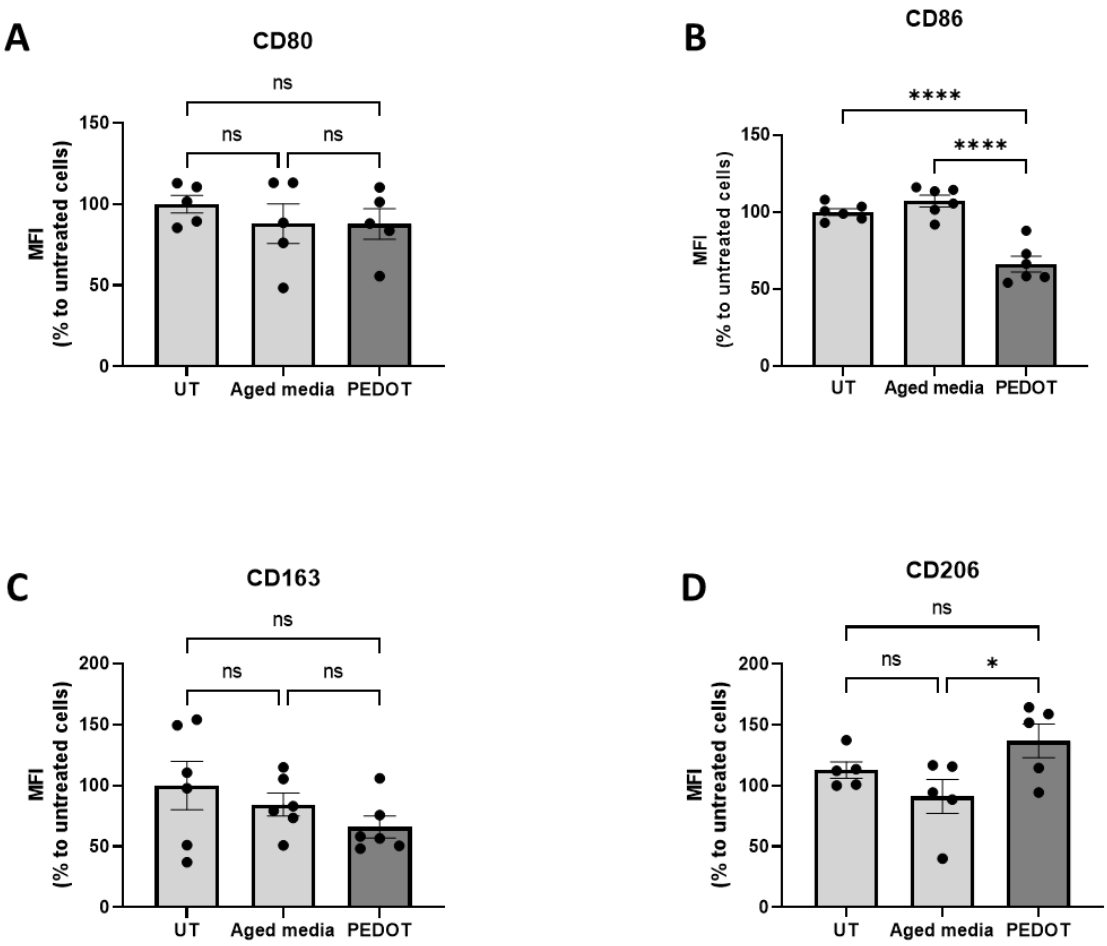

Figure 7-11 - Extraction media from PEDOT: PSS (GOPS) reduces expression of surface maturation marker CD86 in primary human macrophages

Primary human macrophages (1 x 10^6 cells/ml) were left untreated or treated with either aged media or conditioned media from PEDOT: PSS (GOPS) scaffolds for 24 hours. Cells were then stained for CD80, CD86, CD163, CD206 and analysed by flow cytometry. (**A-D**) Bar graphs showing pooled data of % MFI relative to untreated macrophages (N = 5). Data is shown as mean ± SEM and analysed using One Way ANOVA and Tukey's post-test. *p≤0.05, ****p ≤0.0001

7.4.10 PEDOT: PSS (GOPS) extraction media does not drive production of pro-inflammatory or anti-inflammatory cytokines in primary human macrophages

Having observed potential differences in macrophage response to 2D films of PEDOT: PSS and indirect contact with 3D scaffolds, through gene expression, potential changes in cytokine production were next investigated. Primary human macrophages were treated with PEDOT: PSS (GOPS) extraction media for 24 hours. Additionally, macrophages were left untreated or treated with LPS (100 ng/ ml) as negative and positive controls respectively. Levels of TNF, IL-6, IL-8, and IL-10 were assessed from cell supernatants by ELISA. Results demonstrate no significant changes in cytokine levels in PEDOT-treated macrophages compared to untreated cells (Figure 7.12). Interestingly, there appeared to be no basal production of IL-8, in contrast to that observed with 2D films of the material. In combination with the findings obtained with real-time PCR, these results suggest that macrophage response is dependent on direct contact with PEDOT: PSS.

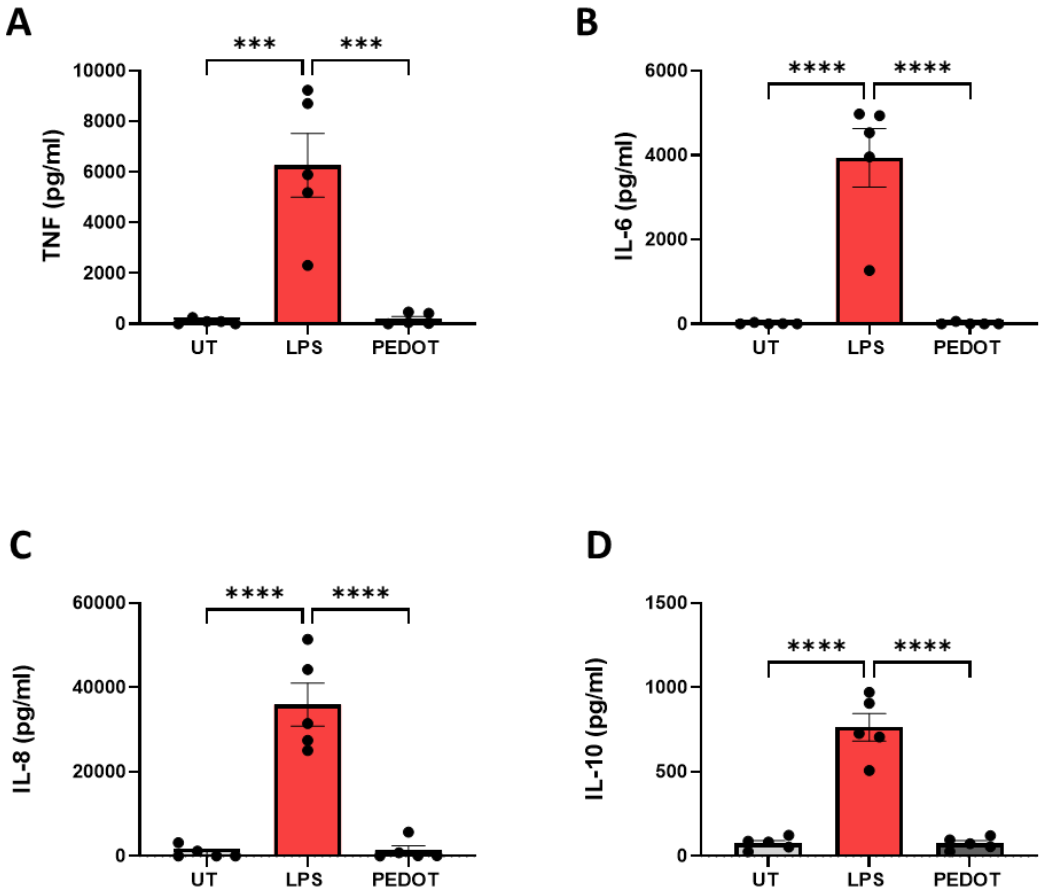

Figure 7-12 - Extraction media from PEDOT: PSS (GOPS) does not drive pro/anti-inflammatory cytokine production in primary human macrophages

Primary human macrophages (1 x 10^6 cells/ml) were left untreated or treated with LPS (100 ng/ml) or conditioned media from PEDOT: PSS (GOPS) scaffolds for 24 hours. (**A-D**) Levels of TNF, IL-6, IL-8 and IL-10 were assessed in cell supernatants by ELISA (N =5, n = 3). All data is shown as mean ± SEM and analysed using One Way ANOVA with Tukey's post-test. *** ≤0.001, ****p ≤0.0001

7.4.11 Primary human macrophages exhibit a significant response to TLR4 stimulation in the presence of PEDOT: PSS (GOPS) extraction media

Having established that PEDOT: PSS media itself had no significant impact on M1/M2 gene expression or cytokine production, it was next investigated if macrophages were still capable of responding to LPS or IL-4 stimulation, to ensure that PEDOT: PSS extraction media did not hinder cell response. Primary human macrophages were treated with PEDOT: PSS (GOPS) extraction media, in addition to LPS (100 ng/ml) or IL-4 (20 ng/ml) for 24 hours. Cell supernatants were assessed by ELISA to measure levels of cytokine in response to cell treatments. Significant levels of TNF, IL-6, IL-8 and IL-10 were observed in response to LPS stimulation in PEDOT-treated macrophages (Figure 7.13), demonstrating that primary human macrophages are capable of a significant response to TLR4 stimulant LPS, in the presence of PEDOT extraction media. These results agree with the previous findings using 2D films.

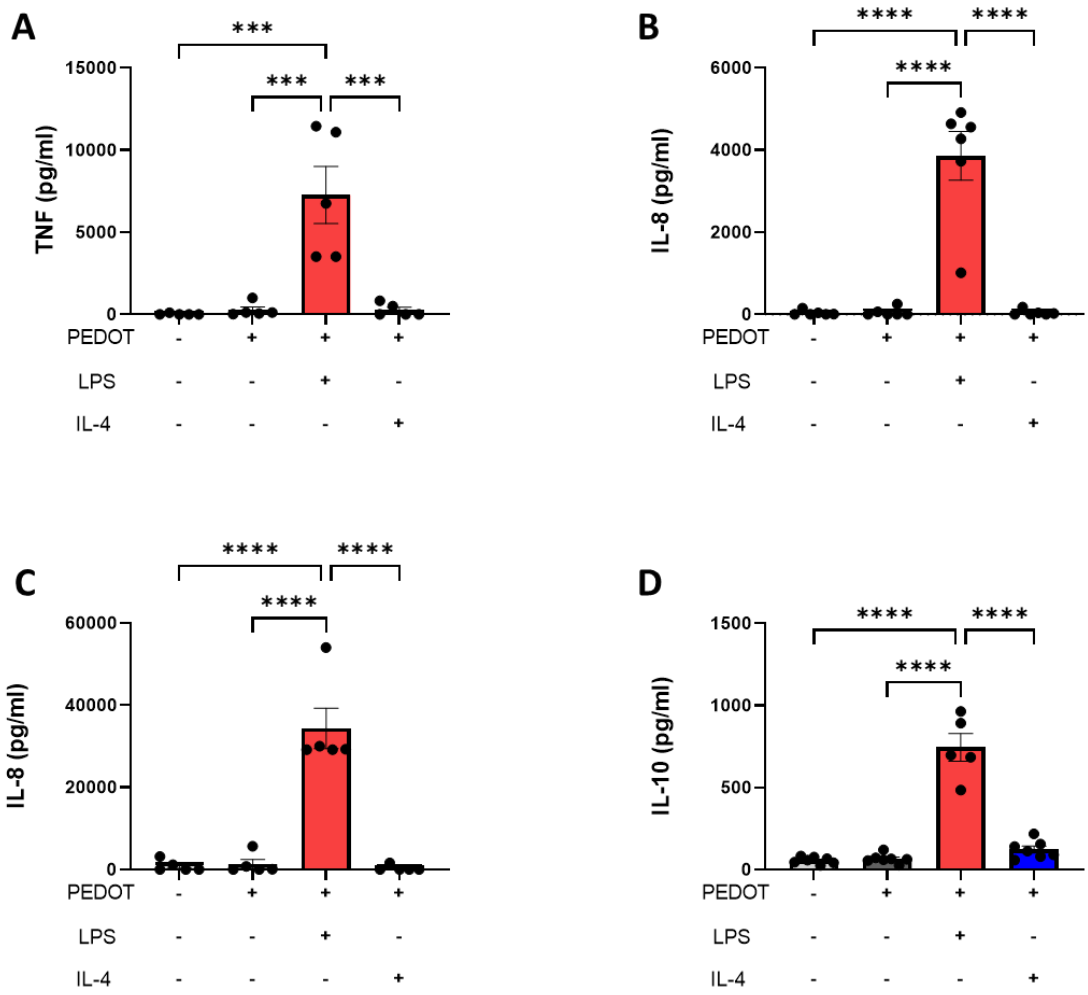

Figure 7-13 - Primary human macrophages exhibit a significant response to TLR4 stimulation in the presence of PEDOT: PSS (GOPS) extraction media

Primary human macrophages (1 x 10^6 cells/ml) were left untreated or treated with conditioned media from PEDOT: PSS (GOPS) scaffolds in the presence/absence of LPS (100 ng/ml) or IL-4 (20 ng/ml) for 24 hours. (**A-D**) Levels TNF, IL-6, IL-8, and IL-10 were assessed in cell supernatants by ELISA (N =5, n = 3). All data is shown as mean ± SEM and analysed using One Way ANOVA with Tukey's post-test. *** ≤0.001, ****p ≤0.0001

7.4.12 Primary human macrophages show significant response to cholesterol crystal stimulation in the presence of PEDOT: PSS (GOPS) extraction media.

Activation of macrophages occurs in both incidence of infection and sterile inflammation. As demonstrated in chapter 5 of this thesis, macrophages can be activated by endogenous DAMPs such as cholesterol crystals. It was of interest in this study to explore if PEDOT: PSS had any effect on macrophage response to DAMPs, as an alternative to LPS stimulation. Primary human macrophages were treated with PEDOT: PSS (GOPS) extraction media for 24 hours in addition to cholesterol crystals (500 µg/ml). Levels of IL-8 were assessed in cell supernatants by ELISA. A significant increase in IL-8 production was observed in response to cholesterol crystal stimulation, compared to PEDOT media alone, and untreated cells (Figure 7.14). This result suggests that PEDOT: PSS does not interfere with DAMP-mediated activation of macrophages, in addition to LPS activation.

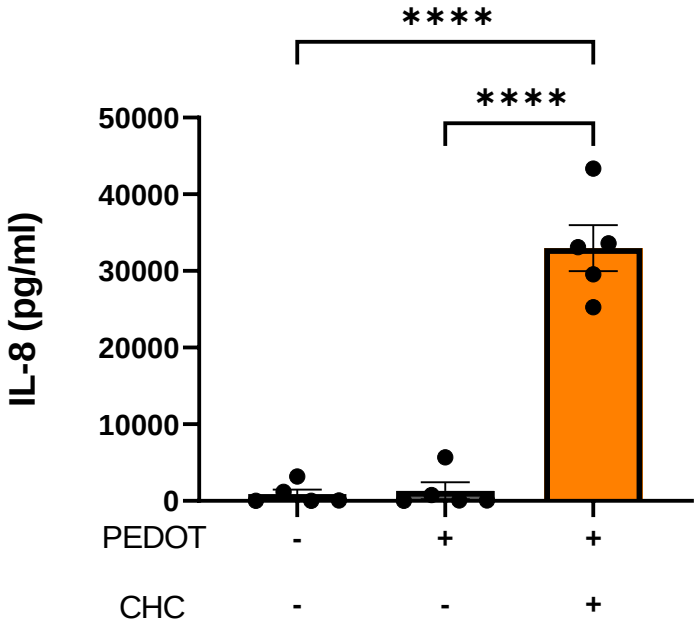

Figure 7-14 - Primary human macrophages show significant response to cholesterol crystal stimulation in the presence of PEDOT: PSS (GOPS) extraction media.

Primary human macrophages (1 x 10^6 cells/ml) were left untreated or treated with conditioned media from PEDOT: PSS (GOPS) scaffolds in the presence/absence of cholesterol crystals (CHC) (500 µg/ml) for 24 hours. Levels IL-8 were assessed in cell supernatants by ELISA (N =5, n = 3). All data is shown as mean ± SEM and analysed using One Way ANOVA with Tukey's post-test. ****p ≤0.0001

7.4.13 Primary human macrophages are capable of M1/M2 polarisation in response to LPS or IL-4 stimulation in the presence of PEDOT: PSS (GOPS) extraction media.

To further affirm that PEDOT media does not interfere with macrophage activation, expression of M1-associated and M2-associated genes were next assessed. Primary human macrophages were treated with PEDOT: PSS (GOPS) extraction media, in addition to LPS (100 ng/ml) or IL-4 (20 ng/ml) for 24 hours. mRNa levels of *CXCL9*, *CXCL10, MRC1*, and *CCL13* were assessed by real time PCR. Similar to the findings with PEDOT: PSS films, a significant increase in expression of *CXCL9* and *CXCL10* was observed in response to LPS treatment compared to PEDOT media alone (Figure 7.15 A-B). Additionally, a significant increase in *MRC1* and *CCL13* was observed in IL-4 treated macrophages compared to PEDOT media alone (Figure 7.15 C-D). Collectively these results show that primary human macrophages are capable of both M1 and M2 polarisation in the presence of PEDOT: PSS extraction media.

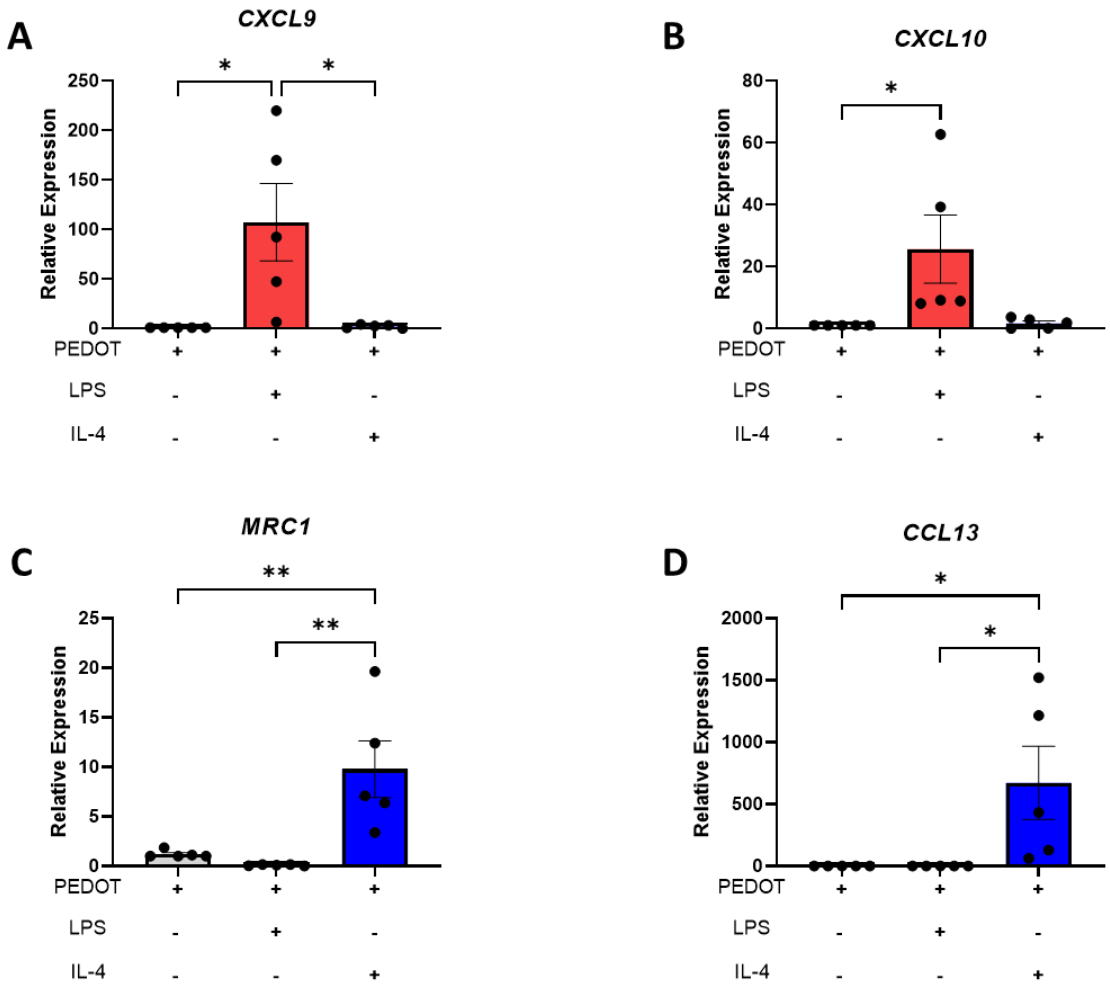

Figure 7-15 - Primary human macrophages are capable of M1/M2 polarisation in response to LPS or IL-4 stimulation in the presence of PEDOT: PSS (GOPS) extraction media.

Primary human macrophages (1 x 10^6 cells/ml) were left untreated or treated with conditioned media from PEDOT: PSS (GOPS) scaffolds in the presence/absence of LPS (100 ng/ml) or IL-4 (20 ng/ml) for 24 hours. (**A-D**) mRNA expression of M1 associated genes *CXCL9, CXCL10* and M2 associated genes *MRC1, CCL13* was assessed by real-time PCR (N =5, n = 3). All data is shown as mean ± SEM and analysed using One Way ANOVA with Tukey's post-test. *p≤0.05, **p≤0.01

7.4.14 Primary human macrophages show increased expression of maturation markers in response to LPS/IL-4 stimulation in the presence of PEDOT: PSS (GOPS) extraction media

As final confirmation that PEDOT: PSS does not interfere or impede macrophage activation, cell response to LPS and IL-4 was assessed at the protein level through flow cytometry. Primary human macrophages were treated with PEDOT: PSS extraction media for 24 hours in addition to treatment with LPS (100 ng/ml) or IL-4 (20 ng/ml). Expression of surface maturation markers CD80, CD86, CD163, and CD206 were assessed by flow cytometry. A significant increase in expression of M1-associated maturation markers CD80 and CD86 was observed in response to LPS treatment, relative to treatment with PEDOT media alone (Figure 7.16 A-B). A significant increase was also observed in expression if M2-associated maturation markers CD163 and CD206 in response to IL-4 treatments (Figure 7.16 C-D). These findings support the results obtained with real-time PCR, showing that indirect contact with 3D PEDOT: PSS (GOPS) scaffolds does not hinder macrophage polarisation in response to LPS or IL-4.

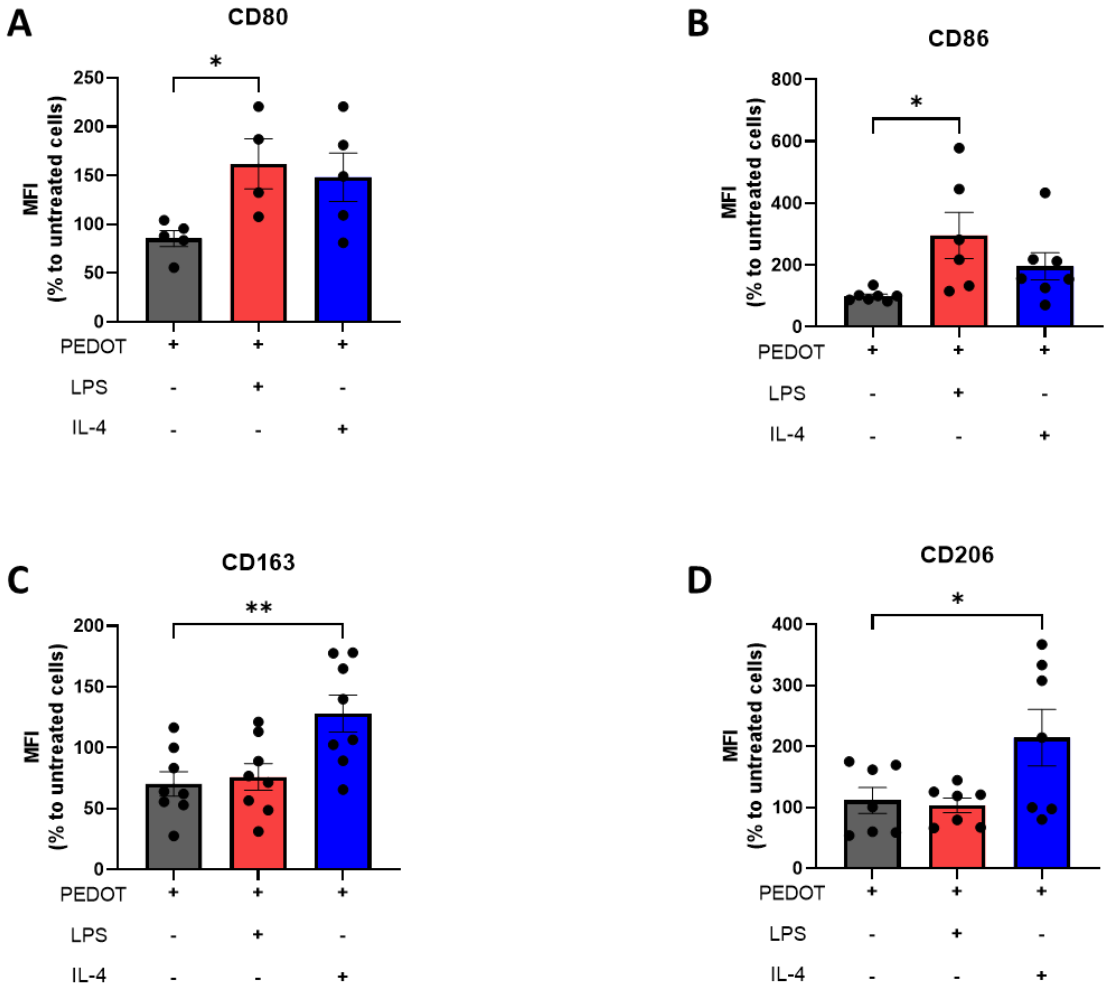

Figure 7-16 - Primary human macrophages show increased expression of maturation markers in response to LPS/IL-4 stimulation in the presence of PEDOT: PSS (GOPS) extraction media

Primary human macrophages (1 x 10^6 cells/ml) were left untreated or treated with conditioned media from PEDOT: PSS (GOPS) scaffolds in the presence/absence of LPS (100 ng/ml) or IL-4 (20 ng/ml) for 24 hours. Cells were stained for CD80, CD86, CD163, and CD206 and assessed by flow cytometry. (**A-D**) Bar graphs depict pooled data of % MFI relative to cells treated with PEDOT media alone (UT) (N = 5-8). All data is shown as mean ± SEM and analysed using One Way ANOVA with Tukey's post-test. *p≤0.05, **p≤0.01

7.5 Discussion

Electroconductive materials are often implemented in studies as a means of enhancing cell response to external delivery of electrical stimulation. In a study led by Ryan *et al*., it was shown that the incorporation of electroconductive biomaterials in electrical pacing of CMs not only facilitated cell response to stimulation but additionally resulted in an improved response compared to stimulation alone [359].The application of PEDOT: PSS has previously proven beneficial to the culture of numerous cell types including CMs [154, 181]. However, immune cell response to PEDOT: PSS has yet to be characterised. The results of this chapter demonstrate that PEDOT: PSS, cross-linked with GOPS, is compatible with culture of primary human macrophages, therefore supporting future application of this material in macrophage culture, potentially in the study of macrophage-CM interactions. Direct contact with PEDOT: PSS films was found to neither promote adverse inflammatory responses in primary human macrophages, nor hinder their stimulation with polarising factors LPS, or IL-4. These findings indicate that PEDOT: PSS is well tolerated by primary human macrophages and can act as an inert platform for the culture of macrophages, supporting both their pro-inflammatory and anti-inflammatory function. This is particularly important for future studies investigating the impact of pro/anti-inflammatory macrophages in disease models.

The effects of 3D scaffolds of PEDOT: PSS were investigated in this study using extraction media from PEDOT scaffolds. This is an established technique adopted from the ISO10993-5 standard test method as a measure of *in vitro* biocompatibility and cytotoxicity of medical devices [360]. Findings from this study demonstrated that the cross-linker PEGDE is cytotoxic to primary human macrophages, and therefore an unsuitable candidate for cross-linking PEDOT: PSS. Cytotoxicity of PEGDE has been previously reported by one other study, where Kim *et al.* discovered that subcutaneous injection of PEGDE in mice resulted in severe toxic effects [361]. Observed cytotoxic effects may also be due to release of PSS into extraction media, as unpublished findings from the Monaghan lab have observed increased degradation of PEDOT: PSS when cross-linked with PEGDE in comparison to GOPS. Published work by Spencer *et al.* investigating PEDOT: PSS in GelMa hydrogels has demonstrated cytotoxic effects with high concentrations of PEDOT, potentially due to excess PSS creating an anionic

environment unfavourable to cell culture [362]. Thus, it is likely that the reduction in cell viability arises as a combined result of direct interaction with PEGDE as well as increased degradation/release of PSS from the scaffold. Cross-linking PEDOT scaffolds with GOPS effectively prevents degradation/release of the PSS into cell media, which is reflected by the high percentage of viability retained by macrophages following 24-hour treatment with PEDOT: PSS (GOPS) extraction media. Moving forward, GOPS appears to be best suited for the generation of biocompatible PEDOT scaffolds, however further work with long-term biodegradation studies is required to confirm this.

Findings from experiments of extraction media also highlight a potential difference in macrophage response to PEDOT: PSS (GOPS), dependent on cell contact with the material. For example, a significant decrease in M1-associated gene *CXCL9* was observed in macrophages seeded directly onto PEDOT films, but not in response to PEDOT: PSS extraction media. Similarly, basal production of the chemokine IL-8 was observed in macrophages seeded directly on PEDOT: PSS films, but not in response to PEDOT conditioned media. While IL-8 production did not appear significant in comparison to cells seeded on TCP controls, the results do suggest that macrophage response to PEDOT: PSS relies on the direct interaction with the material itself and is worthy of further investigation. This in part, may be attributed to mechanical cues provided by the biomaterial, as it has been extensively reported in the literature that direct interactions between biomaterial surfaces and macrophages can greatly influence macrophage form and function [350].

In addition to the use of PEDOT: PSS as an *in vitro* cell platform, its application may also be useful in the generation of cardiac patches for therapy. Implantation of electroconductive patches can promote propagation in the heart following MI, as demonstrated with studies of conductive polymers polyanaline (PANI), polypyrole (PPy), and gold nanosheets [363-366]. Additionally, pre-seeding these patches with iPSC-CMs prior to implantation has been shown to significantly improve cardiac function in rat models of MI [366]. PEDOT: PSS represents a potential candidate for this application, as 3D forms of the material can be generated which recapitulate the anisotropic alignment of the native myocardium, thus supporting CM alignment and contraction [192, 346]. However, often one common property of biomaterials is the induction of an adverse

immune response which can interfere with normal tissue function or repair [367]. Characterisation of the immune response to any chosen biomaterial is therefore an important step in overcoming potential limitation of any implanted biomaterial.

The assessment of cell response to PEDOT extraction media provides useful insight into the potential effects the material may have when implanted into the host. Extraction media from PEDOT: PSS (GOPS) scaffolds showed to have no major effects on macrophage phenotype or function, as demonstrated by the lack of change in phagocytic capacity, cytokine production, and expression of M1/M2 associated markers. Similar to the results with PEDOT: PSS films, lack of response from macrophages was not due to inhibition of function, as treatment with LPS or IL-4 in the presence of the extraction media resulted in significant production of cytokines, as well increased expression of M1/M2 genes depending on the stimulant. Furthermore, macrophage response to DAMPs was also not hindered in the presence of PEDOT extraction media, as indicated by robust production of IL-8 in response to cholesterol crystal treatment. These results suggest that in an *in vivo* setting, PEDOT: PSS may not promote an adverse foreign body response, mediated by macrophages, nor interfere with either pro/anti-inflammatory macrophage function, which is crucial to cardiac tissue repair following incidence of injury such as MI [85].

For future consideration, to address the limitation of conductivity associated with GOPS cross-linking, additional post-treatments may be implemented, for example crystallisation of PEDOT: PSS (GOPS) with sulfuric acid. Previous work led by Solazzo *et al*. demonstrated that treatment of PEDOT: PSS (GOPS) scaffolds with 100% sulfuric acid causes a significant increase in conductivity of the material (1000-fold), while importantly, allowing the material to retain its stability and cytocompatibility [192]. This may provide an effective solution for the application of PEDOT: PSS (GOPS) as cardiac patches and is worthy of further investigation to examine the impact of crystallised PEDOT scaffolds on the immune response, in addition to non-crystallised scaffolds.

In summary, this study has determined that PEDOT: PSS is well tolerated by primary human macrophages, and thus potentially suitable as an *in vitro* platform for the culture of both primary human macrophages and iPSC-CMs. It was further demonstrated that extraction media from PEDOT: PSS (GOPS) scaffolds did not drive an adverse response in

primary human macrophages, highlighting the potential for PEDOT: PSS as an implantable material in the host. Importantly, neither direct contact with PEDOT: PSS films or indirect contact with PEDOT: PSS scaffolds was found to hinder macrophage function, as demonstrated through robust responses to polarising stimulants LPS and IL-4. These results indicate that PEDOT: PSS can act as compatible platform for cell culture and will not interfere with cell response as a result of macrophage-CM interactions, while also highlighting the potential for its use as an *in vivo* cardiac patch.

Chapter 8 : General discussion and future work

8.1 General Discussion

CVD and heart failure remain the leading cause of death worldwide. Incidence of CVD are on the rise globally, presenting a socio-economic burden to the healthcare system, thus the generation of novel therapies to combat disease is a must. The immune response, specifically that mediated by macrophages, has become increasingly acknowledged for its pathogenic role in CVD and represents a prime therapeutic target in patients. However, there are still substantial gaps in our knowledge regarding the interactions of the immune response at a cellular level. This is further complicated by the fact that current disease models either fail to incorporate a multicellular environment, or are carried out in animal models, which can largely lack translational capacity. The aim therefore of this thesis was to examine the role of macrophages in the cardiac environment at a simpler cellular level, with the intention of elucidating the functional role of macrophages in the heart, gaining insight to the mechanisms which advance CVD, and ultimately identifying potential therapeutic strategies for future treatments of heart failure.

Objective 1 of this thesis aimed to investigate the interactions between macrophages and cardiomyocytes, as a means of understanding how macrophages support cardiac function at a cellular level, and where this fails under inflammatory settings. The motivation for this study arose from established knowledge surrounding the limitations of animal models, and the desire to generate human *in vitro* models of cardiac disease. It was intended that the successful generation of a co-culture model of human macrophages and CMs would pave the way towards the application of macrophages in tissue engineered cardiac diseased models. The findings from this study highlighted an important requirement in the generation of multicellular models, in that all factors necessary for the maintenance of each cell type must be assessed for cross-compatibility. Indeed, it was observed that B-27™ supplement, necessary for the maintenance of iPSC-CMs, evoked an inflammatory response in primary human macrophages, driving significant production of pro-inflammatory cytokines and expression of gap junction protein connexin 43. To my knowledge there are no reports of this response in previously published models of macrophage-CM interactions, however it is acknowledged in neural models, where B-27™ is preferentially omitted

from co-culture studies with microglia [211]. The lack of discussion surrounding B-27™-induced responses is surprising, given that cardiomyocytes are receptive to cytokine signalling, with IL-6 and IL-8 previously proven detrimental to CM function [216, 217]. The use of an alternative supplement that does not elicit such a response in macrophages would be ideal to overcome this limitation, however, this does not appear to be readily available with current methods of iPSC-CM culture. Instead, further detailed characterisation of macrophage phenotype induced by B-27™ may be advantageous, to fully understand the impact of B-27™ on macrophage function. The findings of this study demonstrated that B-27™ does not drive maturation of macrophages, as indicated by a lack of increased expression of surface markers CD80 or CD86, as well as observed retention of phagocytic capacity compared to unstimulated cells. That is not to say however that other aspects of macrophage function are not impacted by the supplement, therefore broader analysis of the effects of B-27™, perhaps via transcriptome analysis would be beneficial. Elucidating the complete impact of B-27™ alone, compared to untreated macrophages, or those in culture with CMs will allow us to delineate the effects of B-27™, and identify specifically the impact of CMs and CM-derived factors on macrophage phenotype and function.

Despite the adverse response driven by B-27™, some novel insight was gained in this study regarding macrophage-CM interactions. Indeed, it was observed that in the presence of both CMs, or CM-derived secreted factors, a significant reduction of levels of IL-6 and IL-8 in B-27™-treated macrophages occurred. No reduction in levels of IL-10 were observed, suggesting that CMs may elicit an anti-inflammatory effect on primary human macrophages, targeting pro-inflammatory cytokine production. It would be ideal to investigate this effect under typical inflammatory settings, for example with the established TLR stimulant LPS, and not in B-27™-treated macrophages, to fully investigate the nature of this response. Characterisation of this potential anti-inflammatory effect would be limited in current experimental conditions, given that B-27™-induced cytokine production would mask any effects of LPS-macrophages. Nevertheless, there exists a potential immunomodulatory function of CMs worthy of further exploration. Tissue resident macrophages in the myocardium are reported to exhibit an anti-inflammatory “M2c” phenotype, as reported by studies of murine models

[220]. It is plausible that signals from local CMs contribute to this phenotype via secreted factors. Future work characterising these immunomodulatory factors in CM conditioned media may give way to a potential therapeutic strategy, utilising CM-derived factors as anti-inflammatory therapies.

Interestingly, these results also highlight a further potential benefit of stem cell therapy, one previously not considered in this therapeutic strategy. Transplantation of iPSC-CMs to the infarcted myocardium is currently under consideration as a novel therapy to address the limited regenerative capacity of the myocardium following injury. In a clinically relevant non-human primate model of ischemia/reperfusion injury, direct intramyocardial (IM) injection of iPSC-CMs improved cardiac contractile function at 4 and 12 weeks after transplantation. The grafted cells exhibited electrical coupling with host cardiomyocytes as assessed by use of the fluorescent calcium indicator G-CaMP7.09 [368]. Engineered cardiac muscle patches comprised of iPSC-derived CMs, endothelial cells (ECs) and smooth muscle cells (SMCs) have furthered this treatment strategy, with ECs and SMCs improving host vasculature around the implanted patch and iPSC-CMs overall improving cardiac function in porcine models of MI [369]. It is thought that the observed benefits of iPSC-CM transplant are due in large part to the paracrine effects of these cells following implantation [370]. Indeed, transplantation of iPSC-CMs to the injured myocardium in murine models is shown to significantly improve cardiac function through paracrine effects of secreted factors [370]. In my own findings I have observed a further possible advantage to the use of iPSC-CMs, in that their secreted factors additionally exert an anti-inflammatory effect on primary human macrophages. Dampening of the inflammatory macrophage response in MI has proven to greatly improve cardiac fate and function in murine models [371]. The findings from chapter 4 suggest that implanted iPSC-CMs could modulate this, while having no impact on anti-inflammatory IL-10 production, which is known to facilitate cardiac tissue repair and improve cardiac performance [372]. This effect is certainly worth exploring in future studies, with the hope of unveiling a novel immunomodulatory advantage to stem cell based therapies in the future.

The second objective of this thesis examined the role of macrophages in advancing CVD, specifically atherosclerosis. It is well established that macrophages play a prominent role

in atherosclerosis, advancing plaque formation and eventual destabilisation and rupture. Transcriptome analysis of mouse models reveals that non-foamy pro-inflammatory macrophages are key contributors to lesion inflammation and destabilisation, rather than macrophage-derived foam cells which subside in the plaque [74]. The findings from chapter 5 of this thesis outline that cholesterol crystals, found in early stages of atherosclerotic plaques contribute to this pro-inflammatory phenotype, via alterations to macrophage metabolism. This is the first study, to my knowledge, which demonstrates the ability of cholesterol crystals to promote metabolic reprogramming of macrophages and M1 polarisation. This has significant impact to the study of atherosclerosis, given previous observations of high rates of glycolysis in plaques associated with a high-risk of destabilisation and adverse outcome in patients [231]. The data presented in chapter 5 supports the idea of potentially targeting macrophage metabolism as a therapeutic strategy, given that inhibition of glycolysis in cholesterol crystal treated cells, either directly via treatment with glycolytic inhibitors 2-DG or 3PO, or else indirectly via inhibition of PKM2 with TEPP-46, successfully abrogated the M1 phenotype of cholesterol crystal-treated macrophages.

This is not the first study to suggest immunometabolism as a therapeutic target. Indeed, inhibition of glycolysis in murine models of atherosclerosis via deletion of either GLUT1 or glucose-6-phosphate dehydrogenase effectively reduces atherosclerotic lesions in mice. However, more refined targets are required, due to the necessary requirement of glycolysis in all cell types, including anti-inflammatory macrophages which aid plaque stabilisation [9]. Therefore, the identification of disease-specific metabolic regulators is ideal, with PKM2 presented in this study as a prime example. PKM2 was identified as a key regulator of glycolysis in cholesterol crystal-treated macrophages, and therefore a potential therapeutic target in atherosclerosis. Inhibition of PKM2 activity via treatment with TEPP-46 appeared to only impact cholesterol crystal-induced levels of glycolysis, as cell respiration in macrophages remained unaffected. These findings suggest the potential of PKM2 as a therapeutic target with potentially minimal off-target effects. Excitingly, the recently published work of Dodderpattar *et al*. further exemplifies this potential, as myeloid specific deletion of PKM2 in $LDLr^{-/-}$ mice resulted in a decrease of inflammation and reduced plaque progression [262]. Furthermore, deletion of PKM2

improved lipid uptake and efferocytosis in macrophages, suggesting that the benefits of PKM2 inhibition extend beyond limiting metabolic reprogramming, and overall improve healthy macrophage function in atherosclerotic plaques. Ultimately this tell us that immunometabolism is an attractive target for novel therapies of CVD, with the findings from chapter 5 supporting this.

The third objective of this thesis aimed to examine the impact of electrical stimulation on primary human macrophages and with this, gain potential understanding of the macrophage phenotype in the cardiac environment, where electrical signalling is a prominent feature. Findings from this study reveal electrical stimulation to have an immunomodulatory effect on primary human macrophages, promoting polarisation toward as anti-inflammatory pro-regenerative phenotype. This resembles the M2 phenotype of cardiac resident macrophages, which has previously been characterised in murine models [220]. Based on the findings from my own study, it is possible that biophysical cues native to the cardiac environment contribute towards this anti-inflammatory phenotype and are an important factor in maintaining homeostasis in the healthy myocardium. This raises the question of whether dysregulation of electrical signalling, for example in incidence of tachycardia or arrythmia, also impact macrophage phenotype in the myocardium. It would be of great interest to investigate this in future studies, thus opening the potential for anti-inflammatories as an effective treatment strategy for cardiac arrythmia. Already there is pre-existing evidence to suggest anti-arrythmic effects with anti-inflammatory steroids hydrocortisone and prednisone [373], however, much remains to be explored regarding the role of the immune response in these conditions.

Additionally, based on the observations of chapter 5, it would be of immense interest in future studies to compare the phenotype of electrically stimulated macrophages to resident cells of the myocardium, to fully elucidate the role of electrical signalling in shaping resident macrophage phenotype and function, in particular, with blood-derived macrophages which repopulate the heart following injury. If similarities are indeed identified between resident and ES-macrophages, it presents the opportunity to further develop electrical stimulation as an effective strategy for the generation of “cardiac macrophages” for future *in vitro* models of the heart. Studies of resident macrophages

to date have been limited to animal models, therefore novel strategies which can reproduce this cell population using human cells are greatly welcomed and certainly worth exploring.

Additionally, the potential added benefit of macrophage co-cultures with electrical pacing of CMs should also be examined. Already the benefits of electrical stimulation to the generation of functional cardiac models have been observed via electrical pacing of iPSC-CMs [156]. It is plausible that the presence of macrophages may improve CM maturation under these settings, compared to electrical stimulation alone, potentially through gap junction coupling between cells, particularly given that electrical stimulation was shown to promote expression of the gap junction protein Connexin 43 in macrophages. This would have significant impact in the field of cardiac tissue engineering, ultimately improving EHTs for either therapeutic implant, or as *in vitro* cardiac models to model disease.

The results of chapter 6 also have significance for broader applications of tissue engineering and regenerative medicine as it has become increasingly evident that regulation of the immune response is an attractive approach in regenerative medicine [374]. The use of external electrical stimulation has become an adopted strategy by many researchers to recapitulate the pro-reparative effects of endogenous electrical fields [269]. Now with the findings in chapter 6, the established benefits of external electrical stimulation can be extended to include immunomodulation of macrophages. A greater understanding of the underlying mechanisms responsible for this effect, for example calcium signalling or the PI3K-Akt pathway, will bring us closer to the possibility of being able to control macrophage function, to later translate into new treatments that promote regenerative responses. Furthermore, the impact of electrical stimulation on other immune cells could also be investigated, to expand the immunomodulatory potential of this stimulus, especially given the importance of immune cell cross-talk *in vivo*.

In recent years, electroconductive materials have received widespread attention due to their ability to not only provide the necessary support for cell culture but also facilitate additional electrical stimulation known to regulate specific cell or tissue functions [375]. Having observed that primary human macrophages were indeed responsive to electrical

stimulation, this provided rationale to investigate potential use of electroconductive materials in macrophage culture. Hence the fourth and final objective of this thesis was to characterise the response of primary human macrophages to electroconductive material PEDOT: PSS. Findings of this chapter demonstrated that PEDOT: PSS, cross-linked with GOPS, is well tolerated by primary human macrophages, proving to hinder neither M1 nor M2 polarisation of macrophages. This highlights the material as a suitable inert platform, supporting either pro-inflammatory or anti-inflammatory function of primary human macrophages. This is necessary for future studies assessing the influence of electrical stimulation on these activation states in the presence of PEDOT: PSS, and furthermore, the potential use of PEDOT: PSS as a co-culture platform for macrophage-CM interactions. An important requisite for the latter is that the material itself does not interfere with normal cell function. It has been previously established that PEDOT: PSS is compatible with CM culture, even enhancing function of these cells [154]. The results of chapter 7 have now demonstrated that PEDOT: PSS is additionally compatible with macrophage culture. This will allow for future incorporation of the material in the study of macrophage-CM interactions, either under settings of homeostasis or inflammation.

Additionally, this study provided useful insight to the potential interactions of PEDOT: PSS upon implantation inside a host, as it was demonstrated that extraction media from PEDOT: PSS (GOPS) scaffolds did not elicit any adverse inflammatory reaction in primary human macrophages. Given that macrophages are key mediators of the host's FBR to implanted materials, lack of response to PEDOT extraction media bodes well for the longevity of this material *in vivo*. To further validate these findings, long term degradation studies would be beneficial, in addition to the study of direct interactions of macrophages with PEDOT: PSS scaffolds.

8.2 Limitations and Future Work

- As previously discussed, the culture of macrophages with B-27™ supplement presented a limitation to the study of macrophage-CM interactions. For future co-culture studies involving these cell populations, an alternative media supplement should be considered, one that successfully supports the culture and function of both cell types without any major adverse response. Failing this,

detailed characterisation of macrophage phenotype induced by B-27™ may be a promising solution. Full understanding of the impact of B-27™ supplement on macrophage form and function will allow us to distinguish the effects of CM-derived factors from B-27™-mediated effects.

- Electrical stimulation was shown to induce a "pro-healing" phenotype in macrophages, including increased expression of pro-angiogenic factors. It would be of interest in future studies to validate the pro-angiogenic effects of electrically stimulated macrophages through co-culture experiments with endothelial cells. Moreover, to additionally investigate the impact of electrical stimulation directly on endothelial cells, given that there is pre-existing evidence showing that electrical field stimulation of 100-150 mV promotes migration and proliferation of HUVEC endothelial cells [170]. Additionally, given that electrically stimulated macrophages promoted migration of MSCs, it would be of interest to further explore the differentiation potential of these cells, investigating whether macrophage-derived factors skew MSCs towards specific lineage, e.g., osteogenesis, chondrogenesis or adipogenesis.
- Given the observed phenotype of electrical stimulated macrophages to resemble that of resident macrophages native to the heart, detailed characterisation of electrically stimulated macrophages and comparison with cardiac resident macrophages would be of great interest, for example via RNA-sequencing analysis. Future work investigating the potential for macrophages to electrically couple with iPSC-CMs is warranted, both in the absence or presence of external electrical stimulation is also warranted, to potentially give rise to a novel method for *in vitro* maturation of iPSC-CMs.
- Brief insight into the impact of macrophage metabolism was gained in the study of electrically stimulated macrophages. It would be of interest in future work to build on this data, characterising the metabolic profile of electrically stimulated macrophages through either Seahorse XF assays, or FLIM analysis, therefore unveiling a potential underlying mechanism of macrophage polarisation in response to electrical stimulation.

- PEDOT: PSS (GOPS) was shown in chapter 7 to be compatible with the culture of primary human macrophages both directly with films of PEDOT: PSS and indirectly with extraction media from PEDOT: PSS scaffolds. To advance this work, characterising macrophage response to direct contact with 3D PEDOT: PSS scaffolds would be advantageous. This work may include detailed investigation of various parameters of PEDOT: PSS scaffolds including porosity, anisotropy vs isotropy architecture, (both of which can be altered through varying freeze-drying protocols), as well as HCL-crystallisation to improve conductivity of 3D GOPS scaffolds.
- Previous published studies of electroconductive materials have demonstrated the ability of these materials to enhance effects of electrical stimulation in targeted cells [329, 359]. This was not investigated in my own study of PEDOT: PSS as implementation of PEDOT: PSS films into the bioreactor system requires further optimisation. Currently, the PEDOT: PSS films have the potential to move inside the cell plate of the bioreactor and as a result, the orientation of EFs experienced by cells can be altered. To prevent this in future studies, a rig may be developed to hold PEDOT: PSS coverslips in place. Additionally, with advances into characterisation of macrophage response to 3D PEDOT scaffolds, a mould may be required to hold PEDOT: PSS scaffolds in place in the bioreactor also.

8.3 Conclusion

In conclusion, the data presented herein has provided further insight to cellular mechanisms of human macrophages both in the cardiac environment and in CVD settings. Investigations of macrophage-CM interactions revealed a potential immunomodulatory function of CM-derived factors, while simultaneously highlighting technical limitations of current *in vitro* models worth exploring in the future. Characterisation of macrophage phenotype in response to cholesterol crystals revealed metabolic reprogramming to be a key feature of atherogenic macrophages, bringing to light immunometabolism as a potential therapeutic strategy in atherosclerosis. Finally, electrical stimulation, known to be a key feature of the cardiac environment, was shown to modulate macrophage function, skewing cells towards a favourable pro-regenerative phenotype, with PEDOT: PSS identified as a suitable platform for future studies of

electrical stimulation and cell interactions. Continued work in this field will provide new insights to the supportive role of macrophages in cardiac function, pave the way towards functional *in vitro* cardiac models, and ultimately identify novel therapeutics to target macrophage mediated responses in CVD and heart failure.

Chapter 9 : References

1. James, S., et al., *Life expectancy for community-based patients with heart failure from time of diagnosis.* Int J Cardiol, 2015. **178**: p. 268-74.
2. Isomi, M., T. Sadahiro, and M. Ieda, *Progress and Challenge of Cardiac Regeneration to Treat Heart Failure.* J Cardiol, 2019. **73**(2): p. 97-101.
3. Bacmeister, L., et al., *Inflammation and fibrosis in murine models of heart failure.* Basic Res Cardiol, 2019. **114**(3): p. 19.
4. Van Linthout, S. and C.J.C.H.F.R. Tschöpe, *Inflammation – Cause or Consequence of Heart Failure or Both?* Curr Heart Fail Rep, 2017. **14**(4): p. 251-265.
5. Martinez, F.O., et al., *Macrophage activation and polarization.* Front Biosci, 2008. **13**: p. 453-61.
6. Martinez, F.O. and S. Gordon, *The M1 and M2 paradigm of macrophage activation: time for reassessment.* F1000prime reports, 2014. **6**: p. 13-13.
7. Murray, P.J., et al., *Macrophage activation and polarization: nomenclature and experimental guidelines.* Immunity, 2014. **41**(1): p. 14-20.
8. Chavez-Sanchez, L., et al., *Innate immune system cells in atherosclerosis.* Arch Med Res, 2014. **45**(1): p. 1-14.
9. de Gaetano, M., et al., *M1- and M2-Type Macrophage Responses Are Predictive of Adverse Outcomes in Human Atherosclerosis.* Front immunol, 2016. **7**: p. 275-275.
10. Yurdagul, A., *Crosstalk Between Macrophages and Vascular Smooth Muscle Cells in Atherosclerotic Plaque Stability.* Arterioscler Thromb Vasc Biol, 2022. **42**(4): p. 372-380.
11. Frangogiannis, N.G., *Inflammation in cardiac injury, repair and regeneration.* Curr Opin Cardiol, 2015. **30**(3): p. 240-5.
12. Struthers, M. and A. Pasternak, *CCR2 antagonists.* Curr Top Med Chem, 2010. **10**(13): p. 1278-98.
13. Ridker, P.M., et al., *Relationship of C-reactive protein reduction to cardiovascular event reduction following treatment with canakinumab: a secondary analysis from the CANTOS randomised controlled trial.* Lancet, 2018. **391**(10118): p. 319-328.
14. Mann, D.L., et al., *Targeted anticytokine therapy in patients with chronic heart failure: results of the Randomized Etanercept Worldwide Evaluation (RENEWAL).* Circulation, 2004. **109**(13): p. 1594-602.
15. Padfield, G.J., et al., *Cardiovascular effects of tumour necrosis factor alpha antagonism in patients with acute myocardial infarction: a first in human study.* Heart, 2013. **99**(18): p. 1330-5.
16. Roubille, C., et al., *The effects of tumour necrosis factor inhibitors, methotrexate, non-steroidal anti-inflammatory drugs and corticosteroids on cardiovascular events in rheumatoid arthritis, psoriasis and psoriatic arthritis: a systematic review and meta-analysis.* Ann Rheum Dis, 2015. **74**(3): p. 480-9.
17. Leuschner, F., et al., *Therapeutic siRNA silencing in inflammatory monocytes in mice.* Nat Biotech, 2011. **29**: p. 1005.
18. Majmudar, M.D., et al., *Monocyte-directed RNAi targeting CCR2 improves infarct healing in atherosclerosis-prone mice.* Circulation, 2013. **127**(20): p. 2038-46.
19. Benjamin, E.J., et al., *Heart Disease and Stroke Statistics-2017 Update: A Report From the American Heart Association.* Circulation, 2017. **135**(10): p. e146-e603.
20. Savarese, G. and L.H. Lund, *Global Public Health Burden of Heart Failure.* Card Fail Rev, 2017. **3**(1): p. 7-11.
21. Perbellini, F., et al., *Heterocellularity and Cellular Cross-Talk in the Cardiovascular System.* Front Cardiovasc Med, 2018. **5**: p. 143.
22. Wang, B.X., W. Kit-Anan, and C.M.N. Terracciano, *Many Cells Make Life Work-Multicellularity in Stem Cell-Based Cardiac Disease Modelling.* Int J Mol Sci, 2018. **19**(11).
23. Fountoulaki, K., N. Dagres, and E.K. Iliodromitis, *Cellular Communications in the Heart.* Card Fail Rev, 2015. **1**(2): p. 64-68.

24. Howard, C.M. and T.A. Baudino, *Dynamic cell-cell and cell-ECM interactions in the heart.* J Mol Cell Cardiol, 2014. **70**: p. 19-26.
25. Olsson, A.K., et al., *VEGF receptor signalling - in control of vascular function.* Nat Rev Mol Cell Biol, 2006. **7**(5): p. 359-71.
26. Bryant, D., et al., *Cardiac failure in transgenic mice with myocardial expression of tumor necrosis factor-alpha.* Circulation, 1998. **97**(14): p. 1375-81.
27. Jiang, Y.R., et al., *miRNA-130a improves cardiac function by down-regulating TNF-alpha expression in a rat model of heart failure.* Eur Rev Med Pharmacol Sci, 2018. **22**(23): p. 8454-8461.
28. Ivey, M.J. and M.D. Tallquist, *Defining the Cardiac Fibroblast.* Circ J, 2016. **80**(11): p. 2269-2276.
29. Kanekar, S., et al., *Cardiac fibroblasts form and function.* Cardiovasc Pathol, 1998. **7**(3): p. 127-33.
30. Daskalopoulos, E.P., K.C. Hermans, and W.M. Blankesteijn, *Cardiac (myo)fibroblast: Novel strategies for its targeting following myocardial infarction.* Curr Pharm Des, 2014. **20**(12): p. 1987-2002.
31. Fan, D., et al., *Cardiac fibroblasts, fibrosis and extracellular matrix remodeling in heart disease.* Fibrogenesis Tissue Repair, 2012. **5**(1): p. 15.
32. Murray, P.J. and T.A. Wynn, *Protective and pathogenic functions of macrophage subsets.* Nat Rev Immunol, 2011. **11**(11): p. 723-37.
33. Yang, J., et al., *Monocyte and macrophage differentiation: circulation inflammatory monocyte as biomarker for inflammatory diseases.* Biomark Res, 2014. **2**(1): p. 1-1.
34. Mukhopadhyay, S., L. Peiser, and S. Gordon, *Activation of murine macrophages by Neisseria meningitidis and IFN-gamma in vitro: distinct roles of class A scavenger and Toll-like pattern recognition receptors in selective modulation of surface phenotype.* J Leukoc Biol, 2004. **76**(3): p. 577-84.
35. Fadok, V.A., et al., *Macrophages that have ingested apoptotic cells in vitro inhibit proinflammatory cytokine production through autocrine/paracrine mechanisms involving TGF-beta, PGE2, and PAF.* J Clin Investig, 1998. **101**(4): p. 890-898.
36. Ferrante, C.J., et al., *The adenosine-dependent angiogenic switch of macrophages to an M2-like phenotype is independent of interleukin-4 receptor alpha (IL-4Ralpha) signaling.* Inflammation, 2013. **36**(4): p. 921-31.
37. Martin, C.J., K.N. Peters, and S.M. Behar, *Macrophages clean up: efferocytosis and microbial control.* Curr Opin Microbiol, 2014. **17**: p. 17-23.
38. Galván-Peña, S. and L.A.J. O'Neill, *Metabolic reprograming in macrophage polarization.* Front Immunol, 2014. **5**: p. 420-420.
39. Liu, Y., et al., *Metabolic reprogramming in macrophage responses.* Biomarker Research, 2021. **9**(1): p. 1.
40. Koelwyn, G.J., et al., *Regulation of macrophage immunometabolism in atherosclerosis.* Nat Immunol, 2018. **19**(6): p. 526-537.
41. Warburg, O., *On the origin of cancer cells.* Science, 1956. **123**(3191): p. 309-14.
42. Van den Bossche, J., et al., *Mitochondrial Dysfunction Prevents Repolarization of Inflammatory Macrophages.* Cell Rep, 2016. **17**(3): p. 684-696.
43. Mahon, O.R., et al., *Osteoarthritis-associated basic calcium phosphate crystals alter immune cell metabolism and promote M1 macrophage polarization.* Osteoarthr Cartil, 2020. **28**(5): p. 603-612.
44. Papathanassiu, A.E., et al., *BCAT1 controls metabolic reprogramming in activated human macrophages and is associated with inflammatory diseases.* Nat Commun, 2017. **8**: p. 16040.
45. Qian, X., et al., *Regulation of fatty acid synthesis in immune cells.* Scand J Immunol, 2018. **88**(5): p. e12713.

46. Infantino, V., et al., *A key role of the mitochondrial citrate carrier (SLC25A1) in TNFα- and IFNγ-triggered inflammation.* Biochim Biophys Acta, 2014. **1839**(11): p. 1217-1225.
47. Infantino, V., et al., *ATP-citrate lyase is essential for macrophage inflammatory response.* Biochem Biophys Res Commun, 2013. **440**(1): p. 105-11.
48. Tannahill, G.M., et al., *Succinate is an inflammatory signal that induces IL-1β through HIF-1α.* Nature, 2013. **496**(7444): p. 238-42.
49. Koivunen, P., et al., *Inhibition of Hypoxia-inducible Factor (HIF) Hydroxylases by Citric Acid Cycle Intermediates: Possible Links Between Cell Metabolism, and Stabilisation of HIF.* J Biol Chem, 2007. **282**(7): p. 4524-4532.
50. Palsson-McDermott, E.M., et al., *Pyruvate Kinase M2 Regulates Hif-1alpha Activity and IL-1beta Induction and Is a Critical Determinant of the Warburg Effect in LPS-Activated Macrophages.* Cell Metab, 2015. **21**(2): p. 347.
51. Li, X., et al., *Lactate metabolism in human health and disease.* Signal Transduction and Targeted Therapy, 2022. **7**(1): p. 305.
52. Rabinowitz, J.D. and S. Enerbäck, *Lactate: the ugly duckling of energy metabolism.* Nature Metabolism, 2020. **2**(7): p. 566-571.
53. Zhang, D., et al., *Metabolic regulation of gene expression by histone lactylation.* Nature, 2019. **574**(7779): p. 575-580.
54. Russell, D.G., L. Huang, and B.C. VanderVen, *Immunometabolism at the interface between macrophages and pathogens.* Nat Rev Immunol, 2019. **19**(5): p. 291-304.
55. Jha, A.K., et al., *Network integration of parallel metabolic and transcriptional data reveals metabolic modules that regulate macrophage polarization.* Immunity, 2015. **42**(3): p. 419-30.
56. Genoula, M., et al., *Fatty acid oxidation of alternatively activated macrophages prevents foam cell formation, but Mycobacterium tuberculosis counteracts this process via HIF-1α activation.* PLoS Pathog, 2020. **16**(10): p. e1008929.
57. Houten, S.M. and R.J. Wanders, *A general introduction to the biochemistry of mitochondrial fatty acid β-oxidation.* J Inherit Metab Dis, 2010. **33**(5): p. 469-77.
58. Laplante, M. and D.M. Sabatini, *mTOR signaling at a glance.* J Cell Sci, 2009. **122**(Pt 20): p. 3589-94.
59. Weichhart, T., M. Hengstschläger, and M. Linke, *Regulation of innate immune cell function by mTOR.* Nat Rev Immunol, 2015. **15**(10): p. 599-614.
60. Hallowell, R.W., et al., *mTORC2 signalling regulates M2 macrophage differentiation in response to helminth infection and adaptive thermogenesis.* Nat Comm, 2017. **8**(1): p. 14208.
61. Huang, S.C., et al., *Metabolic Reprogramming Mediated by the mTORC2-IRF4 Signaling Axis Is Essential for Macrophage Alternative Activation.* Immunity, 2016. **45**(4): p. 817-830.
62. Davies, L.C., et al., *Tissue-resident macrophages.* Nat Immunol, 2013. **14**(10): p. 986-95.
63. Chen, B., A. Brickshawana, and N.G. Frangogiannis, *The Functional Heterogeneity of Resident Cardiac Macrophages in Myocardial InjuryCCR2(+) Cells Promote Inflammation, Whereas CCR2(-) Cells Protect.* Circ Res, 2019. **124**(2): p. 183-185.
64. Honold, L. and M. Nahrendorf, *Resident and Monocyte-Derived Macrophages in Cardiovascular Disease.* Am Heart Assoc, 2018. **122**(1): p. 113-127.
65. Bajpai, G., et al., *The human heart contains distinct macrophage subsets with divergent origins and functions.* Nat Med, 2018. **24**(8): p. 1234-1245.
66. Epelman, S., Kory J. Lavine, and Gwendalyn J. Randolph, *Origin and Functions of Tissue Macrophages.* Immunity, 2014. **41**(1): p. 21-35.
67. Leid, J., et al., *Primitive Embryonic Macrophages are Required for Coronary Development and Maturation.* Circ Res, 2016. **118**(10): p. 1498-511.

68. Bajpai, G., et al., *Tissue Resident CCR2- and CCR2+ Cardiac Macrophages Differentially Orchestrate Monocyte Recruitment and Fate Specification Following Myocardial Injury.* Circ Res, 2019. **124**(2): p. 263-278.
69. Dick, S.A., et al., *Self-renewing resident cardiac macrophages limit adverse remodeling following myocardial infarction.* Nat Immunol, 2019. **20**(1): p. 29-39.
70. Hulsmans, M., et al., *Macrophages Facilitate Electrical Conduction in the Heart.* Cell, 2017. **169**(3): p. 510-522.e20.
71. Panek, C.A., et al., *Differential expression of the fractalkine chemokine receptor (CX3CR1) in human monocytes during differentiation.* Cell Mol Immunol, 2015. **12**(6): p. 669-80.
72. Herrington, W., et al., *Epidemiology of Atherosclerosis and the Potential to Reduce the Global Burden of Atherothrombotic Disease.* Circ Res, 2016. **118**(4): p. 535-546.
73. Geovanini, G.R. and P. Libby, *Atherosclerosis and inflammation: overview and updates.* Clin Sci (Lond), 2018. **132**(12): p. 1243-1252.
74. Kim, K., et al., *Transcriptome Analysis Reveals Nonfoamy Rather Than Foamy Plaque Macrophages Are Proinflammatory in Atherosclerotic Murine Models.* Circ Res, 2018. **123**(10): p. 1127-1142.
75. Duewell, P., et al., *NLRP3 inflammasomes are required for atherogenesis and activated by cholesterol crystals.* Nature, 2010. **464**(7293): p. 1357-1361.
76. Liu, W., et al., *OxLDL-induced IL-1 beta secretion promoting foam cells formation was mainly via CD36 mediated ROS production leading to NLRP3 inflammasome activation.* Inflamm Res, 2014. **63**(1): p. 33-43.
77. Rajamäki, K., et al., *Cholesterol crystals activate the NLRP3 inflammasome in human macrophages: a novel link between cholesterol metabolism and inflammation.* PLoS One, 2010. **5**(7): p. e11765.
78. Clarke, M.C., et al., *Apoptosis of vascular smooth muscle cells induces features of plaque vulnerability in atherosclerosis.* Nat Med, 2006. **12**(9): p. 1075-80.
79. Anversa, P. and E.H. Sonnenblick, *Ischemic cardiomyopathy: Pathophysiologic mechanisms.* Prog Cardiovasc Dis, 1990. **33**(1): p. 49-70.
80. Amin, M.N., et al., *Inflammatory cytokines in the pathogenesis of cardiovascular disease and cancer.* SAGE Open Medicine, 2020. **8**: p. 2050312120965752.
81. Debrunner, M., et al., *Proinflammatory cytokines in acute myocardial infarction with and without cardiogenic shock.* Clin Res Cardiol, 2008. **97**(5): p. 298-305.
82. Nian, M., et al., *Inflammatory Cytokines and Postmyocardial Infarction Remodeling.* Circ Res, 2004. **94**(12): p. 1543-1553.
83. Cohn, J.N., R. Ferrari, and N. Sharpe, *Cardiac remodeling--concepts and clinical implications: a consensus paper from an international forum on cardiac remodeling. Behalf of an International Forum on Cardiac Remodeling.* J Am Coll Cardiol, 2000. **35**(3): p. 569-82.
84. Heidt, T., et al., *Differential contribution of monocytes to heart macrophages in steady-state and after myocardial infarction.* Circ Res, 2014. **115**(2): p. 284-95.
85. Ma, Y., A.J. Mouton, and M.L. Lindsey, *Cardiac macrophage biology in the steady-state heart, the aging heart, and following myocardial infarction.* Transl Res, 2018. **191**: p. 15-28.
86. Nahrendorf, M., et al., *The healing myocardium sequentially mobilizes two monocyte subsets with divergent and complementary functions.* J Exp Med, 2007. **204**(12): p. 3037-47.
87. Mouton, A.J., et al., *Mapping macrophage polarization over the myocardial infarction time continuum.* Basic Res Cardiol, 2018. **113**(4): p. 26.
88. Galvan-Pena, S. and L.A. O'Neill, *Metabolic reprograming in macrophage polarization.* Front Immunol, 2014. **5**: p. 420.

89. Cai, S., et al., *Mitochondrial dysfunction in macrophages promotes inflammation and suppresses repair after myocardial infarction.* J Clin Investig, 2022.
90. Wang, N., et al., *Histone Lactylation Boosts Reparative Gene Activation Post–Myocardial Infarction.* Circulation Research, 2022. **131**(11): p. 893-908.
91. Poon, I.K.H., et al., *Apoptotic cell clearance: basic biology and therapeutic potential.* Nat Rev Immunol, 2014. **14**: p. 166.
92. Saraste, A., et al., *Apoptosis in human acute myocardial infarction.* Circulation, 1997. **95**(2): p. 320-3.
93. Yoshimura, C., et al., *Efferocytosis during myocardial infarction.* The Journal of Biochemistry, 2020. **168**(1): p. 1-6.
94. Zhang, S., et al., *Efferocytosis Fuels Requirements of Fatty Acid Oxidation and the Electron Transport Chain to Polarize Macrophages for Tissue Repair.* Cell Metab, 2019. **29**(2): p. 443-456.e5.
95. Yurdagul, A., Jr., et al., *Mechanisms and Consequences of Defective Efferocytosis in Atherosclerosis.* Front Cardiovasc Med, 2017. **4**: p. 86.
96. Gruzdeva, O., et al., *Relationship key factor of inflammation and the development of complications in the late period of myocardial infarction in patients with visceral obesity.* BMC Cardiovas Disord, 2017. **17**(1): p. 36-36.
97. Tilg, H. and A.R. Moschen, *Inflammatory mechanisms in the regulation of insulin resistance.* Mol Med, 2008. **14**(3-4): p. 222-231.
98. Rai, V. and D.K. Agrawal, *The role of damage- and pathogen-associated molecular patterns in inflammation-mediated vulnerability of atherosclerotic plaques.* Can J Physiol Pharmacol, 2017. **95**(10): p. 1245-1253.
99. Silvis, M.J.M., et al., *Damage-Associated Molecular Patterns in Myocardial Infarction and Heart Transplantation: The Road to Translational Success.* Front Immunol, 2020. **11**.
100. Sheedy, F.J., et al., *CD36 coordinates NLRP3 inflammasome activation by facilitating intracellular nucleation of soluble ligands into particulate ligands in sterile inflammation.* Nat Immunol, 2013. **14**(8): p. 812-20.
101. Sunahori, K., et al., *The S100A8/A9 heterodimer amplifies proinflammatory cytokine production by macrophages via activation of nuclear factor kappa B and p38 mitogen-activated protein kinase in rheumatoid arthritis.* Arthritis Res Ther, 2006. **8**(3): p. R69.
102. Jay, A.G., et al., *CD36 binds oxidized low density lipoprotein (LDL) in a mechanism dependent upon fatty acid binding.* J Biol Chem, 2015. **290**(8): p. 4590-4603.
103. Accad, M., et al., *Massive xanthomatosis and altered composition of atherosclerotic lesions in hyperlipidemic mice lacking acyl CoA:cholesterol acyltransferase 1.* J Clin Invest, 2000. **105**(6): p. 711-9.
104. Kligman, D. and D.C. Hilt, *The S100 protein family.* Trends Biochem Sci, 1988. **13**(11): p. 437-43.
105. Xia, C., et al., *S100 Proteins As an Important Regulator of Macrophage Inflammation.* Front Immunol, 2017. **8**: p. 1908.
106. McCormick, M.M., et al., *S100A8 and S100A9 in human arterial wall. Implications for atherogenesis.* J Biol Chem, 2005. **280**(50): p. 41521-9.
107. Healy, A.M., et al., *Platelet expression profiling and clinical validation of myeloid-related protein-14 as a novel determinant of cardiovascular events.* Circulation, 2006. **113**(19): p. 2278-84.
108. Ionita, M.G., et al., *High levels of myeloid-related protein 14 in human atherosclerotic plaques correlate with the characteristics of rupture-prone lesions.* Arterioscler Thromb Vasc Biol, 2009. **29**(8): p. 1220-7.
109. Park, J.S., et al., *Involvement of toll-like receptors 2 and 4 in cellular activation by high mobility group box 1 protein.* J Biol Chem, 2004. **279**(9): p. 7370-7.

110. Andrassy, M., et al., *High-mobility group box-1 in ischemia-reperfusion injury of the heart.* Circulation, 2008. **117**(25): p. 3216-26.
111. Kohno, T., et al., *Role of high-mobility group box 1 protein in post-infarction healing process and left ventricular remodelling.* Cardiovasc Res, 2009. **81**(3): p. 565-73.
112. Tian, Y., et al., *The myocardial infarct-exacerbating effect of cell-free DNA is mediated by the high-mobility group box 1-receptor for advanced glycation end products-Toll-like receptor 9 pathway.* J Thorac Cardiovasc Surg, 2019. **157**(6): p. 2256-2269.e3.
113. Riley, J.S. and S.W. Tait, *Mitochondrial DNA in inflammation and immunity.* EMBO Rep, 2020. **21**(4): p. e49799.
114. Qin, C.Y., et al., *Mitochondrial DNA-induced inflammatory damage contributes to myocardial ischemia reperfusion injury in rats: Cardioprotective role of epigallocatechin.* Mol Med Rep, 2017. **16**(5): p. 7569-7576.
115. Pedersen, T.R., *Randomised trial of cholesterol lowering in 4444 patients with coronary heart disease: the Scandinavian Simvastatin Survival Study (4S).* Atheroscler Supp, 2004. **5**(3): p. 81-87.
116. Rouleau, J., *Improved outcome after acute coronary syndromes with an intensive versus standard lipid-lowering regimen: results from the Pravastatin or Atorvastatin Evaluation and Infection Therapy–Thrombolysis in Myocardial Infarction 22 (PROVE IT–TIMI 22) trial.* Am J Med, 2005. **118**(12, Supplement): p. 28-35.
117. Diamantis, E., et al., *The Anti-Inflammatory Effects of Statins on Coronary Artery Disease: An Updated Review of the Literature.* Curr Cardiol Rev, 2017. **13**(3): p. 209-216.
118. Ridker, P.M., et al., *Rosuvastatin to prevent vascular events in men and women with elevated C-reactive protein.* N Engl J Med, 2008. **359**(21): p. 2195-207.
119. Tousoulis, D., et al., *Effects of rosuvastatin and allopurinol on circulating endothelial progenitor cells in patients with congestive heart failure: the impact of inflammatory process and oxidative stress.* Atherosclerosis, 2011. **214**(1): p. 151-7.
120. Ako, S., et al., *Statins Inhibit Inflammatory Cytokine Production by Macrophages and Acinar-to-Ductal Metaplasia of Pancreatic Cells.* Gastro Hep Advances, 2022. **1**(4): p. 640-651.
121. Hilgendorff, A., et al., *Statins differ in their ability to block NF-kappaB activation in human blood monocytes.* Int J Clin Pharmacol Ther, 2003. **41**(9): p. 397-401.
122. Giugliano, G.R., et al., *Meta-analysis of corticosteroid treatment in acute myocardial infarction.* Am J Cardiol, 2003. **91**(9): p. 1055-9.
123. Gong, K., et al., *The nonspecific anti-inflammatory therapy with methotrexate for patients with chronic heart failure.* Am Heart J, 2006. **151**(1): p. 62-8.
124. Moreira, D.M., et al., *MethotrexaTE THerapy in ST-Segment Elevation MYocardial InfarctionS: A Randomized Double-Blind, Placebo-Controlled Trial (TETHYS Trial).* J Cardiovasc Pharmacol Ther, 2017. **22**(6): p. 538-545.
125. Moreira, D.M., J.L. Vieira, and C.A. Gottschall, *The effects of METhotrexate therapy on the physical capacity of patients with ISchemic heart failure: a randomized double-blind, placebo-controlled trial (METIS trial).* J Card Fail, 2009. **15**(10): p. 828-34.
126. Hausenloy, D.J., E.A. Boston-Griffiths, and D.M. Yellon, *Cyclosporin A and cardioprotection: from investigative tool to therapeutic agent.* Br J Pharmacol, 2012. **165**(5): p. 1235-45.
127. Yingzhong, C., C. Lin, and W. Chunbin, *Clinical effects of cyclosporine A on reperfusion injury in myocardial infarction: a meta-analysis of randomized controlled trials.* Springerplus, 2016. **5**(1): p. 1117.
128. Abbate, A., et al., *Interleukin-1 blockade with anakinra to prevent adverse cardiac remodeling after acute myocardial infarction (Virginia Commonwealth University Anakinra Remodeling Trial [VCU-ART] Pilot study).* Am J Cardiol, 2010. **105**(10): p. 1371-1377.e1.

129. Toldo, S., et al., *Interleukin-1beta blockade improves cardiac remodelling after myocardial infarction without interrupting the inflammasome in the mouse.* Exp Physiol, 2013. **98**(3): p. 734-45.
130. Abbate, A., et al., *Effects of interleukin-1 blockade with anakinra on adverse cardiac remodeling and heart failure after acute myocardial infarction [from the Virginia Commonwealth University-Anakinra Remodeling Trial (2) (VCU-ART2) pilot study].* Am J Cardiol, 2013. **111**(10): p. 1394-400.
131. Morton, A.C., et al., *The effect of interleukin-1 receptor antagonist therapy on markers of inflammation in non-ST elevation acute coronary syndromes: the MRC-ILA Heart Study.* Eur Heart J, 2015. **36**(6): p. 377-84.
132. Sager, H.B., et al., *RNAi targeting multiple cell adhesion molecules reduces immune cell recruitment and vascular inflammation after myocardial infarction.* Sci Transl Med, 2016. **8**(342): p. 342ra80.
133. Monaghan, M., et al., *A Collagen-based Scaffold Delivering Exogenous MicroRNA-29B to Modulate Extracellular Matrix Remodeling.* Mol Ther, 2014. **22**(4): p. 786-796.
134. Monaghan, M.G., et al., *Exogenous miR-29B Delivery Through a Hyaluronan-Based Injectable System Yields Functional Maintenance of the Infarcted Myocardium.* Tissue Eng Part A, 2017. **24**(1-2): p. 57-67.
135. Panahi, M., et al., *Immunomodulatory interventions in myocardial infarction and heart failure: a systematic review of clinical trials and meta-analysis of IL-1 inhibition.* Cardiovasc Res, 2018. **114**(11): p. 1445-1461.
136. van Amerongen, M.J., et al., *Cryoinjury: a model of myocardial regeneration.* Cardiovasc Pathol, 2008. **17**(1): p. 23-31.
137. van Amerongen, M.J., et al., *Macrophage depletion impairs wound healing and increases left ventricular remodeling after myocardial injury in mice.* Am J Pathol, 2007. **170**(3): p. 818-29.
138. Samanta, A., et al., *Abstract 15693: Genetic Deletion of Interleukin-6 Attenuates Left Ventricular Dysfunction and Remodeling After a Reperfused Myocardial Infarction.* Circulation, 2014. **130**(suppl_2): p. A15693-A15693.
139. Sato, T., et al., *Tumor-necrosis-factor-alpha-gene-deficient mice have improved cardiac function through reduction of intercellular adhesion molecule-1 in myocardial infarction.* Circ J, 2006. **70**(12): p. 1635-42.
140. Groff, K., et al., *Review of Evidence of Environmental Impacts of Animal Research and Testing.* Environments, 2014. **1**(1): p. 14-30.
141. Langer, R. and J.P. Vacanti, *Tissue engineering.* Science, 1993. **260**(5110): p. 920-6.
142. Almouemen, N., H.M. Kelly, and C. O'Leary, *Tissue Engineering: Understanding the Role of Biomaterials and Biophysical Forces on Cell Functionality Through Computational and Structural Biotechnology Analytical Methods.* Comput Struct Biotechnol J, 2019. **17**: p. 591-598.
143. Bursac, N., et al., *Cardiac muscle tissue engineering: toward an in vitro model for electrophysiological studies.* Am J Physiol, 1999. **277**(2): p. H433-44.
144. Shadrin, I.Y., et al., *Cardiopatch platform enables maturation and scale-up of human pluripotent stem cell-derived engineered heart tissues.* Nat Commun, 2017. **8**(1): p. 1825.
145. Gintant, G., et al., *Use of Human Induced Pluripotent Stem Cell–Derived Cardiomyocytes in Preclinical Cancer Drug Cardiotoxicity Testing: A Scientific Statement From the American Heart Association.* Circ Res, 2019. **125**(10): p. e75-e92.
146. Magdy, T., et al., *Human Induced Pluripotent Stem Cell (hiPSC)-Derived Cells to Assess Drug Cardiotoxicity: Opportunities and Problems.* Annu Rev Pharmacol Toxicol, 2018. **58**: p. 83-103.

147. Tani, H., et al., *Production of functional cardiomyocytes and cardiac tissue from human induced pluripotent stem cells for regenerative therapy.* J Mol Cell Cardiol, 2022. **164**: p. 83-91.
148. Tani, H. and S. Tohyama, *Human Engineered Heart Tissue Models for Disease Modeling and Drug Discovery.* Front Cell Dev Biol, 2022. **10**: p. 855763.
149. Kamakura, T., et al., *Ultrastructural maturation of human-induced pluripotent stem cell-derived cardiomyocytes in a long-term culture.* Circ J, 2013. **77**(5): p. 1307-14.
150. Dunn, K.K., et al., *Coculture of Endothelial Cells with Human Pluripotent Stem Cell-Derived Cardiac Progenitors Reveals a Differentiation Stage-Specific Enhancement of Cardiomyocyte Maturation.* Biotechnol J, 2019. **14**(8): p. e1800725.
151. Lee, S., et al., *Contractile force generation by 3D hiPSC-derived cardiac tissues is enhanced by rapid establishment of cellular interconnection in matrix with muscle-mimicking stiffness.* Biomaterials, 2017. **131**: p. 111-120.
152. Mohammadi Amirabad, L., et al., *Enhanced Cardiac Differentiation of Human Cardiovascular Disease Patient-Specific Induced Pluripotent Stem Cells by Applying Unidirectional Electrical Pulses Using Aligned Electroactive Nanofibrous Scaffolds.* ACS Appl Mater Interfaces, 2017. **9**(8): p. 6849-6864.
153. Ronaldson-Bouchard, K., et al., *Advanced maturation of human cardiac tissue grown from pluripotent stem cells.* Nature, 2018. **556**(7700): p. 239-243.
154. Roshanbinfar, K., et al., *Electroconductive Biohybrid Hydrogel for Enhanced Maturation and Beating Properties of Engineered Cardiac Tissues.* Adv Funct Mater, 2018. **28**(42): p. 1803951.
155. Eschenhagen, T., et al., *Three-dimensional reconstitution of embryonic cardiomyocytes in a collagen matrix: a new heart muscle model system.* Faseb j, 1997. **11**(8): p. 683-94.
156. Nunes, S.S., et al., *Biowire: a platform for maturation of human pluripotent stem cell-derived cardiomyocytes.* Nat Methods, 2013. **10**(8): p. 781-7.
157. Karbassi, E., et al., *Cardiomyocyte maturation: advances in knowledge and implications for regenerative medicine.* Nat Rev Cardiol, 2020. **17**(6): p. 341-359.
158. da Silva, L.P., et al., *Electric Phenomenon: A Disregarded Tool in Tissue Engineering and Regenerative Medicine.* Trends Biotechnol, 2020. **38**(1): p. 24-49.
159. Tai, G., M. Tai, and M. Zhao, *Electrically stimulated cell migration and its contribution to wound healing.* Burns Trauma, 2018. **6**(1): p. 20.
160. Park, H.J., et al., *Electrical Stimulation Modulates the Expression of Multiple Wound Healing Genes in Primary Human Dermal Fibroblasts.* Tissue Eng Part A, 2015. **21**(13-14): p. 1982-90.
161. Song, B., et al., *Electrical cues regulate the orientation and frequency of cell division and the rate of wound healing in vivo.* Proc Natl Acad Sci U S A, 2002. **99**(21): p. 13577-82.
162. Thakral, G., et al., *Electrical stimulation to accelerate wound healing.* Diabet Foot Ankle, 2013. **4**.
163. Shao, S., et al., *Osteoblast function on electrically conductive electrospun PLA/MWCNTs nanofibers.* Biomaterials, 2011. **32**(11): p. 2821-33.
164. Hernandez, D., et al., *Electrical Stimulation Promotes Cardiac Differentiation of Human Induced Pluripotent Stem Cells.* Stem Cells Int, 2016. **2016**: p. 1718041.
165. Chan, Y.C., et al., *Electrical stimulation promotes maturation of cardiomyocytes derived from human embryonic stem cells.* J Cardiovasc Transl Res, 2013. **6**(6): p. 989-99.
166. Kim, I.S., et al., *Novel Effect of Biphasic Electric Current on In Vitro Osteogenesis and Cytokine Production in Human Mesenchymal Stromal Cells.* Tissue Eng Part A, 2009. **15**(9): p. 2411-2422.
167. Wang, Y., M. Rouabhia, and Z. Zhang, *Pulsed electrical stimulation benefits wound healing by activating skin fibroblasts through the TGFβ1/ERK/NF-κB axis.* Biochim Biophys Acta Gen Subj 2016. **1860**(7): p. 1551-1559.

168. Radisic, M., et al., *Functional assembly of engineered myocardium by electrical stimulation of cardiac myocytes cultured on scaffolds.* Proc Natl Acad Sci U S A, 2004. **101**(52): p. 18129-34.
169. Li, Y., et al., *Enhanced adhesion and proliferation of human umbilical vein endothelial cells on conductive PANI-PCL fiber scaffold by electrical stimulation.* Mater Sci Eng C Mater Biol Appl, 2017. **72**: p. 106-112.
170. Cunha, F., A.M. Rajnicek, and C.D. McCaig, *Electrical Stimulation Directs Migration, Enhances and Orients Cell Division and Upregulates the Chemokine Receptors CXCR4 and CXCR2 in Endothelial Cells.* J Vasc Res, 2019. **56**(1): p. 39-53.
171. Hoare, J.I., et al., *Electric fields are novel determinants of human macrophage functions.* J Leukoc Biol, 2016. **99**(6): p. 1141-51.
172. Srirussamee, K., et al., *Direct electrical stimulation enhances osteogenesis by inducing Bmp2 and Spp1 expressions from macrophages and preosteoblasts.* Biotechnol Bioeng, 2019. **116**(12): p. 3421-3432.
173. Solazzo, M., et al., *The rationale and emergence of electroconductive biomaterial scaffolds in cardiac tissue engineering.* APL Bioeng, 2019. **3**(4): p. 041501.
174. Hopley, E.L., et al., *Carbon nanotubes leading the way forward in new generation 3D tissue engineering.* Biotechnol Adv, 2014. **32**(5): p. 1000-14.
175. Shin, S.R., et al., *Carbon-nanotube-embedded hydrogel sheets for engineering cardiac constructs and bioactuators.* ACS Nano, 2013. **7**(3): p. 2369-80.
176. Madani, S.Y., A. Mandel, and A.M. Seifalian, *A concise review of carbon nanotube's toxicology.* Nano Rev, 2013. **4**.
177. Shevach, M., et al., *Gold nanoparticle-decellularized matrix hybrids for cardiac tissue engineering.* Nano Lett, 2014. **14**(10): p. 5792-6.
178. Chiang, C.K., et al., *Electrical Conductivity in Doped Polyacetylene.* Phy Rev Lett, 1977. **39**(17): p. 1098-1101.
179. Elschner, A., et al., *PEDOT: Principles and applications of an intrinsically conductive polyme*. 2010. 1-380.
180. Groenendaal, L., et al., *Poly(3,4-ethylenedioxythiophene) and Its Derivatives: Past, Present, and Future.* J Adv Mater, 2000. **12**(7): p. 481-494.
181. Šafaříková, E., et al., *Conductive Polymer PEDOT:PSS-Based Platform for Embryonic Stem-Cell Differentiation.* Int J Mol Sci, 2022. **23**(3).
182. Wen, J.Y., et al., *Maturation-Based Model of Arrhythmogenic Right Ventricular Dysplasia Using Patient-Specific Induced Pluripotent Stem Cells.* Circ J, 2015. **79**(7): p. 1402-8.
183. Rother, J., et al., *Crosstalk of cardiomyocytes and fibroblasts in co-cultures.* Open Biol, 2015. **5**(6): p. 150038.
184. Noguchi, R., et al., *Development of a three-dimensional pre-vascularized scaffold-free contractile cardiac patch for treating heart disease.* J Heart Lung Transplant, 2016. **35**(1): p. 137-145.
185. Garzoni, L.R., et al., *Dissecting coronary angiogenesis: 3D co-culture of cardiomyocytes with endothelial or mesenchymal cells.* Exp Cell Res, 2009. **315**(19): p. 3406-18.
186. Camelliti, P., T.K. Borg, and P. Kohl, *Structural and functional characterisation of cardiac fibroblasts.* Cardiovasc Res, 2005. **65**(1): p. 40-51.
187. Narmoneva, D.A., et al., *Endothelial cells promote cardiac myocyte survival and spatial reorganization: implications for cardiac regeneration.* Circulation, 2004. **110**(8): p. 962-8.
188. Mironov, V., et al., *Organ printing: tissue spheroids as building blocks.* Biomaterials, 2009. **30**(12): p. 2164-74.
189. Zavadzkas, J.A., et al., *Direct regulation of membrane type 1 matrix metalloproteinase following myocardial infarction causes changes in survival, cardiac function, and remodeling.* Am J Physiol Heart Circ Physiol, 2011. **301**(4): p. H1656-66.

190. Noel, G., et al., *A primary human macrophage-enteroid co-culture model to investigate mucosal gut physiology and host-pathogen interactions.* Sci Rep, 2017. **7**: p. 45270.
191. Lian, X., et al., *Robust cardiomyocyte differentiation from human pluripotent stem cells via temporal modulation of canonical Wnt signaling.* PNAS, 2012. **109**(27): p. E1848-E1857.
192. Solazzo, M. and M.G. Monaghan, *Structural crystallisation of crosslinked 3D PEDOT:PSS anisotropic porous biomaterials to generate highly conductive platforms for tissue engineering applications.* Biomater Sci, 2021. **9**(12): p. 4317-4328.
193. Solazzo, M. and M.G. Monaghan, *A guide to the manufacture of sustainable, ready to use in vitro platforms for the electric-field pacing of cellularised 3D porous scaffolds.* bioRxiv, 2022: p. 2022.10.04.510868.
194. Nuccitelli, R., *Endogenous ionic currents and DC electric fields in multicellular animal tissues.* Bioelectromagnetics, 1992. **Suppl 1**: p. 147-57.
195. Hwang, T.J. and A.S. Kesselheim, *Challenges in the Development of Novel Cardiovascular Therapies.* Clin Pharmacol Ther, 2017. **102**(2): p. 194-196.
196. Fang, L., A.J. Murphy, and A.M. Dart, *A Clinical Perspective of Anti-Fibrotic Therapies for Cardiovascular Disease.* Front Pharmacol, 2017. **8**: p. 186.
197. Clevers, H., *Modeling Development and Disease with Organoids.* Cell, 2016. **165**(7): p. 1586-1597.
198. Lancaster, M.A. and J.A. Knoblich, *Organogenesis in a dish: modeling development and disease using organoid technologies.* Science, 2014. **345**(6194): p. 1247125.
199. Smith, A.S., et al., *Human iPSC-derived cardiomyocytes and tissue engineering strategies for disease modeling and drug screening.* Biotechnol Adv, 2017. **35**(1): p. 77-94.
200. Kerr, C.M., et al., *Multicellular Human Cardiac Organoids Transcriptomically Model Distinct Tissue-Level Features of Adult Myocardium.* Int J Mol Sci, 2021. **22**(16).
201. Jang, Y., et al., *Modulating cardiomyocyte and fibroblast interaction using layer-by-layer deposition facilitates synchronisation of cardiac macro tissues.* Soft Matter, 2020. **16**(2): p. 428-434.
202. Hanif, W., et al., *Left atrial remodeling, hypertrophy, and fibrosis in mouse models of heart failure.* Cardiovasc Pathol, 2017. **30**: p. 27-37.
203. Houser, S.R., et al., *Animal Models of Heart Failure.* Circ Res, 2012. **111**(1): p. 131-150.
204. Ai, X., et al., *Microfluidic Coculture Device for Monitoring of Inflammation-Induced Myocardial Injury Dynamics.* Anal Chem, 2018. **90**(7): p. 4485-4494.
205. Wrona, E.A., et al., *Effects of polarized macrophages on the in vitro gene expression after Co-Culture of human pluripotent stem cell-derived cardiomyocytes.* J Tissue Eng Regen Med, 2019. **4**: p. 100018.
206. Hitscherich, P.G., et al., *The effects of macrophages on cardiomyocyte calcium-handling function using in vitro culture models.* Physiol Rep, 2019. **7**(13): p. e14137.
207. Almeida Paiva, R., et al., *Ischaemia alters the effects of cardiomyocyte-derived extracellular vesicles on macrophage activation.* J Cell Mol Med, 2019. **23**(2): p. 1137-1151.
208. Feng, X., et al., *Lipopolysaccharide inhibits macrophage phagocytosis of apoptotic neutrophils by regulating the production of tumour necrosis factor α and growth arrest-specific gene 6.* Immunology, 2011. **132**(2): p. 287-95.
209. Schulz, D., et al., *In-Depth Characterization of Monocyte-Derived Macrophages using a Mass Cytometry-Based Phagocytosis Assay.* Sci Rep, 2019. **9**(1): p. 1925.
210. Kaikita, K., et al., *Targeted deletion of CC chemokine receptor 2 attenuates left ventricular remodeling after experimental myocardial infarction.* Am J Pathol, 2004. **165**(2): p. 439-47.

211. Haenseler, W., et al., *A Highly Efficient Human Pluripotent Stem Cell Microglia Model Displays a Neuronal-Co-culture-Specific Expression Profile and Inflammatory Response.* Stem Cell Rep, 2017. **8**(6): p. 1727-1742.
212. Zhong, H.J., et al., *Low concentrations of corticosterone exert stimulatory effects on macrophage function in a manner dependent on glucocorticoid receptors.* Int J Endocrinol, 2013. **2013**: p. 405127.
213. Dambrot, C., et al., *Serum supplemented culture medium masks hypertrophic phenotypes in human pluripotent stem cell derived cardiomyocytes.* J Cell Mol Med, 2014. **18**(8): p. 1509-18.
214. Wei, J., et al., *Serum deprivation induced apoptosis in macrophage is mediated by autocrine secretion of type I IFNs.* Apoptosis, 2006. **11**(4): p. 545-54.
215. Yamauchi-Takihara, K. and T. Kishimoto, *Cytokines and their receptors in cardiovascular diseases--role of gp130 signalling pathway in cardiac myocyte growth and maintenance.* Int J Exp Pathol, 2000. **81**(1): p. 1-16.
216. Jin, H., et al., *Epac activation inhibits IL-6-induced cardiac myocyte dysfunction.* J of Physiol Sci, 2018. **68**(1): p. 77-87.
217. Buoncervello, M., et al., *Inflammatory cytokines associated with cancer growth induce mitochondria and cytoskeleton alterations in cardiomyocytes.* J Cell Physiol, 2019. **234**(11): p. 20453-20468.
218. Yang, L., et al., *An Immuno-Cardiac Model for Macrophage-Mediated Inflammation in COVID-19 Hearts.* Circ Res, 2021. **129**(1): p. 33-46.
219. Zhou, J.Y., et al., *Corticosterone exerts immunostimulatory effects on macrophages via endoplasmic reticulum stress.* Br J Surg, 2010. **97**(2): p. 281-93.
220. Pinto, A.R., et al., *An Abundant Tissue Macrophage Population in the Adult Murine Heart with a Distinct Alternatively-Activated Macrophage Profile.* PLos One, 2012. **7**(5): p. e36814.
221. Ishida, Y., J.L. Gao, and P.M. Murphy, *Chemokine receptor CX3CR1 mediates skin wound healing by promoting macrophage and fibroblast accumulation and function.* J Immunol, 2008. **180**(1): p. 569-79.
222. Lusis, A.J., *Atherosclerosis.* Nature, 2000. **407**(6801): p. 233-41.
223. Khallou-Laschet, J., et al., *Macrophage plasticity in experimental atherosclerosis.* PLoS One, 2010. **5**(1): p. e8852.
224. Moore, K.J., F.J. Sheedy, and E.A. Fisher, *Macrophages in atherosclerosis: a dynamic balance.* Nature Rev Immunol, 2013. **13**(10): p. 709-721.
225. Loftus, R.M. and D.K. Finlay, *Immunometabolism: Cellular Metabolism Turns Immune Regulator.* J Biol Chem, 2016. **291**(1): p. 1-10.
226. San-Millán, I. and G.A. Brooks, *Reexamining cancer metabolism: lactate production for carcinogenesis could be the purpose and explanation of the Warburg Effect.* Carcinogenesis, 2017. **38**(2): p. 119-133.
227. Altenberg, B. and K.O. Greulich, *Genes of glycolysis are ubiquitously overexpressed in 24 cancer classes.* Genomics, 2004. **84**(6): p. 1014-20.
228. Luo, W., et al., *Pyruvate kinase M2 is a PHD3-stimulated coactivator for hypoxia-inducible factor 1.* Cell, 2011. **145**(5): p. 732-44.
229. Knight, M. and S. Stanley, *HIF-1α as a central mediator of cellular resistance to intracellular pathogens.* Curr Opin Immunol, 2019. **60**: p. 111-116.
230. Viola, A., et al., *The Metabolic Signature of Macrophage Responses.* Front Immunol, 2019. **10**: p. 1462-1462.
231. Tomas, L., et al., *Altered metabolism distinguishes high-risk from stable carotid atherosclerotic plaques.* Eur Heart J, 2018. **39**(24): p. 2301-2310.

232. Folco, E.J., et al., *Hypoxia but not inflammation augments glucose uptake in human macrophages: Implications for imaging atherosclerosis with 18fluorine-labeled 2-deoxy-D-glucose positron emission tomography.* J Am Coll Cardiol, 2011. **58**(6): p. 603-14.
233. Ballinger, S.W., et al., *Mitochondrial integrity and function in atherogenesis.* Circulation, 2002. **106**(5): p. 544-9.
234. Mabile, L., et al., *Mitochondrial function is involved in LDL oxidation mediated by human cultured endothelial cells.* Arterioscler Thromb Vasc Biol, 1997. **17**(8): p. 1575-82.
235. Corr, E.M., C.C. Cunningham, and A. Dunne, *Cholesterol crystals activate Syk and PI3 kinase in human macrophages and dendritic cells.* Atherosclerosis, 2016. **251**: p. 197-205.
236. Wang, R., et al., *Activation of NLRP3 inflammasomes contributes to hyperhomocysteinemia-aggravated inflammation and atherosclerosis in apoE-deficient mice.* Lab Invest, 2017. **97**(8): p. 922-934.
237. Hall, C.J., et al., *Blocking fatty acid-fueled mROS production within macrophages alleviates acute gouty inflammation.* J Clin Investig, 2018. **128**(5): p. 1752-1771.
238. Diskin, C. and E.M. Palsson-McDermott, *Metabolic Modulation in Macrophage Effector Function.* Front Immunol, 2018. **9**: p. 270.
239. Freemerman, A.J., et al., *Metabolic reprogramming of macrophages: glucose transporter 1 (GLUT1)-mediated glucose metabolism drives a proinflammatory phenotype.* J Biol Chem, 2014. **289**(11): p. 7884-96.
240. Van den Bossche, J., J. Baardman, and M.P. de Winther, *Metabolic Characterization of Polarized M1 and M2 Bone Marrow-derived Macrophages Using Real-time Extracellular Flux Analysis.* J Vis Exp, 2015(105).
241. Neto, N., R.I. Dmitriev, and M.G. Monaghan, *Seeing Is Believing: Noninvasive Microscopic Imaging Modalities for Tissue Engineering and Regenerative Medicine*, in *Cell Eng Regen*, J.M. Gimble, et al., Editors. 2020, Springer International Publishing: Cham. p. 599-638.
242. Kapetanovic, R., et al., *Lipopolysaccharide promotes Drp1-dependent mitochondrial fission and associated inflammatory responses in macrophages.* Immunol Cell Biol, 2020. **98**(7): p. 528-539.
243. Otera, H., et al., *Mff is an essential factor for mitochondrial recruitment of Drp1 during mitochondrial fission in mammalian cells.* J Cell Biol, 2010. **191**(6): p. 1141-1158.
244. Wang, Y., et al., *Macrophage mitochondrial oxidative stress promotes atherosclerosis and nuclear factor-kappaB-mediated inflammation in macrophages.* Circ Res, 2014. **114**(3): p. 421-33.
245. Finucane, O.M., et al., *The NLRP3 inflammasome modulates glycolysis by increasing PFKFB3 in an IL-1β-dependent manner in macrophages.* Sci Rep, 2019. **9**(1): p. 4034.
246. Shirai, T., et al., *The glycolytic enzyme PKM2 bridges metabolic and inflammatory dysfunction in coronary artery disease.* J Exp Med, 2016. **213**(3): p. 337-54.
247. Anastasiou, D., et al., *Inhibition of pyruvate kinase M2 by reactive oxygen species contributes to cellular antioxidant responses.* Science, 2011. **334**(6060): p. 1278-83.
248. Hotamisligil, G.S., *Foundations of Immunometabolism and Implications for Metabolic Health and Disease.* Immunity, 2017. **47**(3): p. 406-420.
249. Morgan, M.J. and Z.-g. Liu, *Crosstalk of reactive oxygen species and NF-κB signaling.* Cell Res, 2011. **21**(1): p. 103-115.
250. Hoffmann, E., et al., *Multiple control of interleukin-8 gene expression.* J Leukoc Biol, 2002. **72**(5): p. 847-55.
251. Holtmann, H., et al., *Induction of interleukin-8 synthesis integrates effects on transcription and mRNA degradation from at least three different cytokine- or stress-activated signal transduction pathways.* Mol Cell Biol, 1999. **19**(10): p. 6742-53.

252. Liu, J., et al., *High resolution FDG-microPET of carotid atherosclerosis: plaque components underlying enhanced FDG uptake.* Int J Cardiovasc Imaging, 2016. **32**(1): p. 145-52.
253. van Tuijl, J., et al., *Immunometabolism orchestrates training of innate immunity in atherosclerosis.* Cardiovasc Res, 2019. **115**(9): p. 1416-1424.
254. Karshovska, E., et al., *HIF-1α (Hypoxia-Inducible Factor-1α) Promotes Macrophage Necroptosis by Regulating miR-210 and miR-383.* Arterioscler Thromb Vasc Biol, 2020. **0**(0): p. ATVBAHA.119.313290.
255. Christofk, H.R., et al., *The M2 splice isoform of pyruvate kinase is important for cancer metabolism and tumour growth.* Nature, 2008. **452**(7184): p. 230-233.
256. Mazurek, S., et al., *Pyruvate kinase type M2 and its role in tumor growth and spreading.* Semin Cancer Biol, 2005. **15**(4): p. 300-8.
257. Combadiere, C., et al., *Combined inhibition of CCL2, CX3CR1, and CCR5 abrogates Ly6C(hi) and Ly6C(lo) monocytosis and almost abolishes atherosclerosis in hypercholesterolemic mice.* Circulation, 2008. **117**(13): p. 1649-57.
258. Segers, D., et al., *Atherosclerotic Plaque Stability Is Affected by the Chemokine CXCL10 in Both Mice and Humans.* Int J Inflam, 2011. **2011**: p. 936109.
259. Moreau, M., et al., *Interleukin-8 Mediates Downregulation of Tissue Inhibitor of Metalloproteinase-1 Expression in Cholesterol-Loaded Human Macrophages.* Circulation, 1999. **99**(3): p. 420-426.
260. Abboud, G., et al., *Inhibition of Glycolysis Reduces Disease Severity in an Autoimmune Model of Rheumatoid Arthritis.* Front Immunol, 2018. **9**: p. 1973.
261. Pålsson-McDermott, E.M. and L.A.J. O'Neill, *Targeting immunometabolism as an anti-inflammatory strategy.* Cell Res, 2020. **30**(4): p. 300-314.
262. Doddapattar, P., et al., *Myeloid Cell PKM2 Deletion Enhances Efferocytosis and Reduces Atherosclerosis.* Circ Res, 2022. **130**(9): p. 1289-1305.
263. Zhang, X. and D.M. Mosser, *Macrophage activation by endogenous danger signals.* J Pathol, 2008. **214**(2): p. 161-78.
264. McWhorter, F.Y., C.T. Davis, and W.F. Liu, *Physical and mechanical regulation of macrophage phenotype and function.* Cell Mol Life Sci, 2015. **72**(7): p. 1303-1316.
265. Pugin, J., et al., *Activation of human macrophages by mechanical ventilation in vitro.* Am J Physiol, 1998. **275**(6): p. L1040-50.
266. Rich, A. and A.K. Harris, *Anomalous preferences of cultured macrophages for hydrophobic and roughened substrata.* J Cell Sci, 1981. **50**: p. 1-7.
267. Sridharan, R., et al., *Material stiffness influences the polarization state, function and migration mode of macrophages.* Acta Biomater, 2019. **89**: p. 47-59.
268. Higgins, D.M., et al., *Localized Immunosuppressive Environment in the Foreign Body Response to Implanted Biomaterials.* Am J Pathol, 2009. **175**(1): p. 161-170.
269. Balint, R., N.J. Cassidy, and S.H. Cartmell, *Electrical stimulation: a novel tool for tissue engineering.* Tissue Eng Part B Rev, 2013. **19**(1): p. 48-57.
270. *The principles of nerve cell communication.* Alcohol Health Res World, 1997. **21**(2): p. 107-8.
271. Das, R., et al., *Electrical Stimulation for Immune Modulation in Cancer Treatments.* Front Bioeng Biotechnol, 2021. **9**: p. 795300.
272. Brighton, C.T., et al., *Signal transduction in electrically stimulated bone cells.* J Bone Joint Surg Am, 2001. **83**(10): p. 1514-23.
273. Sundelacruz, S., M. Levin, and D.L. Kaplan, *Membrane potential controls adipogenic and osteogenic differentiation of mesenchymal stem cells.* PLoS One, 2008. **3**(11): p. e3737.
274. Chen, C., et al., *Electrical stimulation as a novel tool for regulating cell behavior in tissue engineering.* Biomater Res, 2019. **23**: p. 25.

275. Santos, N.F., et al., *Diamond-Graphite Nanoplatelet Surfaces as Conductive Substrates for the Electrical Stimulation of Cell Functions.* ACS Appl Mater Interfaces, 2017. **9**(2): p. 1331-1342.
276. Zhu, W., et al., *Enhanced neural stem cell functions in conductive annealed carbon nanofibrous scaffolds with electrical stimulation.* Nanomedicine, 2018. **14**(7): p. 2485-2494.
277. Dodel, M., et al., *Electrical stimulation of somatic human stem cells mediated by composite containing conductive nanofibers for ligament regeneration.* Biologicals, 2017. **46**: p. 99-107.
278. Park, S.Y., et al., *Enhanced differentiation of human neural stem cells into neurons on graphene.* Adv Mater, 2011. **23**(36): p. H263-7.
279. Hronik-Tupaj, M., et al., *Osteoblastic differentiation and stress response of human mesenchymal stem cells exposed to alternating current electric fields.* Biomed Eng Online, 2011. **10**: p. 9.
280. Wang, Y., et al., *Modulation of Osteogenesis in MC3T3-E1 Cells by Different Frequency Electrical Stimulation.* PLoS One, 2016. **11**(5): p. e0154924.
281. Evans, R.D., D. Foltz, and K. Foltz, *Electrical stimulation with bone and wound healing.* Clin Podiatr Med Surg, 2001. **18**(1): p. 79-95, vi.
282. Gu, J., et al., *Effects of electrical stimulation on cytokine-induced macrophage polarization.* J Tissue Eng Regen Med, 2022. **16**(5): p. 448-459.
283. Li, C., M. Levin, and D.L. Kaplan, *Bioelectric modulation of macrophage polarization.* Sci Rep, 2016. **6**(1): p. 21044.
284. Sheng, R., et al., *EGCG inhibits cardiomyocyte apoptosis in pressure overload-induced cardiac hypertrophy and protects cardiomyocytes from oxidative stress in rats.* Acta Pharmacologica Sinica, 2007. **28**(2): p. 191-201.
285. Aiba, T., et al., *Electrophysiological consequences of dyssynchronous heart failure and its restoration by resynchronization therapy.* Circulation, 2009. **119**(9): p. 1220-30.
286. Prinzen, F.W., et al., *Electrical management of heart failure: from pathophysiology to treatment.* Eur Heart J, 2022. **43**(20): p. 1917-1927.
287. Kroll, K., et al., *Electro-mechanical conditioning of human iPSC-derived cardiomyocytes for translational research.* Prog Biophys Mol Biol, 2017. **130**(Pt B): p. 212-222.
288. Waataja, J.J., K.S. Tweden, and C.N. Honda, *Effects of high-frequency alternating current on axonal conduction through the vagus nerve.* J Neural Eng, 2011. **8**(5): p. 056013.
289. Patel, B., et al., *CCR2+ Monocyte-Derived Infiltrating Macrophages Are Required for Adverse Cardiac Remodeling During Pressure Overload.* JACC: Basic Transl Sci, 2018. **3**(2): p. 230-244.
290. Crestani, T., et al., *Electrical stimulation applied during differentiation drives the hiPSC-CMs towards a mature cardiac conduction-like cells.* Biochem Biophys Res Comm, 2020. **533**(3): p. 376-382.
291. Bertani, F.R., et al., *Classification of M1/M2-polarized human macrophages by label-free hyperspectral reflectance confocal microscopy and multivariate analysis.* Sci Rep, 2017. **7**(1): p. 8965.
292. Kelly, B. and L.A. O'Neill, *Metabolic reprogramming in macrophages and dendritic cells in innate immunity.* Cell Res, 2015. **25**(7): p. 771-84.
293. Semenov, I., et al., *Cell stimulation and calcium mobilization by picosecond electric pulses.* Bioelectrochemistry, 2015. **105**: p. 65-71.
294. Staehlke, S., et al. *Pulsed Electrical Stimulation Affects Osteoblast Adhesion and Calcium Ion Signaling*. Cells, 2022. **11**, DOI: 10.3390/cells11172650.
295. White, J.A., et al., *Stimulation of Capacitative Calcium Entry in HL-60 Cells by Nanosecond Pulsed Electric Fields *.* J Biol Chem, 2004. **279**(22): p. 22964-22972.

296. Chauhan, A., et al., *M1 Macrophage Polarization Is Dependent on TRPC1-Mediated Calcium Entry.* iScience, 2018. **8**: p. 85-102.
297. Nascimento Da Conceicao, V., et al., *Resolving macrophage polarization through distinct Ca2+ entry channel that maintains intracellular signaling and mitochondrial bioenergetics.* iScience, 2021. **24**(11): p. 103339.
298. De Bock, M., et al., *Connexin 43 hemichannels contribute to cytoplasmic Ca2+ oscillations by providing a bimodal Ca2+-dependent Ca2+ entry pathway.* J Biol Chem, 2012. **287**(15): p. 12250-66.
299. Scheraga, R.G., et al., *TRPV4 Mechanosensitive Ion Channel Regulates Lipopolysaccharide-Stimulated Macrophage Phagocytosis.* J Immunol, 2016. **196**(1): p. 428-36.
300. Braga, T.T., J.S. Agudelo, and N.O. Camara, *Macrophages During the Fibrotic Process: M2 as Friend and Foe.* Front Immunol, 2015. **6**: p. 602.
301. Ayala-Cuellar, A.P., et al., *Roles of Mesenchymal Stem Cells in Tissue Regeneration and Immunomodulation.* Biomol Ther (Seoul), 2019. **27**(1): p. 25-33.
302. Pittenger, M.F., et al., *Mesenchymal stem cell perspective: cell biology to clinical progress.* NPJ Regen, 2019. **4**(1): p. 22.
303. Wu, T., et al., *The roles of mesenchymal stem cells in tissue repair and disease modification.* Curr Stem Cell Res Ther, 2014. **9**(5): p. 424-31.
304. Falanga, V., et al., *Autologous bone marrow-derived cultured mesenchymal stem cells delivered in a fibrin spray accelerate healing in murine and human cutaneous wounds.* Tissue Eng, 2007. **13**(6): p. 1299-312.
305. Ravari, H., et al., *Treatment of non-healing wounds with autologous bone marrow cells, platelets, fibrin glue and collagen matrix.* Cytotherapy, 2011. **13**(6): p. 705-711.
306. Shi, Y., et al., *How mesenchymal stem cells interact with tissue immune responses.* Trends Immunol, 2012. **33**(3): p. 136-43.
307. Yu, B., et al., *Macrophage-Associated Osteoactivin/GPNMB Mediates Mesenchymal Stem Cell Survival, Proliferation, and Migration Via a CD44-Dependent Mechanism.* J Cell Biochem, 2016. **117**(7): p. 1511-21.
308. Martinotti, S. and E. Ranzato, *Scratch Wound Healing Assay.* Methods Mol Biol, 2020. **2109**: p. 225-229.
309. Mahon, O.R., et al., *Nano-particle mediated M2 macrophage polarization enhances bone formation and MSC osteogenesis in an IL-10 dependent manner.* Biomaterials, 2020. **239**: p. 119833.
310. Wynn, T.A. and K.M. Vannella, *Macrophages in Tissue Repair, Regeneration, and Fibrosis.* Immunity, 2016. **44**(3): p. 450-462.
311. Litviňuková, M., et al., *Cells of the adult human heart.* Nature, 2020. **588**(7838): p. 466-472.
312. Eugenín, E.A., et al., *TNF-α Plus IFN-γ Induce Connexin43 Expression and Formation of Gap Junctions Between Human Monocytes/Macrophages That Enhance Physiological Responses.* J Immun, 2003. **170**(3): p. 1320-1328.
313. Cox, C.B., et al., *IL-10 and TGF-β Increase Connexin-43 Expression and Membrane Potential of HL-1 Cardiomyocytes Coupled with RAW 264.7 Macrophages.* ImmunoHorizons, 2022. **6**(6): p. 334-343.
314. Juhas, M., et al., *Incorporation of macrophages into engineered skeletal muscle enables enhanced muscle regeneration.* Nat Biomed Eng, 2018. **2**(12): p. 942-954.
315. Zhao, M., et al., *Electrical signals control wound healing through phosphatidylinositol-3-OH kinase-gamma and PTEN.* Nature, 2006. **442**(7101): p. 457-60.
316. Arranz, A., et al., *Akt1 and Akt2 protein kinases differentially contribute to macrophage polarization.* Proc Natl Acad Sci U S A, 2012. **109**(24): p. 9517-22.

317. White, J.A., et al., *Stimulation of Capacitative Calcium Entry in HL-60 Cells by Nanosecond Pulsed Electric Fields *.* Journal of Biological Chemistry, 2004. **279**(22): p. 22964-22972.
318. Nguyen, T.-N., et al., *Diverse Roles of TRPV4 in Macrophages: A Need for Unbiased Profiling.* Front Immunol, 2022. **12**.
319. Scheraga, R.G., et al., *The Role of TRPV4 in Regulating Innate Immune Cell Function in Lung Inflammation.* Front Immunol, 2020. **11**.
320. Jetten, N., et al., *Anti-inflammatory M2, but not pro-inflammatory M1 macrophages promote angiogenesis in vivo.* Angiogenesis, 2014. **17**(1): p. 109-18.
321. Frangogiannis, N., *Transforming growth factor-β in tissue fibrosis.* J Exp Med, 2020. **217**(3): p. e20190103.
322. Guo, Y., et al., *The therapeutic potential of mesenchymal stem cells for cardiovascular diseases.* Cell Death Dis, 2020. **11**(5): p. 349.
323. Maggini, J., et al., *Mouse bone marrow-derived mesenchymal stromal cells turn activated macrophages into a regulatory-like profile.* PLoS One, 2010. **5**(2): p. e9252.
324. Xu, R., et al., *Exosomes derived from pro-inflammatory bone marrow-derived mesenchymal stem cells reduce inflammation and myocardial injury via mediating macrophage polarization.* J Cell Mol Med, 2019. **23**(11): p. 7617-7631.
325. Guo, J., et al., *Anti-inflammation role for mesenchymal stem cells transplantation in myocardial infarction.* Inflammation, 2007. **30**(3-4): p. 97-104.
326. Orlic, D., et al., *Bone marrow cells regenerate infarcted myocardium.* Nature, 2001. **410**(6829): p. 701-705.
327. Ju, C., et al., *Transplantation of Cardiac Mesenchymal Stem Cell-Derived Exosomes Promotes Repair in Ischemic Myocardium.* J Cardiovasc Transl Res, 2018. **11**(5): p. 420-428.
328. Kishore, R., et al., *Bone marrow progenitor cell therapy-mediated paracrine regulation of cardiac miRNA-155 modulates fibrotic response in diabetic hearts.* PLoS One, 2013. **8**(4): p. e60161.
329. Roshanbinfar, K., et al., *Carbon nanotube doped pericardial matrix derived electroconductive biohybrid hydrogel for cardiac tissue engineering.* Biomater Sci, 2019. **7**(9): p. 3906-3917.
330. Cancian, G., et al., *Carbon nanotubes play an important role in the spatial arrangement of calcium deposits in hydrogels for bone regeneration.* J Mater Sci Mater Med, 2016. **27**(8): p. 126.
331. Wang, W., et al., *Enhancing the Hydrophilicity and Cell Attachment of 3D Printed PCL/Graphene Scaffolds for Bone Tissue Engineering.* Materials (Basel), 2016. **9**(12).
332. Alarcon, E.I., et al., *Safety and efficacy of composite collagen–silver nanoparticle hydrogels as tissue engineering scaffolds.* Nanoscale, 2015. **7**(44): p. 18789-18798.
333. Kang, S., et al., *Covalent conjugation of mechanically stiff graphene oxide flakes to three-dimensional collagen scaffolds for osteogenic differentiation of human mesenchymal stem cells.* Carbon, 2015. **83**: p. 162-172.
334. Navaei, A., et al., *Gold nanorod-incorporated gelatin-based conductive hydrogels for engineering cardiac tissue constructs.* Acta Biomater, 2016. **41**: p. 133-46.
335. Guo, B. and P.X. Ma, *Conducting Polymers for Tissue Engineering.* Biomacromolecules, 2018. **19**(6): p. 1764-1782.
336. Qazi, T.H., R. Rai, and A.R. Boccaccini, *Tissue engineering of electrically responsive tissues using polyaniline based polymers: a review.* Biomaterials, 2014. **35**(33): p. 9068-86.
337. Thrivikraman, G., G. Madras, and B. Basu, *Intermittent electrical stimuli for guidance of human mesenchymal stem cell lineage commitment towards neural-like cells on electroconductive substrates.* Biomaterials, 2014. **35**(24): p. 6219-35.

338. Tsui, J.H., et al., *Conductive Silk-Polypyrrole Composite Scaffolds with Bioinspired Nanotopographic Cues for Cardiac Tissue Engineering.* J Mater Chem B, 2018. **6**(44): p. 7185-7196.
339. Kai, D., et al., *Polypyrrole-contained electrospun conductive nanofibrous membranes for cardiac tissue engineering.* J Biomed Mater Res A, 2011. **99**(3): p. 376-85.
340. Çetin, M.Z. and P. Camurlu, *An amperometric glucose biosensor based on PEDOT nanofibers.* RSC Adv, 2018. **8**(35): p. 19724-19731.
341. Xu, C., et al., *A PEDOT:PSS conductive hydrogel incorporated with Prussian blue nanoparticles for wearable and noninvasive monitoring of glucose.* Chem Eng J, 2022. **431**: p. 134109.
342. Park, M., et al., *Fast and Stable Ionic Electroactive Polymer Actuators with PEDOT:PSS/(Graphene–Ag-Nanowires) Nanocomposite Electrodes.* Sensors, 2018. **18**(9): p. 3126.
343. Cellot, G., et al., *PEDOT:PSS Interfaces Support the Development of Neuronal Synaptic Networks with Reduced Neuroglia Response In vitro.* Front Neurosci, 2015. **9**: p. 521.
344. Magaz, A., et al., *Modulation of Neuronal Cell Affinity on PEDOT–PSS Nonwoven Silk Scaffolds for Neural Tissue Engineering.* ACS Biomater Sci Eng, 2020. **6**(12): p. 6906-6916.
345. Khasim, S., et al., *Post treated PEDOT-PSS films with excellent conductivity and optical properties as multifunctional flexible electrodes for possible optoelectronic and energy storage applications.* Opt Mater, 2022. **125**: p. 112109.
346. Solazzo, M., et al., *PEDOT:PSS interfaces stabilised using a PEGylated crosslinker yield improved conductivity and biocompatibility.* J Mater Chem B, 2019. **7**(31): p. 4811-4820.
347. Håkansson, A., et al., *Effect of (3-glycidyloxypropyl)trimethoxysilane (GOPS) on the electrical properties of PEDOT:PSS films.* J Polym Sci B Polym Phys, 2017. **55**(10): p. 814-820.
348. Wei, Y., et al., *Preparation and characterization of PEGDE crosslinked silk fibroin film.* J Wuhan Univ Technol Mater Sci Ed, 2014. **29**(5): p. 1083-1089.
349. Heller, A. and B. Feldman, *Electrochemical glucose sensors and their applications in diabetes management.* Chem Rev, 2008. **108**(7): p. 2482-505.
350. Liu, Y. and T. Segura, *Biomaterials-Mediated Regulation of Macrophage Cell Fate.* Front Bioeng Biotech, 2020. **8**.
351. Gibon, E., et al., *The biological response to orthopaedic implants for joint replacement: Part I: Metals.* J Biomed Mater Res B Appl Biomater, 2017. **105**(7): p. 2162-2173.
352. Frasca, A., et al., *Glycation and Serum Albumin Infiltration Contribute to the Structural Degeneration of Bioprosthetic Heart Valves.* J Am Coll Cardiol Basic Trans Science, 2020. **5**(8): p. 755-766.
353. Zakharchenko, A., et al., *Inhibition of advanced glycation end product formation and serum protein infiltration in bioprosthetic heart valve leaflets: Investigations of anti-glycation agents and anticalcification interactions with ethanol pretreatment.* Biomaterials, 2022. **289**: p. 121782.
354. Whitaker, R., et al., *Immunomodulatory Biomaterials for Tissue Repair.* Chem Rev, 2021. **121**(18): p. 11305-11335.
355. Chen, S., et al., *Characterization of topographical effects on macrophage behavior in a foreign body response model.* Biomaterials, 2010. **31**(13): p. 3479-91.
356. Brodbeck, W.G., et al., *Biomaterial adherent macrophage apoptosis is increased by hydrophilic and anionic substrates in vivo.* Proc Natl Acad Sci U S A, 2002. **99**(16): p. 10287-92.
357. Feng, B., et al., *The effect of pore size on tissue ingrowth and neovascularization in porous bioceramics of controlled architecture in vivo.* Biomed Mater, 2011. **6**(1): p. 015007.

358. Tylek, T., et al., *Precisely defined fiber scaffolds with 40 µm porosity induce elongation driven M2-like polarization of human macrophages.* Biofabrication, 2020. **12**(2): p. 025007.
359. Ryan, A.J., et al., *Electroconductive Biohybrid Collagen/Pristine Graphene Composite Biomaterials with Enhanced Biological Activity.* Adv Mater, 2018. **30**(15): p. e1706442.
360. Jain, K.G., et al., *Culture & differentiation of mesenchymal stem cell into osteoblast on degradable biomedical composite scaffold: In vitro study.* Indian J Med Res, 2015. **142**(6): p. 747-58.
361. Kim, D.H., et al., *Toxicity Assessment of a Single Dose of Poly(ethylene glycol) Diglycidyl Ether (PEGDE) Administered Subcutaneously in Mice.* Toxics, 2021. **9**(12).
362. Spencer, A.R., et al., *Electroconductive Gelatin Methacryloyl-PEDOT:PSS Composite Hydrogels: Design, Synthesis, and Properties.* ACS Biomater Sci Eng, 2018. **4**(5): p. 1558-1567.
363. Kapnisi, M., et al., *Auxetic Cardiac Patches with Tunable Mechanical and Conductive Properties toward Treating Myocardial Infarction.* Adv Funct Mater, 2018. **28**(21): p. 1800618.
364. Mawad, D., et al., *A conducting polymer with enhanced electronic stability applied in cardiac models.* Sci Adv, 2016. **2**(11): p. e1601007.
365. He, S., et al., *Preservation of conductive propagation after surgical repair of cardiac defects with a bio-engineered conductive patch.* J Heart Lung Transplant, 2018. **37**(7): p. 912-924.
366. Saravanan, S., et al., *Graphene Oxide-Gold Nanosheets Containing Chitosan Scaffold Improves Ventricular Contractility and Function After Implantation into Infarcted Heart.* Sci Rep, 2018. **8**(1): p. 15069.
367. Carnicer-Lombarte, A., et al., *Foreign Body Reaction to Implanted Biomaterials and Its Impact in Nerve Neuroprosthetics.* Front Bioeng Biotechnol, 2021. **9**: p. 622524.
368. Kobayashi, H., et al., *Transplantation of Pluripotent Stem Cell-Derived Cardiomyocytes into a Myocardial Infarction Model of Cynomolgus Monkey.* Methods Mol Biol, 2021. **2320**: p. 295-302.
369. Ye, L., et al., *Cardiac repair in a porcine model of acute myocardial infarction with human induced pluripotent stem cell-derived cardiovascular cells.* Cell Stem Cell, 2014. **15**(6): p. 750-61.
370. Tachibana, A., et al., *Paracrine Effects of the Pluripotent Stem Cell-Derived Cardiac Myocytes Salvage the Injured Myocardium.* Circ Res, 2017. **121**(6): p. e22-e36.
371. Wilson, H.M., et al., *Characterization of the Myocardial Inflammatory Response in Acute Stress-Induced (Takotsubo) Cardiomyopathy.* JACC Basic Transl Sci, 2018. **3**(6): p. 766-778.
372. Ip, W.K.E., et al., *Anti-inflammatory effect of IL-10 mediated by metabolic reprogramming of macrophages.* Science, 2017. **356**(6337): p. 513-519.
373. Granier, M., F. Massin, and J.-L. Pasquie, *Pro- and Anti-Arrhythmic Effects of Anti-Inflammatory Drugs.* Antiinflamm Antiallergy Agents Med Chem, 2013. **12**(1): p. 83-93.
374. Shanley, L.C., et al., *Harnessing the innate and adaptive immune system for tissue repair and regeneration: Considering more than macrophages.* Acta Biomater, 2021. **133**: p. 208-221.
375. Liu, Z., et al., *Electroactive Biomaterials and Systems for Cell Fate Determination and Tissue Regeneration: Design and Applications.* Adv Mater, 2021. **33**(32): p. 2007429.